NusA – zentraler Interaktionspartner in Antiterminationsprozessen in *Escherichia coli* und des Phagen λ

Dissertation

Zur Erlangung des akademischen Grades eines Doktors der Naturwissenschaften (Dr. rer. nat.)

an der Fakultät für Biologie, Chemie und Geowissenschaften

der Universität Bayreuth

vorgelegt von

Benjamin Rene Dudenhöffer

aus Heilbronn-Neckargartach

Bayreuth, 2020

Die vorliegende Arbeit wurde in der Zeit von Mai 2016 bis Juli 2020 in Bayreuth am Lehrstuhl Biochemie IV - Biopolymere unter Betreuung von Herrn Prof. Dr. Paul Rösch (05/2016 – 03/2018) und Herrn Dr. Stefan Knauer (04/2018 – 07/2020) angefertigt.

Vollständiger Abdruck der von der Fakultät für Biologie, Chemie und Geowissenschaften der Universität Bayreuth genehmigten Dissertation zur Erlangung des akademischen Grades eines Doktors der Naturwissenschaften (Dr. rer. nat.).

Dissertation eingereicht am: 22.07.2020

Zulassung durch die Promotionskommission: 29.07.2020

Wissenschaftliches Kolloquium: 23.09.2021

Amtierender Dekan: Prof. Dr. Matthias Breuning

Prüfungsausschuss:

Dr.	Stefan Knauer	(Gutachter)
Prof. Dr.	Birte Höcker	(Gutachterin)
Prof. Dr.	Matthias Ullmann	(Vorsitz)
Prof. Dr.	Olaf Stemmann	

Inhaltsverzeichnis

Zusammenfassung III
Summary V
1 Einleitung 1
1.1 Transkription 1
1.2 *Escherichia coli* RNA-Polymerase 2
1.2.1 Transkriptions-Elongations-Komplex 2
1.2.2 Nukleotid-Additions-Zyklus 4
1.3 Bakterieller Transkriptionszyklus 4
1.3.1 Initiation 4
1.3.2 Elongation 6
1.3.3 Termination 7
1.4 Nus-Faktoren 8
1.4.1 NusA 9
1.4.2 NusB und NusE 11
1.4.3 NusG 11
1.5 Ribosomale Antitermination 12
1.6 Phage λ 14
1.6.1 λN-vermittelte Antitermination 15
1.6.2 λQ-vermittelte Antitermination 17
1.7 NMR-Spektroskopie an großen Molekülen 18
2 Zielsetzung 20
3 Synopsis 21
3.1 Strukturelle Untersuchungen von Proteininteraktionen *via* NMR-Spektroskopie 21
3.2 Ribosomale Antitermination in *Escherichia coli* 23
3.2.1 SuhB ist Teil des ribosomalen Antiterminations-Komplexes 23
3.2.2 SuhB interagiert mit NusA-AR2 und hebt die Autoinhibition von NusA auf 25
3.3 λQ-vermittelte Antitermination des Phagen λ 28
3.3.1 λQ interagiert mit NusA-AR2 und hebt die Autoinhibition von NusA auf 30
3.3.2 λQ interagiert mit NusA-NTD 32

3.3.3 λQ interagiert mit der βFTH und repositioniert NusA-NTD an der RNAP 33
3.3.4 λQ verdrängt σ^{70} von der βFTH 37
3.4 NusA - zentraler Interaktionspartner in Antiterminationsprozessen 39
4 Abkürzungsverzeichnis 42
5 Literaturverzeichnis 44
6 Eigenanteil 60
6.1 Einzelarbeit A 60
6.2 Einzelarbeit B 60
6.3 Einzelarbeit C 61
7 Einzelarbeiten 62
7.1 Einzelarbeit A 62
7.2 Einzelarbeit B 91
7.3 Einzelarbeit C 125
8 Publikationsliste 163
9 Danksagung 164
10 (Eidesstattliche) Versicherungen und Erklärungen 165

Zusammenfassung

Die Transkription, die Synthese von Ribonukleinsäure (RNA) basierend auf einer Desoxyribonukleinsäure (DNA)-Matrize, wird durch DNA-abhängige RNA-Polymerasen (RNAPs) katalysiert, deren einfachsten bakteriellen Vertreter aus fünf Untereinheiten (2xα, β, β, ω) aufgebaut sind. Die Aktivität der RNAP wird in allen Phasen des Transkriptionszyklus (Initiation, Elongation, Termination) durch eine Vielzahl von Transkriptionsfaktoren (TFs) reguliert, wie z. B. die bakteriellen *N-utilization substances* (Nus)-Faktoren A, B, E und G. *Escherichia coli* (*E. coli*) NusA besteht aus sechs Domänen: einer N-terminalen Domäne (NTD), einer S1-Domäne, die zusammen mit den zwei folgenden *K homology* (KH)-Domänen KH1 und KH2 die RNA-bindende SKK-Einheit bildet sowie zwei C-terminalen *acidic repeat* (AR)-Domänen (AR1, AR2). Die RNA-Bindung von NusA wird durch die Bildung eines intramolekularen Komplexes von NusA-AR2 mit NusA-KH1 unterbunden, wodurch NusA autoinhibiert wird. Diese Autoinhibition kann durch die Interaktion von NusA-AR2 mit der C-terminalen Domäne der α-Untereinheit der RNAP (RNAPαCTD) aufgehoben werden. Des Weiteren vermittelt die NusA-AR2:RNAPαCTD-Wechselwirkung zusammen mit der Bindung von NusA-NTD an die zweite RNAPαCTD und die am RNA-Ausgangskanal der RNAP liegende β-*flap-tip*-Helix (βFTH) die Bindung von NusA an die RNAP. NusA interagiert während der Elongation mit der RNAP und übt, kontextabhängig, teils konträre Effekte aus. So ist NusA z. B. in der Lage gemeinsam mit den anderen Nus-Faktoren und weiteren Komponenten das Überlesen von Terminationssequenzen zu vermitteln, ein Mechanismus, der als Antitermination (AT) bezeichnet wird und Forschungsgegenstand dieser Arbeit war.

In *E. coli* ist die Expression ribosomaler RNA-Gene durch AT reguliert (*rrn*-AT). Hierbei werden die Nus-Faktoren durch eine RNA-Sequenz an die RNAP rekrutiert und bilden zusammen mit dieser und dem Protein S4 einen *rrn*-AT-Komplex, welcher das Überlesen von Rho-abhängigen Terminatoren ermöglicht. Darüber hinaus wurde eine Beteiligung der Inositolmonophosphatase SuhB postuliert, weshalb die Rolle von SuhB bei der *rrn*-AT im Rahmen dieser Arbeit mit biochemischen und *nuclear magnetic resonance* (NMR)-spektroskopischen Methoden charakterisiert wurde. Es wurde gezeigt, dass SuhB in den an einer *rrn*-AT-Sequenz pausierten *rrn*-AT-Komplex – bestehend aus der RNAP, einem Nukleinsäuregerüst, den Nus-Faktoren sowie optional S4 – integriert wird und spezifisch mit NusA-AR2 interagiert. Durch die Wechselwirkung mit NusA-AR2 kann SuhB außerdem die Autoinhibition von NusA aufheben bzw. die NusA-AR2:RNAPαCTD-Bindung auflösen. Unsere Ergebnisse deuten darauf hin, dass die SuhB:NusA-AR2-Interaktion bei der Rekrutierung von SuhB an den *rrn*-AT-Komplex eine

Rolle spielt sowie die Bindung der SKK-Einheit an die *rrn*-AT-Sequenz erleichtern und eine Repositionierung von NusA an der RNAP induzieren könnte.

Die Nus-Faktoren sind auch an den beiden, durch die Proteine λN bzw. λQ vermittelten, AT-Mechanismen des Phagen λ beteiligt, welche zur Replikation des Phagen-Genoms im Wirtsbakterium *E. coli* dienen. Während in der λN-AT alle Nus-Faktoren zusammen mit λN die RNAP in einen terminationsresistenten Zustand versetzen, ist für die λQ-AT nur eine Beteiligung von NusA postuliert. In dieser Arbeit wurden die strukturellen Grundlagen der λQ-AT sowie die Rolle von NusA in dieser mittels NMR-Spektroskopie untersucht. Es wurde die Bindung von λQ an die βFTH der RNAP strukturell charakterisiert und gezeigt, dass NusA λQ mittels seiner NTD und AR2-Domäne kontaktiert, wobei keine simultane Bindung eines λQ-Moleküls an beide NusA-Domänen möglich ist. λQ ist darüber hinaus in der Lage durch die Interaktion mit NusA-AR2 die Autoinhibition von NusA aufzuheben sowie durch die Wechselwirkung mit der βFTH NusA-NTD von dieser zu verdrängen und damit an der RNAP zu repositionieren. Die durch λQ induzierte Repositionierung von NusA-NTD könnte zu dem AT-fördernden Effekt von NusA führen, während die Aufhebung der Autoinhibition durch λQ die RNA-Bindung der SKK-Einheit – und damit die Rekrutierung von NusA an den λQ-AT-Komplex – erleichtern könnte. Des Weiteren könnte die NusA-AR2:λQ-Interaktion auch der Rekrutierung von λQ dienen. Schließlich wurde gezeigt, dass λQ in hohem molaren Überschuss die Bindung von NusA-NTD bzw. NusA-AR2 an die jeweilige RNAPαCTD auflöst, wodurch die Dissoziation von NusA von der RNAP induziert werden könnte.

Die Ergebnisse dieser Arbeit unterstreichen die zentrale Rolle von NusA in der Regulation der bakteriellen Transkription. NusA ist während dieser über seine NTD an die RNAP gebunden, während NusA-AR2, wie u.a. in dieser Arbeit gezeigt, spezifische Interaktionen mit TFs eingehen kann, was eine Funktion dieser Domäne als multifunktionale Rekrutierungsplattform nahelegt. Die rekrutierten TFs könnten, wie für λQ gezeigt, kontextabhängig NusA repositionieren, was wiederum mit einer Modulation der von NusA ausgeübten Effekte auf die Transkription einhergehen könnte.

Summary

Transcription, the synthesis of ribonucleic acid (RNA) based on a deoxyribonucleic acid (DNA) template, is catalyzed by DNA-dependent RNA polymerases (RNAPs) the simplest bacterial representatives of which are composed of five subunits (2xα, β, β, ω). In all steps of the transcription cycle (initiation, elongation, termination) RNAP activity is regulated by a multitude of transcription factors (TFs), such as the bacterial N-utilization substances (Nus)-factors A, B, E and G. *Escherichia coli* (*E. coli*) NusA consists of six domains: a N-terminal domain (NTD), an S1 domain which forms together with the two following K homology (KH) domains KH1 and KH2 the RNA-binding SKK unit, as well as two C-terminal acidic repeat domains (AR1, AR2). Formation of an intramolecular complex of NusA-AR2 with NusA-KH1 prevents RNA binding by NusA-SKK, thus autoinhibiting NusA. This autoinhibition can be released by the interaction of NusA-AR2 with the C-terminal domain of the α-subunit of RNAP (RNAPαCTD). Furthermore, the NusA-AR2:RNAPαCTD interaction, together with the binding of NusA-NTD to the second RNAPαCTD and the β flap-tip helix (βFTH) located at the RNA exit channel of RNAP, mediates the binding of NusA to RNAP. NusA contacts RNAP throughout elongation and, depending on the context, exerts partially contrary effects. For example, NusA, together with other Nus factors and other components, is able to suppress termination sequences, a mechanism known as antitermination (AT), which was the subject of this work.

In *E. coli* the expression of ribosomal RNA genes is regulated by AT (*rrn*-AT). Nus factors are recruited to the RNAP by a specific RNA sequence and form together with the RNAP and ribosomal protein S4 an *rrn*-AT complex which allows the read-through of Rho-dependent terminators. In addition, it has been postulated that the inositol monophosphatase SuhB was also involved in *rrn*-AT. Thus, the role of SuhB in *rrn*-AT was studied in this work by a combination of biochemical and nuclear magnetic resonance (NMR)-spectroscopic methods. It was shown that SuhB is integrated into an *rrn*-AT complex paused at an *rrn*-AT sequence, consisting of the RNAP, a nucleic acid scaffold, the Nus factors and optionally S4. Moreover, a direct interaction between SuhB and NusA-AR2 was demonstrated. Using this interaction, SuhB is able to release NusA autoinhibition or disrupt the NusA-AR2:RNAPαCTD interaction. Our results suggest that binding of SuhB to NusA-AR2 may play a role in the recruitment of SuhB to the *rrn*-AT complex, and could also facilitate binding of NusA-SKK to the *rrn*-AT sequence and induce repositioning of NusA at the RNAP.

Nus factors are also involved in the two AT mechanisms of phage λ, which are required to replicate the phage's genome in the host bacterium *E. coli* and which are mediated by the proteins λN and λQ, respectively. In λN-AT all Nus factors act together with λN to modify RNAP into a

termination-resistant state, whereas in λQ-AT only a role for NusA has been postulated. In this thesis the structural basics of λQ-AT as well as the role of NusA was investigated by NMR spectroscopy. The binding of λQ to the βFTH of RNAP was structurally characterized and it was shown that NusA contacts λQ via its NTD and AR2 domain, although simultaneous binding of one λQ molecule to both NusA domains is not possible. Similar to SuhB, λQ is able to release the autoinhibition of NusA by interacting with NusA-AR2. Furthermore, λQ interacts with the βFTH, displacing NusA-NTD from it, triggering repositioning of NusA-NTD on the RNAP. λQ induced repositioning of NusA-NTD could lead to the AT-promoting effect of NusA, whereas the release of autoinhibition by λQ could trigger RNA binding by NusA-SKK and therefore recruitment of NusA to the λQ-AT complex. Moreover, the NusA-AR2:λQ-interaction may be involved in the recruitment of λQ. Finally, it was shown that, in high molar excess, λQ can disrupt binding of NusA-NTD and NusA-AR2 to the RNAPαCTD, which might induce the dissociation of NusA from RNAP.

The results of this work underline the central role of NusA in the regulation of bacterial transcription. During transcription NusA is bound to RNAP via its NTD, whereas NusA-AR2, as shown in this work, can interact specifically with various TFs, suggesting that this domain may serve as versatile recruitment platform. Depending on the context the recruited TFs could, as shown for λQ, reposition NusA which, in turn, might result in a modulation of NusA effects on transcription.

1 Einleitung

1.1 Transkription

Die Transkription, das Umschreiben der Erbinformation, gespeichert in Form der Basenabfolge der Desoxyribonukleinsäure (DNA), in Ribonukleinsäure (RNA), ist der erste Schritt der Genexpression und wird in allen drei Domänen des Lebens durch DNA-abhängige RNA-Polymerasen (RNAPs) katalysiert (zusammengefasst in Werner & Grohmann, 2011). Die RNA kann als *messenger* RNA (mRNA) dem Ribosom als Vorlage zur Proteinbiosynthese im zweiten Schritt der Genexpression, der Translation, dienen (zusammengefasst in Choi *et al.*, 2018) oder auch ein biologisch aktives Endprodukt darstellen. So vermitteln z.B. ribosomale RNAs (rRNAs) die katalytische Aktivität des Ribosoms, während transfer-RNAs (tRNAs) Aminosäuren (As) zum Ribosom transportieren und nicht-kodierende (*non-coding*) RNAs an der Regulation der Genexpression beteiligt sind (zusammengefasst in Morris & Mattick, 2014).

Die Transkription kann in einen dreiphasigen Zyklus aus Initiation, Elongation und Termination unterteilt werden. Die Initiation der Transkription erfolgt durch die Rekrutierung der RNAP an eine regulatorische Erkennungssequenz des Gens (Promotor). Die doppelsträngige (ds)DNA des Promotors wird aufgeschmolzen und es beginnt die Synthese des RNA-Strangs entlang des Antisinn-Strangs (*antisense strand*) der DNA. Nach Verlassen der Promotorregion (*promoter escape*) erfolgt der Übergang in die Elongation unter Ausbildung eines stabilen Komplexes zwischen RNAP, DNA und RNA (*transcription elongation complex*, TEC). Die Termination der Transkription wird durch regulatorische Sequenzen des Gens (Terminationssequenzen) induziert und führt zur Dissoziation des TECs, sodass die RNAP für den nächsten Zyklus bereitsteht. Alle Schritte des Transkriptionszyklus werden durch eine Vielzahl von Effektoren, wie z.B. spezifischen Proteinen, welche als Transkriptionsfaktoren (TFs) bezeichnet werden, reguliert (zusammengefasst in Dangkulwanich *et al.*, 2014). So sind z.B. im Modellorganismus *Escherichia coli* (*E. coli*) die *housekeeping*-Faktoren der *N-utilization substances* (Nus)-Klasse (bestehend aus NusA, B, E und G) an der Regulation von Elongation und Termination beteiligt und in der Lage zusammen mit weiteren Faktoren den TEC derart zu modifizieren, dass Terminationssignale überlesen werden (Antitermination, AT) (zusammengefasst in Sen *et al.*, 2014).

Im Nachfolgenden wird ein Überblick über den Transkriptionszyklus in *E. coli*, dessen zentralen Akteur, die RNAP sowie deren Regulation gegeben. Ein besonderes Augenmerk liegt hierbei auf den TFs der Nus-Klasse, dem AT-Mechanismus zur Transkription ribosomaler RNA (*rrn*)-Operons in *E. coli* (*rrn*-AT) sowie den beiden AT-Mechanismen des Phagen λ, der λQ-AT und der λN-AT, welche der Replikation des Phagen-Genoms im Wirtsbakterium *E. coli* dienen.

1.2 *Escherichia coli* RNA-Polymerase

Die RNAPs zur Transkription zellulärer Genome weisen trotz ihres komplexen Aufbaus aus fünf (in Bakterien) bis 17 Untereinheiten (UEs) (in Eukaryonten) in den drei Domänen des Lebens ein gemeinsames Grundgerüst (zusammengefasst in Werner, 2012) und damit einhergehend ein hoch-konserviertes aktives Zentrum mit identischem katalytischen Mechanismus auf (zusammengefasst Werner & Grohmann, 2011). Die einfachsten bakteriellen RNAPs sind aus fünf UEs (α_2, β, β´, ω) aufgebaut, wie z.B. die 390 Kilodalton (kDa) große *E. coli* RNAP (Abb. 1-1A; Murakami, 2013). Die beiden C-terminalen Domänen der α-UEs der *E. coli* RNAP (RNAPαCTDs) üben regulatorische Funktionen aus. So können diese durch Bindung des, in einigen Pomotoren vorhandenen, *upstream promoter* (UP)-Elements die Transkriptionsrate des entsprechenden Gens erhöhen (Estrem *et al.*, 1999; Ross *et al.*, 1993) und als Bindungsplattform für TFs wie NusA dienen (Schweimer *et al.*, 2011; Guo *et al.*, 2018). Die beiden N-terminalen Domänen der α-UEs organisieren zusammen mit der ω-UE die Assemblierung der RNAP (Ghosh *et al.*, 2001; Ishihama, 1981). Die β-UE und β´-UE verleihen durch ihre Zangenform der RNAP eine krebsscherenartige Erscheinung und beherbergen zusammen in der Spalte zwischen den beiden Zangen das aktive Zentrum (Zhang *et al.*, 1999). Die Zangen der β-UE und β´-UE liegen in freier RNAP (*core* RNAP) in einer offenen Konformation vor und binden bei der Transkriptionsinitiation dsDNA, wobei sie in eine geschlossene Konformation übergehen, welche dem TEC eine erhöhte Stabilität und Prozessivität verleiht (Chakraborty *et al.*, 2012).

1.2.1 Transkriptions-Elongations-Komplex

Im TEC (Abb. 1-1B) wird die dsDNA durch die Zangen der β-UE und β´-UE zum aktiven Zentrum hingeleitet und ein Basenpaar (bp) vor diesem (i-1-Position) durch den β-*fork loop* 2 aufgeschmolzen, sodass sich die Transkriptionsblase ausbilden kann (Vassylyev *et al.*, 2007a). Der Sinn-Strang (*sense strand*) wird oberflächenexponiert an der RNAP weitergeleitet (Wang & Landick, 1997), während der Antisinn-Strang um 90° abgeknickt und zum aktiven Zentrum hingeleitet wird. Im aktiven Zentrum liegt nur das erste aufgeschmolzene Nukleotid (nt) des Antisinn-Strangs ungepaart vor (Vassylyev *et al.*, 2007a), sodass immer nur ein komplementäres Nukleosidtriphosphat (NTP) in der Insertionsstelle (i+1-Stelle) des aktiven Zentrums koordiniert und an das 3´-Ende des naszierenden RNA-Strangs gebunden wird (Abbondanzieri *et al.*, 2005; Vassylyev *et al.*, 2007b). Die katalytische Aktivität der RNAP wird durch zwei Mg^{2+}-Ionen im Zusammenspiel mit zwei hochmobilen Elementen der β´-UE, dem *trigger-loop* (TL) und der *bridge-helix* (BH) vermittelt (zusammengefasst in Brueckner *et al.*, 2009). Während das erste Mg^{2+}-Ion (Mg-A) stabil im aktiven Zentrum koordiniert ist (Zaychikov *et al.*, 1996), wird das

zweite Mg^{2+}-Ion (Mg-B) in jedem Zyklus gemeinsam mit dem einzubauenden NTP (Sosunov *et al.*, 2003) über den sekundären Kanal in das aktive Zentrum eingebracht (Zhang *et al.*, 1999, 2015). Im TEC bilden die stromabwärts (*downstream*) gelegenen Nukleotide des Antisinn-Strangs mit der naszierenden RNA ein 8-9 bp langes RNA:DNA-Hybrid aus, welches durch den β´-*lid loop* aufgespalten wird. Der Antisinn-Strang paart sich wieder mit dem Sinn-Strang, sodass die Transkriptionsblase geschlossen und keine ungepaarte Lücke im Antisinn-Strang hinterlassen wird. Die naszierende RNA wird über den RNA-Ausgangskanal aus der RNAP herausgeleitet (Vassylyev *et al.*, 2007a). Die Wand des RNA-Ausgangskanals wird durch die β-*flap* gebildet, an deren Spitze sich die β-*flap-tip helix* (βFTH) befindet, welche wie der β-*gate loop* (βGL) und die β´-*clamp helices* (β´CH) eine Bindungsplattform für regulatorische Proteine darstellt (Deighan *et al.*, 2008; Guo *et al.*, 2018; Kang *et al.*, 2018b; Krupp *et al.*, 2019; Martinez-Rucobo *et al.*, 2011; Murakami, 2013; Sevostyanova *et al.*, 2011).

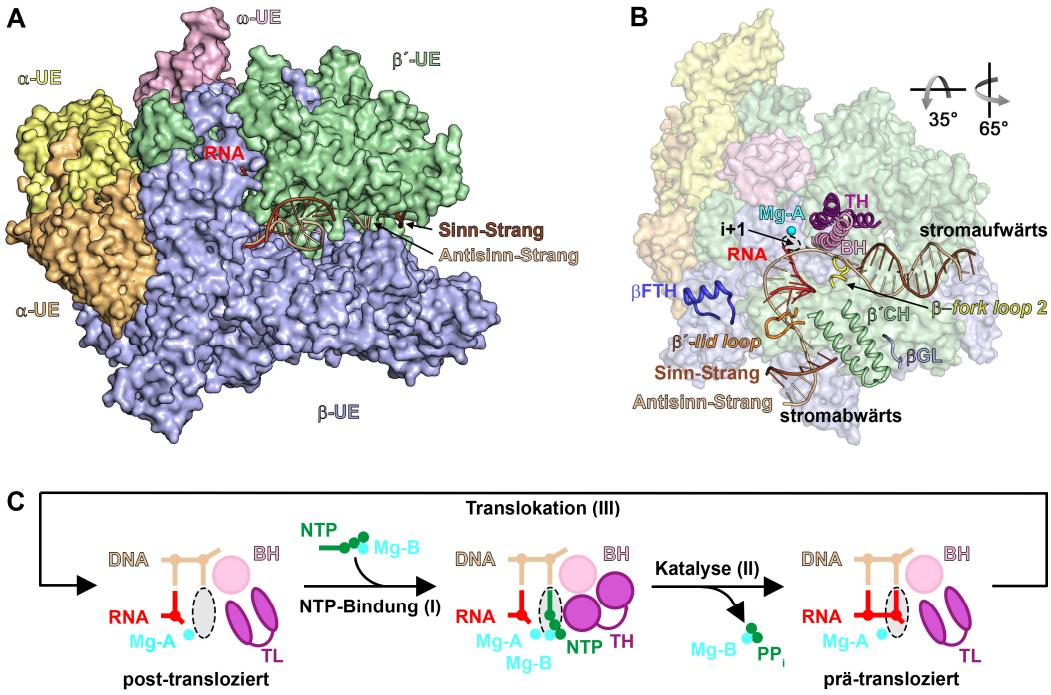

Abbildung 1-1: Struktur des *E. coli* TECs und Nukleotid-Addtions-Zyklus. (A) *E. coli* TEC (*protein data bank identification number* (PDB-ID): 6RH3) in Oberflächendarstellung. Die einzelnen UEs sind farblich hervorgehoben. **(B)** Struktur aus (A) um 65° um die x-Ache und 35° um die y-Achse gedreht in transparenter Oberflächendarstellung. Wichtige Sekundärstrukturelemente sowie die Nukleinsäuren sind in Bänderdarstellung farblich hervorgehoben. Mg-A ist durch eine cyane Kugel dargestellt. Die βFTH ist nicht aufgelöst und wurde aus der mittels Röntgenstrukturanalyse bestimmten Struktur der Holo-RNAP (PDB-ID: 4YG2) in den TEC eingefügt. **(C)** Schematische Darstellung des Zyklus der Nukleotid-Addition. Zu Beginn liegt die NTP-Insertionsstelle (Position i+1, als graues oval hervorgehoben) unbesetzt vor (post-translozierter Zustand). Nach Bindung eines passenden NTPs **(I)** faltet sich der TL zur *trigger-helix* (TH) und positioniert zusammen mit der BH das einzubauende NTP, sodass die Mg^{2+}-abhängige Katalyse der Nukleotid-Addition **(II)** stattfinden kann. Nach der Katalyse entfaltet sich die TH und das PP_i dissoziiert ab (prä-translozierter Zustand). Im Anschluss erfolgt die Translokation **(III)** unter Aufschmelzen des nächsten stromabwärts gelegenen bp der DNA, sodass der Zyklus von neuem beginnen kann. Details siehe Text.

1.2.2 Nukleotid-Additions-Zyklus

Der Zyklus der Nukleotid-Addition (Abb. 1-1C) kann in drei Schritte gegliedert werden: (I) NTP-Bindung, (II) Katalyse der Addition eines Nukelotids an die RNA unter Pyrophosphat (PP_i)-Freisetzung und (III) Translokation der RNAP (zusammengefasst in Brueckner *et al.*, 2009). Zu Beginn des Zyklus liegt die Insertionsstelle i+1 im aktiven Zentrum unbesetzt und der TL ungefaltet vor (post-translozierter Zustand; Kang *et al.*, 2017). Nach Bindung eines passenden NTPs an die Position i+1 (Kaplan *et al.*, 2008; Westover *et al.*, 2004) faltet sich der TL in eine α-helicale Konformation um (*trigger-helix*, TH) und positioniert im Zusammenspiel mit der BH und Mg-B das NTP für die Addition an die 3´ OH-Gruppe der RNA (Vassylyev *et al.*, 2007b, 2007a; Wang *et al.*, 2006). Mg-A vermittelt die katalytische Aktivität der RNAP durch Aktivierung der 3´ OH-Gruppe der RNA, sodass diese einen nukleophilen S_N2-Angriff auf das α-Phosphat des NTPs unter Abspaltung von PP_i durchführen kann. Nach erfolgter Verknüpfung kommt es zur Dissoziation des PP_i mitsamt dem Mg-B (Sosunov *et al.*, 2003; Steitz, 1998). Zugleich entfaltet sich die TH um den Austritt des PP_i aus dem aktiven Zentrum zu erlauben (prä-translozierter Zustand). Im Anschluss schieben TL und BH die RNAP unter Aufschmelzen des nächsten stromabwärts gelegenen bp der DNA, um eine Position entlang dieser weiter (Ratschen-Modell). Der TEC befindet sich im Anschluss wieder im post-translozierten Zustand und ist für einen neuen Nukleotid-Additions-Zyklus bereit (zusammengefasst in Svetlov & Nudler, 2009).

1.3 Bakterieller Transkriptionszyklus

1.3.1 Initiation

Bei der Initiation der Transkription (Abb. 1-2I-IV) erfolgt zunächst die Rekrutierung der RNAP an einen Promotor. Die freie RNAP (Abb. 1-2I) ist katalytisch kompetent, benötigt jedoch die Bindung eines Transkriptionsinitiationsfaktors der σ-Familie zur sequenzspezifischen Bindung an einen Promotor (zusammengefasst in Saecker *et al.*, 2011). In *E. coli* stehen die meisten Gene, welche zur Aufrechterhaltung der lebensnotwendigen Zellfunktionen unabhängig von äußeren Einflüssen exprimiert werden (*housekeeping genes*) unter Kontrolle des σ^{70}-Faktors (zusammengefasst in Ishihama, 2000). Dieser weist vier funktionale Regionen (σ^{70}_1-σ^{70}_4) auf (Lonetto *et al.*, 1992). Promotoren unter der Kontrolle des σ^{70}-Faktors besitzen zwei hexamere Sequenzmotive, das -10-Element (Pribnow Box; Pribnow, 1975) und das -35-Element (Siebenlist *et al.*, 1980). Durch Interaktionen der Region σ^{70}_2 mit den β´CH (Abb. 1-1B) und der Region σ^{70}_4 mit der βFTH (Abb. 1-1B) sowie weiterer Wechselwirkungen der beiden anderen σ^{70}-Regionen mit der RNAP wird die Bildung des Holo-RNAP Komplexes vermittelt (Abb. 1-2II; Murakami, 2013). Die Holo-RNAP wird durch Interaktionen von σ^{70}_2 mit dem -10-Element und von σ^{70}_4 mit

dem -35-Element an den Promotor rekrutiert (geschlossener Komplex) und $\sigma^{70}{}_2$ vermittelt das Aufschmelzen der dsDNA, sodass ein offener Komplex ausgebildet wird (Abb. 1-2III; Bae *et al.*, 2015; Feklistov & Darst, 2011). Im Anschluss ermöglicht σ^{70} die Initiation der Transkription (Pupov *et al.*, 2014), wobei zu Beginn der Transkriptions-Initiations-Komplex (*transcription initiation complex*, TIC) (Abb. 1-2IV; Zuo & Steitz, 2015) fest am Promotor gebunden bleibt und die DNA stromabwärts immer weiter in den offenen Komplex hineingezogen und aufgeschmolzen wird (DNA-*scrunching*). Es wird angenommen, dass das DNA-*scrunching* einen energetisch instabilen „gestressten" Zustand (*stressed state*) des TICs darstellt. Dieser Zustand kann durch Freisetzung des RNA-Transkripts unter bestehender Promotor-Bindung (abortive Initiation) oder durch Beendigung der Interaktionen zwischen der Holo-RNAP und dem Promotor (*promoter escape*) aufgelöst werden, wobei letzteres mit dem Übergang in die Elongation verbunden ist (Kapanidis *et al.*, 2006; Revyakin *et al.*, 2006). Oft werden multiple Zyklen der abortiven Initiation unter Freisetzung kurzer RNA-Stücke (2-12 nt) durchlaufen, bevor es zum *promoter escape* kommt (Hsu, 2002).

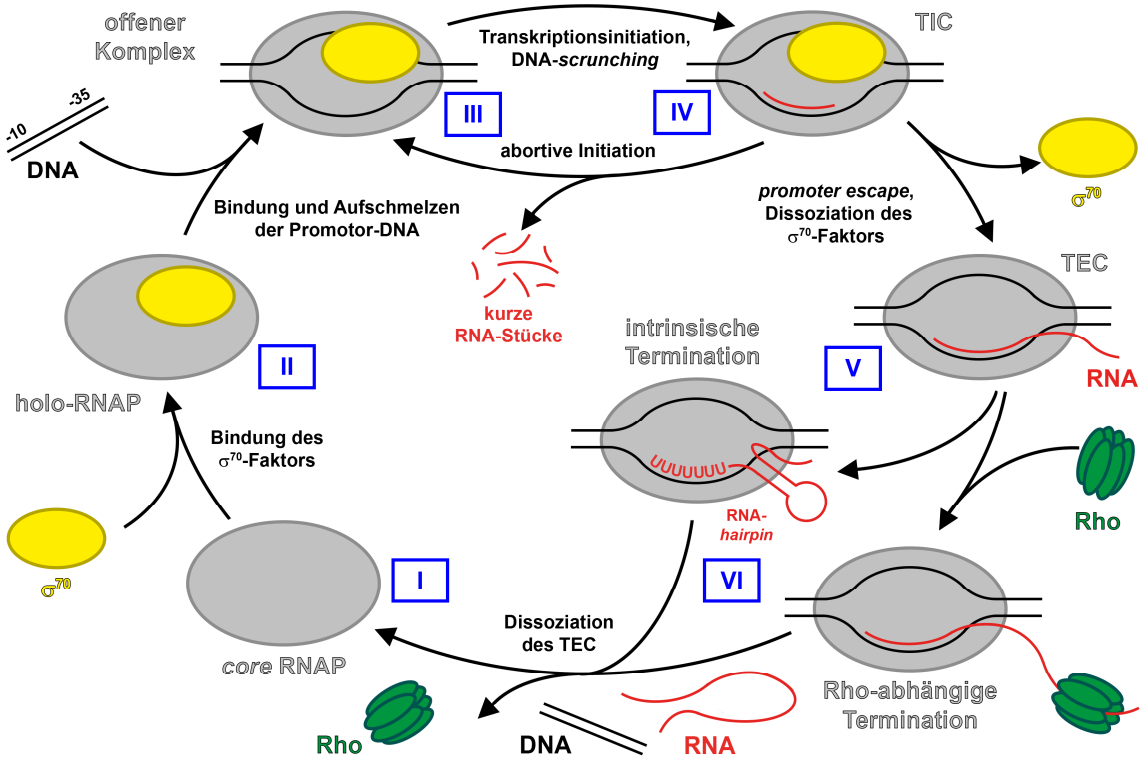

Abbildung 1-2: Der bakterielle Transkriptionszyklus. Zu Initiation der Transkription bindet die freie RNAP **(I)** einen Transkriptionsinitiationsfaktor der σ-Familie (hier σ^{70}), sodass die Holo-RNAP geformt wird **(II)**. Der σ^{70}-Faktor vermittelt die sequenzspezifische Bindung der Holo-RNAP an das -10-Element und das -35-Element des Promotors unter Aufschmelzen von diesem **(III)** sowie die nachfolgende Initiation der Transkription **(IV)**. Nach Überwindung des abortiven Initiationszyklus kommt es zum *promoter escape*, welcher mit dem Übergang in die Elongation einhergeht **(V)**, wobei der σ^{70}-Faktor zumeist dissoziiert. Die Termination der Transkription **(VI)** wird durch einen RNA-*hairpin* gefolgt von einer Poly-Uridin (U)-Sequenz (intrinsische Termination) oder durch den Faktor Rho vermittelt, wobei alle beteiligten Komponenten dissozieren, sodass die freie RNAP im Anschluss für den nächsten Transkriptionszyklus bereitsteht (I). Details siehe Text.

Der Übergang in die Elongation geht zumeist mit der Dissoziation des σ^{70}-Faktors einher, wobei hierfür zwei Modelle postuliert wurden. Entweder dass der σ^{70}-Faktor nach dem *promoter escape* abrupt durch die wachsende RNA verdrängt wird (obligatorisches Modell; Daube & von Hippel, 1999; Metzger *et al.*, 1993) oder während der Elongation nach und nach abdissoziiert (stochastisches Modell; Gill *et al.*, 1991; Shimamoto *et al.*, 1986). Auch eine stabile Integration des σ^{70}-Faktors in den TEC ist möglich (Bar-Nahum & Nudler, 2001; Kapanidis *et al.*, 2005) und wird durch Promotor-proximale σ^{70}-abhängige Pausen gefördert (Harden *et al.*, 2016).

1.3.2 Elongation

Die Elongation (Abb. 1-2V) wird immer wieder von Pausen unterbrochen, wobei in *E. coli* im Schnitt alle ~100 bp Transkriptionspausen auftreten (Adelman *et al.*, 2002; Neuman *et al.*, 2003). Diese ermöglichen (I) die Synchronisation von Transkription und Translation, (II) die Rekrutierung von regulatorischen Proteinen, (III) die Faltung der naszierenden RNA und (IV) die Termination der Transkription (zusammengefasst in Landick, 2006).

Pausen können in zwei Klassen eingeteilt werden: Pausen, die mit der Faltung eines RNA-*hairpins* (HP; Klasse I) und Pausen, die mit dem Zurücklaufen der RNAP (*backtracking*; Klasse II) einhergehen (Artsimovitch & Landick, 2000). Es wird angenommen, dass beiden Klassen von Pausen eine „elementare“ Pause (*elemental pause*, EP) vorausgeht (Landick, 2006), welche durch eine, von ~20 000 im Genom von *E. coli* zu findenden, elementaren Pausierungssequenzen (*elemental pausing sequence*, EPS) induziert werden kann (Larson *et al.*, 2014; Vvedenskaya *et al.*, 2014). Beim Übergang des TECs vom prä- zum post-translozierten Zustand wird durch die EPS in einigen, mit der DNA und RNA in Kontakt stehenden, Elementen der β´-UE sowie in deren Zange (*swivel*-Modul) eine leichte Drehung (~0,5°) induziert (*swiveling*). Hierdurch kann die RNA, nicht jedoch die DNA, in den post-translozierten Zustand übergehen, sodass der TEC in einen kurzlebigen, katalytisch inaktiven, halb-translozierten Pausierungszustand (*elemental paused elongation complex*, ePEC) versetzt wird (Kang *et al.*, 2018a; Saba *et al.*, 2019).

Im Modellsystem für Klasse I-Pausen, der *his*Pause, welche an der Regulation des für Enzyme zur Histidin-Biosynthese kodierenden *his*Operons beteiligt ist (zusammengefasst Gollnick & Babitzke, 2002), wird angenommen, dass die EP der RNA Zeit zur Ausbildung des HPs gibt (Kang *et al.*, 2018a), welcher die Pause um den Faktor 10 verlängert (Hein *et al.*, 2014). Die Nukleation des HP-Stamms im RNA-Ausgangskanal induziert hierbei ein *swiveling* der RNAP um ~3,6°, wodurch die Faltung des TLs im halb-translozierten aktiven Zentrum sterisch blockiert wird (Guo *et al.*, 2018; Kang *et al.*, 2018a). Es wird vermutet, dass hierbei durch eine Interaktion des HP-Stamms mit der βFTH letztere allosterisch zur Konformationsänderung im

aktiven Zentrum des ePECs beitragen kann (Hein *et al.*, 2014; Toulokhonov *et al.*, 2001). Ein translatierendes Ribosom kann die HP-stabilisierte Pause aufheben, wobei im Anschluss Transkription und Translation synchronisiert sind (Landick *et al.*, 1985).

Die EP erlaubt auch das *backtracking* der RNAP (Saba *et al.*, 2019). Hierbei läuft die RNAP unter synchronisiertem Aufschmelzen der stromaufwärts und Rehybridisieren der stromabwärts liegenden DNA in 3´→5´-Richtung entlang der DNA zurück, während sich das 3´-Ende der RNA vom aktiven Zentrum löst und über den sekundären Kanal aus der RNAP herausgeleitet wird (zusammengefasst in Nudler, 2012). Das *backtracking* geht ebenfalls mit einem *swiveling* der RNAP um 1,2 - 2,9° einher (Abdelkareem *et al.*, 2019) und kann durch endonukleolytische Spaltung der zurückgelaufenen RNA aufgehoben werden. Die endonukleolytische Spaltung der RNA wird durch die RNAP selbst katalysiert, wobei der TF GreB stimulierend auf die endonukleolytische RNAP-Aktivität wirkt (Abdelkareem *et al.*, 2019; Sosunova *et al.*, 2003).

1.3.3 Termination

Die Termination der Transkription (Abb. 1-2VI) am 3´-Ende des Gens wird in *E. coli* durch in der DNA kodierte Terminationssequenzen induziert und kann auf zwei Arten erfolgen: intrinsisch oder Rho-abhängig (zusammengefasst in Ray-Soni *et al.*, 2016).

Bei der intrinsischen Termination weist die transkribierte Terminationssequenz eine palindromische, HP-ausbildende, Guanosin (G)- und Cytidin (C)-reiche Sequenz (d'Aubenton Carafa *et al.*, 1990) sowie eine direkt darauffolgende ~8 nt lange Uridin (U)-reiche Sequenz auf (Wilson & von Hippel, 1994). Die Poly-U-Sequenz schwächt das DNA:RNA-Hybrid (Martin & Tinoco, 1980) und induziert eine Pausierung des TECs an dessen 3´-Ende (Gusarov & Nudler, 1999). Die Pause, welche vermutlich einer EP entspricht (Roberts, 2019), bildet ein Zeitfenster zur HP-Nukleation (Gusarov & Nudler, 1999). Die HP-Nukleation geht mit dem Aufschmelzen von 3-4 bp des DNA:RNA-Hybrids und letztlich dem Kollaps der Transkriptionsblase und der Dissoziation des TECs einher (Gusarov & Nudler, 1999; Komissarova *et al.*, 2002).

Im Falle der Rho-abhängigen Termination besitzt die Terminationssequenz ebenfalls zwei Elemente, deren Zusammenspiel die Termination vermittelt: einen 70-80 nt langen unstrukturierten C-reichen Bereich, welcher als Rekrutierungsplattform (*Rho utilization (rut)-site*) für den Terminationsfaktor Rho dient (Chen & Richardson, 1987; Morgan *et al.*, 1985) und eine stromabwärts liegende Pausierungssequenz, welche den Ort der Termination definiert (Morgan *et al.*, 1983). Rho, eine homo-hexamere, ringförmige Helicase, bindet in seiner offenen Konformation an die *rut-site* (Skordalakes & Berger, 2003) und fädelt die RNA durch dessen zentrale Pore, in welcher die sechs Protomere gemeinsam eine sekundäre RNA-Bindungsstelle bilden, die

unspezifisch RNA bindet. Die RNA-Bindung führt zu einer Isomerisierung von Rho in einen geschlossenen Ring (Skordalakes & Berger, 2006; Thomsen & Berger, 2009), welcher *via* seiner ATPase-Aktivität stromabwärts (5´→3´-Richtung) entlang der RNA transloziert (Koslover *et al.*, 2012). Rho und die RNAP weisen ähnliche Geschwindigkeiten der Translokation auf (zusammengefasst in Richardson, 2002), sodass die beiden Enzyme kinetisch gekoppelt sind. Hierdurch werden Pausierungen ausschlaggebend, dass Rho den TEC einholen und die Transkription terminieren kann (Jin *et al.*, 1992). Es wird angenommen, dass es sich bei diesen Pausen um EPs handelt (diskutiert in Ray-Soni *et al.*, 2016), da Klasse I-Pausen und Klasse II-Pausen eine erhöhte Stabilität gegenüber Rho-abhängiger Termination aufweisen (Dutta *et al.*, 2008).

Sowohl bei der Rho-abhängigen, als auch bei der intrinsischen Termination erfolgt die Termination durch eine Destabilisierung des TECs, welche zur Dissoziation von diesem führt. Hierfür wurden verschiedene Theorien postuliert, wobei für beide Terminationsarten gleiche Mechanismen angenommen werden (zusammengefasst in Peters *et al.*, 2011). Einerseits wird vermutet, dass es Rho (Park & Roberts, 2006) bzw. dem Terminator-HP (Santangelo & Roberts, 2004) möglich ist, den TEC vorwärts zu schieben, ohne dass eine Nukleotid-Addition durch diesen stattfindet (*hyper translocation*). Hierdurch verkürzt sich das DNA:RNA-Hybrid und wird destabilisiert. Ein alternatives Modell geht davon aus, dass Rho durch dessen Helicase-Aktivität (diskutiert in Richardson, 2002) bzw. der Terminator-HP durch eine weitere Propagation seines Stammes (Komissarova *et al.*, 2002; Molodtsov *et al.*, 2014) die RNA aus dem TEC herausziehen kann (*hybrid shearing*), sodass es ebenfalls zu einer Verkürzung des DNA:RNA-Hybrids kommt. Auch eine konformationelle Änderung des TECs in Antwort auf die HP-Bildung (Epshtein *et al.*, 2007) bzw. durch die Rho-Bindung (Epshtein *et al.*, 2010) stellt eine diskutierte Möglichkeit der Destabilisierung des TECs dar (*allosteric model*), wobei im Falle der HP-vermittelten Termination der βFTH eventuell eine vermittelnde Rolle hierbei zukommt (Epshtein *et al.*, 2007; Toulokhonov *et al.*, 2001; Toulokhonov & Landick, 2003). Letztlich kommt es in allen Modellen zur Dissoziation des TECs, sodass alle beteiligten Faktoren freigesetzt werden und die RNAP für den nächsten Transkriptionszyklus bereitsteht.

1.4 Nus-Faktoren

Die Transkription ist ein, durch eine Vielzahl von TFs (~300 bis dato in *E. coli* bekannt), hochregulierter Prozess (zusammengefasst in Ishihama, 2018). Eine Klasse von TFs sind die Nus-Faktoren. Ursprünglich als Co-Faktoren bei der durch das Protein λN vermittelten AT des Phagen λ entdeckt und daher als *N-utilization substance* (Nus) bezeichnet (Friedman & Baron, 1974), stellen diese endogene *E. coli* Proteine dar (Bubunenko *et al.*, 2007).

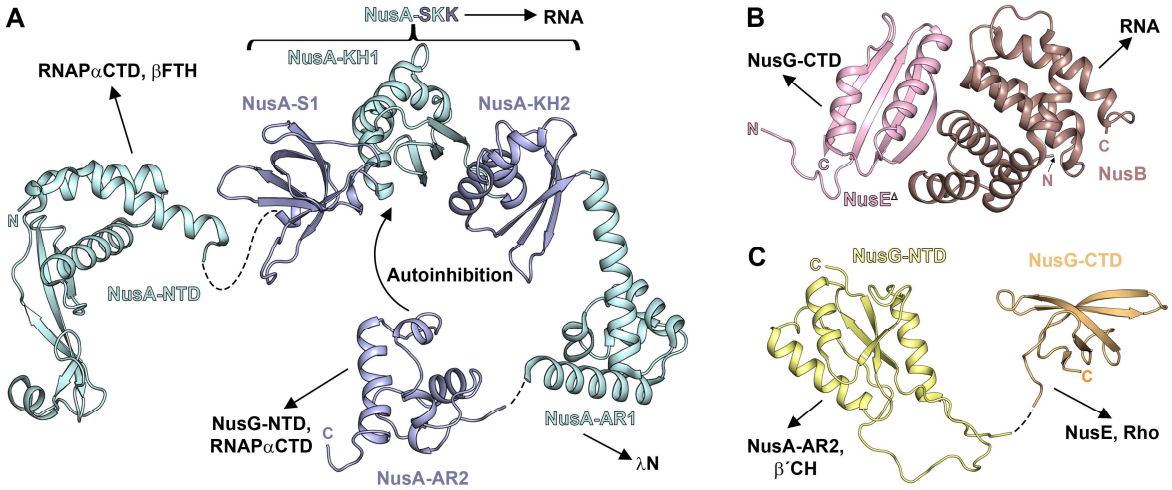

Abbildung 1-3: Die Nus-Faktoren aus *E. coli*. Die Strukturen der Nus-Faktoren sind in Bänderdarstellung wiedergegeben und die *linker* als gestrichelte Linien dargestellt. Die Pfeile zeigen die zugehörigen Interaktionspartner der einzelnen Domänen, bzw. Proteine an. **(A)** NusA (NusA-NTD PDB-ID: 2KWP, NusA-SKK-AR1 (PDB-ID: 5LM9, NusA-AR2 PDB-ID: 1WCN). **(B)** NusB:NusE^{A}-Heterodimer (PDB-ID: 3D3B). Bei NusE ist dessen Ribosomenbindungschleife durch ein Serin ersetzt (NusE^{A}). **(C)** NusG (NusG-NTD PDB-ID: 2K06, NusG-CTD PDB-ID: 2JVV). Details siehe Text.

1.4.1 NusA

Der in Archaeen und Bakterien hochkonservierte TF NusA besteht in *E. coli* aus 495 As (55,0 kDa) und ist in 6 Domänen organisiert (Abb. 1-3A; zusammengefasst in Burmann & Rösch, 2011). NusA ist während der Elongation an den TEC gebunden (Mooney *et al.*, 2009a) und übt in mannigfaltigen Prozessen zum Teil konträre Effekte auf die Transkription aus. So kann NusA (I) die pausierungsfreie Elongationsrate des TECs reduzieren, (II) die Effizienz von EPs erhöhen (Zhou *et al.*, 2011), (III) die Effizienz und Verweildauer an HP-vermittelten Pausen stimulieren (Artsimovitch & Landick, 2000; Ha *et al.*, 2010), (IV) die intrinsische Termination, insbesondere an schwachen Terminatoren, unterstützen (Gusarov & Nudler, 2001; Ha *et al.*, 2010; Mondal *et al.*, 2016), (V) die Rho-abhängige Termination inhibieren (Burns *et al.*, 1998; Qayyum *et al.*, 2016), (VI) zusammen mit AT-Faktoren zur *rrn*-AT in *E. coli* (siehe Abschnitt 1.5) sowie zur λN-AT (siehe Abschnitt 1.6.1) und der λQ-AT (siehe Abschnitt 1.6.2) des Phagen λ beitragen, (VII) die RNA-Faltung unterstützen (Pan *et al.*, 1999) oder (VIII) als Rekrutierungsplattform für Enzyme zur DNA-Reparatur (Cohen *et al.*, 2009; Epshtein *et al.*, 2014) sowie von NusG dienen (Strauß *et al.*, 2016).

Bei der N-terminalen Domäne von NusA (NusA-NTD) handelt es sich um eine L-förmige, aus vier α-Helices und einem zentralen antiprallelen β-Faltblatt aufgebaute Domäne (Drögemüller *et al.*, 2015), welche den stimulierenden Effekt von NusA auf HP-vermittelte Pausen, wie z. B. der *his*Pause vermittelt (Ha *et al.*, 2010). In der *his*Pause interagiert die NusA-NTD mit der RNAPαCTD sowie der βFTH der RNAP (Guo *et al.*, 2018). Es wird angenommen, dass der

stimulierende Effekt von NusA auf die *his*Pause über mehrere Effekte vermittelt wird. Zum einen verstärkt die Bindung von NusA an den ePEC das *swiveling* der RNAP von 0,5° auf 2,6°. Dies erhöht möglicherweise die Dauer der EP und damit das Zeitfenster zur Ausbildung des HPs und erleichtert eventuell auch den Übergang des ePECs in die *his*Pause-Konformation (Guo *et al.*, 2018). Zum anderen stimuliert die NusA-NTD auch die Bildung des HP-Stamms im RNA-Ausgangskanal (Hein *et al.*, 2014; Kolb *et al.*, 2014). Dies ist vermutlich auf die Stabilisierung bzw. Fixierung der flexiblen βFTH zurückzuführen, welche andernfalls mit der Nukleation des HP-Stamms im RNA-Ausgangskanal interferiert (Guo *et al.*, 2018; Hein *et al.*, 2014). Zugleich könnte die βFTH-Fixierung durch NusA-NTD auch den postulierten allosterischen Effekt der βFTH auf die Konformationsänderung des aktiven Zentrums der RNAP im ePEC erhöhen (Guo *et al.*, 2018; Hein *et al*., 2014; Toulokhonov *et al.*, 2001; Toulokhonov & Landick, 2003). Des Weiteren bildet die NusA-NTD durch Bindung an die βFTH zusammen mit NusA-S1 einen positiv geladenen Hohlraum, welcher den RNA-Ausgangskanal verlängert. Dieser Hohlraum begünstigt möglicherweise die HP-Faltung, stabilisiert nachfolgend den HP (Guo *et al.*, 2018) und könnte auch die Funktion von NusA als RNA-Chaperon erklären (Pan *et al.*, 1999). Auch die Stimulation der intrinsischen Termination durch NusA (Gusarov & Nudler, 2001; Ha *et al.*, 2010) insbesondere an suboptimalen Terminationssequenzen (Mondal *et al.*, 2016) ist anhand der beschriebenen Effekte erklärbar (Guo *et al.*, 2018).

Die der NusA-NTD folgende Domäne S1 besteht aus einem viersträngigen, antiparallelen β-Faltblatt und bildet zusammen mit den beiden Domänen K *homology* (KH)1 und KH2, welche jeweils aus drei α-Helices und einem dreisträngigen, antiparallelen β-Faltblatt bestehen, die SKK-Einheit (Said *et al.*, 2017). NusA-SKK ist in der Lage naszierende einzelsträngige RNA zu binden (Prasch *et al.*, 2009), wobei angenommen wird, dass die RNA-Bindung von NusA-SKK durch Verdeckung benachbarter *rut-sites*, auch zur Inhibition der Rho-abhängigen Termination führen kann (Qayyum *et al.*, 2016; Schweimer *et al.*, 2011).

Die auf die SKK-Einheit folgenden beiden C-terminalen Domänen finden sich nur in *E. coli* und einigen anderen α, β und γ-Proteobakterien. In *E. coli* weisen die beiden Domänen eine nahezu identische Struktur auf (Wurzel der mittleren quadratischen Abweichung der Rückgratatome: 1,2 Å) und werden aufgrund ihres negativen Oberflächenpotentials als *acidic repeat* (AR)1 und AR2 bezeichnet (Eisenmann *et al.*, 2005). Für NusA-AR1 ist eine Interaktion mit dem AT-Protein λN bekannt (Prasch *et al.*, 2006), welche während der Assemblierung des λN-AT-Komplexes, nicht jedoch zur Vermittlung der λN-AT selbst eine Rolle spielt (Krupp *et al.*, 2019; Mah *et al.*, 1999; Mishra *et al.*, 2013; Said *et al.*, 2017). NusA-AR2 dient hingegen als autoregulatorisches Element und inhibiert durch Bildung eines intramolekularen Komplexes mit der NusA-KH1-Domäne eine RNA-Bindung von NusA-SKK. Durch Interaktion von NusA-AR2

mit der RNAPαCTD kann die Autoinhibition aufgehoben werden (Schweimer *et al.*, 2011). Der C-terminale Bereich von NusA ist hochflexibel gegenüber der SKK-Einheit (Said *et al.*, 2017) und in der *his*Pause nur lose an die RNAPαCTD gebunden (Guo *et al.*, 2018). Daher ist auch eine hohe Flexibilität und lose Assoziation von NusA-AR2 an den TEC anzunehmen, was die Eigenschaft von NusA-AR2 erklären könnte, als Rekrutierungsplattform für NusG fungieren zu können (Strauß *et al.*, 2016).

1.4.2 NusB und NusE

Bei *E. coli* NusB (139 As, 16,2 kDa) handelt es sich um ein α-helikales Protein (Abb. 1-3B; Altieri *et al.*, 2000), welches sowohl eine Komponente des *rrn*-AT-Komplexes (siehe Abschnitt 1.5) in *E. coli* (Squires *et al.*, 1993) als auch des λN-AT-Komplexes (siehe Abschnitt 1.6.1) des Phagen λ darstellt (DeVito & Das, 1994; Krupp *et al.*, 2019; Said *et al.*, 2017). Im Rahmen beider AT-Mechanismen bindet NusB spezifisch an ein 12 nt langes konserviertes Element (*boxA*) der RNA-Sequenz, welche die am jeweiligen AT-Mechanismus beteiligten Komponenten an den TEC rekrutiert. Zur Bindung von *boxA* formt NusB zusammen mit NusE einen stabilen Komplex (Burmann *et al.*, 2010; Luo *et al.*, 2008), welcher die Affinität von NusB für RNA ~100-fach erhöht (Mühlberger *et al.*, 2003).

NusE (Abb. 1-3B) selbst weist nur eine geringe, unspezifische Affinität für RNA auf (Greive *et al.*, 2005) und ist als Teil des NusB:NusE-Komplexes ebenfalls an der *rrn*-AT (Squires *et al.*, 1993) sowie der λN-AT beteiligt (DeVito & Das, 1994; Said *et al.*, 2017). Als ein *moonlighing*-Protein (Protein mit mehr als einer Funktion) kann NusE, als S10, auch als Teil der 30S-UE des Ribosoms vorliegen. NusE (103 As, 11,8 kDa) selbst ist aus einem antiparallelen β-Faltblatt, zwei α-Helices sowie einer Ribosomenbindungsschleife (As 46-67) aufgebaut, welche sich beim Einbau in das Ribosom zu einem zweisträngigen β-Faltblatt faltet (Noeske *et al.*, 2015).

1.4.3 NusG

NusG als einzig universell konservierter TF (Werner, 2012) ist in *E. coli* (181 As, 20,5 kDa) aus einer N-terminalen (NusG-NTD) und einer C-terminalen Domäne (NusG-CTD) aufgebaut (Abb. 1-3C). Die NusG-NTD, bestehend aus einem zentralen, dreisträngigen, antiparallelen β-Faltblatt, umgeben von drei α-Helices, ist über einen flexiblen Linker mit der NusG-CTD verknüpft, welche sich zu einem fünfsträngigen antiparallelen β-Fass faltet (Mooney *et al.*, 2009b).

NusG ist während der Elongation an den TEC gebunden (Mooney *et al.*, 2009a). Die Interaktion von NusG mit der RNAP wird über die NusG-NTD vermittelt, welche an die β'CH und den βGL

der RNAP bindet und die beiden Zangen der RNAP miteinander verknüpft. Hierdurch wird die geschlossene Konformation der RNAP stabilisiert (Kang *et al.*, 2018b), was zu einer erhöhten Prozessivität des TECs (Chakraborty *et al.*, 2012; Kang *et al.*, 2018b) und damit einhergehend zu einer Steigerung der pausierungsfreien Elongationsrate führt (Herbert *et al.*, 2010). Darüber hinaus induziert die NusG-NTD auch eine Stabilisierung der stromaufwärts gelegenen dsDNA (Kang *et al.*, 2018b), wodurch das Aufschmelzen dieser (Kang *et al.*, 2018b; Turtola & Belogurov, 2016) und damit einhergehend das *backtracking* der RNAP inhibiert wird (Artsimovitch & Landick, 2000).

Während NusG-NTD an den TEC gebunden ist, kann die NusG-CTD durch Bindung an S10 in der 30S-UE des Ribosoms die Kopplung von Transkription und Translation vermitteln (Burmann *et al.*, 2010; Saxena *et al.*, 2018). Am Ende des Gens wird das Ribosom freigesetzt und über dieselbe Bindungsstelle auf NusG-CTD kann Rho gebunden und zur Vermittlung der Rho-abhängigen Termination an den TEC rekrutiert werden. Die Bindung von NusG-CTD an Rho fördert hierbei den Ringschluss von Rho (Lawson *et al.*, 2018), was den stimulierenden Effekt von NusG auf die Rho-abhängige Termination an suboptimalen Terminationssequenzen erklärt (Peters *et al.*, 2012; Sullivan & Gottesman, 1992). Im Gegensatz hierzu ist NusG jedoch auch in der Lage zusammen mit den anderen Nus-Faktoren und weiteren Komponenten im Rahmen der *rrn*-AT in *E. coli* (siehe Abschnitt 1.5) sowie der λN-AT des Phagen λ (siehe Abschnitt 1.6.1) Rho-abhängige Terminatoren zu unterdrücken.

1.5 Ribosomale Antitermination

Terminationssequenzen finden sich nicht nur am 3´-Ende von Genen bzw. Operons, sondern auch an deren Beginn in Leitsequenzen (*leader regions*) sowie in Trenn-Sequenzen (*spacern*) zwischen Operon-Genen und dienen hierbei der Regulation der Genexpression. Das Überlesen von Terminationssequenzen und die Fortsetzung der Transkription wird als (prozessive) AT bezeichnet (zusammengefasst in Santangelo & Artsimovitch, 2011) und stellt in *E. coli* einen wichtigen Mechanismus zur Regulation der Expression von rRNAs dar (Aksoy *et al.*, 1984).

In *E. coli* sind die rRNAs-Gene in sieben *rrn*-Operons (*rrnA*-*rrnE*, *rrnG* und *rrnH*) organisiert (Ellwood & Nomura, 1982). Jedes Operon besteht aus den Genen für 16S, 23S und 5S rRNA sowie für eine oder mehrere tRNAs, wobei die tRNA-Gene im *spacer* zwischen 16S und 23S rRNA-Gen oder/und am 3´-Ende des Operons liegen (Abb. 1-4A; Blattner *et al.*, 1997). Da rRNAs ~84 % des Transkriptoms in *E. coli* ausmachen (Dennis, 1972; Shen & Bremer, 1977), ist ihre Expression stark reguliert. Auf Promotor-Ebene erfolgt die Regulation der *rrn*-Operons durch einen, unter dem Einfluss mehrerer Effektoren stehenden, Tandem-Promotor (*rrn* P1-P2)

(zusammengefasst in Jin *et al.*, 2012). Nachfolgend wird die Expression der *rrn*-Operons durch einen AT-Mechanismus reguliert (*rrn*-AT), welcher durch Unterdrückung der Rho-abhängigen Termination die Transkription der *rrn*-Operons ermöglicht (Albrechtsen *et al.*, 1990).

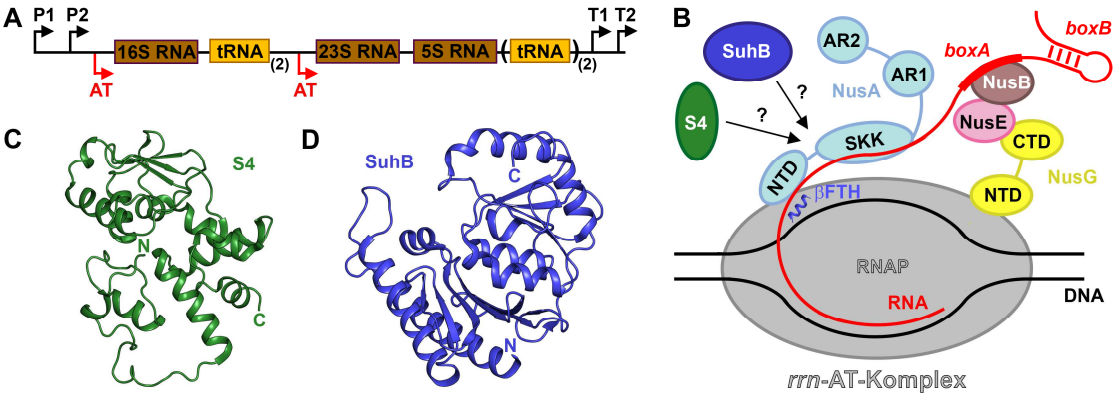

Abbildung 1-4: Die *rrn*-AT in *E. coli*. **(A)** Schematischer Aufbau eines *E. coli rrn*-Operons. Die Lage der Promotoren (P), Terminatoren (T) sowie AT-Sequenzen (in rot) sind durch Pfeile gekennzeichnet. **(B)** Schematischer Aufbau des *rrn*-AT-Komplexes. Es wird ein analoger Aufbau zum λN-AT-Komplex des Phagen λ angenommen (siehe Abschnitt 1.6.1). **(C)** Das ribosomale Protein S4 (PDB-ID: 4YBB). **(D)** Die Inositolmonophosphatase SuhB (PDB-ID: 2QFL). Details siehe Text.

In der *rrn*-AT dient eine RNA-Sequenz bestehend aus *boxA*, *boxB* und *boxC* (*rrn*-AT-Sequenz) zur Rekrutierung der an der *rrn*-AT beteiligten Komponenten an den TEC (Li *et al.*, 1984). Die *rrn*-AT-Sequenz ist dem *rrn* P2-Promotor folgend in der Leitsequenz der *rrn*-Operons, in der Reihenfolge *boxB-boxA-boxC* sowie im *spacer* zwischen dem 16SRNA-Gen und 23SRNA-Gen in Form einer *boxB-boxA*-Sequenz zu finden (Berg *et al.*, 1989), wobei letztere essentiell für die Expression des nachfolgenden 23S RNA-Gens ist (Pfeiffer & Hartmann, 1997). *boxA* alleine ist ausreichend zur Vermittlung der *rrn*-AT (Berg *et al.*, 1989; Heinrich *et al.*, 1995) und stellt wie *boxC* ein konserviertes Element dar, wohingegen *boxB* nicht-konserviert ist und einen HP ausbildet (Berg *et al.*, 1989). Im *rrn*-AT-Komplex (Abb. 1-4B) bindet der NusB:NusE-Komplex *boxA* (Greive *et al.*, 2005; Nodwell & Greenblatt, 1993). Ebenso stellen das ribosomale Protein S4 (Torres *et al.*, 2001), NusG (Li *et al.*, 1992) und NusA (Vogel & Jensen, 1997) essentielle Komponenten zur Vermittlung der *rrn*-AT dar, wobei NusA-SKK vorzugsweise an den *spacer* zwischen *boxA* und *boxC* bindet (Prasch *et al.*, 2009). Neben den Nus-Faktoren und S4 konnte auch eine Beteiligung der Inositolmonophosphatase SuhB an der *rrn*-AT gezeigt werden (Singh *et al.*, 2016). Es wird angenommen, dass der *rrn*-AT-Komplex neben der Vermittlung der AT auch der RNA-Faltung dienen könnte (Bubunenko *et al.*, 2013). So könnte zwischen dem NusB:NusE-Komplex und dem TEC:NusG:NusA-Komplex ein geschützter Raum zur Faltung naszierender RNA gebildet werden, wobei SuhB ein zusätzliches RNA-Chaperon darstellen würde (Singh *et al.*, 2016). Bis dato ist jedoch unklar, ob die RNA-Faltung oder die AT Hauptaufgabe des *rrn*-AT-Komplexes ist.

Das ribosomale Protein S4 (269 As, 29,5 kDa) ist ein überwiegend α-helikales Protein mit einem fünfsträngigen antiparallelen βFaltblatt (Abb. 1-4C). Als *moonlighting*-Protein kann S4 als Teil der 30S-UE des Ribosoms vorliegen (Noeske *et al.*, 2015) sowie als Translationsrepressor fungierend, die Expression der ribosomalen Proteine S13, S11, S4 und L17 regulieren (Jinks-Robertson & Nomura, 1982; Thomas *et al.*, 1987). Bei SuhB (207 As, 23,7 kDa) handelt es sich um eine Inositolmonophosphatase (Matsuhisa *et al.*, 1995), welche aus zwei zentralen antiparallelen β-Faltblättern umgeben von acht α-Helices aufgebaut ist (Abb. 1-4D) und in einem Gleichgewicht zwischen Monomer und Dimer vorliegt (Wang *et al.*, 2007). Es wird angenommen, dass die enzymatische Aktivität von SuhB aufgrund des Fehlens von Inositol-Verbindungen in *E. coli* keine physiologische Bedeutung hat (Kozloff *et al.*, 1991). Neben einer Bindung an die RNAP (Wang *et al.*, 2007) sowie der Beteiligung an der *rrn*-AT (Singh *et al.*, 2016) ist bis dato wenig über die Rolle von SuhB in *E. coli* bekannt.

1.6 Phage λ

Die Replikation des Phagen λ in seinem Wirt *E. coli* kann über zwei Strategien erfolgen. Einerseits kann sich der Phage λ selbst replizieren und Phagenpartikel produzieren, welche durch Lyse der Wirtszelle freigesetzt werden (lytischer Zyklus). Zum anderen kann der Phage λ sein Genom in das Wirtsgenom von *E. coli* integrieren (Prophage), sodass dieses bei der Zellteilung zusammen mit dem Wirtsgenom repliziert wird (lysogener Zyklus) (zusammengefasst in Oppenheim *et al.*, 2005). Die Entscheidung zwischen lysogenem und lytischem Zyklus ist durch ein komplexes Netzwerk einer Vielzahl von Faktoren reguliert (zusammengefasst in Casjens & Hendrix, 2015) und daher im Folgenden vereinfacht dargestellt.

Zu Beginn kommt es zur Expression der „frühen" Gene *cro* und *n* des Phagen-Genoms (Abb. 1-5) unter Kontrolle der Promotoren p_R und p_L, bis zu den Terminationssequenzen t_{L1} und t_{R1}. Das im Gen *cro* kodierte Protein Cro fungiert als Repressor des Promotors p_{RM}, unter dessen Kontrolle das für den λ-Repressor kodierende Gen *cI* steht. Das Produkt des Gens *n* das AT-Protein λN wird an der *n utilization-site* (*nut*) *R* bzw. *nutL* gemeinsam mit den Nus-Faktoren an den TEC rekrutiert und vermittelt zusammen mit diesen das Überlesen der Terminatoren t_{L1} und t_{R1} durch den TEC (λN-AT, siehe Abschnitt 1.6.1). Hierdurch werden die „verspäteten frühen" Gene *o*, *p* und *ren*, welche für die Replikation des Phagen-Genoms im lytischen und lysogenen Zyklus essentiell sind sowie das für das AT-Protein λQ kodierende Gen *q* exprimiert. λQ ermöglicht durch Bindung an den TEC das Überlesen der Terminationssequenz $t_{R'}$ (λQ-AT, siehe Abschnitt 1.6.2) und hierdurch die Expression der „späten" Gene für Packung und Zelllyse im lytischen Zyklus (zusammengefasst in Court *et al.*, 2007). Darüber hinaus werden durch die

λN-AT auch die Gene *int*, *cII* und *cIII* exprimiert, welche den Übergang in den lysogenen Zyklus einleiten können. Die im Gen *int* kodierte Integrase katalysiert die Integration des Phagen-Genoms in das Wirtsgenom und CIII erhöht die Stabilität von CII. CII stimuliert die Expression der Gene für die Integrase sowie den λ-Repressor und reprimiert die Expression des Gens *q*. Der λ-Repressor wiederum reprimiert p_L und p_R, sodass die Expression des Phagen-Genoms nahezu stillgelegt wird. Lediglich das für den λ-Repressor kodierende Gen *cI*, unter Kontrolle des Promotors p_{RM}, bliebt aktiv und wird durch den λ-Repressor selbst reguliert, sodass der Prophage stabil im lysogenen Zyklus vorliegt (zusammengefasst in Oppenheim *et al.*, 2005).

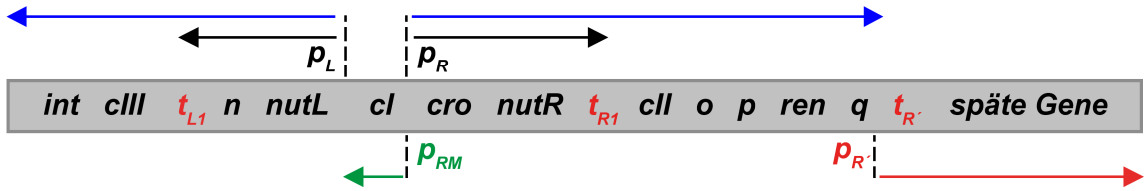

Abbildung 1-5: Ausschnitt aus der Genkarte des Phagen λ. Das Genom ist grau unterlegt. Gene sind in schwarz und Terminationssequenzen in rot dargestellt. Schwarze Pfeile kennzeichnen die Transkripte der „frühen Gene" des Phagen λ unter Kontrolle der Promotoren p_L und p_R und die blauen Pfeile die entsprechenden Transkripte nach Rekrutierung des AT-Proteins λN. Der rote Pfeil markiert das Transkript der „späten Gene" für den lytischen Zyklus unter Kontrolle des Promotor $p_{R'}$ und nach Rekrutierung des AT-Proteins λQ. Der grüne Pfeil zeigt das Transkript unter Kontrolle des Promotors p_{RM} im Prophagen (Abbildung erstellt nach Court *et al.*, 2007). Details siehe Text.

1.6.1 λN-vermittelte Antitermination

In der λN-AT ermöglicht das Zusammenspiel des intrinsisch ungeordneten AT-Proteins λN (Mogridge *et al.*, 1998) mit den Nus-Faktoren (DeVito & Das, 1994) das Überlesen von Rho-abhängigen und intrinsischen Terminatoren durch den TEC (Gottesman *et al.*, 1980). Die Rekrutierung von λN und den Nus-Faktoren an den TEC wird durch die *nut-site* (Salstrom & Szybalski, 1978), eine RNA-Sequenz bestehend aus einem konservierten *boxA*-Element und einem HP-ausbildenden *boxB*-Element vermittelt (zusammengefasst in Friedman & Gottesmann, 1983).

Im λN-AT-Komplex (Abb. 1-6A) erfolgt die Bindung von *boxA* durch das NusB:NusE-Dimer. Die *spacer*-Sequenz zwischen *boxA* und *boxB* wird durch die NusA-KH1-Domäne und der *boxB*-HP durch NusA-KH2 gebunden (Krupp *et al.*, 2019; Said *et al.*, 2017). Der *boxB*-HP fungiert als Rekrutierungsplattform für λN (Mogridge *et al.*, 1995), welches mit seiner N-terminalen α_1-Helix an den *boxB*-HP und an NusA-KH2 bindet. Die α_2-Helix von λN wird in einem, zwischen NusA und NusE ausgebildeten, Hohlraum eingebettet (Said *et al.*, 2017) während die α_3-Helix von λN an NusA-NTD bindet und gemeinsam mit dieser die βFTH der RNAP kontaktiert. λN induziert hierbei eine konformationelle Änderung der βFTH, welche vermutlich die

Bildung von Terminator-HPs sterisch hindert. Zudem vermittelt λN eine Auflösung der Bindung von NusA-NTD an die RNAPαCTD (Krupp *et al.*, 2019). Hierdurch nimmt NusA im Vergleich zur *his*Pause (Abb. 1-6B) eine geänderte globale Konformation ein (Guo *et al.*, 2018; Krupp *et al.*, 2019), welche mögliche positive Effekte von NusA auf die RNA- bzw. Terminator-HP-Faltung inhibieren könnte.

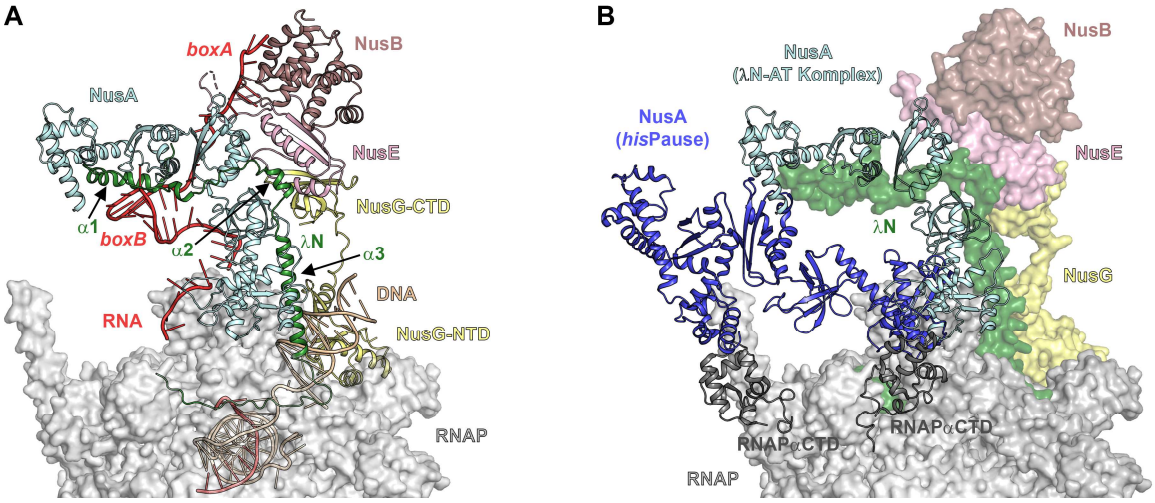

Abbildung 1-6: Der λN-AT-Komplex des Phagen λ. (A) Der λN-AT-Komplex (PDB-ID: 6GOV). Die RNAP ist transparent in Oberflächendarstellung wiedergegeben. Alle weiteren beteiligten Komponenten des λN-AT-Komplexes, einschließlich der Nukleinsäuren, sind als Bändermodelle farblich hervorgehoben. **(B)** Position von NusA im λN-AT-Komplex im Vergleich zu dessen Position im *his*pausierten TEC (PDB-ID: 6FLQ). NusA und die beiden RNAPαCTDs des TECs sind in Bänderdarstellung hervorgehoben, während die restlichen Faktoren des λN-AT-Komplexes, ebenso wie die RNAP transparent in Oberflächendarstellung wiedergegeben sind. Die Nukleinsäuren sind zur besseren Übersichtlichkeit nicht dargestellt. Details siehe Text.

Der unstrukturierte C-Terminus von λN verknüpft einige Elemente des *swivel*-Moduls miteinander, sodass vermutlich das *swiveling* der RNAP erschwert wird. Darüber hinaus kontaktiert der C-Terminus von λN auch das DNA-RNA-Hybrid im Inneren der RNAP sowie die stromaufwärts liegende dsDNA und wirkt möglicherweise stabilisierend auf diese, wodurch *backtracking* (Klasse II-Pausen) als auch Termination entgegengewirkt werden könnte. Ebenso kontaktiert die NusG-NTD die stromaufwärts liegende dsDNA und übt durch Stabilisierung dieser einen *backtracking*-inhibierenden Effekt aus. Des Weiteren verknüpft die NusG-NTD im λN-AT-Komplex durch Bindung an die β'CH und den βGL die beiden Zangen der RNAP miteinander (Krupp *et al.*, 2019), sodass die geschlossene Konformation des TECs stabilisiert und damit einhergehend möglicherweise dessen Prozessivitiät erhöht wird (Chakraborty *et al.*, 2012; Kang *et al.*, 2018b; Krupp *et al.*, 2019). Die zweite Domäne von NusG, die NusG-CTD bindet im λN-AT-Komplex an NusE (Krupp *et al.*, 2019), wodurch die Rho-Bindungsstelle von NusG-CTD verdeckt und hierdurch vermutlich die Rho-abhängige Termination inhibiert wird (Krupp *et al.*, 2019; Lawson *et al.*, 2018).

1.6.2 λQ-vermittelte Antitermination

Die späten Gene des Phagen λ für Packung und Zelllyse sind in einem 26 kB großen Operon organisiert, dessen Expression durch den Promotor $p_{R'}$ sowie nachfolgende Terminatoren im Operon reguliert wird (zusammengefasst in Casjens & Hendrix, 2015). Das AT-Protein λQ ermöglicht dem TEC die Expression des Operons (Deighan & Hochschild, 2007) über Rho-abhängige und intrinsische Terminatoren hinweg (Luk & Szybalski, 1983), wobei ein stimulierender Effekt für NusA auf die AT-Effizienz von λQ gezeigt wurde (Grayhack *et al.*, 1985). Bei λQ (207 As, 22,6 kDa) selbst handelt es sich um ein leicht elongiertes Protein, bestehend aus sechs α-Helices sowie einem zweisträngigen, antiparallelen β-Faltblatt, welches ein Zink-Finger-Motiv sowie einen 60 As langen N-Terminus aufweist, von dem angenommen wird, dass er flexibel ist (Abb.1-7A; Vorobiev *et al.*, 2014).

Die Rekrutierung von λQ an den TEC wird durch das Zusammenspiel von drei DNA-Elementen in der Promotor-Region $p_{R'}$ des Phagen λ (Abb. 1-7B) vermittelt, (I) dem λQ-bindenden Element (QBE) (Yarnell & Roberts, 1992), (II) einer, aus einem -10-artigen Element (Ring *et al.*, 1996) und einem -35-artigen Element (Nickels *et al.*, 2002; Perdue & Roberts, 2010) bestehenden, Promotor-proximalen σ^{70}-abhängigen Pause sowie (III) einer EP (Bird *et al.*, 2016; Strobel & Roberts, 2015). Bei der Transkriptionsinitiation (Abb. 1-7C-I) ist das zwischen dem σ^{70}-Promotor eingebettete QBE zunächst durch die Bindung von σ^{70}_2 an das -10-Element und von σ^{70}_4 an das -35-Element des σ^{70}-Promotors verdeckt (Nickels *et al.*, 2002). Nach dem Verlassen des Promotors kommt es durch die Bindung von σ^{70}_2 an das -10-artige Element (Ring *et al.*, 1996) und σ^{70}_4 an das -35-artige Element (Nickels *et al.*, 2002; Perdue & Roberts, 2010) der σ^{70}-abhängigen Pause ab Position +13 zu DNA-*scrunching* (Strobel & Roberts, 2014). An Position +16 wird durch die EP eine Pausierung des TECs induziert (Bird *et al.*, 2016; Strobel & Roberts, 2015) und λQ an das, durch den *promoter escape* freigegebene, QBE (Nickels *et al.*, 2002) rekrutiert (Abb. 1-7C-II). Das QBE enthält zwei postulierte λQ-Bindungsstellen (QBEI und QBEII), wobei eine Bindung von je einem λQ-Protein an eine QBE-Bindungsstelle angenommen wird (Guo & Roberts, 2004) und für den AT-Mechanismus des verwandten Phagen Φ21 gezeigt wurde (Yin *et al.*, 2019). Im AT-Mechanismus des Phagen Φ21 kontaktieren die beiden an die DNA rekrutierten Q21-Proteine zugleich die pausierte Holo-RNAP. Hierbei bindet ein Q21-Protein an die βFTH der RNAP, wodurch σ^{70}_4 von dieser verdrängt und damit einhergehend die σ^{70}-Bindung an die RNAP geschwächt wird, während das zweite Q21-Protein mit seinem N-Terminus einen Ring (*torus*) am RNA-Ausgangskanal der RNAP ausbildet. Die naszierende RNA wird durch diesen Ring gefädelt, wodurch wahrscheinlich die Bildung von Pausierungs-, bzw. Terminator-HPs im weiteren Verlauf der Transkription inhibiert wird (Shi *et al.*, 2019; Yin *et al.*, 2019). Ein ähnliches Schema der Rekrutierung an den pausierten TEC sowie ein ähnlicher

Mechanismus der Vermittlung der AT wird auch für λQ angenommen. So konnte für λQ sowohl eine Interaktion mit der βFTH (Deighan *et al.*, 2008), als auch mit σ^{70}_4 nachgewiesen werden (Nickels *et al.*, 2002), wobei vermutet wird, dass der σ^{70}_4:βFTH-Komplex durch die Interaktion von λQ mit σ^{70}_4 (Nickels *et al.*, 2002) sowie durch DNA-*scrunching* destabilisiert wird (Nickels *et al.*, 2006), um die Bindung von λQ an die βFTH zu erleichtern (Deighan *et al.*, 2008). Nach der Translokation des TECs auf Position +17 kann es, getrieben durch DNA-*scrunching*, zur Dissoziation von σ^{70} und zum Übergang in die Elongation kommen (Strobel & Roberts, 2015, 2014), wobei λQ nachfolgend als stabiler Bestandteil des TECs AT vermittelt (Deighan & Hochschild, 2007). Sollte σ^{70} nicht dissoziieren kommt es zum *backtracking* des TECs auf Position +16. Das *backtracking* wird durch Spaltung der zurückgelaufenen RNA aufgehoben, wobei GreB stimulierend auf die RNA-Spaltung durch RNAP wirkt. Im Anschluss beginnt der Zyklus von Neuem (Bird *et al.*, 2016; Strobel & Roberts, 2015, 2014).

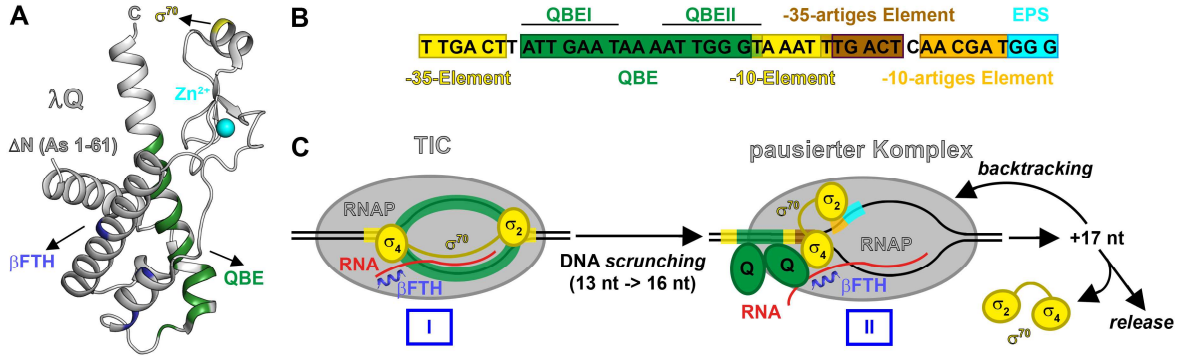

Abbildung 1-7: Die λQ-vermittelte AT des Phagen λ. **(A)** Bänderdarstellung der mittels Röntgenstrukturanalyse bestimmten Struktur einer N-terminal deletierten Variante von λQ (PDB-ID: 4MO1). Farblich hervorgehoben sind die postulierten Bindungsstellen von λQ für das QBE (grün), die βFTH (blau) und σ^{70}_4 (gelb) sowie das durch λQ koordinierte Zn^{2+}-Ion (cyan). **(B)** Die Promotor-Region $p_{R'}$ des Phagen λ. Das QBE (grün) ist zwischen dem -35-Element und dem -10-Element des σ^{70}-Promotors (gelb) eingebettet und die beiden postulierten λQ-Bindungsstellen im QBE (QBEI und QBEII) sind durch schwarze Balken gekennzeichnet. Das auf dem σ^{70}-Promotor folgende -35-artige Element (braun) bildet zusammen mit dem -10-artigen Element (orange) die Promotor-proximale σ^{70}-abhängige Pause, welcher eine EPS (cyan) folgt. **(C)** Im TIC ist das QBE durch die Bindung von σ^{70}_2 an das -10-Element sowie von σ^{70}_4 an das -35-Element verdeckt **(I)**. Nach dem *promoter escape* kommt es durch Bindung von σ^{70}_2 an das -10-artige-Element und σ^{70}_4 an das -35-artige-Element der σ^{70}-abhängigen Pause zu DNA-*scrunching* und an Position +16 zu einer durch die EPS induzierten Pausierung der TECs **(II)**, welche den Rekrutierungsort für λQ an den TEC darstellst. Details siehe Text.

1.7 NMR-Spektroskopie an großen Molekülen

Die Transkription wird durch eine Vielzahl von TFs alleine oder im Verbund mit anderen Komponenten reguliert (siehe Abschnitt 1.4 - 1.6). Hierbei sind Interaktionen von TFs mit der RNAP, mit Nukleinsäuren sowie mit anderen TFs von Bedeutung, für deren Untersuchung die *nuclear magnetic resonance* (NMR)-Spektroskopie eine geeignete Methode darstellt (zusammengefasst in Liu *et al.*, 2016).

Die Isotope ^{1}H, ^{13}C und ^{15}N ermöglichen die strukturelle Charakterisierung von Proteinen mittels NMR-Spektroskopie. So können mittels dreidimensionaler (3D)-[^{1}H,^{13}C,^{15}N]-Korrelationsexperimente NMR-Signale zu den zugehörigen As des Peptidrückgrats des Proteins zugeordnet werden und unter Nutzung des Kern-Overhauser-Effekts räumliche Abstandsinformationen zur *de novo*-Strukturbestimmung gewonnen werden (zusammengefasst in Wüthrich, 1990). Die NMR-Spektroskopie ist jedoch größenlimitiert. So führen Dipol-Dipol-Wechselwirkungen bei zunehmender Molekülgröße zu einer schnelleren Relaxation der Magnetisierung, was zu einer Linienverbreiterung und letztlich zu einem Verlust an Signalintensität im NMR-Spektrum führt. Um diesem Effekt entgegenzuwirken kann das Protein deuteriert werden. Hierdurch können die Wasserstoffatome nicht mehr zu Dipol-Dipol Wechselwirkungen beitragen, womit die Relaxation der Magnetisierung verlangsamt wird (zusammengefasst in Gardner & Kay, 1998). Ebenso ermöglichen Pulsprogramme wie *transverse relaxation optimized spectroscopy* (TROSY) eine höhere Sensitivität und Linienschärfung, um eine höhere Spektren-Qualität bei größeren Molekülen zu erreichen (Pervushin *et al.*, 1997; Salzmann *et al.*, 1998). Das derzeit größte Protein, für welches mittels einer Kombination aus Deuterierung und TROSY-Pulsprogrammen eine Rückgrat-Zuordnung durchgeführt werden konnte, ist die Malatsynthase G (81,4 kDa) (Tugarinov *et al.*, 2002).

Eine Möglichkeit zur Untersuchung größerer NMR-Systeme stellt die [^{1}H,^{13}C]-Markierung endständiger Methylgruppen in einem ansonsten deuterierten und unmarkierten Protein dar. [^{1}H,^{13}C]-markierte endständige As-Methylgruppen sind als NMR-Sonden besonders geeignet, da sich die Signale der dazugehörigen Methylprotonen aufgrund ihrer Entartung aufaddieren, wodurch die Methylgruppen besonders sensitiv sind. Zum anderen weisen endständige Methylgruppen von As eine höhere Dynamik als das Peptidrückgrat auf, wodurch deren Relaxation verlangsamt wird. In der Praxis erfolgt häufig die [^{1}H,^{13}C]-Markierung der endständigen Methylgruppen der As Isoleucin, Leucin und Valin ([I,L,V]-Markierung), da diese in der Proteinsequenz relativ gleichmäßig verteilt sind (zusammengefasst in Tugarinov & Kay, 2005). Im Gegensatz zur [^{1}H,^{13}C,^{15}N]-Markierung ist bei der [I,L,V]-Markierung weder eine Aussage über jede As des Proteins noch eine *de novo*-Strukturbestimmung möglich, sodass sich die Untersuchungen mit [I,L,V]-markierten Proteinen auf Interaktionen und Dynamiken beschränken (zusammengefasst in Wiesner & Sprangers, 2015).

2 Zielsetzung

In der Transkription, dem ersten Schritt der Genexpression, wird die RNA-Synthese basierend auf einer DNA-Matrize durch das Enzym RNAP katalysiert. Die Aktivität der RNAP wird in allen Phasen des Transkriptionszyklus (Initiation, Elongation, Termination) durch eine Vielzahl von TFs reguliert. So sind beispielsweise die TFs der Nus-Klasse (bestehend aus NusA, B, E und G) in der Lage zusammen mit weiteren Komponenten das Überlesen von Terminationssequenzen durch den TEC zu vermitteln, ein Mechanismus der als AT bezeichnet wird und erstmalig für den Phagen λ beschrieben wurde. Hier regulieren zwei AT-Mechanismen, die λN-AT und die λQ-AT, die Replikation des Phagen-Genoms im Wirtsbakterium *E. coli*. Darüber hinaus besitzt *E. coli* selbst einen endogenen AT-Mechanismus. Dieser ist für die Regulation der Expression von ribosomalen RNA-Genen zuständig (*rrn*-AT). Im Gegensatz zur λN-AT ist über die molekulare Basis der *rrn*-AT und λQ-AT nur wenig bekannt. Aus diesem Grund waren diese beiden AT-Mechanismen Forschungsgegenstand dieser Arbeit und ihre strukturellen Grundlagen sollten mittels biochemischer, biophysikalischer und NMR-spektroskopischer Methoden auf molekularer Ebene untersucht werden.

Zur Vermittlung der *rrn*-AT werden die Nus-Faktoren durch eine RNA-Sequenz an die RNAP rekrutiert und versetzen zusammen mit dem Protein S4 den TEC in einen terminations-resistenten Zustand (*rrn*-AT-Komplex). Darüber hinaus wurde auch eine Beteiligung der Inositolmonophosphatase SuhB an der *rrn*-AT postuliert. Um Aufschluss über die Rolle von SuhB in der *rrn*-AT zu erlangen, sollte in dieser Arbeit untersucht werden, ob SuhB in den *rrn*-AT-Komplex integriert wird und welche Interaktionen SuhB mit den an der *rrn*-AT beteiligten Komponenten eingeht, um Ideen über die Funktion von SuhB in der *rrn*-AT zu erhalten.

Im Falle der λQ-AT bindet das AT-Protein λQ an die βFTH der RNAP und erlaubt die Transkription der späten Gene des Phagen λ für Packung und Zelllyse über intrinsische und Rho-abhängige Terminatoren hinweg. Im Rahmen dieser Arbeit sollten das AT-Protein λQ und die βFTH der RNAP NMR-spektroskopisch zugänglich gemacht und ihre Interaktion strukturell charakterisiert werden. Da NusA einen stimulatorischen Effekt auf die λQ-AT besitzt und sich λQ und NusA die βFTH als Bindungsstelle auf der RNAP teilen, sollte außerdem die Rolle von NusA bei der λQ-AT untersucht werden. Dies sollte insgesamt zum besseren Verständnis der zentralen Rolle von NusA in der bakteriellen Transkriptionsregulation beitragen.

3 Synopsis

3.1 Strukturelle Untersuchungen von Proteininteraktionen *via* NMR-Spektroskopie

Im Rahmen dieser Arbeit wurde zur Untersuchung von Interaktionen in AT-Prozessen und deren strukturellen Charakterisierung die NMR-Spektroskopie (siehe Abschnitt 1.7) als primäre Methode angewandt. Die NMR-Spektroskopie ermöglicht im Gegensatz zur Röntgenstrukturanalyse und Kryo-Elektronenmikroskopie Interaktionsuntersuchungen in Lösung und ist auch zur Untersuchung transienter Wechselwirkungen geeignet (zusammengefasst in Liu *et al.*, 2016).

Zur Charakterisierung von Protein:Protein-Interaktionen und Bestimmung der zugehörigen Interaktionsflächen wurden NMR-Titrationen durchgeführt. Hierbei wurde jeweils eines der beiden Proteine ^{15}N-markiert vorgelegt und der unmarkierte Interaktionspartner schrittweise zugegeben. Nach jedem Titrationsschritt wurden NMR-Spektren mittels zweidimensionaler (2D)-[^{1}H,^{15}N] *hetero single quantum coherence* (HSQC)-Experimente (Bodenhausen & Ruben, 1980), bzw. mittels 2D-[^{1}H,^{15}N]-TROSY-Experimente aufgenommen (Pervushin *et al.*, 1997), wobei die TROSY-Experimente zur schnelleren Datenaquisition mit *Band-selective Excitation Short Transient* (BEST)-Experimenten kombiniert wurden (Schanda *et al.*, 2006). In den zugehörigen 2D-[^{1}H,^{15}N]-Korrelationsspektren werden für jedes Wasserstoffatom, welches direkt an ein ^{15}N-Stickstoffatom gebunden ist, die chemischen Verschiebungen beider Kerne miteinander korreliert, sodass sich für jede As aus dem Peptidrückgrat des ^{15}N-markierten Proteins mit Ausnahme von Prolin ein Signal ergibt. Da die chemische Verschiebung des Signals einer As durch dessen chemische Umgebung bestimmt wird und die Bindung eines Interaktionspartners an das ^{15}N-markierte Protein zu einer Änderung der chemischen Umgebung der von der Interaktion betroffenen As führt, ändert sich dementsprechend auch die chemische Verschiebung des zu dieser As zugehörigen Signals. Dieser Effekt bildet die Grundlage für strukturelle Interaktionsuntersuchungen mittels NMR-Spektroskopie und kann sich abhängig vom chemischen Austausch im 2D-NMR-Spektrum auf unterschiedliche Arten äußern. Im Falle des „schnellen chemischen Austauschs“ ist die chemische Austauschrate zwischen freiem und komplexiertem Zustand höher als der Frequenzunterschied der zu diesen beiden Zuständen zugehörigen Signale der As, sodass sich ein gemitteltes Signal der beiden Zustände ergibt. Das gemittelte Signal „wandert“ während der NMR-Titration von der chemischen Verschiebung des Signals im freien Zustand zur chemischen Verschiebung des Signals im komplexierten Zustand, wobei die Signalposition proportional zum Verhältnis zwischen freiem und komplexiertem Zustand des ^{15}N-markierten Proteins ist. Ist die chemische Austauschrate von freiem zu komplexiertem Zustand kleiner als der Frequenzunterschied der zu diesen beiden Zuständen zugehörigen Signale

der As, spricht man vom „langsamen chemischen Austausch“. Hierbei kommt es zu einem Intensitätsverlust des zu dem freien Zustand zugehörigen Signals, bei simultanem Intensitätsgewinn des zu dem komplexierten Zustand zugehörigen Signals, wobei die Intensitätsverhältnisse der beiden Signale zueinander proportional zum Verhältnis zwischen freiem und komplexiertem Zustand des ^{15}N-markierten Proteins ist. Zu einem Signalintensitätsverlust des zum freien Zustand zugehörigen Signals während der NMR-Titration kommt es auch beim „intermediären chemischen Austausch“. Hier ist die chemische Austauschrate zwischen freiem und komplexiertem Zustand in derselben Größenordnung wie der Frequenzunterschied der zu diesen beiden Zuständen zugehörigen Signale der As. Dies führt während der NMR-Titration zu einer Linienverbreiterung und damit zu einem Intensitätsverlust des zu dem freien Zustand zugehörigen Signals. In der Nähe des Endpunktes der Titration kommt es zu einer Linienverschmälerung und damit Intensitätszunahme des zu dem komplexierten Zustand zugehörigen Signals (zusammengefasst in Cavanagh *et al*., 1996). Im Falle des schnellen chemischen Austausches erfolgte die Bestimmung der Bindungsfläche auf dem ^{15}N-markierten Protein über die Berechnung der normierten Änderung der chemischen Verschiebung ($\Delta\delta_{norm}$) der einzelnen As. Befand sich das NMR-System im langsamen oder intermediären chemischen Austausch, erfolgte eine Analyse der Rest-Signalintensitäten der einzelnen As zur Ermittlung der Bindungsfläche auf dem ^{15}N-markierten Protein (Details zum Vorgehen: siehe Einzelarbeiten A-C).

Zur Untersuchung von Protein:Protein-Interaktionen, bei denen die Komplexgröße keine quantitative Analyse *via* 2D-[^{1}H,^{15}N]-Korrelationsspektren erlaubten, wurden NMR-Titrationen durchgeführt, in welchen das kleinere Protein ^{15}N-markiert vorgelegt, der größere Interaktionspartner unmarkiert hinzugegeben und eindimensionale (1D)-[^{1}H,^{15}N]-HSQC-Experimente aufgenommen wurden. Im Falle einer Interaktion führt die zunehmende Molekülgröße aufgrund der Komplexbildung zu einer schnelleren Relaxation der Magnetisierung des ^{15}N-markierten Proteins. Dies äußert sich in dem zugehörigen 1D-[^{1}H,^{15}N]-HSQC-Spektrum der Amidprotonen in einem Signalintensitätsverlust. Die strukturelle Charakterisierung dieser Protein:Protein-Interaktionen erfolgte einerseits, indem Einzeldomänen, bzw. Teile des Gesamtproteins, welche für 2D-[^{1}H,^{15}N]-Korrelationsexperimente zugänglich sind, eingesetzt wurden. Zum anderen wurden Proteine *via* [I,L,V]-Markierung sowie unter Nutzung von 2D-[^{1}H,^{13}C]-Methyl-TROSY-Experimenten für NMR-basierte Interaktionsstudien in makromolekularen Systemen zugänglich gemacht, wobei die Auswertung der zugehörigen 2D-[^{1}H,^{13}C]-Methyl-TROSY-Spektren zur Bestimmung der Interaktionsfläche auf dem [I,L,V]-markierten Protein analog zur Auswertung von 2D-[^{1}H,^{15}N]-Korrelationsspektren erfolgte.

3.2 Ribosomale Antitermination in *Escherichia coli*

Die Transkriptionsregulation der für rRNAs kodierenden *rrn*-Operons in *E. coli* erfolgt unter anderem durch Rho-abhängige Terminatoren in den Leit- und Trennsequenzen der Operons (zusammengefasst in Jin *et al.*, 2012). Vermittelt durch eine *rrn*-AT-Sequenz, bestehend aus den drei Elementen *boxA*, *boxB* und *boxC* (Li *et al.*, 1984), werden die Nus-Faktoren A, B, E und G an den TEC rekrutiert (Squires *et al.*, 1993) und ermöglichen im Zusammenspiel mit dem ribosomalen Protein S4 (Torres *et al.*, 2001) das Überlesen Rho-abhängiger Terminatoren in einem als *rrn*-AT bezeichneten Prozess (siehe Abschnitt 1.5). Jedoch sind weder die Nus-Faktoren alleine (Squires *et al.*, 1993) noch zusammen mit S4 in der Lage die volle *rrn*-AT-Effizienz zu gewährleisten (Torres *et al.*, 2001). Gen-Reporter-Tests haben gezeigt, dass *in vivo* ein zusätzlicher Faktor, die Inositolmonophosphatase SuhB, an der *rrn*-AT beteiligt ist, wobei anhand von Chromatin-Immunpräzipitation-Analysen eine Assoziation von SuhB in NusB- und *boxA*-abhängigerweise an den TEC vorgeschlagen wurde (Singh *et al.*, 2016). Im Rahmen der Einzelarbeit A wurde untersucht, ob SuhB stabil in den *rrn*-AT-Komplex integriert wird und welche Interaktionen SuhB mit den an der *rrn*-AT beteiligten Komponenten eingeht.

3.2.1 SuhB ist Teil des ribosomalen Antiterminations-Komplexes

Mittels analytischer Gelfiltration wurde untersucht, ob SuhB in den an einer *rrn*-AT-Sequenz pausierten *rrn*-AT-Komplex integriert wird. Die Analyse der Eluat-Fraktionen auf Proteinebene erfolgte mittels Natriumdodecylsulfat-Polyacrylamid-Gelelektrophorese (SDS-PAGE) und Coomassie-Färbung sowie mittels *urea*-PAGE und Toluidin-Färbung auf RNA-Ebene. Zur Generierung des an einer *rrn*-AT-Sequenz pausierten TECs wurde ein Nukleinsäure-Gerüst mit der *rrnG*-RNA (Einzelarbeit A, Abb. S1A), der *rrn*-AT-Sequenz für die Assemblierung des *rrn*-AT-Komplexes im *rrnG*-Operon, verwendet. Für NusE wurde aus Löslichkeits- und Stabilitätsgründen eine Deletionsvariante, in welcher die Ribosomenbindungsschleife durch ein Serin ersetzt wurde ($NusE^{\Delta}$), im Komplex mit NusB (NusB:$NusE^{\Delta}$) eingesetzt (Luo *et al.*, 2008). Bei dem analytischen Gelfiltrationslauf von SuhB zusammen mit dem *rrn*-AT-Komplex, bestehend aus dem TEC sowie NusA, NusB:$NusE^{\Delta}$ und NusG co-eluierten alle Komponenten, einschließlich SuhB (Abb. 3-1A). Folglich wird SuhB in den *rrn*-AT-Komplex integriert. Auch in Anwesenheit von S4 (Einzelarbeit A, Abb. 1F) co-eluierte SuhB mit allen anderen Faktoren des *rrn*-AT-Komplexes, einschließlich S4. Es kann demnach zeitgleich auch eine Integration von S4 und SuhB in den *rrn*-AT-Komplex stattfinden. Zur Untersuchung der zugrundeliegenden binären Interaktionen wurden analytische Gelfiltrationsläufe von SuhB mit den Einzelkomponenten des *rrn*-AT-Komplexes durchgeführt. Hierbei co-eluierte SuhB mit der *rrnG*-RNA (Abb. 3-1B),

nicht jedoch mit einer *random* RNA (Abb. 3-1C), sodass eine spezifische Interaktion von SuhB mit der *rrnG*-RNA angenommen werden kann. Dieses Ergebnis ist in Übereinstimmung mit der Hypothese, dass SuhB in *boxA*-abhängigerweise an den TEC rekrutiert wird (Singh *et al.*, 2016). Ebenso co-eluierte SuhB mit NusA (Abb. 3-1D), nicht jedoch mit einer C-terminal deletierten Variante von NusA (NusA$^{\Delta AR2}$) (Abb. 3-1E). Daher liegt eine Interaktion von SuhB mit NusA über dessen AR2-Domäne nahe. In einem weiteren analytischen Gelfiltrationslauf des *rrn*-AT-Komplexes mit SuhB und NusA$^{\Delta AR2}$ co-eluierte SuhB mitsamt aller anderen Faktoren (Abb. 3-1F), sodass angenommen werden kann, dass die Interaktion zwischen SuhB und NusA-AR2 nicht essentiell für die Integration von SuhB in den *rrn*-AT-Komplex ist.

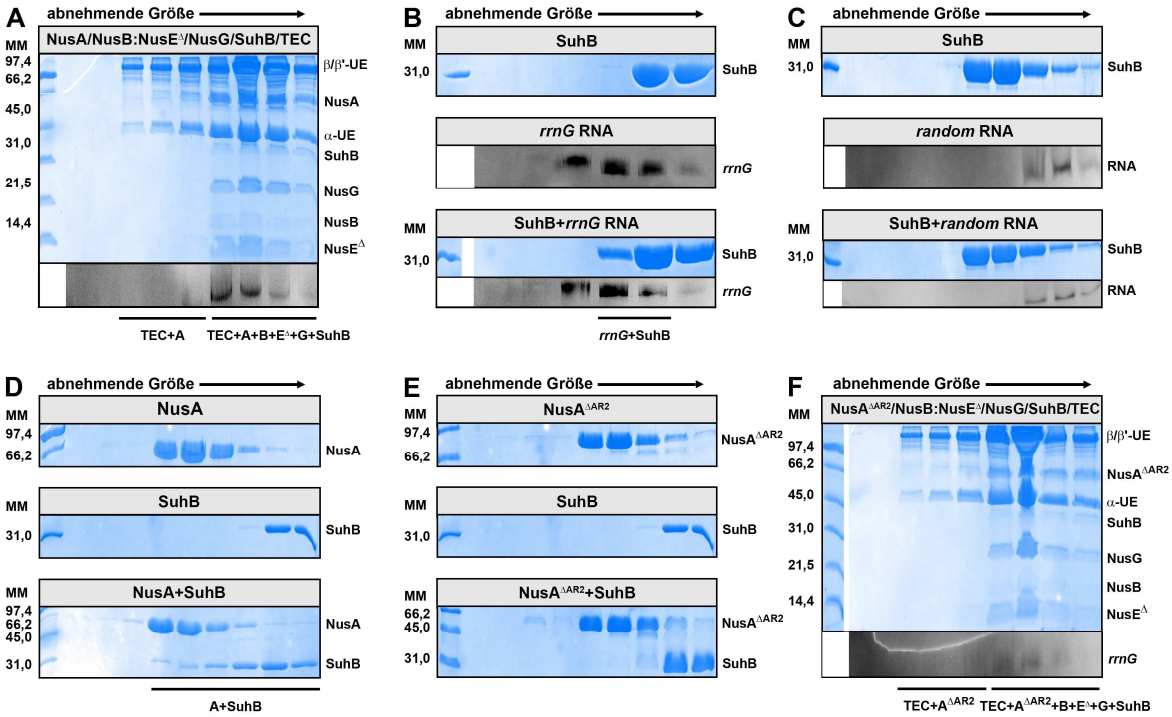

Abbildung 3-1: Interaktionsstudien von SuhB mit den Komponenten des *rrn*-AT-Komplexes. Mittels SDS-PAGE und Coomassie-Färbung (Proteine, blau) sowie mittels *urea*-PAGE und Toluidin-Färbung (RNA, grau) erfolgte die Analyse der analytischen Gelfiltrationsläufe auf Interaktionen zwischen **(A)** SuhB, NusA, NusB:NusE$^{\Delta}$, NusG und dem an der *rrnG*-RNA pausierten TEC, **(B)** SuhB und *rrnG*-RNA, **(C)** SuhB und *random* RNA, **(D)** SuhB und NusA, **(E)** SuhB und NusA$^{\Delta AR2}$, **(F)** SuhB, NusA$^{\Delta AR2}$, NusB:NusE$^{\Delta}$, NusG und dem an der *rrnG*-RNA pausierten TEC. In den Boxen über den Gelen sind die Einzelkomponenten der im jeweiligen Gelfiltrationslauf aufgetragenen Proben angegeben. Links ist jeweils die Bahn des Markers (SDS-PAGE *Standards Low Range*, BioRad) gezeigt und die zur jeweiligen Bande des Markers zugehörige Molekülmasse (MM) angegeben. Rechts sind die zu den jeweiligen Banden gehörenden Proteine und unter den Gelen die jeweils gebildeten Komplexe angegeben. Die Abbildung wurde aus Dudenhoeffer *et al.*, 2019 (Abb.1 und Abb. S1) entnommen und abgeändert.

Komplementär zu den analytischen Gelfiltrationsexperimenten wurden NMR-Titrationen von SuhB mit den einzelnen Proteinkomponenten des *rrn*-AT-Komplexes durchgeführt, wobei die NMR-Titrationen von SuhB mit den Nus-Faktoren (Einzelarbeit A, Abb. S2A-D) die Ergebnisse der analytischen Gelfiltrationsläufe bestätigten. So wurde nur eine Interaktion zwischen SuhB

und NusA gesehen, welche nachfolgend charakterisiert wurde (siehe Abschnitt 3.2.2). Auch die NMR-Titration von SuhB mit RNAP (Einzelarbeit A, Abb. S7A) weist auf eine Interaktion zwischen beiden Proteinen hin. Eine Wechselwirkung zwischen SuhB und der RNAP wurde bereits zuvor gezeigt (Wang *et al.*, 2007), konnte jedoch *via* analytischer Gelfiltration (Einzelarbeit A, Abb. S1F) nicht nachgewiesen werden. Daher ist anzunehmen, dass es sich um eine schwache Wechselwirkung zwischen SuhB und der RNAP handelt, wobei NMR-Titrationen von SuhB mit den RNAP-Domänen (Einzelarbeit A, Abb. S7B-E) darauf hindeuten, dass die Interaktion zwischen SuhB und der RNAP über die β-UE und β´-UE der RNAP vermittelt wird.

3.2.2 SuhB interagiert mit NusA-AR2 und hebt die Autoinhibition von NusA auf

Analytische Gelfiltrationsläufe sowie NMR-Titrationen haben gezeigt, dass SuhB mit NusA als einzigem Nus-Faktor interagiert. Zur Bestimmung der mit SuhB interagierenden Domäne wurden NMR-Titrationen von SuhB mit ^{15}N-NusA-NTD (Einzelarbeit A, Abb. S2E), ^{2}H,^{15}N-NusA-SKK (Einzelarbeit A, Abb. S2F) sowie ^{15}N-NusA-AR1-AR2 (Einzelarbeit A, Abb. 2A,B) durchgeführt. Hierbei konnte nur für ^{15}N-NusA-AR1-AR2 in Gegenwart von SuhB eine signifikante Änderung im zugehörigen NMR-Spektrum, ein Verlust an Signalintensität, beobachtet werden, welcher die Bestimmung der SuhB-Bindungsfläche auf ^{15}N-NusA-AR1-AR2 erlaubte. Hierbei zeigte sich, dass trotz der hohen Homologie in Topologie und Ladungsverteilung von NusA-AR1 und NusA-AR2 (Eisenmann *et al.*, 2005) nur Signale der NusA-AR2-Domäne von der SuhB-Bindung betroffen sind (Einzelarbeit A, Abb. 2C). Daher kann in Übereinstimmung mit den Ergebnissen der analytischen Gelfiltrationsläufe von einer spezifischen Interaktion von SuhB mit NusA *via* der AR2-Domäne ausgegangen werden. Die Bindungsfläche von NusA-AR2 auf SuhB konnte nicht bestimmt werden, da trotz Nutzung von TROSY-Pulssequenzen eine ^{2}H,^{13}C,^{15}N-markierte Probe von SuhB ein zu geringes Signal-Rausch-Verhältnis in den zugehörigen 3D-NMR-Spektren aufwies, um eine Zuordnung der [^{1}H,^{15}N]-NMR-Signale zu den zugehörigen As von dessen Peptidrückgrat durchzuführen. Daher wurde basierend auf der SuhB-Bindungsfläche auf NusA-AR2 mittels HDOCK (Yan *et al.*, 2017) ein Modell der Bindung von SuhB an NusA-AR2 erstellt (Abb. 3-2). Die von der SuhB-Bindung betroffenen As auf NusA-AR2 sind überwiegend in der aziden Helix α5* lokalisiert. Diese kontaktiert im Modell des SuhB:NusA-AR2-Komplexes die positiv geladene Oberfläche von SuhB, während die beiden der Helix α5* folgenden C-terminalen As Trp490 und Phe491 gegen den hydrophoben C-Terminus der Helix α6 von SuhB packen. Die zugehörige Dissoziationskonstante (K_D) konnte mittels Fluoreszenz-Anisotropie-Titrationen von SuhB mit einer Fluorescein-markierten Cystein-Variante von NusA-AR2 (NusA-AR2^{D443C}) auf 83±4 µM (Einzelarbeit A, S3C) bestimmt werden (Details: siehe Einzelarbeit A).

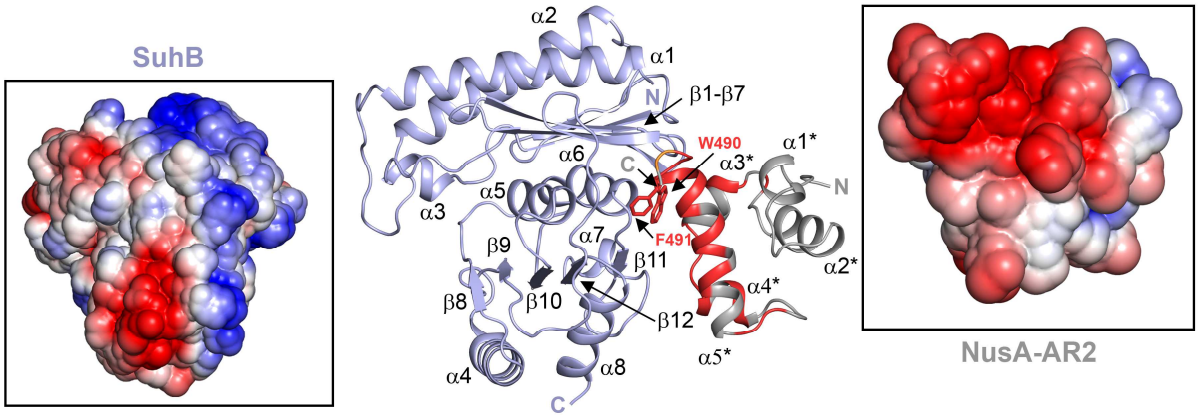

Abbildung 3-2: Interaktion von SuhB mit NusA-AR2. Modell des SuhB:NusA-AR2-Komplexes. NusA-AR2 (PDB-ID: 1WCN; grau) und SuhB (PDB-ID: 2QFL; hellblau) sind jeweils in Bänderdarstellung wiedergegeben. Sekundärstrukurelemente und Termini sind beschriftet. Die auf NusA-AR2 betroffenen Reste der Titration von ^{15}N-NusA-AR1-AR2 mit SuhB sind farblich hervorgehoben (moderat betroffen: orange; stark betroffen: rot). Für die beiden stark betroffenen C-terminalen As Trp490 und Phe491 ist die Seitenkette gezeigt. Die beiden Kästen zeigen das elektrostatische Oberflächenpotential von SuhB (links), bzw. NusA-AR2 (rechts) von -3 kT/e$^-$ (dunkelrot) bis +3 kT/e$^-$ (dunkelblau). Die Abbildung wurde aus Dudenhoeffer *et al.*, 2019 (Abb. 2 und Abb. S3) entnommen und abgeändert.

Die SuhB-Bindungsstelle auf NusA-AR2 überlappt mit der für RNAPαCTD (Schweimer *et al.*, 2011) und NusG-NTD (Strauß *et al.*, 2016) bestimmten Bindungsstelle auf NusA-AR2. In allen Fällen sind auf Seiten von NusA-AR2 die Helix α5* und die beiden C-terminalen As Trp490 und Phe491 von der Bindung des entsprechenden Partners betroffen. Durch NMR-basierte Verdrängungsexperimente wurde gezeigt, dass sich die Bindungsstellen von NusG-NTD und RNAPαCTD auf NusA-AR2 überschneiden (Strauß *et al.*, 2016). Um zu überprüfen, ob auch die Bindungsstellen von RNAPαCTD und SuhB auf NusA-AR2 überlappen wurden NMR-basierte Verdrängungsexperimente durchgeführt (Einzelarbeit A, Abb. 3). Hierbei zeigte sich, dass sich SuhB und RNAPαCTD durch einen Überschuss des jeweils anderen Proteins von NusA-AR2 verdrängen lassen, sodass davon ausgegangen werden kann, dass sich die Bindungsstellen von SuhB und RNAPαCTD auf NusA-AR2 überschneiden.

Die AR2-Domäne von NusA fungiert als autoinhibitorisches Element und verhindert durch Bindung an NusA-SKK eine RNA-Bindung dieser (Schweimer *et al.*, 2011). NMR-basierte Verdrängungsexperimente haben gezeigt, dass die RNAPαCTD in der Lage ist NusA-AR2 von NusA-SKK zu verdrängen, sodass die Autoinhibition von NusA aufgehoben wird (Schweimer *et al.*, 2011). Zur Überprüfung, ob auch NusG-NTD und SuhB in der Lage sind NusA-AR2 von NusA-SKK zu verdrängen, wurden NMR-Titrationen von ^{2}H,^{15}N-NusA-SKK mit NusA-AR2 durchgeführt (Abb. 3-3A) und nachfolgend NusG-NTD (Abb. 3-3B), bzw. SuhB (Abb. 3-3C) hinzugegeben. Wie es bereits für die RNAPαCTD beobachtet werden konnte (Schweimer *et al.*, 2011), zeigte sich auch in Anwesenheit von SuhB bzw. NusG-NTD eine Verdrängung der NusA-AR2 von ^{2}H,^{15}N-NusA-SKK.

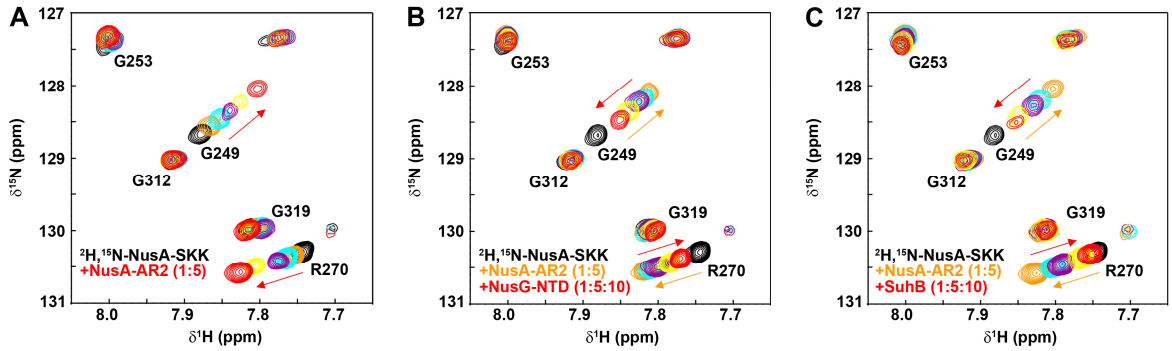

Abbildung 3-3: NusG-NTD und SuhB verdrängen NusA-AR2 von NusA-SKK. (A) Ausschnitt aus dem 2D-[^{1}H,^{15}N]-BEST-TROSY-Spektrum von ^{2}H,^{15}N-NusA-SKK in Abwesenheit (schwarz) und in Anwesenheit von NusA-AR2 (molare Verhältnisse 1:0,5, orange; 1:1, cyan; 1:2, lila; 1:3, gelb; 1:5, rot). Zugeordnete Signale sind beschriftet und die Pfeile zeigen die Richtung der Änderung der chemischen Verschiebung einzelner Signale durch Zugabe von NusA-AR2 (rot) an. **(B,C)** Ausschnitt aus den 2D-[^{1}H,^{15}N]-BEST-TROSY-Spektren des Komplexes von ^{2}H,^{15}N-NusA-SKK (1:0, schwarz) mit NusA-AR2 (1:5, orange) in Anwesenheit steigender Konzentrationen von NusG-NTD (B), bzw. SuhB (C) (molare Verhältnisse 1:5:1, cyan; 1:5:2, lila; 1:5:5, gelb; 1:5:10, rot). Zugeordnete Signale sind beschriftet und die Pfeile zeigen die Richtung der Änderung der chemischen Verschiebung der einzelnen Signale durch Zugabe von NusA-AR2 (orange) sowie von NusG-NTD (rot) bzw. SuhB (rot) an. Die zu den gezeigten Ausschnitten zugehörigen NMR-Spektren sind in Einzelarbeit A, Abb. 4 zu finden. Die Abbildung wurde aus Dudenhoeffer *et al.*, 2019 (Abb. 4) entnommen und abgeändert.

Da NusA-AR2 und NusA-SKK intramolekular miteinander verknüpft sind, ist eine höhere lokale Konzentration und damit auch eine höhere Interaktionswahrscheinlichkeit der beiden Domänen im Volllängenprotein zu erwarten. Daher wurde die Aufhebung der Autoinhibition auch an dem NusA Volllängenprotein untersucht. Hierfür wurde NusA (54,9 kDa) [I,L,V]-markiert und 2D-[^{1}H,^{13}C]-Methyl-TROSY-Titrationen mit SuhB (Einzelarbeit A, Abb. 5) sowie NusG-NTD (Einzelarbeit A, Abb. S5) durchgeführt. Eine quantitative Auswertung der NMR-Titrationen zeigte, dass sowohl durch die Zugabe von SuhB als auch von NusG-NTD, NMR-Sonden der SKK-Einheit sowie von NusA-AR2 betroffen waren, sodass in Übereinstimmung mit den NMR-basierten Verdrängungsexperimenten eine Aufhebung der Autoinhibition von NusA durch SuhB und NusG-NTD angenommen werden kann.

Für SuhB wurde eine NusB- und *boxA*-abhängige Rekrutierung an den TEC sowie eine anschließende Mitwirkung an der *rrn*-AT postuliert (Singh *et al.*, 2016). Die Ergebnisse der Einzelarbeit A zeigen, dass SuhB mit NusA, der RNAP sowie der *rrnG*-RNA interagiert und stabil in den *rrn*-AT-Komplex integriert wird. Während die Interaktion von SuhB mit NusA über deren AR2-Domäne vermittelt wird und zur Aufhebung der Autoinhibition von NusA führt, konnte für NusB keine Interaktion mit SuhB gesehen werden, sodass von einer indirekten Abhängigkeit ausgegangen werden kann. Die SuhB:NusA-AR2-Interaktion ist nicht essentiell für die Integration von SuhB in den *rrn*-AT-Komplex, dennoch könnte NusA-AR2 als Bindungsplattform zur Rekrutierung von SuhB an den *rrn*-AT-Komplex dienen und die SuhB:NusA-AR2-Interaktion könnte nachfolgend zur Assemblierung bzw. Stabilisierung des *rrn*-AT-Komplexes beitragen.

NusA wird beim Übergang in die Elongation an den TEC rekrutiert (Mooney *et al.*, 2009a), wobei durch Bindung von NusA-AR2 an die RNAPαCTD die Autoinhibition von NusA aufgehoben wird (Schweimer *et al.*, 2011). Hierdurch kann eine Bindung von NusA-SKK an den *spacer* zwischen *boxA* und *boxB* der *rrn*-AT-Sequenz erfolgen (Prasch *et al.*, 2009), welche den Zugang für das NusB:NusE-Heterodimer zu *boxA* (Greive *et al.*, 2005; Nodwell & Greenblatt, 1993) blockieren bzw. erschweren könnte (Einzelarbeit A, Abb. 6A). SuhB könnte durch Interaktionen mit NusA-AR2, der RNAP und der *rrn*-AT-Sequenz die NusA-SKK:RNA-Bindung derart beeinflussen, dass die *boxA*-Bindung von NusA-SKK aufgehoben und die Rekrutierung des NusB:NusE-Heterodimers an *boxA* zur Assemblierung des *rrn*-AT-Komplexes erleichtert bzw. erst ermöglicht wird. Ebenso könnte SuhB durch Auflösung der Bindung von NusA-AR2 an die RNAPαCTD auch eine Repositionierung von NusA in eine AT-stimulierende Konformation induzieren bzw. durch Inhibition einer NusA-AR2:RNAPαCTD-Interaktion eine AT-stimulierende NusA-Konformation im *rrn*-AT-Komplex stabilisieren (Einzelarbeit A, Abb. 6B).

Parallel zu dieser Arbeit wurde eine mittels Röntgenstrukturanalyse bestimmte Struktur des SuhB:NusA-AR2-Komplexes (PDB-ID: 6IB) von Huang *et al.* publiziert, in welcher SuhB, wie in dieser Arbeit gezeigt, von NusA-AR2 über deren beiden As Trp490 und Phe491 kontaktiert wird. In Übereinstimmung mit den Ergebnissen der Einzelarbeit A konnte auch eine Interaktion von SuhB mit der *rrnG*-RNA gezeigt werden. Weiterführende Studien von Huang *et al.* legen eine Bindung von SuhB an den *spacer* zwischen *boxA* und *boxB* und/oder der *boxC* der *rrn*-AT-Sequenz nahe und zeigen, dass diese Interaktion essentiell für die Integration von SuhB in den *rrn*-AT-Komplex ist. Des Weiteren wurde auch gezeigt, dass SuhB, wie in dieser Arbeit postuliert, die Integration des NusB:NusE-Heterodimers in den *rrn*-AT-Komplex ermöglicht und für das Überlesen Rho-abhängiger Terminatoren durch den *rrn*-AT-Komplex benötigt wird, wobei der AT-Effekt von SuhB nur im Zusammenspiel mit den Nus-Faktoren vermittelt wird und hierfür die SuhB:NusA-AR2-Interaktion von Bedeutung ist (Huang *et al.* 2019).

3.3 λQ-vermittelte Antitermination des Phagen λ

Neben der *rrn*-AT in *E. coli* sind die Nus-Faktoren auch an der λN-AT (siehe Abschnitt 1.6.1) und der λQ-AT (siehe Abschnitt 1.6.2) des Phagen λ beteiligt, welche der Replikation seines Genoms im Wirtsbakterium *E. coli* dienen. Im Falle der λQ-AT wird das AT-Protein λQ in der Promotorregion $p_{R'}$ des Phagen-Genoms durch das Zusammenspiel des QBEs (Guo & Roberts, 2004; Yarnell & Roberts, 1992) mit einer σ^{70}-abhängigen Pause (Nickels *et al.*, 2002; Perdue & Roberts, 2010; Ring *et al.*, 1996) und einer EP (Bird *et al.*, 2016; Strobel & Roberts, 2015) an

den TEC rekrutiert. Nachfolgend ermöglicht λQ die Transkription der „späten Gene“ des Phagen λ für Packung und Zelllyse durch den TEC (Deighan & Hochschild, 2007) über intrinsische und Rho-abhängige Terminatoren hinweg (Luk & Szybalski, 1983). Mutagenese-Studien haben gezeigt, dass der N-Terminus von λQ zu dessen AT-Effizienz beiträgt (Deighan & Hochschild, 2007). Zum anderen legen *in-vitro* Transkriptionsassays auch einen AT-Effizienz steigernden Effekt von NusA auf die λQ-AT nahe (Grayhack *et al.*, 1985), wobei weder etwas über eine Wechselwirkung von λQ mit NusA noch über eine Beteiligung der anderen Nus-Faktoren an der λQ-AT bekannt ist. Im Rahmen der Einzelarbeit B wurden die [^{1}H,^{15}N]-NMR-Signale von λQ zu den zugehörigen As des Peptidrückgrats zugeordnet und mittels NMR-Titrationen untersucht, welche Interaktionen λQ mit den Nus-Faktoren eingeht.

Für λQ war trotz hoher Löslichkeit und ausreichender Langzeitstabilität auch nach Deuterierung und unter Nutzung von TROSY-Pulssequenzen das Signal-Rausch-Verhältnis in den zugehörigen 3D-NMR-Spektren zu niedrig, um eine Zuordnung der [^{1}H,^{15}N]-NMR-Signale zu den zugehörigen As des Peptidrückgrats von ^{2}H,^{13}C,^{15}N-λQ durchzuführen. Daher wurde eine um 36 As N-terminal deletierte ^{2}H,^{13}C,^{15}N-markierte Variante von λQ (λQ$^{\Delta 36}$) hergestellt. Die 3D-NMR-Spektren von ^{2}H,^{13}C,^{15}N-λQ$^{\Delta 36}$ wiesen ein ausreichend hohes Signal-Rausch-Verhältnis auf, sodass eine Zuordnung der [^{1}H,^{15}N]-NMR-Signale zu den zugehörigen As von dessen Peptidrückgrat möglich war (*Biological Magnetic Resonance Data Bank* (BMRB)-ID: 28043). Der Vergleich der [^{1}H,^{15}N]-BEST-TROSY-Spektren von λQ mit λQ$^{\Delta 36}$ (siehe Einzelarbeit B, Abb. 1B) zeigt, dass die Signale der 36 N-terminalen As von λQ allesamt chemische Verschiebungen zwischen 7,5 ppm und 8,5 ppm in der ^{1}H-Dimension aufweisen, wie sie typisch für As in unstrukturierten Bereichen sind. Zur weiteren Charakterisierung von λQ$^{\Delta 36}$ wurde mittels der chemischen Verschiebungen für C_α und C_O der *chemical shift index* (CSI) berechnet (Einzelarbeit B, Abb. 1C; Wishart *et al.*, 1992; Wishart & Sykes, 1994), welcher Auskunft über die Sekundärstruktur gibt. Dieser zeigt, dass definierte Sekundärstrukturen von λQ$^{\Delta 36}$ erst ab As 66 beginnen und diese mit den Sekundärstrukturen in der mittels Röntgenstrukturanalyse bestimmten Struktur einer um 38 As N-terminal deletierten Variante von λQ (Vorobiev *et al.*, 2014) übereinstimmen. Daher kann davon ausgegangen werden, dass der N-Terminus von λQ, wie postuliert (Vorobiev *et al.*, 2014), in Lösung unstrukturiert vorliegt.

Zur Untersuchung von etwaigen Interaktionen von λQ mit den Nus-Faktoren wurden NMR-Titrationen von ^{15}N-λQ mit NusA, NusB, NusE$^{\Delta}$:NusB und NusG durchgeführt (Einzelarbeit B, Abb. S3), wobei nur für NusA eine Interaktion mit ^{15}N-λQ gesehen wurde; in Übereinstimmung mit Ergebnissen, dass NusA die AT-Effizienz von λQ stimuliert (Grayhack *et al.*, 1985).

3.3.1 λQ interagiert mit NusA-AR2 und hebt die Autoinhibition von NusA auf

Wie NMR-Titrationen gezeigt haben, interagiert λQ mit NusA als einzigem Nus-Faktor. Zur weitergehenden strukturellen Charakterisierung dieser Interaktion erfolgten NMR-Titrationen von λQ mit NusA-NTD (Einzelarbeit B, Abb. 2A,B und Abb. S4A,B), NusA-SKK (Einzelarbeit B, Abb. S7A,B), NusA-AR1 (Einzelarbeit B, Abb. S7C,D) sowie NusA-AR2 (Einzelarbeit B, Abb. 3A,B und Abb. S8A,B). Hierbei zeigte sich, dass λQ sowohl mit NusA-NTD (siehe Abschnitt 3.3.2) als auch mit NusA-AR2 spezifisch interagiert. Für die Interaktion von λQ mit NusA-AR2 wurde durch quantitative Auswertung der zugehörigen NMR-Titrationen die Bindungsflächen auf beiden Proteinen bestimmt. Die von der NusA-AR2-Bindung auf ^{15}N-λQ betroffenen Reste finden sich vorwiegend in den Helices α1, α3 und α5, während von der λQ-Bindung auf NusA-AR2 dessen Helix α5* sowie der C-Terminus betroffen sind (Abb. 3-4). In dem anhand der ermittelten Bindungsflächen erstellten HADDOCK-Modell (Dominguez *et al.*, 2003) des NusA-AR2:λQ-Komplexes packt die Helix α5* von NusA-AR2 gegen die Helix α3 und α5 von λQ, wobei die beiden C-terminalen As Trp490 und Phe491 von NusA-AR2 einen zentralen Bestandteil der Interaktionsfläche darstellen (Abb. 3-4). Analog zur Bestimmung des K_D-Werts der SuhB:NusA-AR2-Interaktion wurde mittels Fluoreszenz-Anisotropie-Titrationen von λQ mit Fluorescein-markierten NusA-AR2^{D443C} (Einzelarbeit B, Abb. S8F) der K_D-Wert der λQ:NusA-AR2-Interaktion auf 268±17 µM bestimmt (Details: siehe Einzelarbeit B). Des Weiteren zeigte eine NMR-Titration von ^{15}N-NusA-AR2 mit λQ$^{\Delta 36}$ (Einzelarbeit B, Abb. S8G-I), im Vergleich zu λQ, keine Unterschiede in der Bindungsfläche auf ^{15}N-NusA-AR2, sodass angenommen werden kann, dass der N-Terminus von λQ keinen Einfluss auf die Interaktion mit NusA-AR2 hat.

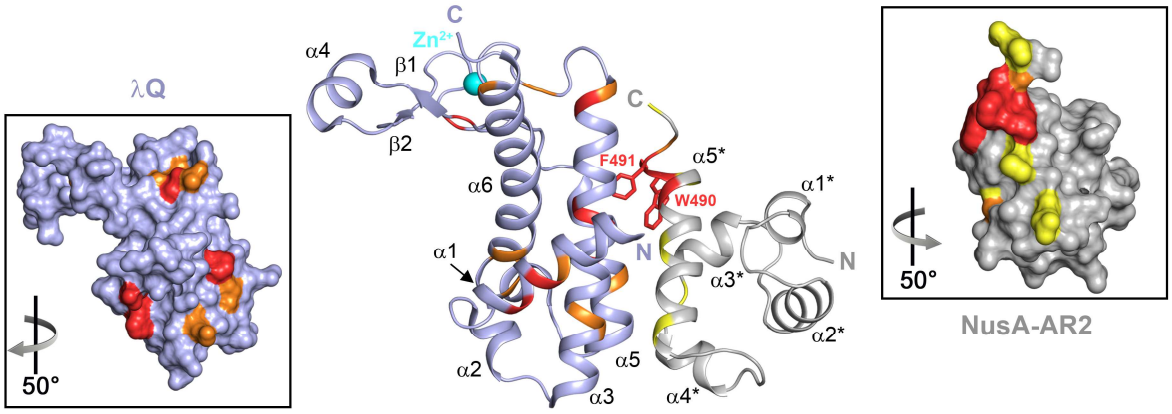

Abbildung 3-4: Interaktion von λQ mit NusA-AR2. Modell des λQ:NusA-AR2-Komplexes. NusA-AR2 (PDB-ID: 1WCN; grau) und λQ (PDB-ID: 4MO1; hellblau) sind jeweils in Bänderdarstellung wiedergegeben. Betroffene Reste der Interaktion sind farblich hervorgehoben (λQ: moderat betroffen: orange; stark betroffen: rot; NusA-AR2: leicht betroffen: gelb; moderat betroffen: orange; stark betroffen: rot). Für Trp490 und Phe491 ist die Seitenkette gezeigt. Sekundärstrukturelemente und Termini sind beschriftet und das Zn^{2+}-Ion ist als cyane Kugel dargestellt. Die Kästen links (λQ), bzw. rechts (NusA-AR2) zeigen die Oberflächendarstellung der beiden Proteine (Farbschema wie im Komplex). Die Abbildung wurde aus Dudenhoeffer *et al.*, 2020 (Abb. 3) entnommen und abgeändert.

Die Bindungsfläche von λQ auf NusA-AR2 beinhaltet wie auch für die Interaktion von NusA-AR2 mit SuhB (Abb. 3-2), RNAPαCTD (Schweimer *et al.*, 2011) und NusG-NTD (Strauß *et al.*, 2016) gesehen die C-terminale Helix α5* und die beiden As Trp490 und Phe491. NMR-basierte Verdrängungsexperimente haben gezeigt, dass die Bindungsfläche von NusG-NTD (Strauß *et al.*, 2016) bzw. SuhB (Einzelarbeit A, Abb. 3) auf NusA-AR2 mit der Bindungsfläche von RNAPαCTD auf NusA-AR2 überlappt. Daher wurden ebenfalls NMR-basierte Verdrängungsexperimente von λQ mit RNAPαCTD und NusA-AR2 durchgeführt (Einzelarbeit B, Abb.4 und Abb. S10A,B), welche bestätigten, dass sich auch die Bindungsflächen von λQ und RNAPαCTD auf NusA-AR2 überschneiden. Da die RNAPαCTD durch Verdrängung der NusA-AR2 von NusA-SKK die Autoinhibition von NusA aufheben kann (Schweimer *et al.*, 2011), wurde untersucht, ob λQ ebenfalls hierzu in der Lage ist. In Analogie zu SuhB wurde eine NMR-Titration von λQ mit [I,L,V]-NusA durchgeführt, wobei aufgrund von Präzipitation eine Auswertung dieses NMR-Systems nicht möglich war. Ebenso erfolgten analog zu den Untersuchungen mit SuhB NMR-basierte Verdrängungsexperimente von ^{2}H,^{15}N-NusA-SKK mit NusA-AR2 (Abb. 3-5A) und λQ (Abb. 3-5B), bzw. λQ$^{\Delta 36}$ (Abb. 3-5C).

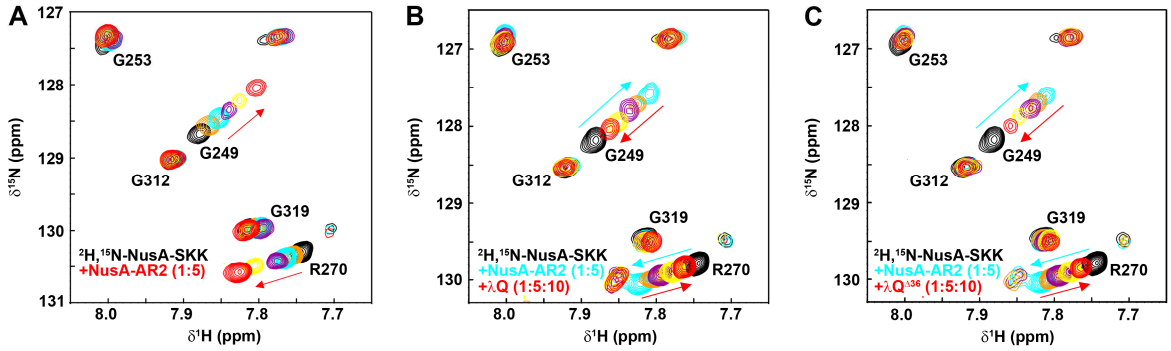

Abbildung 3-5: λQ verdängt NusA-AR2 von NusA-SKK. (A) Ausschnitt aus den 2D-[^{1}H,^{15}N]-BEST-TROSY-Spektren der Titration von ^{2}H,^{15}N-NusA-SKK mit NusA-AR2 (molare Verhältnisse 1:0, schwarz; 1:0,5, orange; 1:1, cyan; 1:2, lila; 1:3, gelb; 1:5, rot). Zugeordnete Signale sind beschriftet und die Pfeile zeigen die Richtung der Änderung der chemischen Verschiebung ausgewählter Signale durch Zugabe von NusA-AR2 (rot) an. **(B,C)** Ausschnitt aus den 2D-[^{1}H,^{15}N]-BEST-TROSY-Spektren des Komplexes von ^{2}H,^{15}N-NusA-SKK (1:0, schwarz) mit NusA-AR2 (1:5, cyan) in Anwesenheit steigender Konzentrationen von λQ (B), bzw. λQ$^{\Delta 36}$ (C) (molare Verhältnisse 1:5:1, orange; 1:5:2, lila; 1:5:5, gelb; 1:5:10, rot). Zugeordnete Signale sind beschriftet und die Pfeile zeigen die Richtung der Änderung der chemischen Verschiebung ausgewählter Signale durch Zugabe von NusA-AR2 (cyan) sowie λQ (rot) bzw. λQ$^{\Delta 36}$ (rot) an. Die zu den Ausschnitten zugehörigen NMR-Spektren sind in Einzelarbeit B, Abb. S11 zu finden. Die Abbildung wurde aus Dudenhoeffer *et al.*, 2020 (Abb. 5) entnommen und abgeändert.

Sowohl die Zugabe von λQ als auch von λQ$^{\Delta 36}$ führte zur Verdrängung der NusA-AR2 von ^{2}H,^{15}N-NusA-SKK, wie es auch für NusG-NTD (Abb. 3-3B), SuhB (Abb. 3-3C) sowie RNAPαCTD (Schweimer *et al.*, 2011) beobachtet werden konnte. Daher liegt eine Aufhebung

der Autoinhibition von NusA durch λQ unabhängig von dessen N-Terminus nahe, auch wenn aufgrund von Präzipitation im NMR-System von [I,L,V]-NusA mit λQ dieses Ergebnis nicht im NusA Volllängenprotein bestätigt werden konnte.

3.3.2 λQ interagiert mit NusA-NTD

Die Bestimmung der mit λQ interagierenden NusA-Domäne zeigte, dass NusA λQ sowohl über seine AR2-Domäne als auch seine NTD kontaktiert. Durch quantitative Analyse der zu den NMR-Titrationen von λQ mit NusA-NTD (Einzelarbeit B, Abb. 2A,B und Abb. S4) zugehörigen 2D-[^{1}H,^{15}N]-Korrelationsspektren wurden die Bindungsflächen der beiden Proteine aufeinander bestimmt sowie anhand dieser ein HADDOCK-Modell (Dominguez *et al.*, 2003) des NusA-NTD:λQ-Komplexes erstellt (Abb. 3-6). Während die von der NusA-NTD-Bindung betroffenen Reste auf λQ im C- und N-terminalen Bereich des Zink-Finger-Motivs und in den Helices α3, α5 und α6 zu finden sind, ist auf Seiten von NusA-NTD deren azide Kopfregion mitsamt der Helix α3* betroffen, welche im NusA-NTD:λQ-Komplex den C- und N-terminalen Bereich des Zink-Finger-Motivs von λQ kontaktiert. Darüber hinaus legt eine NMR-Titration von ^{15}N-NusA-NTD mit λQ$^{\Delta 36}$ (Einzelarbeit B, Abb. S5) den Schluss nahe, dass der N-Terminus von λQ keinen Einfluss auf die Interaktion mit NusA-NTD hat.

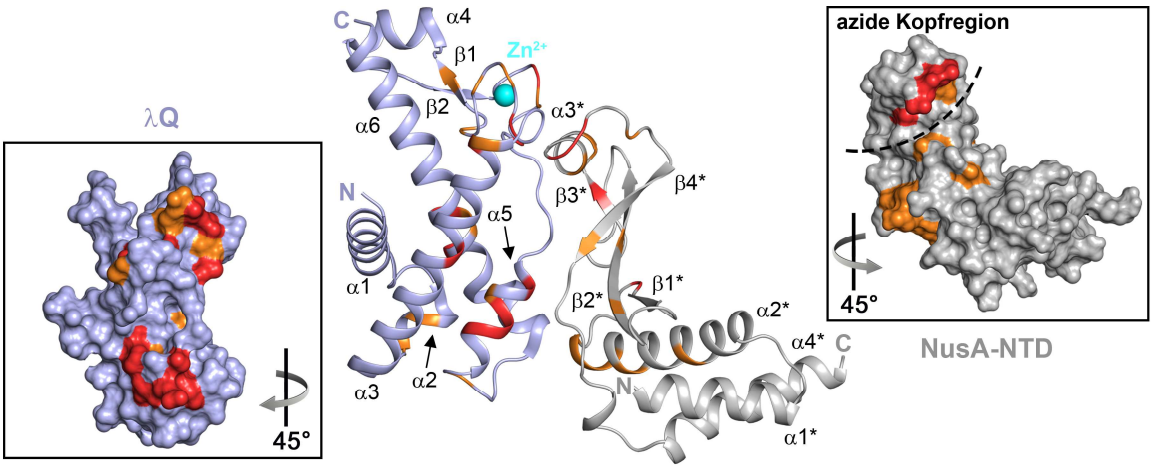

Abbildung 3-6: Interaktion von λQ mit NusA-NTD. Modell des λQ:NusA-NTD-Komplexes. NusA-NTD (PDB-ID: 2KWP; grau) und λQ (PDB-ID: 4MO1; hellblau) sind jeweils in Bänderdarstellung wiedergegeben. Betroffene Reste der Interaktion sind farblich hervorgehoben (moderat betroffen: orange; stark betroffen: rot). Sekundärstrukturelemente und Termini sind beschriftet und das Zn^{2+}-Ion ist als cyane Kugel dargestellt. In den Kästen links (λQ), bzw. rechts (NusA-NTD) sind die beiden Proteine in Oberflächendarstellung wiedergegeben (Farbschema wie im Komplex). Die azide Kopfregion von NusA-NTD ist durch eine getrichelte Linie gekennzeichnet. Die Abbildung wurde aus Dudenhoeffer *et al.*, 2020 (Abb. 2) entnommen und abgeändert.

Von der Bindung der NusA-Domänen NTD und AR2 sind auf Seiten von λQ in beiden Fällen die Helices α3 und α5 betroffen, sodass eine Überlappung der Bindungsflächen beider NusA-Domänen auf λQ naheliegt. Aus diesem Grund wurden NMR-basierte Verdrängungsexperimente

mit NusA-NTD, NusA-AR2 und λQ durchgeführt (Einzelarbeit B, Abb. 3D,E und Abb. S9) welche bestätigten, dass sich die Bindungsflächen von NusA-NTD und NusA-AR2 auf λQ überschneiden, sodass keine simultane Bindung von einem λQ-Molekül an NusA-NTD und NusA-AR2 stattfinden kann. Auf Seiten von NusA-NTD überlappt die für λQ bestimmte Bindungsfläche mit der RNAPαCTD-Bindungsfläche auf NusA-NTD (Guo *et al.*, 2018). Daher wurden ebenfalls NMR-basierte Verdrängungsexperimente von NusA-NTD mit RNAPαCTD und λQ durchgeführt (Einzelarbeit B, Abb. 3D,E und Abb. S6A,B), wobei λQ und RNAPαCTD durch einen Überschuss des jeweils anderen Proteins von NusA-NTD verdrängt werden konnte. Daher kann davon ausgegangen werden, dass sich die Bindungsflächen von λQ und RNAPαCTD auch auf NusA-NTD überschneiden.

Die Ergebnisse der Einzelarbeit B zeigen, dass λQ von allen Nus-Faktoren nur mit NusA interagiert. NusA kontaktiert λQ mittels seiner NTD und AR2-Domäne, wobei keine simultane Bindung eines λQ-Moleküls an beide NusA-Domänen möglich ist. Im Falle der Interaktion von λQ mit NusA-AR2 ist es denkbar, dass NusA-AR2 als Bindungsplattform zur Rekrutierung von λQ-Molekülen an den TEC im Verlaufe der Transkription der „späten" Gene des Phagen λ fungieren könnte. Darüber hinaus ist λQ in der Lage durch die Interaktion mit NusA-AR2 die Autoinhibition von NusA aufzuheben, was wiederum die RNA-Bindung von NusA-SKK und damit einhergehend die Rekrutierung von NusA an den λQ-AT-Komplex erleichtern könnte. Da sich die Bindungsflächen von λQ und RNAPαCTD auf NusA-NTD und NusA-AR2 überlappen, ist es auch möglich, dass λQ durch Interaktion mit der jeweiligen NusA-Domäne deren Bindung an die RNAPαCTD auflösen und hierdurch eine Repositionierung von NusA in eine AT-stimulierende Konformation induzieren könnte. Ebenso könnte λQ auch eine Inhibition der RNAPαCTD-Bindung durch die jeweilige NusA-Domäne bewirken, sodass eine AT-stimulierende Konformation von NusA im λQ-AT-Komplex stabilisiert werden könnte.

3.3.3 λQ interagiert mit der βFTH und repositioniert NusA-NTD an der RNAP

Wie in Einzelarbeit B gezeigt, interagiert λQ mit NusA-NTD. Die NusA-NTD bindet ihrerseits im *his*pausierten NusA:TEC-Komplex über die RNAPαCTD sowie die βFTH an die RNAP (Guo *et al.*, 2018), wobei die βFTH auch für λQ als Bindungsstelle an die RNAP postuliert wurde (Deighan *et al.*, 2008). Daher wurde im Rahmen der Einzelarbeit C die βFTH der *E. coli* RNAP *via* eines Konstruktes für die NMR-Spektroskopie zugänglich gemacht, um sowohl die Interaktion von λQ mit der RNAP strukturell zu charakterisieren, als auch den Einfluss von λQ auf die Bindung von NusA-NTD an die RNAP weitergehend zu untersuchen.

Um die βFTH der *E. coli* RNAP (As 897-906 der β-UE) für NMR-basierte Untersuchungen zugänglich zu machen wurde ein Konstrukt (βFlap) hergestellt, welches den Sequenzbereich von As 829 bis As 1060 der β-UE ohne die beiden i9 Helices (As 937-1040) umfasst (Einzelarbeit C, Abb. 1A). Mit einer $^{2}H,^{13}C,^{15}N$-markierten Probe von βFlap erfolgte die Zuordnung der $[^{1}H,^{15}N]$-NMR-Signale zu den zugehörigen As des βFlap-Rückgrats. Nachfolgend wurde der CSI des βFlap-Konstrukts berechnet (Einzelarbeit C, Abb. 1B; Wishart *et al.*, 1992; Wishart & Sykes, 1994). Dieser zeigt, dass die Sekundärstrukturen des βFlap-Konstrukts in guter Übereinstimmung mit den Sekundärstrukturen der βFlap-Region in der mittels Röntgenstrukturanalyse bestimmten Struktur der *E. coli* RNAP (PDB ID: 4KMU; Molodtsov *et al.*, 2013) sind und die βFTH (As 897-906) des βFlap-Konstrukts eine definierte α-Helix ausbildet.

Die Interaktion von NusA-NTD mit der βFTH der RNAP wurde bereits strukturell charakterisiert (Guo *et al.*, 2018). Daher wurde diese Interaktion genutzt, um zu überprüfen, ob das βFlap-Konstrukt dieselben Interaktionseigenschaften wie die βFlap-Region der RNAP aufweist und somit funktional ist. Hierzu wurden NMR-Titrationen von NusA-NTD mit βFlap durchgeführt (Einzelarbeit C, Abb. 2) und zur strukturellen Charakterisierung der Interaktion quantitativ ausgewertet. Hierbei zeigte sich, dass auf Seiten von βFlap die Interaktion mit NusA-NTD über die βFTH vermittelt wird, welche durch die Helices α1, α2 und α4 der NusA-NTD gebunden wird. Dieses Ergebnis ist in Übereinstimmung mit der Bindungsfläche der NusA-NTD:βFTH-Interaktion in der mittels Kryo-Elektronenmikroskopie bestimmten Struktur des *his*pausierten NusA:TEC-Komplexes (Guo *et al.*, 2018). Daher kann davon ausgegangen werden, dass das βFlap-Konstrukt als Modell der βFlap-Region der *E. coli* RNAP geeignet ist.

Da die βFTH auch für λQ als Bindungsstelle an die RNAP postuliert wurde (Deighan *et al.*, 2008), erfolgten NMR-Titrationen von λQ mit dem βFlap-Konstrukt (Einzelarbeit C, Abb. 4A,B und Abb. S3A,B), um die Bindung von λQ an die RNAP strukturell zu charakterisieren. Die quantitative Analyse der zugehörigen 2D-$[^{1}H,^{15}N]$-Korrelationsspektren zeigte, dass auf Seiten von λQ die von der βFlap-Bindung betroffenen Reste in den Helices α1, α3 und α5 lokalisiert sind (Abb. 3-7A), während die Bindungsfläche von λQ auf βFlap die βFTH darstellt (Abb. 3-7B). Beide ermittelten Bindungsflächen sind in Übereinstimmung mit der *via* Mutagenese und *bacterial two-hybrid*-Systemen bestimmten Bindungsfläche für die λQ:RNAP-Interaktion (Deighan *et al.*, 2008) und eine NMR-Titration von ^{15}N-βFlap mit $\lambda Q^{\Delta 36}$ (Einzelarbeit C, Abb. S3C) zeigte im Vergleich zu λQ keine Unterschiede im Bindungsmuster auf ^{15}N-βFlap, sodass angenommen werden kann, dass der N-Terminus von λQ keinen Einfluss auf die Bindung an die βFlap hat.

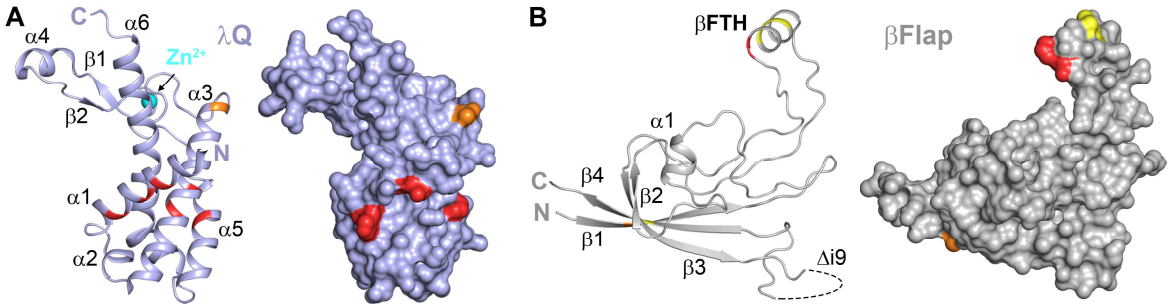

Abbildung 3-7: Interaktion von λQ mit βFlap. λQ (PDB-ID: 4MO1; hellblau) **(A)** und βflap (PDB-ID: 4KMU; grau) **(B)** sind jeweils links in Bänderdarstellung und rechts in Oberflächendarstellung wiedergegeben. Betroffene Reste der Interaktion sind farblich hervorgehoben (λQ: moderat betroffen: orange; stark betroffen: rot; βFlap: leicht betroffen: gelb; moderat betroffen: orange; stark betroffen: rot). Sekundärstrukturelemente und Termini sind beschriftet und das Zn^{2+}-Ion von λQ ist als cyane Kugel dargestellt. Die Abbildung wurde aus Einzelarbeit C (Abb. 4) entnommen und abgeändert.

Da sowohl für NusA-NTD als auch für λQ die Bindungsfläche auf βFlap die βFTH darstellt und λQ ebenfalls mit NusA-NTD interagiert (Abb. 3-6) wurde ein NMR-basiertes Verdrängungsexperiment mit βFlap und λQ an $^{2}H,^{15}N$-NusA-NTD durchgeführt (Einzelarbeit C, Abb. 4C und Abb. S4A). Hierbei zeigte sich, dass keine Interaktion von NusA-NTD mit λQ in Anwesenheit von βFlap stattfindet, sondern NusA-NTD durch λQ von der βFTH verdrängt wird. Daher kann sowohl eine simultane Bindung von λQ und NusA-NTD an die βFTH als auch die Bildung eines ternären Komplexes mit NusA-NTD als zentralem Protein ausgeschlossen werden.

Im *his*pausierten NusA:TEC-Komplex bindet NusA-NTD an die βFTH und an die RNAPαCTD (Guo *et al.*, 2018). Die mittels einer NMR-Titration von [I,L,V]-NusA-NTD mit RNAP (Einzelarbeit C, Abb. 3B) bestimmte Bindungsfläche von RNAP auf NusA-NTD zeigt, dass NusA-NTD dasselbe Bindungsmuster wie im *his*pausierten NusA:TEC-Komplex aufweist, also auch die *core* RNAP simultan über die βFTH sowie die RNAPαCTD kontaktiert. Folglich kann davon ausgegangen werden, dass die Bindung von NusA-NTD an die βFTH und die RNAPαCTD den „normalen" Bindungsmodus von NusA-NTD an die RNAP darstellt. Um den Einfluss von λQ auf die NusA-Positionierung an der RNAP zu untersuchen, wurde daher eine NMR-Titration von $^{2}H,^{15}N$-NusA-NTD mit RNAPαCTD und βFlap durchgeführt (Abb. 3-8A) und nachfolgend λQ (Abb. 3-8B) zugegeben. Bei Zugabe von RNAPαCTD und βFlap zu $^{2}H,^{15}N$-NusA-NTD traten jeweils Änderungen der chemischen Verschiebungen auf, wie sie auch in den binären NMR-Systemen von ^{15}N-NusA-NTD mit RNAPαCTD (Einzelarbeit C, Abb. S1A) bzw. βFlap (Einzelarbeit C, Abb. 2A) beobachtet werden konnten, sodass davon ausgegangen werden kann, dass ein ternärer Komplex assembliert wird. Ebenso sind die Bindungsflächen von RNAPαCTD und βFlap auf NusA-NTD im ternären Komplex in Übereinstimmung mit den Interaktionsflächen der RNAP auf NusA-NTD im *his*pausierten NusA:TEC-Komplex (Guo *et al.*, 2018) bzw. der *core* RNAP auf NusA-NTD. Folglich gibt der $^{2}H,^{15}N$-NusA-NTD:RNAPαCTD:βFlap-Komplex den Bindungszustand von NusA-NTD an der RNAP wieder. Durch Zugabe von λQ zu dem

^{2}H,^{15}N-NusA-NTD:RNAPαCTD:βFlap-Komplex und der anschließenden Bestimmung der Bindungsfläche auf NusA-NTD wurde der Einfluss von λQ auf die NusA-Positionierung an der RNAP untersucht. Hierbei zeigte sich, dass NusA-NTD durch λQ von der βFTH verdrängt wird und keine Änderungen für die Interaktionsfläche von RNAPαCTD auf NusA-NTD sichtbar sind. Der Einfluss von λQ auf die NusA-NTD-Positionierung an der RNAP wurde auch mit der RNAP selbst untersucht, indem eine NMR-Titration von [I,L,V]-NusA-NTD mit RNAP durchgeführt und λQ hinzugegeben wurde (Abb. 3-8C).

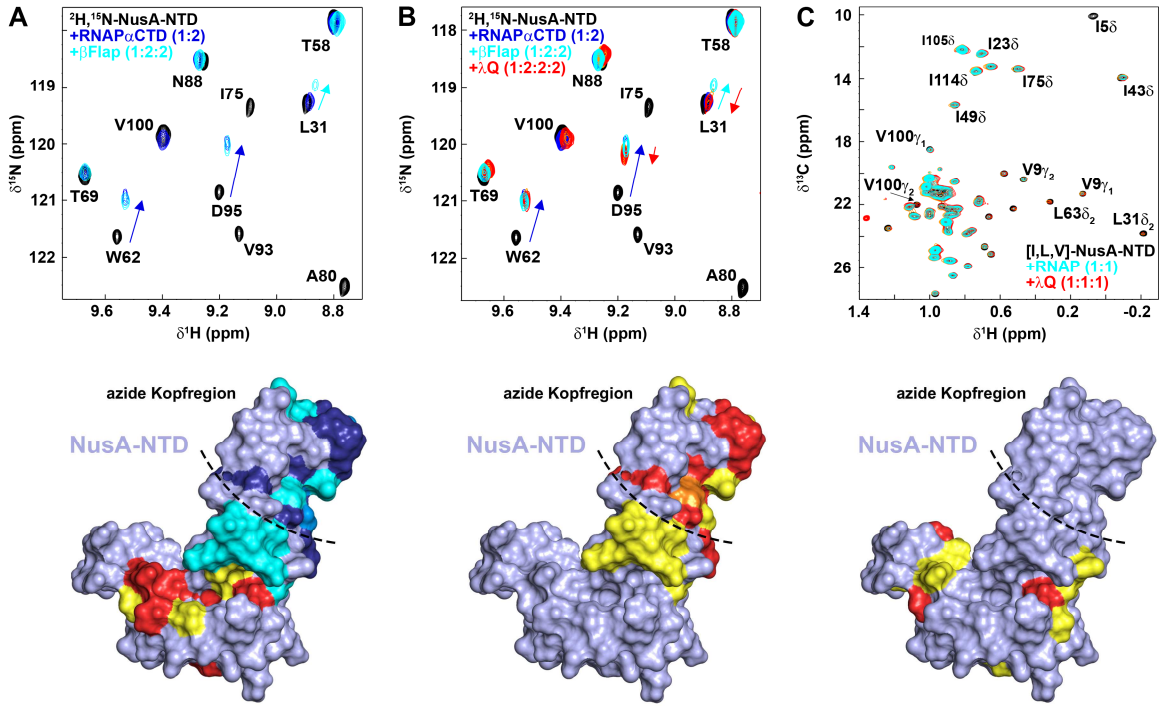

Abbildung 3-8: λQ ist in der Lage NusA-NTD von der βFTH zu verdrängen. **(A)** NusA-NTD-Bindung an die RNAPαCTD und βFlap. **(oben)** Ausschnitt aus den 2D-[^{1}H,^{15}N]-HSQC-Spektren der Titration von ^{2}H,^{15}N-NusA-NTD mit RNAPαCTD und βFlap (molare Verhältnisse: 1:0:0, schwarz; 1:2:0, blau; 1:2:2, cyan). **(unten)** Markierung der von der RNAPαCTD-Bindung (leicht betroffen: cyan; moderat betroffen: marineblau; stark betroffen: dunkelblau) sowie βFlap-Bindung (leicht betroffen: gelb; moderat betroffen: orange; stark betroffen: rot) betroffenen Reste auf die Struktur von NusA-NTD (PDB-ID: 2KWP; hellblau, Oberflächendarstellung). **(B)** NusA-NTD-Bindung an die RNAPαCTD und βFlap in Anwesenheit von λQ. **(oben)** Ausschnitt aus den 2D-[^{1}H,^{15}N]-HSQC-Spektren der Titration von ^{2}H,^{15}N-NusA-NTD mit RNAPαCTD, βFlap und λQ (molare Verhältnisse: 1:0:0:0, schwarz; 1:2:0:0, blau; 1:2:2:0 cyan; 1:2:2:2, rot). **(unten)** Markierung der in Anwesenheit von RNAPαCTD, βFlap und λQ betroffenen Reste (leicht betroffen: gelb; moderat betroffen: orange; stark betroffen: rot) auf NusA-NTD (PDB-ID: 2KWP; hellblau, Oberflächendarstellung). **(C)** NusA-NTD-Bindung an RNAP in Anwesenheit von λQ **(oben)** 2D-[^{1}H,^{13}C]-Methyl-TROSY-Spektren der Titration von [I,L,V]-NusA-NTD mit RNAP und λQ (molare Verhältnisse: 1:0:0, schwarz; 1:1:0, cyan; 1:1:1, rot). **(unten)** Markierung der durch Zugabe von λQ betroffenen Reste auf NusA-NTD (PDB-ID: 2KWP; hellblau, Oberflächendarstellung). As mit betroffenen ILV-Sonden sind rot und zwei As auf jeder Seite um die betroffene ILV-Sonde sind in gelb hervorgehoben, sofern keine nicht betroffene ILV-Sonde in diesem Bereich liegt. Ausgewählte Signale in (A-C) sind beschriftet und die Pfeile in (A,B) zeigen die Richtung der Änderung der chemischen Verschiebung von Signalen durch Zugabe von RNAPαCTD (blau), βflap (cyan) sowie λQ (rot) an. Die azide Kopfregion der NusA-NTD (A-C) ist durch eine getrichelte Linie hervorgehoben. Die zu den in (A,B) gezeigten Ausschnitten zugehörigen NMR-Spektren sind in Einzelarbeit C, Abb. S2C bzw. Abb. S4B zu finden. Die Abbildung wurde aus Einzelarbeit C (Abb. 3 und Abb. 5) entnommen und abgeändert.

Während die Zugabe von RNAP zu [I,L,V]-NusA-NTD zu einem Signalintensitätsverlust führte, konnte bei der nachfolgenden Zugabe von λQ eine Zunahme der Intensitäten einzelner Signale von [I,L,V]-NusA-NTD beobachtet werden. Daher erfolgte die quantitative Auswertung des NMR-Systems von [I,L,V]-NusA-NTD mit RNAP und λQ über die Berechnung der Zunahme der Rest-Signalintensitäten dieses NMR-Systems im Vergleich zu dem NMR-System von [I,L,V]-NusA-NTD mit RNAP (Details: siehe Einzelarbeit C). Die Markierung der durch λQ-Zugabe betroffenen Reste auf die Struktur von NusA-NTD zeigt, dass sich die Anwesenheit von λQ nur auf die βFTH-Bindungsfläche auf der NusA-NTD auswirkt, nicht jedoch auf den aziden Kopfbereich der NusA-NTD, welcher die Interaktion von NusA-NTD mit der RNAPαCTD vermittelt. Dieses Ergebnis ist in Übereinstimmung mit dem Ergebnis für λQ im ^{2}H,^{15}N-NusA-NTD:RNAPαCTD:βFlap-Komplex, sodass davon ausgegangen werden kann, dass λQ in der Lage ist NusA-NTD von der βFTH zu verdrängen.

3.3.4 λQ verdrängt σ^{70} von der βFTH

Zur Vermittlung der AT wird λQ in der Promotor-Region $p_{R'}$ des Phagen λ durch das QBE (Guo & Roberts, 2004; Yarnell & Roberts, 1992) an den pausierten TEC rekrutiert, dessen Pausierung durch das Zusammenspiel einer σ^{70}-abhängigen Pause (Nickels *et al.*, 2002; Perdue & Roberts, 2010; Ring *et al.*, 1996) mit einer EP (Bird *et al.*, 2016; Strobel & Roberts, 2015) vermittelt wird (siehe Abschnitt 1.6.2). Das Verlassen der σ^{70}-abhängigen Pause geht mit der σ^{70}-Dissoziation von der RNAP einher. Es wurden zwei Kräfte für die Dissoziation von σ^{70} postuliert, die λQ vermittelte Destabilisierung der σ^{70}:RNAP-Interaktion (Shi *et al.*, 2019; Yin *et al.*, 2019) sowie DNA-*scrunching* (Strobel & Roberts, 2014). Da σ$^{70}_{R4}$ (Geszvain *et al.*, 2004), NusA-NTD (Guo *et al.*, 2018) sowie λQ (Deighan *et al.*, 2008) mit der βFTH interagieren wurde untersucht, ob λQ bzw. NusA-NTD in der Lage ist σ^{70} von der βFTH zu verdrängen und somit die Holo-RNAP zu destabilisieren.

Hierzu wurden NMR-basierte Verdrängungsexperimente an ^{15}N-βFlap mit σ^{70} und NusA-NTD (Abb. 3-9A) bzw. λQ (Abb. 3-9B) durchgeführt. Bei Zugabe von σ^{70} zu ^{15}N-βFlap konnte ein starker Signalintensitätsverlust beobachtet werden, welcher auf eine Komplexbildung von ^{15}N-βFlap mit σ^{70} schließen lässt. Während die nachfolgende Zugabe von NusA-NTD zu dem ^{15}N-βFlap:σ^{70}-Komplex zu keinen signifikanten Änderungen der Signalintensitäten führte, konnte bei Zugabe von λQ zu dem ^{15}N-βFlap:σ^{70}-Komplex eine Signalintensitätszunahme sowie eine Änderung der chemischen Verschiebung einiger zu den As der βFTH zugehörigen Signale von ^{15}N-βFlap beobachtet werden. Daher kann davon ausgegangen werden, dass λQ durch Bindung an die βFTH in der Lage ist, σ^{70} von dieser zu verdrängen. Um den Einfluss von

NusA-NTD und λQ auf die Holo-RNAP, dem physiologisch relevanten System, zu untersuchen, wurde σ^{70} mittels ^{15}N-Markierung für 1D-[^{1}H,^{15}N]-HSQC-basierte Verdrängungsexperimente zugänglich gemacht. Durch Zugabe eines äquimolaren Verhältnisses an RNAP zu ^{15}N-σ^{70} wurde die Holo-RNAP assembliert und NusA-NTD (Abb. 3-9C) bzw. λQ (Abb. 3-9D) zu dieser hinzugegeben. Die Zugabe von RNAP zu ^{15}N-σ^{70} führte zu einem starken Signalverlust aufgrund der Größenzunahme durch die Holo-RNAP-Bildung, während die nachfolgende Zugabe von NusA-NTD keine Änderung der Signalintensität bewirkte. Im Gegensatz hierzu führte die Zugabe von λQ zu dem ^{15}N-σ^{70}:RNAP-Komplex zu einer signifikanten Signalintensitätszunahme, sodass angenommen werden kann, dass λQ nicht nur in der Lage ist σ^{70} von der βFTH zu verdrängen, sondern auch den Holo-RNAP-Komplex zu destabilisieren.

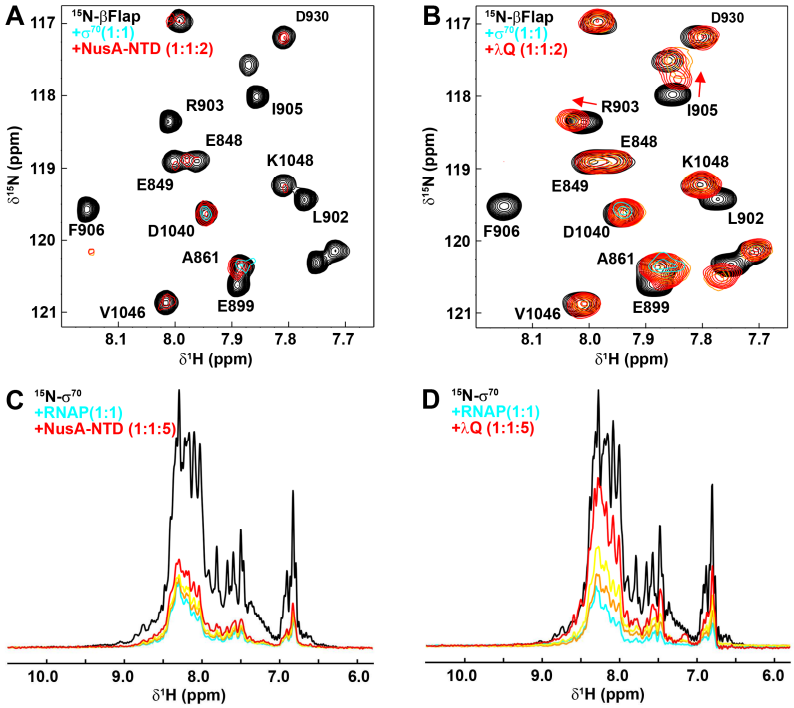

Abbildung 3-9: λQ kann σ^{70} von der βFTH verdrängen und die σ^{70}:RNAP-Interaktion schwächen. (A,B) Ausschnitt aus den 2D-[^{1}H,^{15}N]-HSQC-Spektren der Titration von ^{15}N-βFlap mit σ^{70} und NusA-NTD (A) bzw. λQ (B). Molare Verhältnisse 1:0:0, schwarz; 1:1:0, cyan; 1:1:2, rot. Zugeordnete Signale sind beschriftet und die Pfeile zeigen die Richtung der Änderung der chemischen Verschiebung ausgewählter Signale durch Zugabe von λQ (rot) an. **(C,D)** 1D-[^{1}H,^{15}N]-HSQC-Titration von ^{15}N-σ^{70} mit RNAP und NusA-NTD (C) bzw. λQ (D). Molare Verhältnisse 1:0:0, schwarz; 1:1:0, cyan; 1:1:5, rot. Die zu den Ausschnitten in (A,B) zugehörigen NMR-Spektren sind in Einzelarbeit C, Abb. S5 zu finden. Die Abbildung wurde aus Einzelarbeit C (Abb. 6 und Abb. S5) entnommen und abgeändert.

Zusammenfassend lässt sich festhalten, dass NusA-NTD, wie im *his*pausierten TEC gesehen, auch mit der *core* RNAP über die RNAPαCTD und die βFTH wechselwirkt und λQ nicht nur NusA-NTD, sondern auch σ^{70} von der βFTH verdrängen sowie den σ^{70}:RNAP-Komplex destabilisieren kann. Die destabilisierende Wirkung von λQ auf den Holo-RNAP-Komplex deutet darauf hin, dass λQ die treibende Kraft für die Dissoziation von σ^{70} und damit zum Verlassen

der Promotor-proximalen σ^{70}-abhängigen Pause ist, so wie es auch für das AT-Protein Q21 des verwandten Phagen Φ21 angenommen wird (Shi *et al.*, 2019; Yin *et al.*, 2019). λQ ist ebenso in der Lage NusA-NTD von der βFTH zu verdrängen, wobei keine Änderungen für die Interaktionsfläche von RNAPαCTD auf NusA-NTD sichtbar sind (Abb. 3-8B,C). Es ist daher denkbar, dass λQ durch Verdrängung der NusA-NTD von der βFTH eine Repositionierung von NusA in eine AT-stimulierende Konformation induziert, wobei NusA-NTD über die RNAPαCTD an der RNAP gebunden bleibt, welche als Drehpunkt für die Repositionierung von NusA-NTD an der RNAP fungieren könnte; in Übereinstimmung mit Ergebnissen, dass die Interaktion von NusA-NTD mit der RNAPαCTD für die AT-Effizienz der λQ-AT relevant ist (Liu *et al.*, 1996). Da λQ und RNAPαCTD über dieselbe Bindungsfläche mit NusA-NTD interagieren, wäre es auch möglich, dass λQ durch Interaktion mit NusA-NTD die RNAPαCTD-Bindung von NusA-NTD auflöst, ohne dass dies über eine Änderung der Interaktionsfläche auf NusA-NTD beobachtbar wäre. NMR-basierte Verdrängungsexperimente legen jedoch nahe, dass λQ nur bei einem hohen molekularen Überschuss in der Lage ist RNAPαCTD von NusA-NTD (Einzelarbeit B, Abb. 2D,E und Abb. S6A,B) sowie auch von NusA-AR2 (Einzelarbeit B, Abb. 4 und Abb. S10A,B) zu verdrängen. Somit könnte ein hoher molarer Überschuss von λQ zur Dissoziation von NusA von der RNAP führen, wodurch der AT-Effizienz steigernde Effekt von NusA inhibiert werden würde; in Übereinstimmung mit Ergebnissen, dass bei dem AT-Mechanismus des Phagen Φ82 hohe Konzentrationen von Q82 den stimulierenden Effekt von NusA auf die Q82-AT inhibiert (Wells *et al.*, 2016).

3.4 NusA - zentraler Interaktionspartner in Antiterminationsprozessen

NusA stellt ein zentrales regulatorisches Protein der Transkription dar, welches in vielfältigen Prozessen zum Teil gegensätzliche Effekte auf diese ausübt (siehe Abschnitt 1.4.1). Neben der Regulation der Elongationsrate des TECs (Zhou *et al.*, 2011) sowie der Stimulation von HP-vermittelten Pausen (Artsimovitch & Landick, 2000; Ha *et al.*, 2010) und der intrinsischen Termination (Gusarov & Nudler, 2001; Ha *et al.*, 2010; Mondal *et al.*, 2016) zeigen die Ergebnisse dieser Arbeit, dass NusA auch ein zentraler Interaktionspartner in AT-Prozessen ist. So konnte gezeigt werden, dass NusA nicht nur mit dem AT-Protein λN (Krupp *et al.*, 2019; Said *et al.*, 2017), sondern auch mit dem AT-Protein λQ (Einzelarbeit B) sowie im Rahmen der *rrn*-AT in *E. coli* mit SuhB (Einzelarbeit A) interagiert.

Während NusA-NTD im *his*pausierten NusA:TEC-Komplex zugleich an die βFTH sowie an die RNAPαCTD bindet, bildet in der λN-AT das AT-Protein λN einen ternären Komplex mit NusA-NTD und der βFTH aus und löst zugleich die NusA-NTD:RNAPαCTD-Interaktion auf.

Die Auflösung der Interaktion von NusA-NTD mit der RNAPαCTD ermöglicht NusA eine geänderte globale Konformation im Vergleich zur *his*Pause einzunehmen (Abb. 1-6B), welche mögliche positive Einflüsse von NusA auf die Faltung von Terminator-HPs inhibieren und/oder den RNA-Zugang für Rho blockieren könnte (Guo *et al.*, 2018; Krupp *et al.*, 2019). Im Gegensatz zur λN-AT verdrängt in der λQ-AT das AT-Protein λQ NusA-NTD von der βFTH, während die Bindung von NusA-NTD an die RNAPαCTD bei einem äquimolaren Verhältnis von λQ erhalten bleibt (Abb. 3-8B,C), sodass die RNAPαCTD als Drehpunkt für eine Repositionierung von NusA in einen terminationsresistenten Zustand fungieren könnte. Folglich erscheint eine Repositionierung von NusA im Vergleich zu deren Konformation im *his*pausierten NusA:TEC-Komplex (Guo *et al.*, 2018) ein gemeinsames Schema der AT-Mechanismen des Phagen λ darzustellen. In Übereinstimmung mit den Ergebnissen von Liu *et al.*, welche zeigen, dass die NusA-NTD:RNAPαCTD-Interaktion für die Effizienz der λQ-AT, nicht aber für die λN-AT-Effizienz relevant ist (Liu *et al.*, 1996), legen die Ergebnisse dieser Arbeit nahe, dass NusA-NTD in der λQ-AT und in der λN-AT jeweils eine unterschiedliche Konformation einnimmt und folglich auf unterschiedliche Art und Weise zur AT-Effizienz beitragen kann.

NusA-AR2 ist in der Lage durch Bildung eines intramolekularen Komplexes mit NusA-KH1 die RNA-Bindung von NusA zu inhibieren, wodurch NusA autoinhibiert wird (Schweimer *et al.*, 2011). Im Rahmen dieser Arbeit wurde mittels NMR-Titrationen von NusA-SKK mit NusA-AR2 die Bindungsflächen dieser beiden NusA-Domänen aufeinander bestimmt (Einzelarbeit B, Abb. 5A,B und Abb. S11A,B) sowie anhand dieser ein HADDOCK-Modell (Dominguez *et al.*, 2003) des autoinhibierten Zustands von NusA-SKK erstellt (Abb. 3-10A). Auf Seiten von NusA-AR2 wird die Autoinhibition durch die C-terminale Helix α5 sowie die beiden As Tyr490 und Phe491 vermittelt, welche auch an der Interaktion von NusA-AR2 mit RNAPαCTD (Schweimer *et al.*, 2011), NusG-NTD (Strauß *et al.*, 2016), SuhB (Abb. 3-2) und λQ (Abb. 3-4) beteiligt sind. Mittels NMR-basierter Verdrängungsexperimente konnte in dieser Arbeit gezeigt werden, dass neben der RNAPαCTD (Schweimer *et al.*, 2011) auch die NusG-NTD (Abb. 3-3B), SuhB (Abb. 3-3C) sowie λQ (Abb. 3-5B) in der Lage sind NusA-AR2 von NusA-SKK zu verdrängen. Folglich kann angenommen werden, dass SuhB, NusG-NTD und λQ als Effektoren wirkend die Autoinhibition von NusA aufheben und hierdurch eine kontextabhängige RNA-Bindung von NusA erleichtern bzw. induzieren können.

NusA bindet nach Verlassen des σ^{70}-Faktors mit seiner NTD und AR2-Domäne an den TEC und bleibt während der Elongation an diesen gebunden (Mooney *et al.*, 2009a). Da NusA-AR2 eine hohe intramolekulare Flexibilität aufweist (Eisenmann *et al.*, 2005; Said *et al.*, 2017), im TEC nur lose an der RNAPαCTD gebunden ist (Guo *et al.*, 2018) und spezifische Interaktionen mit den TFs SuhB (Abb. 3-2), λQ (Abb. 3-4) und NusG-NTD (Strauß *et al.*, 2016) eingeht, ist es

ebenso denkbar, dass NusA-AR2 als eine multifunktionale Rekrutierungsplattform für TFs während der Elongation dient (Abb. 3-10B). Die rekrutierten TFs könnten zum einen, wie für λQ gezeigt, NusA kontextabhängig repositionieren und damit einhergehend die Effekte von NusA auf die Transkription modulieren oder aber, wie für SuhB gezeigt, in regulatorische Komplexe integriert werden, welche ihrerseits die RNAP-Aktivität regulieren.

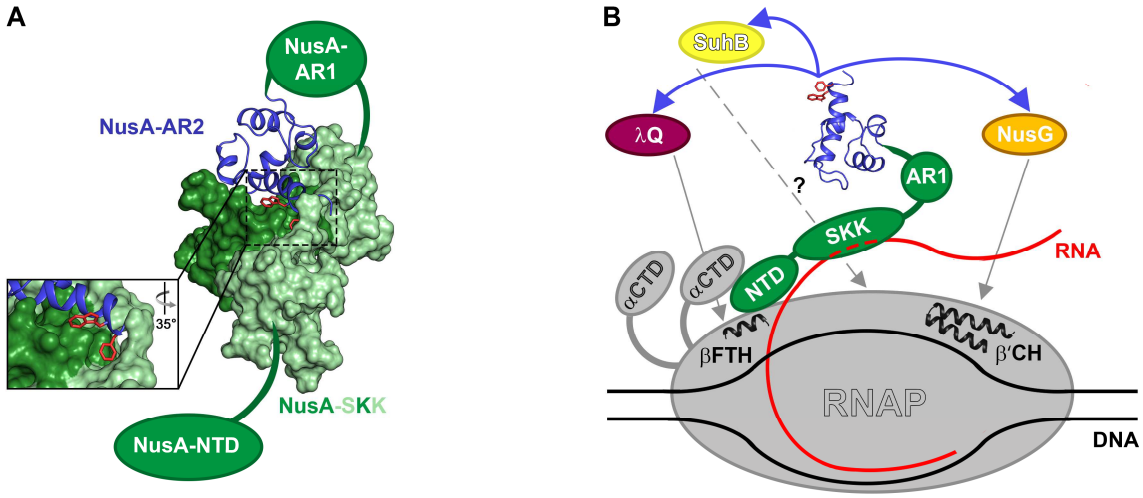

Abbildung 3-10: NusA als Rekrutierungsplattform in der Transkription. (A) Modell des autoinhibierten Zustands von NusA. NusA-AR2 (PDB-ID: 1WCN; blau) ist in Bänderdarstellung und NusA-SKK (PDB-ID: 5LM9; grün) ist in Oberflächendarstellung wiedergegeben. Die Seitenketten von Trp490 und Phe491 sind in rot hervorgehoben und NusA-NTD sowie NusA-AR1 sind jeweils als grüner Ellipsoid wiedergegeben. Der Ausschnitt links zeigt eine Vergrößerung der Bindung von NusA-AR2 an NusA-KH1. **(B)** NusA als Rekrutierungsplattform des TECs. NusA-AR2 (PDB-ID: 1WCN; blau) ist in Bänderdarstellung wiedergegeben und die Seitenketten der beiden As Trp490 und Phe491 sind in rot hervorgehoben. Alle anderen NusA-Domänen sowie Proteine sind als Ellipsoide dargestellt. Ausgewählte Bindungsstellen auf der RNAP sind als Ellipsoide, bzw. in Bänderdarstellung hervorgehoben und entsprechend beschriftet. Die blauen Pfeile zeigen Interaktionspartner von NusA-AR2 und die grauen Pfeile die Bindungsplattform der durch NusA-AR2 rekrutierten Proteine auf der RNAP an. Die Abbildung wurde aus Dudenhoeffer *et al.*, 2020 (Abb. 6) entnommen und abgeändert.

Zusammenfassend unterstreichen die Ergebnisse dieser Arbeit die zentrale Rolle von NusA in der Regulation der bakteriellen Transkription, wobei NusA, obwohl nicht im *rpo*-Operon kodiert, nicht nur als TF, sondern ähnlich wie der σ-Faktor, als akzessorische UE der RNAP während der Transkription betrachtet werden könnte.

4 Abkürzungsverzeichnis

1D	eindimensional
2D	zweidimensional
3D	dreidimensional
AR	*acidic repeat*
As	Aminosäure
AT	Antitermination
β´CH	β´-*clamp helices*
BEST	*band-selective excitation short transient*
βFTH	β-*flap-tip helix*
βGL	β-*gate loop*
BH	*bridge-helix*
BMRB	*Biological Magnetic Resonance Data Bank*
bp	Basenpaar
C	Cytidin
CSI	*chemical shift index*
CTD	C-terminale Domäne
DNA	Desoxyribonukleinsäure
ds	doppelsträngig
E. coli	*Escherichia coli*
EP	*elemental pause*
ePEC	*elemental paused elongation complex*
EPS	*elemental pause sequence*
G	Guanosin
*his*Pause	Pause in der Leitsequenz des Histidin-Operons
HP	*hairpin*
HSQC	*heteronuclear single quantum coherence*
[I,L,V]	[^{1}H,^{13}C]-Markierung der endständigen Methylgruppen der Aminosäuren Isoleucin, Leucin und Valin in einem deuterierten Protein
K_D	Dissoziationskonstante
kDa	Kilodalton
KH	K *homology*
Mg-A	stabil im aktiven Zentrum der RNAP koordiniertes Mg^{2+}-Ion

Mg-B	gemeinsam mit dem einzubauenden NTP in das aktive Zentrum der RNAP eingebrachtes Mg^{2+}-Ion
MM	Molekülmasse
mRNA	*messenger* RNA
NMR	*nuclear magnetic resonance*
nt	Nukleotid
NTD	N-terminale Domäne
NTP	Nukleosidtriphospaht
Nus	N-*utilization substances*
nut	N *utilization-site*
PDB-ID	*protein data bank identification number*
PPi	Pyrophosphat
QBE	Q-bindendes Element
RNA	Ribonukleinsäure
RNAP	DNA-abhängige RNA-Polymerase
RNAPαCTD	C-terminale Domäne der α-Untereinheit der RNA-Polymerase
rRNA	ribosomale RNA
rrn-AT	Anitermination der ribosomalen RNA-Operons
rrn-Operons	ribosomale RNA-Operons
rut	Rho *utilization-site*
SDS-PAGE	Natriumdodecylsulfat-Polyacrylamidgelelektrophorese
SKK	S1-KH1-KH2-Einheit von NusA
TEC	*transcription elongation complex*
TF	Transkriptionsfaktor
TH	*trigger-helix*
TIC	*transcription initiation complex*
TL	*trigger-loop*
tRNA	transfer RNA
TROSY	*transverse relaxation optimized spectroscopy*
U	Uridin
UE	Untereinheit
UP	*upstream promoter*
Urea-PAGE	Urea-Polyacrylamidgelelektrophorese

5 Literaturverzeichnis

Abbondanzieri EA, Greenleaf WJ, Shaevitz JW, Landick R und Block SM (2005) Direct observation of base-pair stepping by RNA polymerase. *Nature* **438:** 460–465

Abdelkareem M, Saint-André C, Takacs M, Papai G, Crucifix C, Guo X, Ortiz J und Weixlbaumer A (2019) Structural Basis of Transcription: RNA Polymerase Backtracking and Its Reactivation. *Mol. Cell* **75:** 298-309.e4

Adelman K, La Porta A, Santangelo TJ, Lis JT, Roberts JW und Wang MD (2002) Single molecule analysis of RNA polymerase elongation reveals uniform kinetic behavior. *Proc. Natl. Acad. Sci. U. S. A.* **99:** 13538–13543

Aksoy S, Squires CL und Squires C (1984) Evidence for antitermination in *Escherichia coli* rRNA transcription. *J. Bacteriol.* **159:** 260–264

Albrechtsen B, Squires CL, Li S und Squires C (1990) Antitermination of characterized transcriptional terminators by the *Escherichia coli rrnG* leader region. *J. Mol. Biol.* **213:** 123–134

Altieri AS, Mazzulla MJ, Horita DA, Coats RH, Wingfield PT, Das A, Court DL und Byrd RA (2000) The structure of the transcriptional antiterminator NusB from *Escherichia coli*. *Nat. Struct. Biol.* **7:** 470–474

Artsimovitch I und Landick R (2000) Pausing by bacterial RNA polymerase is mediated by mechanistically distinct classes of signals. *Proc. Natl. Acad. Sci. U. S. A.* **97:** 7090–7095

Bae B, Feklistov A, Lass-Napiorkowska A, Landick R und Darst SA (2015) Structure of a bacterial RNA polymerase holoenzyme open promoter complex. *eLife* **4:** e08504

Bar-Nahum G und Nudler E (2001) Isolation and characterization of σ70-retaining transcription elongation complexes from *Escherichia coli*. *Cell* **106:** 443–451

Berg KL, Squires C und Squires CL (1989) Ribosomal RNA operon anti-termination. Function of leader and spacer region *box B-box A* sequences and their conservation in diverse micro-organisms. *J. Mol. Biol.* **209:** 345–358

Bird JG, Strobel EJ und Roberts JW (2016) A universal transcription pause sequence is an element of initiation factor σ70-dependent pausing. *Nucleic Acids Res.* **44:** 6732–6740

Blattner FR, Plunkett G, Bloch CA, Perna NT, Burland V, Riley M, Collado-Vides J, Glasner JD, Rode CK, Mayhew GF, Gregor J, Davis NW, Kirkpatrick HA, Goeden MA, Rose DJ, Mau B und Shao Y (1997) The complete genome sequence of *Escherichia coli* K-12. *Science* **277:** 1453–1462

Bodenhausen G und Ruben DJ (1980) Natural abundance nitrogen-15 NMR by enhanced heteronuclear spectroscopy. *Chem. Phys. Lett.* **69:** 185–189

Brueckner F, Ortiz J und Cramer P (2009) A movie of the RNA polymerase nucleotide addition cycle. *Curr. Opin. Struct. Biol.* **19:** 294–299

Bubunenko M, Baker T und Court DL (2007) Essentiality of ribosomal and transcription antitermination proteins analyzed by systematic gene replacement in *Escherichia coli*. *J. Bacteriol.* **189:** 2844–2853

Bubunenko M, Court DL, Al Refaii A, Saxena S, Korepanov A, Friedman DI, Gottesman ME und Alix JH (2013) Nus transcription elongation factors and RNase III modulate small ribosome subunit biogenesis in *Escherichia coli*. *Mol. Microbiol.* **87:** 382–393

Burmann BM und Rösch P (2011) The role of *E. coli* Nus-factors in transcription regulation and transcription:translation coupling: From structure to mechanism. *Transcription* **2:** 130–134

Burmann BM, Schweimer K, Luo X, Wahl MC, Stitt BL, Gottesman ME und Rösch P (2010) A NusE:NusG complex links transcription and translation. *Science* **328:** 501–504

Burns CM, Richardson LV und Richardson JP (1998) Combinatorial effects of NusA and NusG on transcription elongation and Rho-dependent termination in *Escherichia coli*. *J. Mol. Biol.* **278:** 307–316

Casjens SR und Hendrix RW (2015) Bacteriophage lambda: Early pioneer and still relevant. *Virology* **479–480:** 310–330

Cavanagh J, Fairbrother WJ, Palmer AG III und Skelton NJ (1996). Chemical-Exchange Effects in NMR Spectroscopy in *Protein NMR spectroscopy: principles and practice*, 1st ed., Academic Press, San Diego: 290-300

Chakraborty A, Wang D, Ebright YW, Korlann Y, Kortkhonjia E, Kim T, Chowdhury S, Wigneshweraraj S, Irschik H, Jansen R, Nixon BT, Knight J, Weiss S und Ebright RH (2012) Opening and closing of the bacterial RNA polymerase clamp. *Science* **337:** 591–595

Chen CY und Richardson JP (1987) Sequence elements essential for rho-dependent transcription termination at λ*tR1*. *J. Biol. Chem.* **262:** 11292–11299

Choi J, Grosely R, Prabhakar A, Lapointe CP, Wang J und Puglisi JD (2018) How Messenger RNA and Nascent Chain Sequences Regulate Translation Elongation. *Annu. Rev. Biochem.* **87:** 421–449

Cohen SE, Godoy VG und Walker GC (2009) Transcriptional modulator NusA interacts with translesion DNA polymerases in *Escherichia coli*. *J. Bacteriol.* **191:** 665–672

Court DL, Oppenheim AB und Adhya SL (2007) A new look at bacteriophage lambda genetic networks. *J. Bacteriol.* **189:** 298–304

Dangkulwanich M, Ishibashi T, Bintu L und Bustamante C (2014) Molecular mechanisms of transcription through single-molecule experiments. *Chem. Rev.* **114:** 3203–3223

Daube SS und von Hippel PH (1999) Interactions of *Escherichia coli* σ70 within the transcription elongation complex. *Proc. Natl. Acad. Sci. U. S. A.* **96:** 8390–8395

d'Aubenton Carafa Y, Brody E und Thermes C (1990) Prediction of rho-independent *Escherichia coli* transcription terminators. A statistical analysis of their RNA stem-loop structures. *J. Mol. Biol.* **216:** 835–858

Deighan P, Diez CM, Leibman M, Hochschild A und Nickels BE (2008) The bacteriophage lambda Q antiterminator protein contacts the β-flap domain of RNA polymerase. *Proc. Natl. Acad. Sci. U. S. A.* **105:** 15305–15310

Deighan P und Hochschild A (2007) The bacteriophage lambdaQ anti-terminator protein regulates late gene expression as a stable component of the transcription elongation complex. *Mol. Microbiol.* **63:** 911–920

Dennis PP (1972) Stable ribonucleic acid synthesis during the cell division cycle in slowly growing *Escherichia coli* B/r*. *J. Biol. Chem.* **247:** 204–208

DeVito J und Das A (1994) Control of transcription processivity in phage lambda: Nus factors strengthen the termination-resistant state of RNA polymerase induced by N antiterminator. *Proc. Natl. Acad. Sci. U. S. A.* **91:** 8660–8664

Dominguez C, Boelens R und Bonvin AMJJ (2003) HADDOCK: a protein-protein docking approach based on biochemical or biophysical information. *J. Am. Chem. Soc.* **125:** 1731–1737

Drögemüller J, Strauß M, Schweimer K, Jurk M, Rösch P und Knauer SH (2015) Determination of RNA polymerase binding surfaces of transcription factors by NMR spectroscopy. *Sci. Rep.* **5:** 16428

Dudenhoeffer BR, Borggraefe J, Schweimer K und Knauer SH (2020) NusA directly interacts with antitermination factor Q from phage λ**.** *Sci. Rep.* **10:** 6607

Dudenhoeffer BR, Schneider H, Schweimer K und Knauer SH (2019) SuhB is an integral part of the ribosomal antitermination complex and interacts with NusA. *Nucleic Acids Res.* **47:** 6504–6518

Dutta D, Chalissery J und Sen R (2008) Transcription termination factor rho prefers catalytically active elongation complexes for releasing RNA. *J. Biol. Chem.* **283:** 20243–20251

Eisenmann A, Schwarz S, Prasch S, Schweimer K und Rösch P (2005) The *E. coli* NusA carboxy-terminal domains are structurally similar and show specific RNAP- and λN interaction. *Protein Sci. Publ. Protein Soc.* **14:** 2018–2029

Ellwood M und Nomura M (1982) Chromosomal locations of the genes for rRNA in *Escherichia coli* K-12. *J. Bacteriol.* **149:** 458–468

Epshtein V, Cardinale CJ, Ruckenstein AE, Borukhov S und Nudler E (2007) An allosteric path to transcription termination. *Mol. Cell* **28:** 991–1001

Epshtein V, Dutta D, Wade J und Nudler E (2010) An allosteric mechanism of Rho-dependent transcription termination. *Nature* **463:** 245–249

Epshtein V, Kamarthapu V, McGary K, Svetlov V, Ueberheide B, Proshkin S, Mironov A und Nudler E (2014) UvrD facilitates DNA repair by pulling RNA polymerase backwards. *Nature* **505:** 372–377

Estrem ST, Ross W, Gaal T, Chen ZW, Niu W, Ebright RH und Gourse RL (1999) Bacterial promoter architecture: subsite structure of UP elements and interactions with the carboxy-terminal domain of the RNA polymerase α subunit. *Genes Dev.* **13:** 2134–2147

Feklistov A und Darst SA (2011) Structural basis for promoter-10 element recognition by the bacterial RNA polymerase σ subunit. *Cell* **147:** 1257–1269

Friedman DI und Baron LS (1974) Genetic characterization of a bacterial locus involved in the activity of the N function of phage λ. *Virology* **58:** 141–148

Friedman DI und Gottesman M (1983) Lytic mode of lambda development in *Lambda II*. Editors: Hendrix R, Roberts J, Stahl FW, Weisberg R. Cold Spring Harbor Laboratory Press, New York: 21-52

Gardner KH und Kay LE (1998) The use of 2H, 13C, 15N multidimensional NMR to study the structure and dynamics of proteins. *Annu. Rev. Biophys. Biomol. Struct.* **27:** 357–406

Geszvain K, Gruber TM, Mooney RA, Gross CA und Landick R (2004) A hydrophobic patch on the flap-tip helix of *E.coli* RNA polymerase mediates σ70 region 4 function. *J. Mol. Biol.* **343:** 569–587

Ghosh P, Ishihama A und Chatterji D (2001) *Escherichia coli* RNA polymerase subunit omega and its N-terminal domain bind full-length beta' to facilitate incorporation into the alpha2beta subassembly. *Eur. J. Biochem.* **268:** 4621–4627

Gill SC, Weitzel SE und von Hippel PH (1991) *Escherichia coli* σ70 and NusA proteins. I. Binding interactions with core RNA polymerase in solution and within the transcription complex. *J. Mol. Biol.* **220:** 307–324

Gollnick P und Babitzke P (2002) Transcription attenuation. *Biochim. Biophys. Acta* **1577:** 240–250

Gottesman ME, Adhya S und Das A (1980) Transcription antitermination by bacteriophage lambda N gene product. *J. Mol. Biol.* **140:** 57–75

Grayhack EJ, Yang XJ, Lau LF und Roberts JW (1985) Phage lambda gene Q antiterminator recognizes RNA polymerase near the promoter and accelerates it through a pause site. *Cell* **42:** 259–269

Greive SJ, Lins AF und von Hippel PH (2005) Assembly of an RNA-protein complex. Binding of NusB and NusE (S10) proteins to *boxA* RNA nucleates the formation of the antitermination complex involved in controlling rRNA transcription in *Escherichia coli*. *J. Biol. Chem.* **280:** 36397–36408

Guo J und Roberts JW (2004) DNA binding regions of Q proteins of phages λ and Φ80. *J. Bacteriol.* **186:** 3599–3608

Guo X, Myasnikov AG, Chen J, Crucifix C, Papai G, Takacs M, Schultz P und Weixlbaumer A (2018) Structural Basis for NusA Stabilized Transcriptional Pausing. *Mol. Cell* **69:** 816-827.e4

Gusarov I und Nudler E (2001) Control of intrinsic transcription termination by N and NusA: the basic mechanisms. *Cell* **107:** 437–449

Gusarov I und Nudler E (1999) The mechanism of intrinsic transcription termination. *Mol. Cell* **3:** 495–504

Ha KS, Toulokhonov I, Vassylyev DG und Landick R (2010) The NusA N-terminal domain is necessary and sufficient for enhancement of transcriptional pausing via interaction with the RNA exit channel of RNA polymerase. *J. Mol. Biol.* **401:** 708–725

Harden TT, Wells CD, Friedman LJ, Landick R, Hochschild A, Kondev J und Gelles J (2016) Bacterial RNA polymerase can retain σ70 throughout transcription. *Proc. Natl. Acad. Sci. U. S. A.* **113:** 602–607

Hein PP, Kolb KE, Windgassen T, Bellecourt MJ, Darst SA, Mooney RA und Landick R (2014) RNA polymerase pausing and nascent-RNA structure formation are linked through clamp-domain movement. *Nat. Struct. Mol. Biol.* **21:** 794–802

Heinrich T, Condon C, Pfeiffer T und Hartmann RK (1995) Point mutations in the leader *boxA* of a plasmid-encoded *Escherichia coli rrnB* operon cause defective antitermination *in vivo*. *J. Bacteriol.* **177:** 3793–3800

Herbert KM, Zhou J, Mooney RA, Porta AL, Landick R und Block SM (2010) *E. coli* NusG inhibits backtracking and accelerates pause-free transcription by promoting forward translocation of RNA polymerase. *J. Mol. Biol.* **399:** 17–30

Hsu LM (2002) Promoter clearance and escape in prokaryotes. *Biochim. Biophys. Acta* **1577:** 191–207

Huang YH, Said N, Loll B und Wahl MC (2019) Structural basis for the function of SuhB as a transcription factor in ribosomal RNA synthesis. *Nucleic Acids Res.* **47:** 6488–6503

Ishihama A (2018) Building a complete image of genome regulation in the model organism *Escherichia coli*. *J. Gen. Appl. Microbiol.* **63:** 311–324

Ishihama A (2000) Functional modulation of *Escherichia coli* RNA polymerase. *Annu. Rev. Microbiol.* **54:** 499–518

Ishihama A (1981) Subunit of assembly of *Escherichia coli* RNA polymerase. *Adv. Biophys.* **14:** 1–35

Jin DJ, Burgess RR, Richardson JP und Gross CA (1992) Termination efficiency at rho-dependent terminators depends on kinetic coupling between RNA polymerase and rho. *Proc. Natl. Acad. Sci. U. S. A.* **89:** 1453–1457

Jin DJ, Cagliero C und Zhou YN (2012) Growth rate regulation in *Escherichia coli*. *FEMS Microbiol. Rev.* **36:** 269–287

Jinks-Robertson S und Nomura M (1982) Ribosomal protein S4 acts in trans as a translational repressor to regulate expression of the α operon in *Escherichia coli*. *J. Bacteriol.* **151:** 193–202

Kang JY, Mishanina TV, Bellecourt MJ, Mooney RA, Darst SA und Landick R (2018a) RNA Polymerase Accommodates a Pause RNA Hairpin by Global Conformational Rearrangements that Prolong Pausing. *Mol. Cell* **69:** 802-815.e5

Kang JY, Mooney RA, Nedialkov Y, Saba J, Mishanina TV, Artsimovitch I, Landick R und Darst SA (2018b) Structural Basis for Transcript Elongation Control by NusG Family Universal Regulators. *Cell* **173:** 1650-1662.e14

Kang JY, Olinares PDB, Chen J, Campbell EA, Mustaev A, Chait BT, Gottesman ME und Darst SA (2017) Structural basis of transcription arrest by coliphage HK022 Nun in an *Escherichia coli* RNA polymerase elongation complex. *eLife* **6:** e25478

Kapanidis AN, Margeat E, Ho SO, Kortkhonjia E, Weiss S und Ebright RH (2006) Initial transcription by RNA polymerase proceeds through a DNA-scrunching mechanism. *Science* **314:** 1144–1147

Kapanidis AN, Margeat E, Laurence TA, Doose S, Ho SO, Mukhopadhyay J, Kortkhonjia E, Mekler V, Ebright RH und Weiss S (2005) Retention of transcription initiation factor σ70 in transcription elongation: single-molecule analysis. *Mol. Cell* **20:** 347–356

Kaplan CD, Larsson K-M und Kornberg RD (2008) The RNA polymerase II trigger loop functions in substrate selection and is directly targeted by α-amanitin. *Mol. Cell* **30:** 547–556

Kolb KE, Hein PP und Landick R (2014) Antisense oligonucleotide-stimulated transcriptional pausing reveals RNA exit channel specificity of RNA polymerase and mechanistic contributions of NusA and RfaH. *J. Biol. Chem.* **289:** 1151–1163

Komissarova N, Becker J, Solter S, Kireeva M und Kashlev M (2002) Shortening of RNA:DNA hybrid in the elongation complex of RNA polymerase is a prerequisite for transcription termination. *Mol. Cell* **10:** 1151–1162

Koslover DJ, Fazal FM, Mooney RA, Landick R und Block SM (2012) Binding and translocation of termination factor Rho studied at the single-molecule level. *J. Mol. Biol.* **423:** 664–676

Kozloff LM, Turner MA, Arellano F und Lute M (1991) Phosphatidylinositol, a phospholipid of ice-nucleating bacteria. *J. Bacteriol.* **173:** 2053–2060

Krupp F, Said N, Huang Y-H, Loll B, Bürger J, Mielke T, Spahn CMT und Wahl MC (2019) Structural Basis for the Action of an All-Purpose Transcription Anti-termination Factor. *Mol. Cell* **74:** 143-157.e5

Landick R (2006) The regulatory roles and mechanism of transcriptional pausing. *Biochem. Soc. Trans.* **34:** 1062–1066

Landick R, Carey J und Yanofsky C (1985) Translation activates the paused transcription complex and restores transcription of the *trp* operon leader region. *Proc. Natl. Acad. Sci. U. S. A.* **82:** 4663–4667

Larson MH, Mooney RA, Peters JM, Windgassen T, Nayak D, Gross CA, Block SM, Greenleaf WJ, Landick R und Weissman JS (2014) A pause sequence enriched at translation start sites drives transcription dynamics *in vivo*. *Science* **344:** 1042–1047

Lawson MR, Ma W, Bellecourt MJ, Artsimovitch I, Martin A, Landick R, Schulten K und Berger JM (2018) Mechanism for the Regulated Control of Bacterial Transcription Termination by a Universal Adaptor Protein. *Mol. Cell* **71:** 911-922.e4

Li J, Horwitz R, McCracken S und Greenblatt J (1992) NusG, a new *Escherichia coli* elongation factor involved in transcriptional antitermination by the N protein of phage λ. *J. Biol. Chem.* **267:** 6012–6019

Li SC, Squires CL und Squires C (1984) Antitermination of *E. coli* rRNA transcription is caused by a control region segment containing lambda *nut*-like sequences. *Cell* **38:** 851–860

Liu K, Zhang Y, Severinov K, Das A und Hanna MM (1996) Role of *Escherichia coli* RNA polymerase alpha subunit in modulation of pausing, termination and anti-termination by the transcription elongation factor NusA. *EMBO J.* **15:** 150–161

Liu Z, Gong Z, Dong X und Tang C (2016) Transient protein-protein interactions visualized by solution NMR. *Biochim. Biophys. Acta* **1864:** 115–122

Lonetto M, Gribskov M und Gross CA (1992) The σ70 family: sequence conservation and evolutionary relationships. *J. Bacteriol.* **174:** 3843–3849

Luk KC und Szybalski W (1983) Tandem transcription-termination sites in the late rightward operon of bacteriophage lambda. *Mol. Gen. Genet. MGG* **189:** 289–297

Luo X, Hsiao H-H, Bubunenko M, Weber G, Court DL, Gottesman ME, Urlaub H und Wahl MC (2008) Structural and functional analysis of the *E. coli* NusB-S10 transcription antitermination complex. *Mol. Cell* **32:** 791–802

Mah TF, Li J, Davidson AR und Greenblatt J (1999) Functional importance of regions in *Escherichia coli* elongation factor NusA that interact with RNA polymerase, the bacteriophage λ N protein and RNA. *Mol. Microbiol.* **34:** 523–537

Martin FH und Tinoco I (1980) DNA-RNA hybrid duplexes containing oligo(dA:rU) sequences are exceptionally unstable and may facilitate termination of transcription. *Nucleic Acids Res.* **8:** 2295–2299

Martinez-Rucobo FW, Sainsbury S, Cheung ACM und Cramer P (2011) Architecture of the RNA polymerase-Spt4/5 complex and basis of universal transcription processivity. *EMBO J.* **30:** 1302–1310

Matsuhisa A, Suzuki N, Noda T und Shiba K (1995) Inositol monophosphatase activity from the *Escherichia coli suhB* gene product. *J. Bacteriol.* **177:** 200–205

Metzger W, Schickor P, Meier T, Werel W und Heumann H (1993) Nucleation of RNA chain formation by *Escherichia coli* DNA-dependent RNA polymerase. *J. Mol. Biol.* **232:** 35–49

Mishra S, Mohan S, Godavarthi S und Sen R (2013) The interaction surface of a bacterial transcription elongation factor required for complex formation with an antiterminator during transcription antitermination. *J. Biol. Chem.* **288:** 28089–28103

Mogridge J, Legault P, Li J, Van Oene MD, Kay LE und Greenblatt J (1998). Independent ligand-induced folding of the RNA-binding domain and two functionally distinct antitermination regions in the phage lambda N protein. *Mol. Cell* **1**: 265-275

Mogridge J, Mah TF und Greenblatt J (1995) A protein-RNA interaction network facilitates the template-independent cooperative assembly on RNA polymerase of a stable antitermination complex containing the λ N protein. *Genes Dev.* **9:** 2831–2845

Molodtsov V, Anikin M und McAllister WT (2014) The presence of an RNA:DNA hybrid that is prone to slippage promotes termination by T7 RNA polymerase. *J. Mol. Biol.* **426:** 3095–3107

Molodtsov V, Nawarathne IN, Scharf NT, Kirchhoff PD, Showalter HDH, Garcia GA und Murakami KS (2013) X-ray crystal structures of the *Escherichia coli* RNA polymerase in complex with benzoxazinorifamycins. *J. Med. Chem.* **56:** 4758–4763

Mondal S, Yakhnin AV, Sebastian A, Albert I und Babitzke P (2016) NusA-dependent transcription termination prevents misregulation of global gene expression. *Nat. Microbiol.* **1:** 15007

Mooney RA, Davis SE, Peters JM, Rowland JL, Ansari AZ und Landick R (2009a) Regulator trafficking on bacterial transcription units *in vivo*. *Mol. Cell* **33:** 97–108

Mooney RA, Schweimer K, Rösch P, Gottesman M und Landick R (2009b) Two structurally independent domains of *E. coli* NusG create regulatory plasticity via distinct interactions with RNA polymerase and regulators. *J. Mol. Biol.* **391:** 341–358

Morgan WD, Bear DG, Litchman BL und von Hippel PH (1985) RNA sequence and secondary structure requirements for rho-dependent transcription termination. *Nucleic Acids Res.* **13:** 3739–3754

Morgan WD, Bear DG und von Hippel PH (1983) Rho-dependent termination of transcription. II. Kinetics of mRNA elongation during transcription from the bacteriophage λ *PR* promoter. *J. Biol. Chem.* **258:** 9565–9574

Morris KV und Mattick JS (2014) The rise of regulatory RNA. *Nat. Rev. Genet.* **15:** 423–437

Mühlberger R, Robelek R, Eisenreich W, Ettenhuber C, Sinner EK, Kessler H, Bacher A und Richter G (2003) RNA DNA discrimination by the antitermination protein NusB. *J. Mol. Biol.* **327:** 973–983

Murakami KS (2013) X-ray crystal structure of *Escherichia coli* RNA polymerase σ70 holoenzyme. *J. Biol. Chem.* **288:** 9126–9134

Neuman KC, Abbondanzieri EA, Landick R, Gelles J und Block SM (2003) Ubiquitous transcriptional pausing is independent of RNA polymerase backtracking. *Cell* **115:** 437–447

Nickels BE, Roberts CW, Roberts JW und Hochschild A (2006) RNA-mediated destabilization of the σ70 region 4/β flap interaction facilitates engagement of RNA polymerase by the Q antiterminator. *Mol. Cell* **24:** 457–468

Nickels BE, Roberts CW, Sun H, Roberts JW und Hochschild A (2002) The σ70 subunit of RNA polymerase is contacted by the λQ antiterminator during early elongation. *Mol. Cell* **10:** 611–622

Nodwell JR und Greenblatt J (1993) Recognition of *boxA* antiterminator RNA by the *E. coli* antitermination factors NusB and ribosomal protein S10. *Cell* **72:** 261–268

Noeske J, Wasserman MR, Terry DS, Altman RB, Blanchard SC und Cate JHD (2015) High-resolution structure of the *Escherichia coli* ribosome. *Nat. Struct. Mol. Biol.* **22:** 336–341

Nudler E (2012) RNA polymerase backtracking in gene regulation and genome instability. *Cell* **149:** 1438–1445

Oppenheim AB, Kobiler O, Stavans J, Court DL und Adhya S (2005) Switches in bacteriophage lambda development. *Annu. Rev. Genet.* **39:** 409–429

Pan T, Artsimovitch I, Fang XW, Landick R und Sosnick TR (1999) Folding of a large ribozyme during transcription and the effect of the elongation factor NusA. *Proc. Natl. Acad. Sci. U. S. A.* **96:** 9545–9550

Park J-S und Roberts JW (2006) Role of DNA bubble rewinding in enzymatic transcription termination. *Proc. Natl. Acad. Sci. U. S. A.* **103:** 4870–4875

Perdue SA und Roberts JW (2010) A backtrack-inducing sequence is an essential component of *Escherichia coli* σ70-dependent promoter-proximal pausing. *Mol. Microbiol.* **78:** 636–650

Pervushin K, Riek R, Wider G und Wüthrich K (1997) Attenuated T2 relaxation by mutual cancellation of dipole-dipole coupling and chemical shift anisotropy indicates an avenue to NMR structures of very large biological macromolecules in solution. *Proc. Natl. Acad. Sci. U. S. A.* **94:** 12366–12371

Peters JM, Mooney RA, Grass JA, Jessen ED, Tran F und Landick R (2012) Rho and NusG suppress pervasive antisense transcription in *Escherichia coli*. *Genes Dev.* **26:** 2621–2633

Peters JM, Vangeloff AD und Landick R (2011) Bacterial transcription terminators: the RNA 3'-end chronicles. *J. Mol. Biol.* **412:** 793–813

Pfeiffer T und Hartmann RK (1997) Role of the spacer *boxA* of *Escherichia coli* ribosomal RNA operons in efficient 23 S rRNA synthesis *in vivo*. *J. Mol. Biol.* **265:** 385–393

Prasch S, Jurk M, Washburn RS, Gottesman ME, Wöhrl BM und Rösch P (2009) RNA-binding specificity of *E. coli* NusA. *Nucleic Acids Res.* **37:** 4736–4742

Prasch S, Schwarz S, Eisenmann A, Wöhrl BM, Schweimer K und Rösch P (2006) Interaction of the intrinsically unstructured phage λ N Protein with *Escherichia coli* NusA. *Biochemistry* **45:** 4542–4549

Pribnow D (1975) Nucleotide sequence of an RNA polymerase binding site at an early T7 promoter. *Proc. Natl. Acad. Sci. U. S. A.* **72:** 784–788

Pupov D, Kuzin I, Bass I und Kulbachinskiy A (2014) Distinct functions of the RNA polymerase σ subunit region 3.2 in RNA priming and promoter escape. *Nucleic Acids Res.* **42:** 4494–4504

Qayyum MZ, Dey D und Sen R (2016) Transcription Elongation Factor NusA Is a General Antagonist of Rho-dependent Termination in *Escherichia coli*. *J. Biol. Chem.* **291:** 8090–8108

Ray-Soni A, Bellecourt MJ und Landick R (2016) Mechanisms of Bacterial Transcription Termination: All Good Things Must End. *Annu. Rev. Biochem.* **85:** 319–347

Revyakin A, Liu C, Ebright RH und Strick TR (2006) Abortive initiation and productive initiation by RNA polymerase involve DNA scrunching. *Science* **314:** 1139–1143

Richardson JP (2002) Rho-dependent termination and ATPases in transcript termination. *Biochim. Biophys. Acta* **1577:** 251–260

Ring BZ, Yarnell WS und Roberts JW (1996) Function of *E. coli* RNA polymerase σ factor σ70 in promoter-proximal pausing. *Cell* **86:** 485–493

Roberts JW (2019) Mechanisms of Bacterial Transcription Termination. *J. Mol. Biol.* **431:** 4030–4039

Ross W, Gosink KK, Salomon J, Igarashi K, Zou C, Ishihama A, Severinov K und Gourse RL (1993) A third recognition element in bacterial promoters: DNA binding by the α subunit of RNA polymerase. *Science* **262:** 1407–1413

Saba J, Chua XY, Mishanina TV, Nayak D, Windgassen TA, Mooney RA und Landick R (2019) The elemental mechanism of transcriptional pausing. *eLife* **8:** e40981

Saecker RM, Record MT und Dehaseth PL (2011) Mechanism of bacterial transcription initiation: RNA polymerase - promoter binding, isomerization to initiation-competent open complexes, and initiation of RNA synthesis. *J. Mol. Biol.* **412:** 754–771

Said N, Krupp F, Anedchenko E, Santos KF, Dybkov O, Huang Y-H, Lee C-T, Loll B, Behrmann E, Bürger J, Mielke T, Loerke J, Urlaub H, Spahn CMT, Weber G und Wahl MC (2017) Structural basis for λN-dependent processive transcription antitermination. *Nat. Microbiol.* **2:** 17062

Salstrom JS und Szybalski W (1978) Coliphage *λnut*L$^-$: a unique class of mutants defective in the site of gene N product utilization for antitermination of leftward transcription. *J. Mol. Biol.* **124:** 195–221

Salzmann M, Pervushin K, Wider G, Senn H und Wüthrich K (1998) TROSY in triple-resonance experiments: new perspectives for sequential NMR assignment of large proteins. *Proc. Natl. Acad. Sci. U. S. A.* **95:** 13585–13590

Santangelo TJ und Artsimovitch I (2011) Termination and antitermination: RNA polymerase runs a stop sign. *Nat. Rev. Microbiol.* **9:** 319–329

Santangelo TJ und Roberts JW (2004) Forward translocation is the natural pathway of RNA release at an intrinsic terminator. *Mol. Cell* **14:** 117–126

Saxena S, Myka KK, Washburn R, Costantino N, Court DL und Gottesman ME (2018) *Escherichia coli* transcription factor NusG binds to 70S ribosomes. *Mol. Microbiol.* **108:** 495–504

Schanda P, Van Melckebeke H und Brutscher B (2006) Speeding up three-dimensional protein NMR experiments to a few minutes. *J. Am. Chem. Soc.* **128:** 9042–9043

Schweimer K, Prasch S, Sujatha PS, Bubunenko M, Gottesman ME und Rösch P (2011) NusA interaction with the α subunit of *E. coli* RNA polymerase is via the UP element site and releases autoinhibition. *Struct. Lond. Engl. 1993* **19:** 945–954

Sen R, Chalissery J, Qayyum MZ, Vishalini V und Muteeb G (2014) Nus Factors of *Escherichia coli*. *EcoSal Plus* **6:** ESP-0008-2013

Sevostyanova A, Belogurov GA, Mooney RA, Landick R und Artsimovitch I (2011) The β subunit gate loop is required for RNA polymerase modification by RfaH and NusG. *Mol. Cell* **43:** 253–262

Shen V und Bremer H (1977) Chloramphenicol-induced changes in the synthesis of ribosomal, transfer, and messenger ribonucleic acids in *Escherichia coli* B/r. *J. Bacteriol.* **130:** 1098–1108

Shi J, Gao X, Tian T, Yu Z, Gao B, Wen A, You L, Chang S, Zhang X, Zhang Y und Feng Y (2019) Structural basis of Q-dependent transcription antitermination. *Nat. Commun.* **10:** 2925

Shimamoto N, Kamigochi T und Utiyama H (1986) Release of the σ subunit of *Escherichia coli* DNA-dependent RNA polymerase depends mainly on time elapsed after the start of initiation, not on length of product RNA. *J. Biol. Chem.* **261:** 11859–11865

Siebenlist U, Simpson RB und Gilbert W (1980) *E. coli* RNA polymerase interacts homologously with two different promoters. *Cell* **20:** 269–281

Singh N, Bubunenko M, Smith C, Abbott DM, Stringer AM, Shi R, Court DL und Wade JT (2016) SuhB Associates with Nus Factors To Facilitate 30S Ribosome Biogenesis in *Escherichia coli*. *mBio* **7:** e00114

Skordalakes E und Berger JM (2006) Structural insights into RNA-dependent ring closure and ATPase activation by the Rho termination factor. *Cell* **127:** 553–564

Skordalakes E und Berger JM (2003) Structure of the Rho transcription terminator: mechanism of mRNA recognition and helicase loading. *Cell* **114:** 135–146

Sosunov V, Sosunova E, Mustaev A, Bass I, Nikiforov V und Goldfarb A (2003) Unified two-metal mechanism of RNA synthesis and degradation by RNA polymerase. *EMBO J.* **22:** 2234–2244

Sosunova E, Sosunov V, Kozlov M, Nikiforov V, Goldfarb A und Mustaev A (2003) Donation of catalytic residues to RNA polymerase active center by transcription factor Gre. *Proc. Natl. Acad. Sci. U. S. A.* **100:** 15469–15474

Squires CL, Greenblatt J, Li J, Condon C und Squires CL (1993) Ribosomal RNA antitermination *in vitro*: requirement for Nus factors and one or more unidentified cellular components. *Proc. Natl. Acad. Sci. U. S. A.* **90:** 970–974

Steitz TA (1998) A mechanism for all polymerases. *Nature* **391:** 231–232

Strauß M, Vitiello C, Schweimer K, Gottesman M, Rösch P und Knauer SH (2016) Transcription is regulated by NusA:NusG interaction. *Nucleic Acids Res.* **44:** 5971–5982

Strobel EJ und Roberts JW (2015) Two transcription pause elements underlie a σ70-dependent pause cycle. *Proc. Natl. Acad. Sci. U. S. A.* **112:** E4374-4380

Strobel EJ und Roberts JW (2014) Regulation of promoter-proximal transcription elongation: enhanced DNA scrunching drives λQ antiterminator-dependent escape from a σ70-dependent pause. *Nucleic Acids Res.* **42:** 5097–5108

Sullivan SL und Gottesman ME (1992) Requirement for *E. coli* NusG protein in factor-dependent transcription termination. *Cell* **68:** 989–994

Svetlov V und Nudler E (2009) Macromolecular micromovements: how RNA polymerase translocates. *Curr. Opin. Struct. Biol.* **19:** 701–707

Thomas MS, Bedwell DM und Nomura M (1987) Regulation of α operon gene expression in *Escherichia coli*. A novel form of translational coupling. *J. Mol. Biol.* **196:** 333–345

Thomsen ND und Berger JM (2009) Running in reverse: the structural basis for translocation polarity in hexameric helicases. *Cell* **139:** 523–534

Torres M, Condon C, Balada JM, Squires C und Squires CL (2001) Ribosomal protein S4 is a transcription factor with properties remarkably similar to NusA, a protein involved in both non-ribosomal and ribosomal RNA antitermination. *EMBO J.* **20:** 3811–3820

Toulokhonov I, Artsimovitch I und Landick R (2001) Allosteric control of RNA polymerase by a site that contacts nascent RNA hairpins. *Science* **292:** 730–733

Toulokhonov I und Landick R (2003) The flap domain is required for pause RNA hairpin inhibition of catalysis by RNA polymerase and can modulate intrinsic termination. *Mol. Cell* **12:** 1125–1136

Tugarinov V und Kay LE (2005) Methyl groups as probes of structure and dynamics in NMR studies of high-molecular-weight proteins. *Chembiochem Eur. J. Chem. Biol.* **6:** 1567–1577

Tugarinov V, Muhandiram R, Ayed A und Kay LE (2002) Four-dimensional NMR spectroscopy of a 723-residue protein: chemical shift assignments and secondary structure of malate synthase g. *J. Am. Chem. Soc.* **124:** 10025–10035

Turtola M und Belogurov GA (2016) NusG inhibits RNA polymerase backtracking by stabilizing the minimal transcription bubble. *eLife* **5:** e18096

Vassylyev DG, Vassylyeva MN, Perederina A, Tahirov TH und Artsimovitch I (2007a) Structural basis for transcription elongation by bacterial RNA polymerase. *Nature* **448:** 157–162

Vassylyev DG, Vassylyeva MN, Zhang J, Palangat M, Artsimovitch I und Landick R (2007b) Structural basis for substrate loading in bacterial RNA polymerase. *Nature* **448:** 163–168

Vogel U und Jensen KF (1997) NusA is required for ribosomal antitermination and for modulation of the transcription elongation rate of both antiterminated RNA and mRNA. *J. Biol. Chem.* **272:** 12265–12271

Vorobiev SM, Gensler Y, Vahedian-Movahed H, Seetharaman J, Su M, Huang JY, Xiao R, Kornhaber G, Montelione GT, Tong L, Ebright RH und Nickels BE (2014) Structure of the DNA-binding and RNA-polymerase-binding region of transcription antitermination factor λQ. *Struct. Lond. Engl. 1993* **22:** 488–495

Vvedenskaya IO, Vahedian-Movahed H, Bird JG, Knoblauch JG, Goldman SR, Zhang Y, Ebright RH und Nickels BE (2014) Interactions between RNA polymerase and the „core recognition element“ counteract pausing. *Science* **344:** 1285–1289

Wang D, Bushnell DA, Westover KD, Kaplan CD und Kornberg RD (2006) Structural basis of transcription: role of the trigger loop in substrate specificity and catalysis. *Cell* **127:** 941–954

Wang D und Landick R (1997) Nuclease cleavage of the upstream half of the nontemplate strand DNA in an *Escherichia coli* transcription elongation complex causes upstream translocation and transcriptional arrest. *J. Biol. Chem.* **272:** 5989–5994

Wang Y, Stieglitz KA, Bubunenko M, Court DL, Stec B und Roberts MF (2007) The structure of the R184A mutant of the inositol monophosphatase encoded by *suhB* and implications for its functional interactions in *Escherichia coli*. *J. Biol. Chem.* **282:** 26989–26996

Wells CD, Deighan P, Brigham M und Hochschild A (2016) Nascent RNA length dictates opposing effects of NusA on antitermination. *Nucleic Acids Res.* **44:** 5378–5389

Werner F (2012) A nexus for gene expression-molecular mechanisms of Spt5 and NusG in the three domains of life. *J. Mol. Biol.* **417:** 13–27

Werner F und Grohmann D (2011) Evolution of multisubunit RNA polymerases in the three domains of life. *Nat. Rev. Microbiol.* **9:** 85–98

Westover KD, Bushnell DA und Kornberg RD (2004) Structural basis of transcription: nucleotide selection by rotation in the RNA polymerase II active center. *Cell* **119:** 481–489

Wiesner S und Sprangers R (2015) Methyl groups as NMR probes for biomolecular interactions. *Curr. Opin. Struct. Biol.* **35:** 60–67

Wilson KS und von Hippel PH (1994) Stability of *Escherichia coli* transcription complexes near an intrinsic terminator. *J. Mol. Biol.* **244:** 36–51

Wishart DS und Sykes BD (1994) The 13C chemical-shift index: a simple method for the identification of protein secondary structure using 13C chemical-shift data. *J. Biomol. NMR* **4:** 171–180

Wishart DS, Sykes BD und Richards FM (1992) The chemical shift index: a fast and simple method for the assignment of protein secondary structure through NMR spectroscopy. *Biochemistry* **31:** 1647–1651

Wüthrich K (1990) Protein structure determination in solution by NMR spectroscopy. *J. Biol. Chem.* **265:** 22059–22062

Yan Y, Zhang D, Zhou P, Li B und Huang S-Y (2017) HDOCK: a web server for protein-protein and protein-DNA/RNA docking based on a hybrid strategy. *Nucleic Acids Res.* **45:** W365–W373

Yarnell WS und Roberts JW (1992) The phage λ gene Q transcription antiterminator binds DNA in the late gene promoter as it modifies RNA polymerase. *Cell* **69:** 1181–1189

Yin Z, Kaelber JT und Ebright RH (2019) Structural basis of Q-dependent antitermination. *Proc. Natl. Acad. Sci. U. S. A.* **116:** 18384–18390

Zaychikov E, Martin E, Denissova L, Kozlov M, Markovtsov V, Kashlev M, Heumann H, Nikiforov V, Goldfarb A und Mustaev A (1996) Mapping of catalytic residues in the RNA polymerase active center. *Science* **273:** 107–109

Zhang G, Campbell EA, Minakhin L, Richter C, Severinov K und Darst SA (1999) Crystal structure of Thermus aquaticus core RNA polymerase at 3.3 A resolution. *Cell* **98:** 811–824

Zhang L, Silva D-A, Pardo-Avila F, Wang D und Huang X (2015) Structural Model of RNA Polymerase II Elongation Complex with Complete Transcription Bubble Reveals NTP Entry Routes. *PLoS Comput. Biol.* **11:** e1004354

Zhou J, Ha KS, La Porta A, Landick R und Block SM (2011) Applied force provides insight into transcriptional pausing and its modulation by transcription factor NusA. *Mol. Cell* **44:** 635–646

Zuo Y und Steitz TA (2015) Crystal structures of the *E. coli* transcription initiation complexes with a complete bubble. *Mol. Cell* **58:** 534–540

6 Eigenanteil

Alle Arbeiten wurden von Stefan H. Knauer betreut.

6.1 Einzelarbeit A

Benjamin R. Dudenhoeffer, Hans Schneider, Kristian Schweimer und Stefan H. Knauer (2019): **SuhB is an integral part of the ribosomal antitermination complex and interacts with NusA.** *Nucleic Acids Research* **47**, 6504–6518.

Die Klonierung der Gene für die Proteine S4 und SuhB sowie deren Expression und Reinigung erfolgten unter meiner Anleitung durch Hans Schneider. Die NMR-Experimente wurden von Stefan H. Knauer, Kristian Schweimer und mir geplant. Unter meiner Anleitung wurden von Hans Schneider die NMR-Titrationen von SuhB mit den Nus-Faktoren durchgeführt, wobei diese aufgrund von Präzipitationsproblemen unter geänderten Puffer-Bedingungen von mir in meiner Doktorarbeit erneut durchgeführt sowie ausgewertet wurden. Alle NMR-Titrationen mit [I,L,V]-NusA ebenso wie alle NMR-basierten Verdrängungsexperimente wurden von mir in meiner Doktorarbeit durchgeführt und evaluiert. Die Herstellung einer Cystein-Variante von NusA-AR2, deren Fluoreszenz-Markierung und die zugehörigen Fluoreszenz-Anisotropie-Titrationen mit SuhB wurden von mir in meiner Doktorarbeit geplant, durchgeführt und ausgewertet. Die Herstellung der *rrnG*-RNA wurde von Stefan H. Knauer geplant und von mir in meiner Doktorarbeit durchgeführt. Die analytischen GF-Läufe wurden von Stefan H. Knauer geplant, durchgeführt und ausgewertet. Alle Abbildungen wurden von mir erstellt und das Manuskript wurde von Stefan H. Knauer und mir, mit Beiträgen aller Autoren, verfasst.

6.2 Einzelarbeit B

Benjamin R. Dudenhoeffer, Jan Borggraefe, Kristian Schweimer und Stefan H. Knauer (2020): **NusA directly interacts with antitermination factor Q from phage λ.** *Scientific Reports* **10,** 6607-6621.

Unter Anleitung von Stefan H. Knauer erfolgte die Etablierung von Expressions- und Reinigungsprotokollen der um 36 Aminosäuren N-terminal verkürzten Variante von λQ ($\lambda Q^{\Delta 36}$) in Jan Borggraefes Masterarbeit sowie von λQ in meiner Masterarbeit. Die Aufnahmen von NMR-Spektren zur Rückgrat-Zuordnung von λQ sowie zur Bestimmung der zugehörigen Relaxationsraten wurden von Kristian Schweimer durchgeführt. Die Rückgrat-Zuordnung von λQ wurde durch Jan Borggraefe in dessen Masterarbeit begonnen. Unter Anleitung von Kristian

Schweimer wurde von mir in meiner Doktorarbeit die Rückgrat-Zuordnung von λQ zu Ende geführt sowie die zugehörigen Relaxationsraten bestimmt. Die NMR-Titrationen von λQ bzw. $\lambda Q^{\Delta 36}$ mit den Nus-Faktoren wurden von Stefan H. Knauer geplant und für $\lambda Q^{\Delta 36}$ in Jan Borggraefes sowie für λQ in meiner Masterarbeit durchgeführt. Aufgrund von Präzipitationsproblemen wurde von mir in meiner Doktorarbeit eine Puffer-Optimierung durchgeführt und unter neuen Puffer-Bedingungen Jan Borggraefes sowie meine NMR-Titrationen erneut von mir durchgeführt und evaluiert. Die NMR-Titrationen zur Modellierung des autoinhibierten Komplexes von NusA sowie alle NMR-basierten Verdrängungsexperimente wurden von mir in meiner Doktorarbeit geplant, durchgeführt und ausgewertet ebenso wie alle Fluoreszenz-Anisotropie-Titrationen. Alle Abbildungen wurden von mir erstellt und das Manuskript von Stefan H. Knauer und mir, mit Beiträgen aller Autoren, verfasst.

6.3 Einzelarbeit C

Benjamin R. Dudenhoeffer, Marlon Wörner, Jan Bodenschlägel, Kristian Schweimer und Stefan H. Knauer: **Antitermination factor λQ mediates NusA-NTD rearrangement on RNAP βflap.** Manuskript.

In meiner Masterarbeit erfolgte, betreut durch Stefan H. Knauer, die Klonierung, Expression und Reinigung des βFlap-Konstrukts der *E. coli* RNAP. Die NMR-Experimente zur Rückgrat-Zuordnung sowie zur Bestimmung der Relaxationsraten des βFlap-Konstrukts wurden von Kristian Schweimer durchgeführt und unter dessen Anleitung von Jan Bodenschlägel ausgewertet. Die NMR-Titrationen von βFlap mit NusA-NTD, λQ und $\lambda Q^{\Delta 36}$ wurden von Stefan Knauer geplant und in meiner Masterarbeit von mir durchgeführt. Aufgrund von Präzipitationsproblemen wurde von mir in meiner Doktorarbeit eine Puffer-Optimierung durchgeführt und unter meiner Anleitung von Marlon Wörner diese NMR-Titrationen unter geänderten Puffer-Bedingungen erneut durchgeführt und ausgewertet. Die NMR-Titrationen von NusA-NTD mit RNAPαCTD, alle NMR-Titrationen mit [I,L,V]-NusA-NTD sowie alle NMR-basierten Verdrängungsexperimente wurden von mir in meiner Doktorarbeit geplant und unter meiner Anleitung von Marlon Wörner in dessen Masterarbeit durchgeführt und evaluiert. Die Planung, Durchführung und Evaluation der NMR-basierten Verdrängungsexperimente von σ^{70}, λQ und NusA-NTD an βFlap bzw. der RNAP erfolgten meinerseits im Rahmen meiner Doktorarbeit. Alle Abbildungen wurden von mir erstellt und das Manuskript von Stefan H. Knauer und mir, mit Beiträgen aller Autoren, verfasst.

7 Einzelarbeiten

7.1 Einzelarbeit A

Benjamin R. Dudenhoeffer, Hans Schneider, Kristian Schweimer und Stefan H. Knauer (2019): **SuhB is an integral part of the ribosomal antitermination complex and interacts with NusA.** *Nucleic Acids Research* **47**, 6504–6518.

Nucleic Acids Research, 2019 **1**
doi: 10.1093/nar/gkz442

SuhB is an integral part of the ribosomal antitermination complex and interacts with NusA

Benjamin R. Dudenhoeffer, Hans Schneider, Kristian Schweimer and Stefan H. Knauer*

Biopolymers, University of Bayreuth, Universitätsstraße 30, 95447 Bayreuth, Germany

Received December 03, 2018; Revised May 06, 2019; Editorial Decision May 07, 2019; Accepted May 08, 2019

ABSTRACT

The synthesis of ribosomal RNA (rRNA) is a tightly regulated central process in all cells. In bacteria efficient expression of all seven rRNA operons relies on the suppression of termination signals (antitermination) and the proper maturation of the synthesized rRNA. These processes depend on N-utilization substance (Nus) factors A, B, E and G, as well as ribosomal protein S4 and inositol monophosphatase SuhB, but their structural basis is only poorly understood. Combining nuclear magnetic resonance spectroscopy and biochemical approaches we show that *Escherichia coli* SuhB can be integrated into a Nus factor-, and optionally S4-, containing antitermination complex halted at a ribosomal antitermination signal. We further demonstrate that SuhB specifically binds to the acidic repeat 2 (AR2) domain of the multidomain protein NusA, an interaction that may be involved in antitermination or posttranscriptional processes. Moreover, we show that SuhB interacts with RNA and weakly associates with RNA polymerase (RNAP). We finally present evidence that SuhB, the C-terminal domain of the RNAP α-subunit, and the N-terminal domain of NusG share binding sites on NusA-AR2 and that all three can release autoinhibition of NusA, indicating that NusA-AR2 serves as versatile recruitment platform for various factors in transcription regulation.

INTRODUCTION

Transcription, the first step in gene expression, is tightly controlled by a multitude of transcriptional regulators at all steps of the transcription cycle, i.e. initiation, elongation, and termination, with RNA polymerase (RNAP) being responsible for RNA synthesis. Under certain circumstances termination signals are suppressed by a process called antitermination (AT), a ubiquitous mechanism to regulate the expression of viral genes in bacteria, bacterial genes, and possibly, genes of archaea and eukaryotes. AT mechanisms were first discovered in context with bacteriophage λ, where they are essential for the phage's life cycle as they control the expression of early and late genes (1). Phage protein λN combines with *Escherichia coli* host proteins, the N-utilization substance (Nus) factors A, B, E, and G, as well as specific RNA sequences, *nutL* and *nutR,* that contain two protein binding elements, *boxA* and *boxB,* and the elongation complex (EC) (2). In the resulting λN- and Nus factor containing antitermination complex (TAC) RNAP is modulated to suppress termination signals (3–7). Nus factors are not only involved in the life cycle of bacteriophages, but are required for the correct expression of genes in bacteria. NusG is member of the only universally conserved family of transcription factors (8) and, in *E. coli*, consists of an N- and a C-terminal domain (NTD, CTD) connected by a flexible linker (9). NusG-NTD binds to RNAP to increase its processivity, NusG-CTD serves as interaction platform for various binding partners, e.g. it interacts with ribosomal protein S10 to couple transcription and translation or with termination factor Rho to stimulate Rho-dependent termination (10,11). During AT NusG-CTD binds to NusE, which is identical to S10, and anchors the NusB:NusE:*boxA* complex to the RNAP (12,13). Highly conserved NusA is composed of six domains in *E. coli* and involved in AT processes (14,15), RNA folding (16), pausing and intrinsic as well as Rho-dependent termination (17). NusA-NTD binds to the β flap tip helix, which forms the mouth of the RNA exit channel, and modulates pausing and termination (5,7,18). The following three domains, S1 and K homology (KH) 1 and KH2, form a compact RNA binding region called NusA-SKK (19). In *E. coli* and other γ-proteobacteria, NusA-SKK is followed by two acidic repeat (AR) domains, AR1 and AR2 (20). NusA-AR1 binds λN during λN-dependent AT (21–23). In free NusA NusA-AR2 interacts with NusA-KH1, autoinhibiting NusA by preventing RNA binding. This autoinhibition can be released by interaction of NusA-AR2 with the CTD of the α subunit of RNAP (αCTD) (24–26). Moreover, NusA-AR2 can bind to NusG-NTD, an interaction that might be involved in NusG recruitment (27).

In many bacteria, Nus factors are also required for the correct expression of ribosomal RNA (rRNA) genes (6,28). rRNA and transfer RNA (tRNA) make up more than 95%

*To whom correspondence should be addressed. Tel: +49 921 553868; Email: stefan.knauer@uni-bayreuth.de

of the total RNA in a bacterial cell and ribosome biosynthesis consumes a major fraction of the energy of the cell (29). Thus, synthesis, cleavage, and maturation of rRNAs as well as their assembly with ribosomal proteins need to be tightly controlled. *E. coli* harbors seven rRNA operons, each comprising the genes coding for 16S, 23S and 5S rRNA. All operons have a leader sequence upstream of the 16S gene and a spacer element between the 16S and the 23S genes. Similar to λN-dependent AT sequences, *E. coli* rRNA operons contain *boxA* and *boxB* elements, both in the leader and in the spacer regions, but in reversed order (30–34). The ribosomal (*rrn*) *boxA* element is essential for *rrn* AT, highly conserved in all seven *rrn* operons in *E. coli* (consensus sequence: UGCUCUUUA), and differs only slightly from λ *boxA* (33). The *boxA* element is specifically recognized by the NusB:NusE heterodimer (35), with NusE being the active AT component while NusB acts as loading factor for NusE (13,36). *boxB* is neither a consensus sequence nor required for *rrn* AT, but has the potential to form an RNA hairpin loop structure (33,34). Additionally, a linear, less well characterized *boxC* element consisting of an alternating GU sequence can be found 3′ of *boxA* in the *rrn* leader region or following *boxB* in lambdoid *nut* sites (33,34). Similar to *boxB, boxC* is not necessary for *rrn* AT (33), but a *boxC* element can also be found in other species such as *Mycobacterium tuberculosis*, where it is part of a binding site that is recognized by NusA (37).

In bacteria, long non-coding RNAs are target for Rho-dependent termination. Thus, RNAP is modified at *boxA* elements of the leader and the spacer region of rRNA operons to suppress Rho-dependent termination *via* assembly of an *rrn* TAC that comprises at least NusA, NusB, NusE and NusG (6,38,39). Complete *rrn* AT cannot be achieved by using purified Nus factors *in vitro* (6), but cell extract is able to stimulate *rrn* AT, and ribosomal protein S4 has been identified as key player in *rrn* AT (40). Moreover, inositol monophosphatase SuhB (41) and translation-associated heat shock protein YbeY (42) are suggested to contribute to correct rRNA biosynthesis. Although AT has long been the accepted role for Nus factors in rRNA synthesis, recent studies suggest that the major role of the Nus factor- and SuhB-modified EC in rRNA operons is to act as RNA chaperone and to co-ordinate transcription with folding of the 16S rRNA and processing by RNase III, ensuring the proper production of 30S subunits (43). Thus, it is unclear if the predominant role of SuhB and Nus factors is to stimulate *rrn* AT or to function post-transcriptionally or if they are essential for both activities as these are not mutually exclusive. It is proposed that SuhB associates directly with RNAP (44), maybe in a NusB-dependent manner (41), and promotes RNA loop formation between elongating RNAP and the *boxA*-bound NusB:NusE complex (41). To date, the structural basis for proper rRNA synthesis ensured by Nus and other factors remains elusive.

Here, we combined biochemical approaches with solution-state nuclear magnetic resonance (NMR) spectroscopy to demonstrate that SuhB can indeed be part of a Nus factor-, and optionally S4-, containing EC halted at an *rrn* AT site. Although it is not yet clear if the resulting complex is involved in AT or acts posttranscriptionally, we will refer to it as *rrn*-TAC. We show that SuhB specifically interacts with NusA-AR2, but that it also binds to RNA as well as to RNAP. Moreover, our analyses reveal that SuhB, RNAP αCTD and NusG-NTD share binding sites on NusA-AR2, and that all three interactions release autoinhibition of NusA, confirming NusA as central regulator in transcription.

MATERIALS AND METHODS

Cloning and mutagenesis

The genes encoding SuhB and S4 were amplified from chromosomal *E. coli* DNA by polymerase chain reaction using the primers listed in Supplementary Table S1. Each gene was cloned into a pETGB1a expression vector (provided by Gunter Stier, EMBL Heidelberg, Germany) *via* BamHI and NcoI restriction sites resulting in the recombinant plasmids pETGB1a_suhb and pETGB1a_s4, respectively. The recombinant target proteins carry a hexa-histidine tag followed by the B1 domain of streptococcal protein G (GB1) and a Tobacco Etch Virus (TEV) cleavage site at their N-termini.

The gene coding for NusA lacking the AR2 domain (amino acids 1–426, NusA$^{\Delta AR2}$) was amplified from pTKK19_NusA(1–495) (27) with primers listed in Supplementary Table S1. The gene was cloned into a modified vector pET19b *via* NdeI and XhoI restriction sites (pET19bmod_nusAΔAR2) so that the resulting fusion protein harbors a hexa-histidine tag followed by a TEV protease cleavage site at its N-terminus.

The exchange of D443 in NusA-AR2 by a cysteine was done according to the QuickChange Site-directed Mutagenesis protocol from Stratagene (Stratagene, La Jolla, USA) using pET19b_nusA-AR2 (24) as template and primers AR2-D443C-FW and AR2-D443C-RV (Supplementary Table S1), resulting in pET19b_nusA-AR2(D443C).

Gene expression and protein purification

Full length NusA was produced as described (27), as was NusA-NTD (45), NusA-SKK (46), NusA-AR1-AR2 (20), NusA-AR2 (27), NusB (12), NusE$^{\Delta}$/B (12), NusG (47), NusG-NTD (47), RNAP (48), α-, β-, β′-, ω-subunit (45) and RNAP α-CTD (20). The production and purification of NusA-AR2^{D443C} were the same as for NusA-AR2.

s4 was expressed in *E. coli* BL21 (λ DE3) (Novagen, Madison, USA) harboring the plasmid pETGB1a_s4. Lysogeny broth (LB) medium supplemented with 30 μg/ml kanamycin was inoculated with a preculture to an optical density at 600 nm (OD_{600}) of 0.2 and grown at 37°C. At an OD_{600} of 0.7 expression was induced by addition of 1 mM isopropyl β-D-1-thiogalactopyranoside (IPTG). Cells were harvested 4 h after induction by centrifugation (6 000 × *g*, 10 min, 4°C), resuspended in buffer S4-A (50 mM tris(hydroxymethyl)aminomethane (Tris)/HCl, pH 7.5, 500 mM NaCl, 10 mM imidazole, 10% (v/v) glycerol, 2 mM Dithiothreitol (DTT)), and lysed by a microfluidizer (Microfluidics, Newton, USA). Upon centrifugation (25 000 × *g*, 30 min, 4°C) the supernatant was applied to a 5 ml HisTrap HP chelating column (GE Healthcare, Chalfont St Giles, UK), which was subsequently washed with buffer S4-A. Elution was carried out *via* a step gradient with increasing imidazole concentrations (10 mM–1 M in buffer S4-

A). Fractions containing His_6-Gb1-S4 were combined and cleaved during overnight dialysis against buffer S4-B (50 mM Tris/HCl, pH 7.5, 400 mM NaCl, 10 mM imidazole, 10% (v/v) glycerol, 2 mM DTT; molecular weight cut-off (MWCO) 3 500 Da) at 4°C by TEV protease. The dialysate was applied to a 5 ml HisTrap HP chelating column connected to a 5 ml Heparin HP column (GE Healthcare, Munich, Germany). After washing with buffer S4-A, the HisTrap HP chelating column was removed and the Heparin HP column was eluted with a constant gradient from 400 mM to 1 M NaCl in buffer S4-A. Fractions containing pure S4 were combined, dialysed against 50 mM 3-(*N*-morpholino)propanesulfonic acid (MOPS) buffer, pH 7.0, 300 mM NaCl, 150 mM D-glucose, 2 mM DTT (MWCO 3 500 Da) at 4°C, concentrated by ultrafiltration (MWCO 3 000 Da), shock frozen in liquid nitrogen, and subsequently stored at −80°C.

Expression of *suhb* was carried out in *E. coli* Rosetta (λ DE3) plysS (Novagen, Madison, USA) containing pETGB1a_suhb. The procedure was the same as for *s4*, except that LB medium was supplemented with 34 μg/ml chloramphenicol in addition to 30 μg/ml kanamycin. Furthermore, 0.5 mM IPTG was used for induction and cells were resuspended in buffer SuhB-A (50 mM Tris/HCl, pH 7.5, 150 mM NaCl, 0.5 mM phenylmethane sulfonyl fluoride (PMSF)). Cell lysis and protein purification were analogous to the procedures described for S4, with buffers as follows. Elution of the first Ni affinity chromatography was performed with a step gradient from 0 to 500 mM imidazole in buffer SuhB-A. Subsequent dialysis and cleavage by TEV protease was carried out in buffer SuhB-B (50 mM Tris/HCl, pH 7.5, 150 mM NaCl). The target protein was eluted from the Heparin HP column *via* a constant gradient with increasing NaCl concentration (150 mM–1 M NaCl in buffer SuhB-B). Pure SuhB was finally dialysed against 50 mM Tris/HCl, pH 7.5, 500 mM NaCl, 10% (v/v) glycerol, 2 mM DTT (MWCO 10 000 Da). Analytical gel filtration on a Superdex 75 10/300 GL column (GE Healthcare, Munich, Germany) showed that the protein existed as monomer in solution.

$NusA^{\Delta AR2}$ was produced in *E. coli* BL21 (λ DE3) harboring the plasmid pET19bmod_nusAΔAR2. The expression procedure resembled the expression of the *s4* gene, with exception that the LB medium was supplemented with 100 μg/ml ampicillin. For purification, cells were resuspended in buffer $NusA^{\Delta AR2}$-A (20 mM Tris/HCl, pH 7.9, 500 mM NaCl, 5 mM imidazole, 1 mM β-mercaptoethanol (β-ME)). Cell lysis and the first step of protein purification (Ni affinity chromatography) were analogous to the procedures described for S4, with a step gradient of 5 mM–1 M imidazole in buffer $NusA^{\Delta AR2}$-A. After cleavage by TEV protease during overnight dialysis at 4°C against buffer $NusA^{\Delta AR2}$-B (20 mM Tris/HCl, pH 8.0, 1 mM β-ME) (MWCO 10 000 Da) the protein solution was applied to a HisTrap HP chelating column coupled to a QXL column (GE Healthcare, Chalfont St Giles, UK). The target protein was eluted from the QXL column *via* a constant gradient with increasing NaCl concentration (150 mM–1 M NaCl in buffer $NusA^{\Delta AR2}$-B). Pure $NusA^{\Delta AR2}$ was dialysed against 50 mM MOPS, pH 7.0, 300 mM NaCl, 150 mM D-glucose, 2 mM DTT (MWCO 3 500 Da) at 4°C, concentrated by ultrafiltration (MWCO 10 000 Da), shock frozen in with liquid nitrogen and stored at −80°C.

Quality control of recombinant proteins

The purity was checked by sodium dodecyl sulfate polyacrylamide gel electrophoresis (SDS-PAGE), the absence of nucleic acids by recording UV/visible spectra on a Nanodrop ND-100 spectrometer (PEQLAB, Erlangen, Germany) from 220 to 600 nm and calculating the ratio of the absorbance at 260 and 280 nm. Concentrations were determined by measuring the absorbance at 280 nm in a 10 mm quartz cuvette (Hellma, Müllheim, Germany) on a Biospectrometer basic (Eppendorf, Hamburg, Germany). The identitiy of SuhB and S4, respectively, was checked by peptide mass finger printing (Department of Biochemistry, University of Bayreuth, Germany). Homogeneity was ensured by analytical gel filtration on a Superdex 75 or a Superdex 200 10/300 GL column (GE Healthcare, Munich, Germany). The folding state was assessed by circular dichroism (CD) spectroscopy (1 mm quartz cuvette; J-1100, JASCO, Pfungstadt, Germany) as well as one dimensional (1D) ^{1}H-NMR spectra in the case of S4 and SuhB.

RNA synthesis and purification

rrnG RNA was produced *via* T7 RNAP-based *in vitro* transcription using T7 RNAP variant P226K (T7 $RNAP^{P226K}$) to enhance transcription efficiency. The *rrnG* DNA template was chemically synthesized (metabion, Planegg, Germany) and contained a T7 promoter, a GGG sequence at the transcription start site to enhance transcription efficiency, and the gene coding for *rrnG* RNA comprising *boxA*, *boxB*, and *boxC* (Supplementary Table S1). Transcription reactions were performed in 40 mM Tris/HCl, pH 8.1, 5 mM DTT, 1 mM spermidine, 28 mM $MgCl_2$, 8% (w/v) polyethylene glycol (PEG) 8 000, 0,01% (v/v) Triton X-100 containing 100 μM *rrnG* DNA template, 4 mM NTPs (ATP, GTP, UTP, CTP) and 100 μg/ml T7 $RNAP^{P226K}$ at 37°C for 4 h. Afterward, the reaction was stopped *via* addition of ethylenediaminetetraacetic acid (EDTA) to a final concentration of 66.8 mM and an ethanol precipitation was performed. The *rrnG* RNA was purified *via* a preparative 20% acrylamide/8 M urea PAGE and subsequent electro elution. The RNA was dialyzed against water, concentrated, lyophilized and stored at −80°C.

Isotopic labeling of proteins

^{15}N-labeled proteins were produced by growing *E. coli* cells in M9 medium (49,50) containing $(^{15}NH_4)_2SO_4$ (Cortec-Net, Voisins-Le-Bretonneux, France). For the production of perdeuterated proteins, *E. coli* cells were grown in M9 medium (49,50) prepared with increasing amounts of D_2O (25% (v/v), 50% (v/v), 99.9% (v/v) D_2O; Eurisotop, Saint-Aubin, France) with d_7-glucose as carbon source. Site-specific [^{1}H,^{13}C]-labeling of Ile, Leu and Val methyl groups ([I,L,V]-labeling) in perdeuterated proteins was performed according to published protocols (51), i.e. expression was carried out as described for the production of perdeuterated proteins, but 60 mg/l 2-keto-3-d_3–4-^{13}C-butyrate and 100

mg/l 2-keto-3-methyl-d_3–3-d_1–4-^{13}C-butyrate (both from Eurisotop, St. Aubin Cedex, France) were added 1 h prior to induction. Expression and purification were as described for the production of unlabeled proteins.

NMR experiments

NMR experiments were carried out on Bruker Avance 700 MHz, Bruker Ascend Aeon 900 MHz and Bruker Ascend Aeon 1 000 MHz spectrometers, equipped with cryogenically cooled inverse triple resonance probes. Data was processed using in-house routines. Two dimensional (2D)/three dimensional (3D) spectra were visualized and analysed by NMRViewJ (One Moon Scientific, Inc., Westfield, NJ, USA), 1D spectra by MatLab (The MathWorks, Inc., Version 7.1.0.183). Assignments for the backbone amide resonances of NusA-AR2 (20), NusA-AR1-AR2(20), NusA-SKK (24) and αCTD (24) were taken from previous studies, the assignment of methyl group signals in full length NusA were adapted from the assignments of individual domains (20,24,52).

All spectra were recorded at 298 K with an initial sample volume of 250 μl, if not stated otherwise. Proteins were in 50 mM MOPS, pH 7.0, 300 mM NaCl, 150 mM D-glucose, 10 mM $MgCl_2$, 2 mM DTT, which was prepared with either H_2O for ^{15}N- and ^{2}H,^{15}N-labeled samples or 99.9% D_2O for [I,L,V]-labeled proteins. 1D spectra and signal intensities of 2D spectra were normalized by protein concentration, number of scans, and length of the 90° proton pulse; the receiver gain was kept constant.

The SuhB binding surface of NusA-AR2 was determined by analyzing the signal intensity in all titration steps of 2D spectra quantitatively. For each titration step the ratios of remaining signal intensities and signal intensities in the spectrum of the free, labeled protein were calculated, yielding relative signal intensities. The mean value of all relative signal intensities in each titration step was determined and thresholds were defined at 1 and 1.5σ of the mean value. Residues with relative signal intensities below these thresholds were classified as moderately or strongly affected, respectively.

Chemical shift changes in methyl-transverse relaxation-optimized spectroscopy (TROSY)-based interaction studies were in the fast regime on the chemical shift timescale and thus analysed by calculating the normalized chemical shift perturbation ($\Delta\delta_{norm}$) according to equation (1) for [^{1}H,^{13}C] correlation spectra.

$$\Delta\delta_{norm} = \sqrt{\left(\Delta\delta^{1}\mathrm{H}\right)^2 + \left[0.25 \cdot \left(\Delta\delta^{13}\mathrm{C}\right)\right]^2} \qquad (1)$$

where Δδ is the resonance frequency difference in ppm.

Leu and Val residues were considered as affected if at least one of the two signals showed a $\Delta\delta_{norm} \geq 0.04$ ppm and only unambiguously assigned signals were used in the analysis. Affected residues were mapped on the 3D structure of NusA with the complete amino acids being highlighted instead of only the methyl group to improve visualization.

Analytical size exclusion chromatography

Analytical size exclusion chromatography on a Superdex 200 Increase 10/300 GL column (GE Helathcare, Munich, Germany) was used to study interactions. Stock solutions of proteins and/or nucleic acids were combined to yield mixtures of equimolar concentration (50 μM of each component; in mixtures containing TACs each component was present at 21 μM). The sequence of the random RNA is given in Supplementary Table S1. 100 μl of the mixtures were incubated for 15 min at room temperature, loaded on the column and chromatographed at 0.3 ml/min at room temperature. 0.5 ml fractions were collected and analyzed by SDS-PAGE (17% PA gels) after trichloracetic acid precipitation or urea PAGE (20% PA gels, 8 M urea) to reveal protein and nucleic acid contents, respectively. The identities of S4 and SuhB were checked by peptide mass finger printing (Department of Biochemistry, University of Bayreuth, Germany). Proteins were in 50 mM Na phosphate buffer, pH 7.0, 75 mM NaCl, 150 mM D-glucose, 2 mM DTT. Quantitative analysis of the PA gels was carried out using the Image Lab Software (Bio-Rad Laboratories, Version 5.2.1).

rrnG-TAC assembly

Assembly of the *rrnG*-TAC and design of the nucleic acids were based on published methods (53). First, an RNA:DNA-hybrid was formed from the template (T) DNA and the RNA (Supplementary Table S1). The stock solution of T DNA (1 mM and in H_2O) was diluted with TAC buffer (50 mM Na phosphate buffer, pH 7.0, 75 mM NaCl, 150 mM D-glucose, 2 mM DTT) by 1:1 and mixed with RNA at an equimolar ratio. The mixture was incubated for 1 min at 95°C, then for 10 min at 70°C, and finally cooled to room temperature within 15 min. RNAP (typically at 50–100 μM) was added at 1.2 molar excess over the hybrid, followed by 10 min incubation at room temperature. Finally, the non-template (NT) DNA strand (Supplementary Table S1; 1 mM stock solution in H_2O; diluted 1:2 with TAC buffer) was added at a molar ratio of 1:1.2:3 (T-DNA/RNA-hybrid:RNAP:NT-DNA) and incubated for 10 min at 37°C.

Fluorescence anisotropy

For fluorescence anisotropy measurements, NusA-AR2^{D443C} was site-specifically labeled with fluorescein-5-maleimide (ThermoFisher Scientific, Waltham, USA) according to the manufacturer's protocol. In brief, 25 μM NusA-AR2^{D443C} were incubated with 750 μM fluorescein-5-maleimide at 4°C overnight (labeling buffer: 20 mM Na phosphate, pH 7.0, 150 mM NaCl). The solution was then applied to a PD MiniTrap Sephadex G-25 gravity column (GE Healthcare, Munich, Germany) equilibrated with fluorescence buffer (50 mM MOPS, pH 7.0, 300 mM NaCl, 150 mM glucose, 5 mM DTT) and eluted with fluorescence buffer to remove non-reacted fluorescein-5-maleimide and to exchange labeling buffer by fluorescence buffer. Finally, the degree of labeling and the protein concentration were determined by UV/vis spectroscopy on a Nanodrop ND-1000 spectrometer (PEQLAB, Erlangen, Germany).

For the titration of NusA-AR2^{D443C} with SuhB individual 100 μl samples were prepared for each titration step, each containing 25 nM labeled NusA-AR2^{D443C} and in-

creasing concentrations of SuhB up to 600 μM. Measurements were done in black, sterile 96-well microtiter plates (Brand, Wertheim, Germany) at 25°C on a Synergy 2 microplate reader (BioTek, Winooski, USA). Both proteins were in fluorescence buffer. Four independent measurements were carried out per titration step and the anisotropy values were averaged. The mean values were plotted against the SuhB concentration. The data was fitted to a two-component binding equation describing the binding equilibrium of a 1:1 binding system to determine the K_D value (54).

Docking

The complex of NusA-AR2 and SuhB was modeled with the HDOCK server (55) using data from the [^{1}H,^{15}N]-heteronuclear single quantum coherence (HSQC) titration of ^{15}N-NusA-AR1-AR2 with SuhB as restraints. Thus, residues 461, 464, 465, 483, 486, 490 and 491 were defined as binding site residues. Model 1 of the NMR ensemble of NusA-AR2 (PDB ID: 1WCN) and chain A of the crystal structure of SuhB (PDB ID: 2QFL) were used as input.

Programs

The PyMOL Molecular Graphics System (Version 1.7, Schrödinger, LLC.) was used for the graphical representation of protein structures.

RESULTS

SuhB integrates into a Nus factor-containing *rrn*-TAC

SuhB is suggested to be part of the rRNA biosynthesis machinery, and thus we probed SuhB interactions in a TAC that is halted at an *rrn* AT site and that harbors all Nus factors by analytical gel filtration using a Superdex 200 column. We produced RNAP, NusA, NusE:NusB, NusG and SuhB recombinantly in *E. coli* and generated an *rrnG* RNA (68 nucleotides) containing linear *boxA* and *boxC* elements as well as a *boxB* hairpin (Supplementary Figure S1A) by *in vitro* transcription. We used a NusE variant lacking the ribosome binding loop (NusE$^{\Delta}$) in complex with NusB to increase its stability (13) in all interaction studies. SuhB existed as monomer in solution. To check the integrity of the *rrnG* RNA we tested its ability to bind to a NusE$^{\Delta}$:NusB heterodimer. The NusE$^{\Delta}$:NusB complex and *rrnG* RNA were mixed in equimolar concentration and NusE$^{\Delta}$:NusB coeluted with the RNA (Supplementary Figure S1B), in agreement with previous findings (12,13,35). Next we assembled a Nus factor- and SuhB-containing TAC resting at the *rrnG* AT site (*rrnG*-TAC). In brief, an EC was assembled using a nucleic acid scaffold (Supplementary Figure S1A, for details see Materials and Methods) that was subsequently incubated with all Nus factors and SuhB. All transcription factors coeluted with RNAP and the *rrnG* RNA (Figure 1A), demonstrating that all components form a complex. However, quantitative analysis revealed that, in contrast to NusA, NusE$^{\Delta}$:B, and NusG, only ∼20% of SuhB coeluted with the *rrnG*-TAC, indicating that the affinity of SuhB for the *rrnG*-TAC is lower than that of the Nus factors. To identify relevant interactions of SuhB in this complex we tested binary systems by mixing SuhB with NusA, NusE$^{\Delta}$:NusB, NusG, RNAP, or RNA in a 1:1 molar ratio (Figure 1B and Supplementary Figure S1C–F). Among the Nus factors SuhB coeluted only with NusA, indicating a direct interaction between them (Figure 1B). Using a NusA variant lacking the AR2 domain (NusA$^{\Delta AR2}$) shows that the SuhB:NusA interaction depends on the presence of AR2 as NusA$^{\Delta AR2}$ and SuhB eluted separately (Figure 1C). However, a SuhB- and Nus factor-containing *rrnG*-TAC could still form when NusA$^{\Delta AR2}$ was used instead of full length NusA (Figure 1D), suggesting that the SuhB:NusA-AR2 interaction is dispensable for SuhB integration if all components are present simultaneously. SuhB also coeluted with *rrnG* RNA (Figure 1E) indicating a direct SuhB:*rrnG* interaction, in agreement with the suggestion that SuhB functions as RNA chaperone and supports RNA loop formation during RNA maturation (41). To test if SuhB exhibits specificity toward *rrnG* RNA a random RNA was analysed. The elution profiles of SuhB and the random RNA overlapped when run separately, but they were not altered at all when the 1:1 mixture was applied to the column (Supplementary Figure S1E), indicating that SuhB might specifically recognize *rrnG* RNA. This finding should, however, be corroborated by an orthogonal technique. Finally, no stable SuhB:RNAP complex could be detected (Supplementary Figure S1F).

Ribosomal protein S4 also contributes to *rrn* AT (40) and, indeed, it coeluted with RNAP, *rrnG* RNA, all Nus factors, and SuhB when all components were present in equimolar concentration (Figure 1F), indicating integration of S4 into a Nus factor- and SuhB-modified *rrnG*-TAC. As observed for SuhB, only a fraction of S4 (∼25%) coeluted with the *rrnG*-TAC, suggesting that its affinity for the *rrnG*-TAC is also lower than that of the Nus factors. A direct interaction between SuhB and S4 could not be detected (Supplementary Figure S1G).

SuhB binds directly to NusA-AR2

We next aimed to corroborate the finding that SuhB directly interacts with NusA-AR2 by solution-state NMR spectroscopy. The addition of full length NusA to ^{15}N-labeled SuhB led to a significant decrease of SuhB signal intensity in the 1D [^{1}H,^{15}N]-heteronuclear single quantum coherence (HSQC) spectrum (Supplementary Figure S2A). The high transversal relaxation rate of the spins of NusA (54.9 kDa) strongly affects magnetization transfer efficiency upon binding, which results in line broadening and thus ultimately in a decrease of signal intensity. Consequently, the loss of ^{15}N-SuhB signal intensity suggests a direct SuhB:NusA interaction. Titrations of ^{15}N-NusE$^{\Delta}$:NusB, ^{15}N-NusB and ^{15}N-NusG with SuhB demonstrated no interaction (Supplementary Figure S2B–D), all in agreement with our gel filtration data. To identify the NusA domain that binds to SuhB, ^{15}N-NusA-NTD, ^{15}N-NusA-SKK and ^{15}N-NusA-AR1-AR2 were titrated with SuhB and 2D [^{1}H,^{15}N]-HSQC spectra were recorded after each step (Figure 2A, B and Supplementary Figure S2E,F). In the presence of SuhB significant changes were only observable in the spectrum of ^{15}N-NusA-AR1-AR2. The chemical shift perturbations were small, but the intensity of sev-

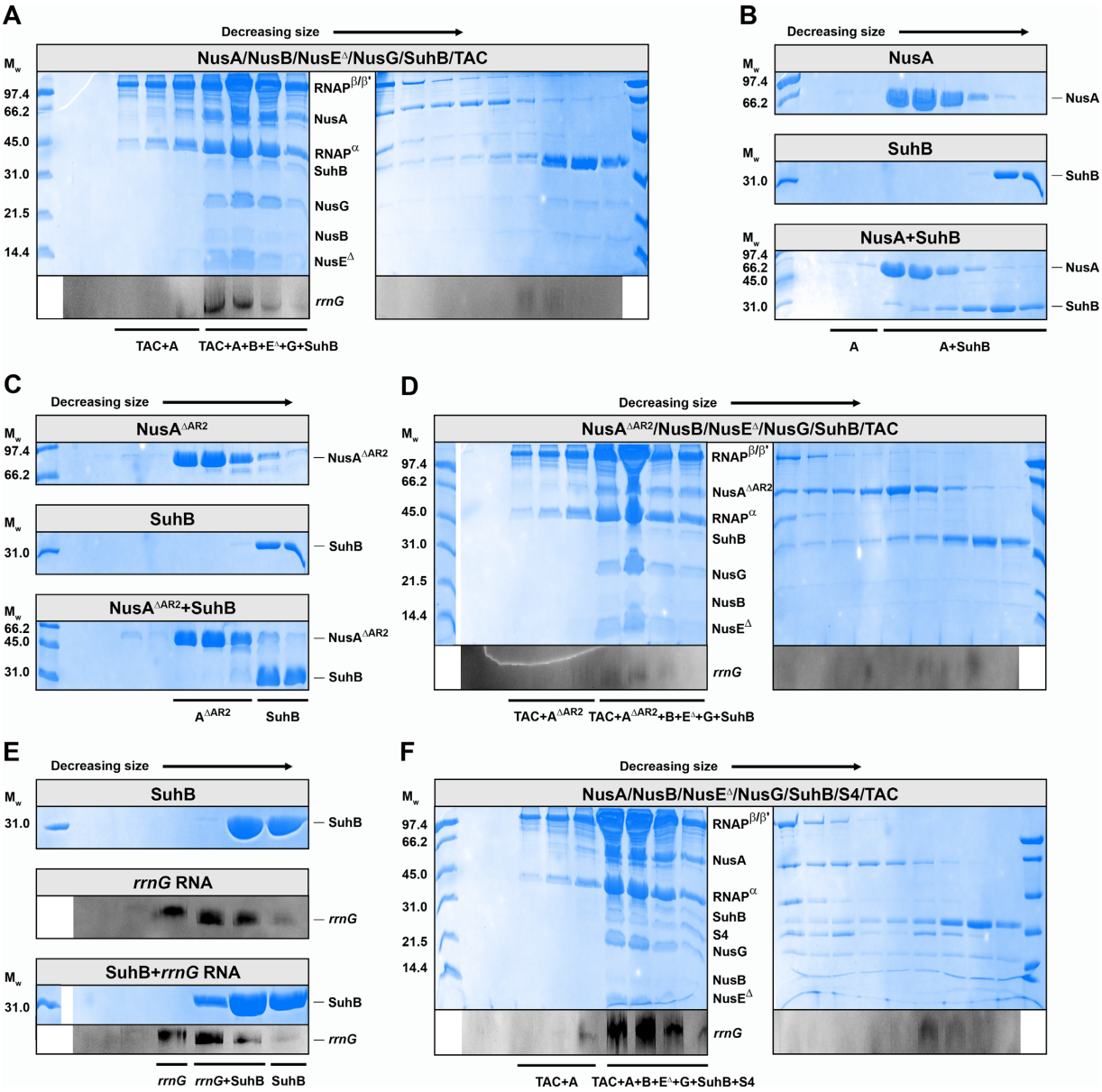

Figure 1. Interaction studies. Analyses of analytical size exclusion chromatography runs by Coomassie-stained SDS-PAGE (proteins, in color) and Toluidine blue-stained urea-PAGE (RNA, in grayscale), monitoring interactions between SuhB, NusA, NusE$^{\Delta}$/B, NusG and the *rrnG*-TAC (**A**), SuhB and NusA (**B**), SuhB and NusA$^{\Delta AR2}$ (**C**), SuhB, NusA$^{\Delta AR2}$, NusE$^{\Delta}$/B, NusG and the *rrnG*-TAC (**D**), SuhB and *rrnG* RNA (**E**), and SuhB, S4, NusA, NusE$^{\Delta}$/B, NusG and the *rrnG*-TAC (**F**). Mixtures loaded for each run are indicated in the boxes above the gels. The left lane shows the marker (SDS-PAGE standard low range, BioRad). Molecular weights (M_W) are indicated on the left, bands are identified on the right or between two gels, and complexes formed are given below the gels. Gels are representative examples of at least two repetitions.

eral signals decreased dramatically, indicating intermediate chemical exchange on the NMR time scale. Plotting the relative signal intensity of ^{15}N-NusA-AR1-AR2 in the presence of 0.5 equivalents of SuhB against the NusA-AR1-AR2 amino acid position clearly shows that only the intensity of signals corresponding to the NusA-AR2 domain were affected (Figure 2C), suggesting that SuhB specifically recognizes and interacts with NusA-AR2, consistent with the results of the analytical gel filtration.

Mapping of the affected residues on the structure of NusA-AR2 reveals that they form a continuous patch at the C-terminal part of NusA-AR2, involving helices α3, α4, α5 and the loops connecting these helices (Figure 2D). The electrostatic surface potential of NusA-AR2 is mostly negative, whereas SuhB exhibits an extensive positively charged area, a large negatively charged region, and a mostly hydrophobic patch, the latter constituting the dimerization interface (Supplementary Figure S3A, B). Based on the affected residues in NusA-AR2 a docking model was generated without conformational rearrangements. In the lowest energy model NusA-AR2 binds to the positively charged area of SuhB *via* helices α3 and α5, positioning NusA-AR2

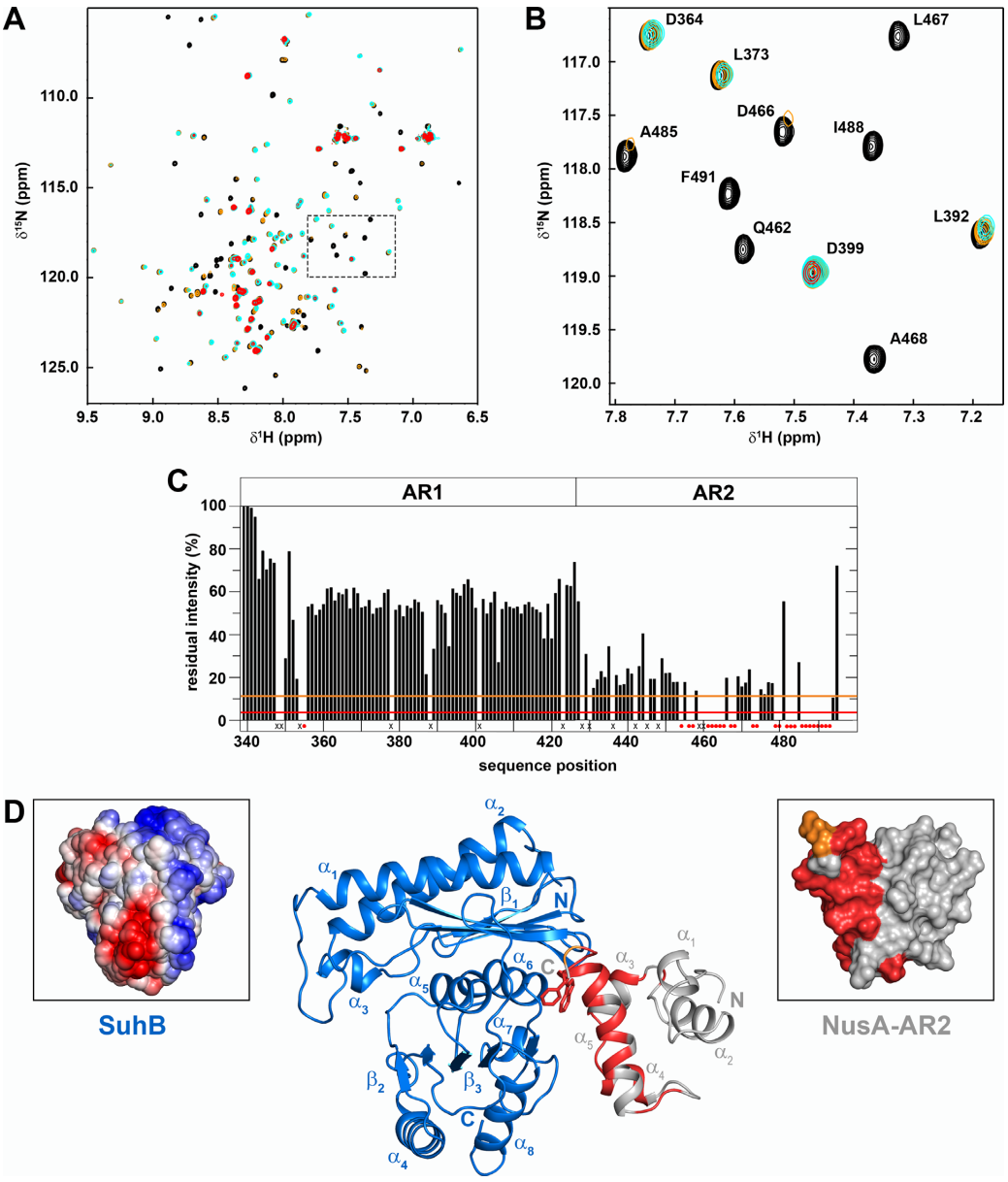

Figure 2. SuhB interacts with NusA-AR2. (**A** and **B**) 2D [^{1}H,^{15}N]-HSQC spectra of the titration of 125 μM ^{15}N-NusA-AR1-AR2 with SuhB. Spectra corresponding to molar ratios 1:0, 1:0.5, 1:1, 1:2 are in black, orange, cyan and red, respectively (stock concentration of SuhB: 471 μM). The dashed box in (**A**) indicates the section as in (**B**). Selected signals are labeled. (**C**) HSQC-derived relative intensity of NusA-AR1-AR2 in the presence of 0.5 equivalents of SuhB. Orange and red lines indicate thresholds for moderately (1 σ of average relative signal intensity) and strongly (1.5 σ of average relative signal intensity) affected signals, respectively. Disappearing signals are indicated by red dots, crosses mark not assigned residues. (**D**) Model of the SuhB:NusA-AR2 complex. The model was generated with HDOCK using the chemical shift perturbations of the [^{1}H,^{15}N]-HSQC titration as restraints for NusA-AR2. The model with the lowest HDOCK score is depicted. SuhB (PDB ID: 2QFL), blue, and NusA-AR2 (PDB ID: 1WCN), gray, are in ribbon representation. Affected residues from (**C**) are mapped on NusA-AR2 (moderately affected residues, orange; strongly affected residues, red). Termini and secondary structure elements are labeled. Panels show the surface representations of SuhB colored according to its electrostatic surface potential (left) and NusA-AR2 colored as in the complex (right).

opposite the dimerization interface of SuhB (Figure 2D). NusA-AR2 residues W490 and F491 located in helix α5 pack against the hydrophobic, C-terminal part of SuhB helix α6.

The K_D of the SuhB:NusA-AR2 interaction was determined by fluorescence anisotropy measurements. For this, D443 in the isolated NusA-AR2 domain, which is located in helix α2 and thus opposite the SuhB binding site, was exchanged by a Cys residue, resulting in NusA-AR2^{D443C}. This NusA-AR2 variant was site-specifically labeled with fluorescein-5-maleimide and titrated with SuhB (Supplementary Figure S3C), yielding a K_D of 83 ± 4 μM. This rather low affinity may be a result of the high salt concen-

tration that had to be present in the buffer to avoid precipitation of SuhB in the stock solution.

SuhB, NusG-NTD and αCTD share binding sites on NusA-AR2

In free NusA the AR2 domain binds to the KH1 domain of the SKK motif, preventing RNA binding by NusA-SKK and rendering NusA autoinhibited (24–26). This autoinhibition can be relieved by the αCTD of RNAP as NusA-SKK and αCTD share binding sites on NusA-AR2 (24). NusA-AR2, however, can also bind to NusG-NTD, an interaction that might be involved in the regulation of Rho-dependent termination or in the recruitment of NusG (27). The binding sites for both NusG-NTD and αCTD on NusA-AR2 involve the C-terminal helix α5 (Supplementary Figure S4). Interestingly, the SuhB binding site of NusA-AR2 also overlaps with the binding sites for αCTD and NusG-NTD (Supplementary Figure S4). All interactions are specific for NusA-AR2 and involve helix α5 of NusA-AR2 with residues W490 and F491 being key determinants (Figure 2C, (24,27)).

To test if interactions of NusA-AR2 with SuhB and αCTD are competitive, we carried out 2D [^{1}H,^{15}N]-HSQC-based displacement experiments with spectra being recorded after each titration step. First, NusA-AR2 was added in equimolar concentration to ^{15}N-αCTD, resulting in chemical shift changes corresponding to ^{15}N-αCTD:NusA-AR2 complex formation (Figure 3A,B), in agreement with previous findings (24). Subsequent titration with SuhB reversed the chemical shift changes (Figure 3A, B), confirming that SuhB displaces the αCTD from NusA-AR2. A reverse displacement experiment was performed (Figure 3C, D) where NusA-AR2 was added to ^{2}H,^{15}N-SuhB in a 1:1 molar ratio, leading to chemical shift perturbations indicating complex formation. Addition of the αCTD reversed those changes, demonstrating the displacement of SuhB from NusA-AR2. The mutual displacement of SuhB and αCTD from NusA-AR2 indicates similar affinities for the SuhB:NusA-AR2 and the αCTD:NusA-AR2 interactions, suggesting that both are physiologically relevant.

SuhB, NusG-NTD and αCTD can release autoinhibition of NusA

The αCTD is able to release autoinhibition of NusA by removing NusA-AR2 from NusA-SKK (24–26). Thus, we probed if NusG-NTD and SuhB have the same capability by NMR-based displacement experiments. We first titrated ^{2}H,^{15}N-labeled NusA-SKK with NusA-AR2 and recorded [^{1}H,^{15}N]-band-selective excitation short-transient transverse relaxation-optimized spectroscopy (BEST-TROSY) spectra after each titration step to determine the chemical shift perturbations caused by binding of NusA-AR2 to the NusA-SKK domain (Figure 4A), which were in agreement with previous data (24). Addition of NusG-NTD to the preformed ^{2}H,^{15}N-NusA-SKK:NusA-AR2 complex led to partial reversal of all shifts, indicating displacement of NusA-AR2 from NusA-SKK (Figure 4B). Similarly, SuhB was able to displace NusA-AR2 from NusA-SKK (Figure 4C).

The interaction probability of NusA-AR2 with NusA-SKK may, however, be higher in full length NusA as the domains are covalently connected resulting in a higher local concentration. Thus, we repeated the displacement experiments in the context of the full length protein. Due to the high molecular mass of the system we used ^{1}H,^{13}C-labeled methyl groups of Ile, Leu, and Val residues in a perdeuterated background as NMR-active probes ([I,L,V]-NusA). SuhB was titrated to [I,L,V]-NusA and methyl-TROSY spectra were recorded after each titration step (Figure 5A,B). Normalized changes of the chemical shifts were calculated to identify affected residues (Supplementary Table S2), which were then mapped on the three dimensional structure of NusA (Figure 5C). Affected residues can only be found in the C-terminal region of NusA-AR2 and the β-sheet of the NusA-KH1 subdomain, indicating that SuhB is able to release NusA autoinhibition as KH1 is the binding site for the AR2 domain in autoinhibted NusA (24) and the C-terminal region of NusA-AR2 is the binding site for SuhB (see Figure 2D). This finding corroborates our gel filtration data as SuhB is able to interact with NusA even in the absence of any other factors (Figure 1B). Similarly, NusG-NTD (Supplementary Table S3 and Supplementary Figure S5) and the αCTD (Supplementary Table S4 and Supplementary Figure S6) can release the autoinhibition of NusA. However, in the presence of the αCTD, several residues in NusA-NTD are also strongly affected and form a patch opposite the β flap tip helix binding site (Supplementary Figure S6C), indicating that the αCTD can also bind to NusA-NTD, in agreement with a cryo electron microscopy structure of NusA bound to a paused EC where one αCTD is bound to NusA-AR2 and the other αCTD interacts with NusA-NTD (18).

SuhB interacts weakly with RNAP

SuhB has been reported to associate with RNAP (44) and the EC (41,56), but SuhB did not coelute with RNAP alone in our gel filtration experiments (Supplementary Figure S1F). Nevertheless, we tested if SuhB can bind to RNAP by solution-state NMR spectroscopy. We recorded 1D [^{1}H,^{15}N]-HSQC spectra of ^{15}N-SuhB in the absence and presence of RNAP (Supplementary Figure S7A). Addition of RNAP led to a significant decrease of ^{15}N-SuhB signal intensity due to enhanced magnetization relaxation upon ^{15}N-SuhB:RNAP complex formation. As binding of SuhB to RNAP was not observable in the gel filtration experiments we conclude that this interaction is only weak and transient and may be not detectable in non-equilibrium methods. To identify the interacting RNAP subunit we added individual RNAP subunits to ^{15}N-labeled SuhB and recorded 1D or 2D [^{1}H,^{15}N]-HSQC spectra (Supplementary Figure S7B–E). The spectrum of ^{15}N-SuhB was only significantly affected in the presence of the β or the β' subunit, suggesting that SuhB might interact with either or both simultaneously.

DISCUSSION

Nus factors and their role in the proper expression of rRNA have been studied for a long time. *rrn* AT is a documented

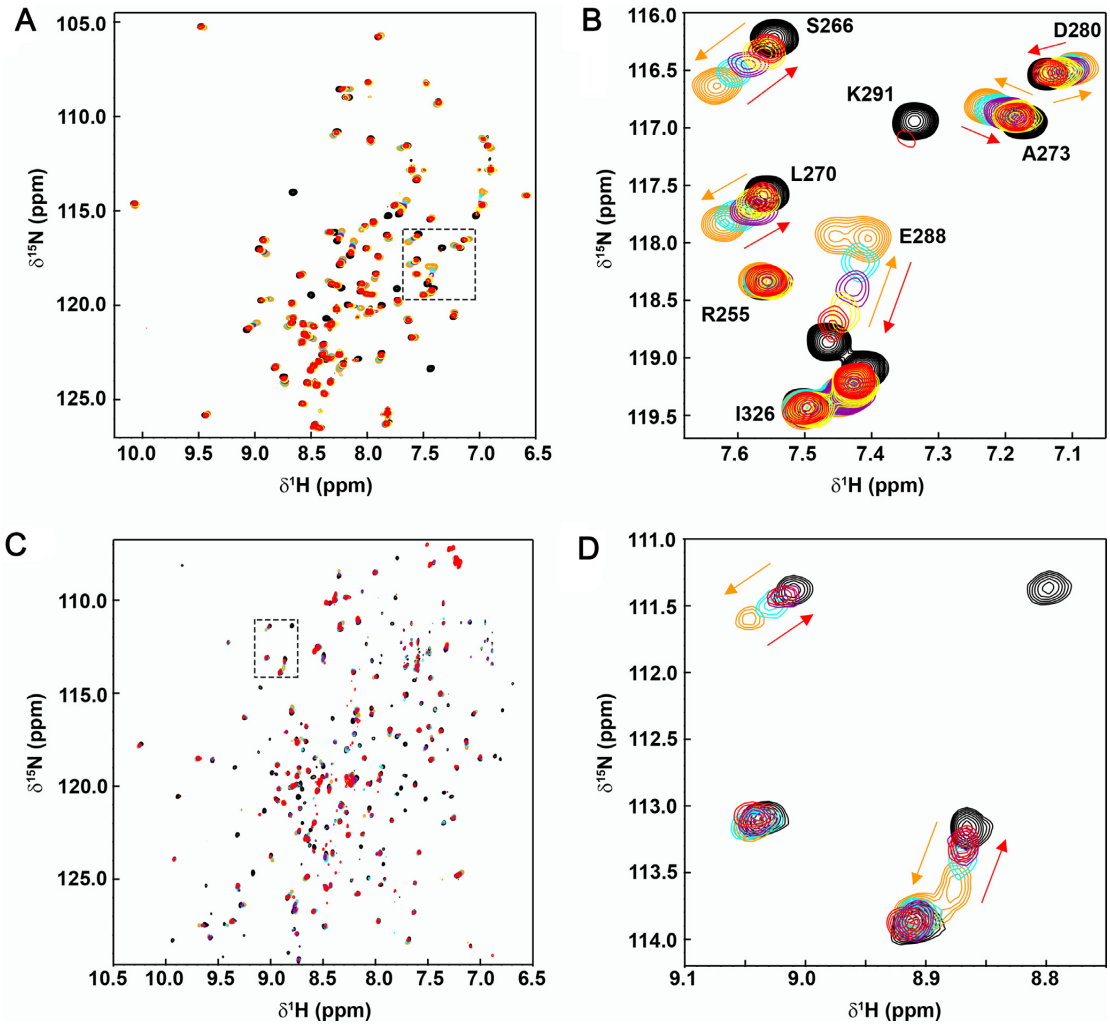

Figure 3. The αCTD and SuhB share binding sites on NusA-AR2. (**A** and **B**) [^{1}H,^{15}N]-HSQC displacement of NusA-AR2 from ^{15}N-αCTD by SuhB. ^{15}N-αCTD:NusA-AR2:SuhB = 1:0:0, black; = 1:1:0, orange; = 1:1:1, cyan; = 1:1:2, purple; = 1:1:5, yellow; = 1:1:10, red. Initial concentration of ^{15}N-αCTD: 200 μM; stock concentrations of NusA-AR2 and SuhB were 941 μM and 597 μM, respectively. The dashed box in (**A**) indicates the section as in (**B**). In (**B**), selected signals are labeled and arrows show the changes in their chemical shifts upon addition of NusA-AR2 (orange) and SuhB (red). (**C** and **D**) [^{1}H,^{15}N]-BEST-TROSY displacement of NusA-AR2 from ^{2}H,^{15}N-SuhB by αCTD. ^{2}H,^{15}N-SuhB:NusA-AR2:αCTD = 1:0:0, black; = 1:1:0, orange; = 1:1:1, cyan; = 1:1:2, purple; = 1:1:5, red. Initial concentration of ^{2}H,^{15}N-SuhB: 250 μM; stock concentrations of NusA-AR2 and αCTD were 759 and 793 μM, respectively. The dashed box in (**C**) indicates the section as in (**D**). In (**D**), arrows show the changes in the chemical shifts of selected signals upon addition of NusA-AR2 (orange) and αCTD (red).

activity of an *rrn*-TAC that comprises minimally RNAP, Nus factors and nucleic acids (6). Highly efficient *rrn* AT, however, cannot be achieved by this 'minimal' *rrn*-TAC, but *rrn* AT is strongly stimulated in the presence of cell extract (6), indicating that additional factors are involved. There is, for example, solid evidence that ribosomal protein S4 plays a central role in *rrn* AT (40). Despite some functional similarities of λN-dependent and *rrn* AT (38,57), no central unstructured component such as λN has yet been identified in *rrn* AT. Inositol monophosphatase SuhB and translation-associated heat shock protein YbeY are also involved in rRNA biosynthesis (41,42).

Here, we show that SuhB can form a complex with a Nus factor-containing TAC halted at an *rrnG* AT site with the RNA harboring *boxA, boxB* and *boxC* motifs (Figure 1A). This finding is in agreement with *in vivo* experiments showing that a *boxA* element and Nus factors recruit SuhB, which then remains associated with RNAP throughout transcription of rRNA (41). S4 is involved in *rrn* AT (40), and we demonstrate that SuhB can also be integrated into a Nus factor- and S4-containing *rrnG*-TAC, but S4 interactions within this complex remain elusive (Figure 1F). We studied the interactions of SuhB with all components in this complex and found that SuhB directly interacts with the AR2 domain of NusA, but highly likely with no other Nus factor or S4 (Figures 1 and 2 and Supplementary Figures S1 and S2). *E. coli* SuhB has an inositol monophosphatase activity, which it exerts—unlike other inositol monophosphatases—as monomer, although it can occur in a monomer-oligomer equilibrium in solution (58). In our experiments SuhB exists as monomer, indicating that SuhB performs its function as transcription factor in its

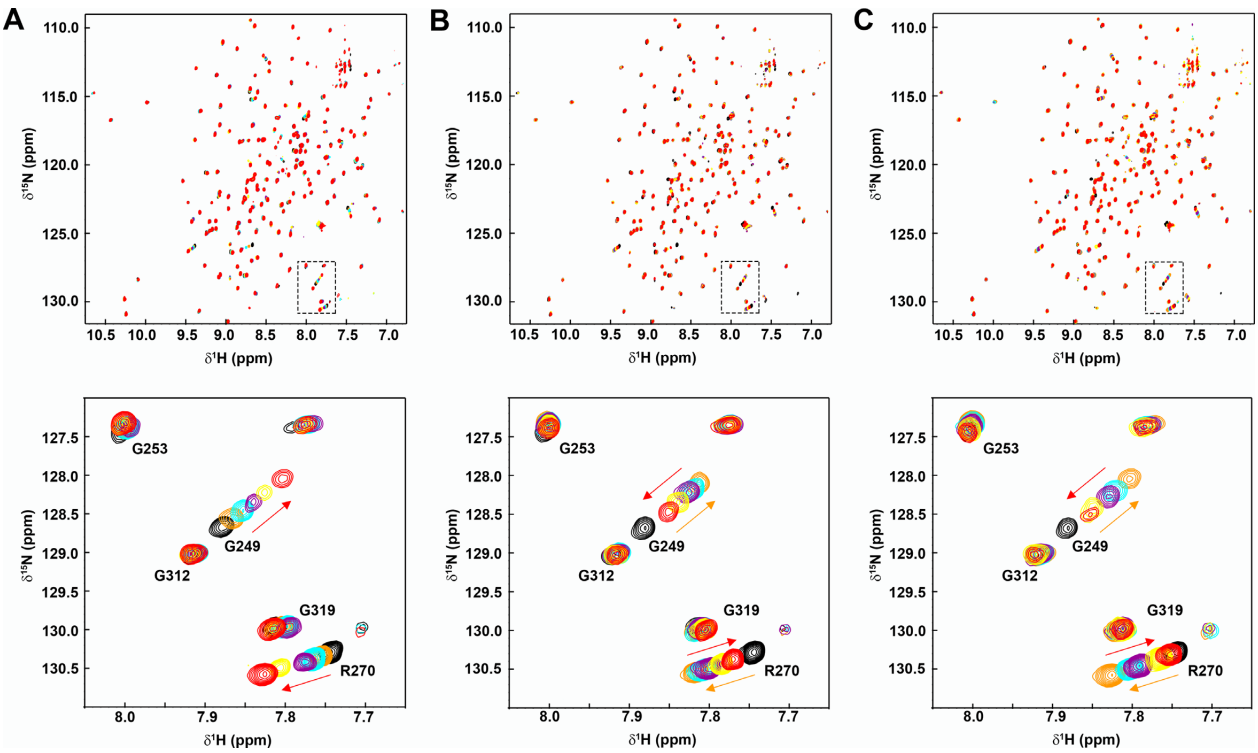

Figure 4. NusG-NTD and SuhB displace NusA-AR2 from NusA-SKK. (**A**) Interaction of NusA-SKK with NusA-AR2. [^{1}H,^{15}N]-BEST-TROSY spectra of the titration of 175 μM ^{2}H,^{15}N-NusA-SKK with NusA-AR2. NusA-AR2 was added in a molar ratio of 1:0, black; 1:0.5, orange; 1:1, cyan; 1:2, purple; 1:3, yellow; 1:5, red. The dashed box in the top panel indicates the section shown in the bottom panel. Selected signals are labeled and the changes in their chemical shifts are indicated by arrows. (**B**) [^{1}H,^{15}N]-BEST-TROSY displacement experiment of NusA-AR2 from ^{2}H,^{15}N-NusA-SKK by NusG-NTD. ^{2}H,^{15}N-NusA-SKK: NusA-AR2:NusG-NTD = 1:0, black; = 1:5, orange; = 1:5:1, cyan; = 1:5:2, purple; = 1:5:5, yellow; = 1:5:10, red. Initial concentration of ^{2}H,^{15}N-NusA-SKK: 200 μM; stock concentrations of NusA-AR2 and NusG-NTD were 941 and 1098 μM, respectively. The dashed box in the top panel indicates the section as in the bottom panel. Selected signals are labeled and arrows show the changes in their chemical shifts upon addition of NusA-AR2 (orange) and NusG-NTD (red). (**C**) [^{1}H,^{15}N]-BEST-TROSY displacement experiment of NusA-AR2 from ^{2}H,^{15}N-NusA-SKK by SuhB. ^{2}H,^{15}N-NusA-SKK: NusA-AR2:SuhB = 1:0, black; = 1:5, orange; = 1:5:1, cyan; = 1:5:2, purple; = 1:5:5, yellow; = 1:5:10, red. Initial concentration of ^{2}H,^{15}N-NusA-SKK: 200 μM; stock concentrations of NusA-AR2 and SuhB were 969 μM and 562 μM, respectively. The dashed box in the top panel indicates the section as in the bottom panel. Selected signals are labeled and arrows show the changes in their chemical shifts upon addition of NusA-AR2 (orange) and SuhB (red).

monomeric state. As there is no requirement for an inositol monophosphatase activity in *E. coli* (59), our findings support the proposal that widely conserved SuhB has two unrelated functions with gene regulation being the primary one (41). The SuhB:NusA-AR2 interaction is dispensable for SuhB integration into a Nus factor containing *rrnG*-TAC if all components are present simultaneously (Figure 1D). However, SuhB not only interacts with NusA-AR2, but it also binds to *rrnG* RNA, in agreement with the finding that it may act as RNA chaperone to support the formation of RNA loops formation during RNA maturation (41). Furthermore, NMR experiments indicated that SuhB can also bind to RNAP (Supplementary Figure S7), although this interaction is weak and transient as it was not observable *via* gel filtration (Supplementary Figure S1F). It has been reported previously that *E. coli* SuhB associates with elongating RNAP (41) and binds to σ factor-containing RNAP (44) and that SuhB from *Pseudomonas aeroguinosa* associates with RNAP *in vivo* (56), but nevertheless it remains to be determined if the SuhB:RNAP interaction detected *via* NMR spectroscopy is specific and of physiological relevance.

Taking together all findings we suggest several functions for the SuhB:NusA-AR2 interaction during *rrn* AT (Figure 6). First, it may be involved in the assembly of the *rrn*-TAC (Figure 6A). Although SuhB can be integrated into a Nus factor-modified *rrn*-TAC in the absence of the AR2 domain (Figure 1D), the SuhB:NusA-AR2 interaction might, nevertheless, contribute to SuhB recruitment if not all components are present at the same time, but if the *rrn*-TAC is assembled in a stepwise manner, as known from other TACs. The λN-dependent TAC, for example, is assembled cooperatively and involves binary interactions that are occasionally not stable when studied in isolation (5,7). However, as SuhB binds to *rrnG* RNA we hypothesize that the RNA:SuhB interaction is the key player in SuhB recruitment, in agreement with reports that SuhB is incorporated in a NusB/*boxA*-dependent manner (41). No direct interaction between SuhB and NusB could be detected *in vitro* (Supplementary Figures S1C and S2B), implying that this dependence is most likely indirect. Alternatively, the SuhB:NusA-AR2 interaction could promote the recruitment of other components of the *rrn*-TAC during the stepwise assembly of the complex, e.g. the NusB:NusE

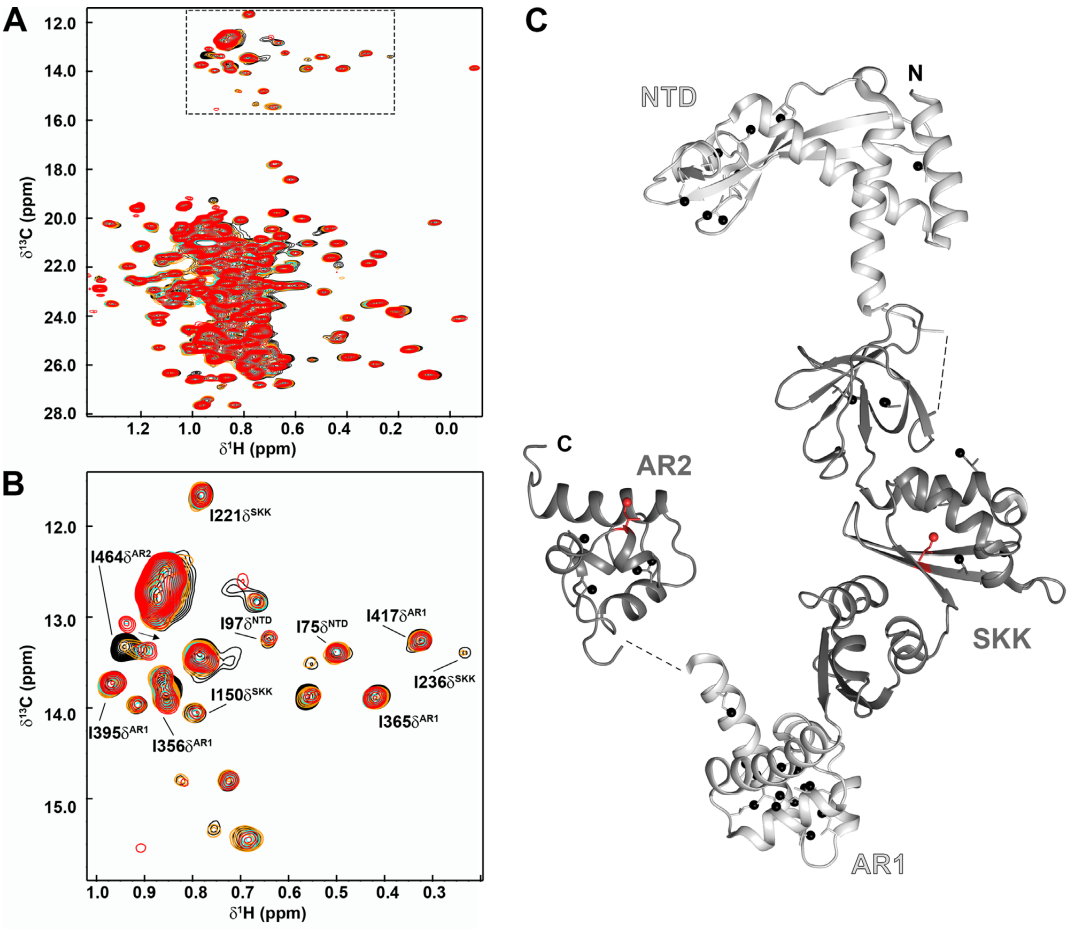

Figure 5. SuhB releases autoinhibition of NusA. (**A** and **B**) [^{1}H,^{13}C]-methyl-TROSY spectra of the titration of 25 μM [I,L,V]-NusA with SuhB. SuhB was added in a molar ratio of 1:0, black; 1:0.5, orange; 1:1, cyan; 1:2, purple; 1:3, yellow; 1:5, red (concentration of SuhB stock: 343 μM). The boxed region in (**A**) indicates the section as in (**B**). Selected signals are labeled. (**C**) Structure of NusA in ribbon representation. Linker regions are indicated by dashed lines. Ile, Leu, and Val residues with assigned methyl groups are shown as sticks with carbon atoms of the methyl groups as black spheres. If a methyl group was affected upon addition of SuhB ($\Delta\delta_{norm} \geq 0.04$ ppm) the whole residue was colored in red (see also Supplementary Table S2). PDB IDs: NusA-NTD: 2KWP, SKK-AR1: 5LM9, NusA-AR2: 1WCN.

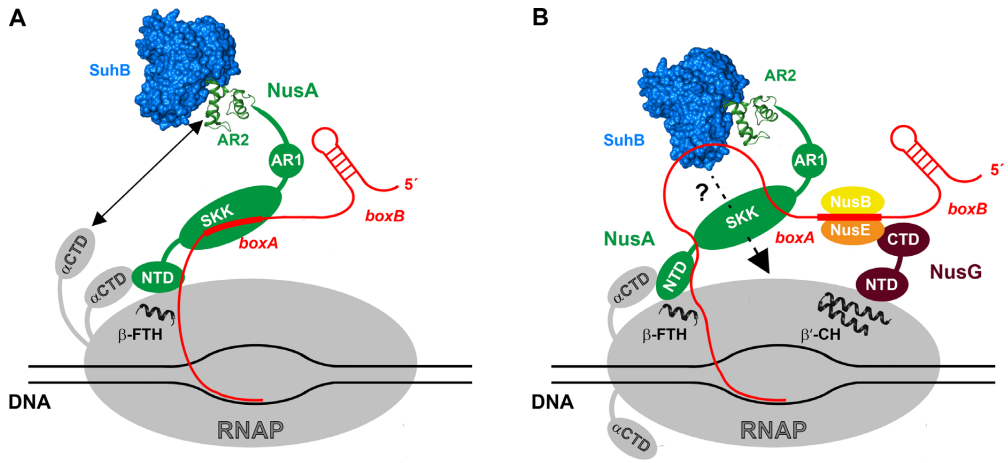

Figure 6. Scheme of the possible functions of the SuhB:NusA-AR2 interaction during *rrn* AT. The SuhB:NusA-AR2 interaction may be involved in the assembly of the SuhB- and Nus factor-containing *rrn*-TAC (**A**) or in suppressing Rho-dependent termination by repositioning of NusA (**B**). SuhB (blue) is depicted in surface, NusA-AR2 (green) in ribbon representation. Important binding sites on RNAP are highlighted in ribbon representation. The solid arrow in (**A**) illustrates the αCTD:NusA-AR2 interaction and thus the competition of the αCTD and SuhB for NusA-AR2, the dashed arrow in (B) indicates the putative SuhB:RNAP interaction. β-FTH: β flap tip helix, β'-CH: β' clamp helices. PDB IDs: SuhB: 2QFL, NusA-AR2: 1WCN.

heterodimer. The NusB:NusE complex binds specifically to *boxA* (12,35), whereas the regions upstream and downstream of *boxA* constitute a binding site for NusA-SKK (46). In a λN-dependent TAC NusA-SKK and NusB:NusE can bind simultaneously to RNA (5,7) as the order of *boxA* and *boxB* is reversed as compared to rRNA operons (33). NusA is recruited early during transcription (60) and could thus hinder the access of NusB:NusE to *boxA via* two ways: (i) NusA could bind in its autoinhbited state to RNAP *via* NusA-NTD, sterically blocking access to *boxA*, or (ii) upon release of autoinhibition by the αCTD, NusA-SKK could bind to the regions flanking *boxA*, masking the NusB:NusE binding site. SuhB binds to *rrnG* RNA (Figure 1E), interacts with NusA-AR2 (Figure 2) and can even release autoinhibition of NusA (Figure 5), and may consequently alter the RNA binding properties of NusA. Thus, the SuhB:NusA-AR2 interaction might affect the overall conformation of NusA or directly the NusA-SKK:RNA interaction in a way that removes NusA from *boxA*, allowing recruitment of NusB:NusE. Finally, the SuhB:NusA-AR2 interaction may additionally stabilize the *rrn*-TAC during processive AT. If the SuhB:NusA-AR2 interaction remains stable throughout complete transcription of rRNA and if SuhB establishes specific contacts with RNAP remains to be determined.

Second, the SuhB:NusA-AR2 interaction could modify RNAP into a termination-resistant state (Figure 6B) *via* different ways: (i) SuhB could affect the positioning of NusA on RNAP. During elongation NusA-NTD interacts with the β flap tip helix at the RNA exit channel while it is concomitantly bound by one of the αCTDs (18). The second αCTD interacts with NusA-AR2, tethering NusA to the RNAP in a defined conformation with limited flexibility (18,46). As indicated by the displacement experiments the affinity of the SuhB:NusA-AR2 and the NusA-AR2:αCTD interaction is similar (Figure 3), and the concentration of SuhB is approximately half the concentration of RNAP molecules (61). Thus, SuhB might displace the αCTD from NusA-AR2 and consequently change the conformation and consequently influence the positioning of NusA, a principle reminiscent of λN-dependent AT (5,7). How this rearrangement could contribute to suppressing Rho-dependent termination remains elusive, although one may speculate that NusA blocks accession of Rho to its recruitment site on the RNA. (ii) SuhB itself could prevent recruitment of Rho by interacting with RNA and thus sterically blocking the Rho binding site of the RNA.

A recent study showed that Nus factors and SuhB can act as RNA chaperones and suggested that this function may be their major role at rRNA operons, ensuring the proper folding of 16S RNA and thus being critical for the biogenesis of the 30S subunit (43). Our results demonstrate that SuhB can be integrated into a Nus factor-containing *rrn*-TAC, a complex that may be involved in *rrn* AT as well as in post-transcriptional processes in rRNA biosynthesis. If the SuhB:NusA-AR2 interaction is required for both RNA chaperone and AT activity or just one of them needs to be determined as does the question if further factors are involved in *rrn* AT. More general, as *boxA* elements, which recruit NusB:NusE, are widespread, the regulation by Nus factors and SuhB may not be limited to rRNA operons, but may play a role in the expression of many genes in diverse bacterial species, including autoregulation of Nus factors (62).

NusA-AR1 and NusA-AR2 share a high sequence identity of 31.5% and exhibit nearly identical structures (root mean square deviation of main chain atoms: 1.2 Å) with a very similar electrostatic potential surface (20). Nevertheless, SuhB exclusively recognizes NusA-AR2 (Figure 2). This binding specificity can probably be attributed to the presence of two residues in the C-terminal helix α5 of NusA-AR2, W490 and F491. In NusA-AR1, a Leu (L414) and an Ala (A415) residue can be found at corresponding positions. NusG-NTD and the αCTD also specifically bind to NusA-AR2 (24,27), while λN only interacts with NusA-AR1 (20,22). The interaction surfaces on NusA-AR2 with αCTD, NusG-NTD, and SuhB overlap and all involve helix α5 (Supplementary Figure S4), in particular residues W490 and F491. The NusA-AR2 domain constitutes the very C-terminus of NusA and all domains are connected *via* linkers conferring NusA high intramolecular flexibility. When attached to RNAP *via* NusA-NTD and to RNA *via* NusA-SKK, the AR domains can still move virtually independently. This together with the high specificity suggests that NusA-AR2 may serve as versatile and efficient recruitment platform for various transcription factors in *E. coli* and other γ-proteobacteria. Upon recruitment, these factors may then be made available to interactions with other factors or RNAP to be integrated into regulatory transcription complexes. Moreover, NusA-AR2 shares some features with the acidic activation domains (ADs) found in eukaryotic transcription activators. Similar to NusA, these transcription factors usually exhibit a modular structure, comprising at least one DNA binding domain and one AD, the latter being essential for the interaction with other transcription factors, RNAP or coactivators (63). Generally, ADs show no apparent sequence conservation and are usually intrinsically disordered regions (IDRs) in the absence of binding partners, but, like NusA-AR2, they interact with structurally diverse binding partners (64). ADs are classified according to the preponderance of certain amino acids with the so called *acidic ADs* containing clusters of negatively charged amino acids ('acidic blobs') and consequently a negative net charge (65,66). Although acidic ADs are enriched in acidic amino acids their interaction with binding partners does usually not rely on these residues (67). Instead, specific recognition is mediated *via* short motifs of bulky hydrophobic residues in the IDRs that are occasionally presented on one side of one or two α-helices which form in the presence of a binding partner (68–71). This recognition mode is reminiscent of NusA-AR2 where W490 and F491, which are located on one side of helix α5 in the mainly negatively charged domain, are the key determinants for the interaction with SuhB, αCTD and NusG-NTD.

Autoinhibition is an important regulatory mechanism that is widespread in nature (72). Intramolecular interactions between different regions of a polypeptide that may even be coupled to conformational changes inhibit the function of at least one of these regions. This negative regulation limits activation of the protein/enzyme to certain physiological conditions and alters the activity of proteins in-

volved in diverse cellular processes, ranging from transcription factors (73) to E3 ubiquitin ligases (74) and protein kinases (75). In NusA the AR2 domain binds to the KH1 domain of the RNA binding SKK motif, preventing RNA binding and thus autoinhibiting NusA to allow context-dependent RNA binding (24,25). NusA autoinhibition can be released by the αCTD (24), NusG-NTD (27) and SuhB that all bind to NusA-AR2 (Figure 5, Supplementary Figures S5 and S6). The ability of NusA-AR2 to specifically recognize various other transcription factors and the fact that these interactions can activate NusA underline the central role of NusA in transcription regulation.

DATA AVAILABILITY

We generated a model of the SuhB:NusA-AR2 complex. Coordinates of SuhB and NusA-AR2 are available in the PDB (2QFL, 1WCN). The coordinates of the best model are provided as Supplementary Data.

Resonance assignments of NusA-AR2, NusA-AR1-AR2, NusA-SKK, NusA-NTD and αCTD were taken from previous studies as indicated in the manuscript.

SUPPLEMENTARY DATA

Supplementary Data are available at NAR Online.

ACKNOWLEDGEMENTS

We thank Paul Rösch for helpful discussions, Ramona Heissmann, Ulrike Persau and Andrea Hager for excellent technical assistance, and the Northern Bavarian NMR Centre (NBNZ) for access to the NMR spectrometers.

FUNDING

German Research Foundation [Ro617/21-1 to P.R.]. Funding for open access charge: German Research Foundation and the University of Bayreuth in the funding program Open Access Publishing.
Conflict of interest statement. None declared.

REFERENCES

1. Gottesman,M.E. and Weisberg,R.A. (2004) Little lambda, who made thee? *Microbiol. Mol. Biol. Rev.*, **68**, 796–813.
2. Roberts,J.W. (1993) RNA and protein elements of *E. coli* and lambda transcription antitermination complexes. *Cell*, **72**, 653–655.
3. de Crombrugghe,B., Mudryj,M., DiLauro,R. and Gottesman,M. (1979) Specificity of the bacteriophage lambda N gene product (pN): *nut* sequences are necessary and sufficient for antitermination by pN. *Cell*, **18**, 1145–1151.
4. Olson,E.R., Flamm,E.L. and Friedman,D.I. (1982) Analysis of *nutR*: a region of phage lambda required for antitermination of transcription. *Cell*, **31**, 61–70.
5. Said,N., Krupp,F., Anedchenko,E., Santos,K.F., Dybkov,O., Huang,Y.-H., Lee,C.-T., Loll,B., Behrmann,E., Bürger,J. *et al.* (2017) Structural basis for λN-dependent processive transcription antitermination. *Nat. Microbiol.*, **2**, 17062.
6. Squires,C.L., Greenblatt,J., Li,J., Condon,C. and Squires,C.L. (1993) Ribosomal RNA antitermination *in vitro*: requirement for Nus factors and one or more unidentified cellular components. *Proc. Natl. Acad. Sci. U.S.A.*, **90**, 970–974.
7. Krupp,F., Said,N., Huang,Y.-H., Loll,B., Bürger,J., Mielke,T., Spahn,C.M.T. and Wahl,M.C. (2019) Structural basis for the action of an all-purpose transcription anti-termination factor. *Mol. Cell*, **74**, 143–157.
8. Werner,F. (2012) A nexus for gene expression-molecular mechanisms of Spt5 and NusG in the three domains of life. *J. Mol. Biol.*, **417**, 13–27.
9. Mooney,R.A., Schweimer,K., Rösch,P., Gottesman,M. and Landick,R. (2009) Two structurally independent domains of *E. coli* NusG create regulatory plasticity *via* distinct interactions with RNA polymerase and regulators. *J. Mol. Biol.*, **391**, 341–358.
10. Burmann,B.M., Schweimer,K., Luo,X., Wahl,M.C., Stitt,B.L., Gottesman,M.E. and Rösch,P. (2010) A NusE:NusG complex links transcription and translation. *Science*, **328**, 501–504.
11. Mitra,P., Ghosh,G., Hafeezunnisa,M. and Sen,R. (2017) Rho protein: roles and mechanisms. *Annu. Rev. Microbiol.*, **71**, 687–709.
12. Burmann,B.M., Luo,X., Rösch,P., Wahl,M.C. and Gottesman,M.E. (2010) Fine tuning of the *E. coli* NusB:NusE complex affinity to *BoxA* RNA is required for processive antitermination. *Nucleic Acids Res.*, **38**, 314–326.
13. Luo,X., Hsiao,H.-H., Bubunenko,M., Weber,G., Court,D.L., Gottesman,M.E., Urlaub,H. and Wahl,M.C. (2008) Structural and functional analysis of the *E. coli* NusB-S10 transcription antitermination complex. *Mol. Cell*, **32**, 791–802.
14. Friedman,D.I. and Baron,L.S. (1974) Genetic characterization of a bacterial locus involved in the activity of the N function of phage lambda. *Virology*, **58**, 141–148.
15. Vogel,U. and Jensen,K.F. (1997) NusA is required for ribosomal antitermination and for modulation of the transcription elongation rate of both antiterminated RNA and mRNA. *J. Biol. Chem.*, **272**, 12265–12271.
16. Pan,T., Artsimovitch,I., Fang,X.W., Landick,R. and Sosnick,T.R. (1999) Folding of a large ribozyme during transcription and the effect of the elongation factor NusA. *Proc. Natl. Acad. Sci. U.S.A.*, **96**, 9545–9550.
17. Artsimovitch,I. and Landick,R. (2000) Pausing by bacterial RNA polymerase is mediated by mechanistically distinct classes of signals. *Proc. Natl. Acad. Sci. U.S.A.*, **97**, 7090–7095.
18. Guo,X., Myasnikov,A.G., Chen,J., Crucifix,C., Papai,G., Takacs,M., Schultz,P. and Weixlbaumer,A. (2018) Structural basis for nusa stabilized transcriptional pausing. *Mol. Cell*, **69**, 816–827.
19. Worbs,M., Bourenkov,G.P., Bartunik,H.D., Huber,R. and Wahl,M.C. (2001) An extended RNA binding surface through arrayed S1 and KH domains in transcription factor NusA. *Mol. Cell*, **7**, 1177–1189.
20. Eisenmann,A., Schwarz,S., Prasch,S., Schweimer,K. and Rösch,P. (2005) The *E. coli* NusA carboxy-terminal domains are structurally similar and show specific RNAP- and lambdaN interaction. *Protein Sci.*, **14**, 2018–2029.
21. Mah,T.F., Li,J., Davidson,A.R. and Greenblatt,J. (1999) Functional importance of regions in *Escherichia coli* elongation factor NusA that interact with RNA polymerase, the bacteriophage lambda N protein and RNA. *Mol. Microbiol.*, **34**, 523–537.
22. Prasch,S., Schwarz,S., Eisenmann,A., Wöhrl,B.M., Schweimer,K. and Rösch,P. (2006) Interaction of the intrinsically unstructured phage lambda N Protein with *Escherichia coli* NusA. *Biochemistry*, **45**, 4542–4549.
23. Bonin,I., Mühlberger,R., Bourenkov,G.P., Huber,R., Bacher,A., Richter,G. and Wahl,M.C. (2004) Structural basis for the interaction of *Escherichia coli* NusA with protein N of phage lambda. *Proc. Natl. Acad. Sci. U.S.A.*, **101**, 13762–13767.
24. Schweimer,K., Prasch,S., Sujatha,P.S., Bubunenko,M., Gottesman,M.E. and Rösch,P. (2011) NusA interaction with the α subunit of *E. coli* RNA polymerase is *via* the UP element site and releases autoinhibition. *Structure*, **19**, 945–954.
25. Mah,T.F., Kuznedelov,K., Mushegian,A., Severinov,K. and Greenblatt,J. (2000) The alpha subunit of *E. coli* RNA polymerase activates RNA binding by NusA. *Genes Dev.*, **14**, 2664–2675.
26. Liu,K., Zhang,Y., Severinov,K., Das,A. and Hanna,M.M. (1996) Role of *Escherichia coli* RNA polymerase alpha subunit in modulation of pausing, termination and anti-termination by the transcription elongation factor NusA. *EMBO J.*, **15**, 150–161.

27. Strauß,M., Vitiello,C., Schweimer,K., Gottesman,M., Rösch,P. and Knauer,S.H. (2016) Transcription is regulated by NusA:NusG interaction. *Nucleic Acids Res.*, **44**, 5971–5982.
28. Arnvig,K.B., Zeng,S., Quan,S., Papageorge,A., Zhang,N., Villapakkam,A.C. and Squires,C.L. (2008) Evolutionary comparison of ribosomal operon antitermination function. *J. Bacteriol.*, **190**, 7251–7257.
29. Bremer,H. and Dennis,P.P. (1996) Modulation of chemical composition and other parameters of the cell by growth rate. In: *Escherichia coli and Salmonella: Cellular and Molecular Biology*. ASM Press, Washington DC, **2**, 1553–1569.
30. Li,S.C., Squires,C.L. and Squires,C. (1984) Antitermination of *E. coli* rRNA transcription is caused by a control region segment containing lambda *nut*-like sequences. *Cell*, **38**, 851–860.
31. Pfeiffer,T. and Hartmann,R.K. (1997) Role of the spacer *boxA* of *Escherichia coli* ribosomal RNA operons in efficient 23 S rRNA synthesis *in vivo*. *J. Mol. Biol.*, **265**, 385–393.
32. Heinrich,T., Condon,C., Pfeiffer,T. and Hartmann,R.K. (1995) Point mutations in the leader *boxA* of a plasmid-encoded *Escherichia coli rrnB* operon cause defective antitermination *in vivo*. *J. Bacteriol.*, **177**, 3793–3800.
33. Berg,K.L., Squires,C. and Squires,C.L. (1989) Ribosomal RNA operon anti-termination. Function of leader and spacer region *box B-box A* sequences and their conservation in diverse micro-organisms. *J. Mol. Biol.*, **209**, 345–358.
34. Friedman,D.I. and Gottesman,M.E. (1983) Lytic mode of lambda development. In: Hendrix,RW, Roberts,JW, Stahl,F and Weisberg,RA (eds). *Lambda II*. Cold Spring Harbor Laboratory Press, NY, Vol. **13**, pp. 21–51.
35. Greive,S.J., Lins,A.F. and von Hippel,P.H. (2005) Assembly of an RNA-protein complex. Binding of NusB and NusE (S10) proteins to *boxA* RNA nucleates the formation of the antitermination complex involved in controlling rRNA transcription in *Escherichia coli*. *J. Biol. Chem.*, **280**, 36397–36408.
36. DeVito,J. and Das,A. (1994) Control of transcription processivity in phage lambda: Nus factors strengthen the termination-resistant state of RNA polymerase induced by N antiterminator. *Proc. Natl. Acad. Sci. U.S.A.*, **91**, 8660–8664.
37. Beuth,B., Pennell,S., Arnvig,K.B., Martin,S.R. and Taylor,I.A. (2005) Structure of a Mycobacterium tuberculosis NusA-RNA complex. *EMBO J.*, **24**, 3576–3587.
38. Li,J., Horwitz,R., McCracken,S. and Greenblatt,J. (1992) NusG, a new *Escherichia coli* elongation factor involved in transcriptional antitermination by the N protein of phage lambda. *J. Biol. Chem.*, **267**, 6012–6019.
39. Condon,C., Squires,C. and Squires,C.L. (1995) Control of rRNA transcription in *Escherichia coli*. *Microbiol. Rev.*, **59**, 623–645.
40. Torres,M., Condon,C., Balada,J.M., Squires,C. and Squires,C.L. (2001) Ribosomal protein S4 is a transcription factor with properties remarkably similar to NusA, a protein involved in both non-ribosomal and ribosomal RNA antitermination. *EMBO J.*, **20**, 3811–3820.
41. Singh,N., Bubunenko,M., Smith,C., Abbott,D.M., Stringer,A.M., Shi,R., Court,D.L. and Wade,J.T. (2016) SuhB associates with nus factors to facilitate 30s ribosome biogenesis in *escherichia coli*. *MBio.*, **7**, e00114.
42. Grinwald,M. and Ron,E.Z. (2013) The *Escherichia coli* translation-associated heat shock protein YbeY is involved in rRNA transcription antitermination. *PLoS ONE*, **8**, e62297.
43. Bubunenko,M., Court,D.L., Al Refaii,A., Saxena,S., Korepanov,A., Friedman,D.I., Gottesman,M.E. and Alix,J.-H. (2013) Nus transcription elongation factors and RNase III modulate small ribosome subunit biogenesis in *Escherichia coli*. *Mol. Microbiol.*, **87**, 382–393.
44. Wang,Y., Stieglitz,K.A., Bubunenko,M., Court,D.L., Stec,B. and Roberts,M.F. (2007) The structure of the R184A mutant of the inositol monophosphatase encoded by *suhB* and implications for its functional interactions in *Escherichia coli*. *J. Biol. Chem.*, **282**, 26989–26996.
45. Drögemüller,J., Strauß,M., Schweimer,K., Wöhrl,B.M., Knauer,S.H. and Rösch,P. (2015) Exploring RNA polymerase regulation by NMR spectroscopy. *Sci. Rep.*, **5**, 10825.
46. Prasch,S., Jurk,M., Washburn,R.S., Gottesman,M.E., Wöhrl,B.M. and Rösch,P. (2009) RNA-binding specificity of *E. coli* NusA. *Nucleic Acids Res.*, **37**, 4736–4742.
47. Burmann,B.M., Scheckenhofer,U., Schweimer,K. and Rösch,P. (2011) Domain interactions of the transcription-translation coupling factor *Escherichia coli* NusG are intermolecular and transient. *Biochem. J.*, **435**, 783–789.
48. Zuber,P.K., Artsimovitch,I., NandyMazumdar,M., Liu,Z., Nedialkov,Y., Schweimer,K., Rösch,P. and Knauer,S.H. (2018) The universally-conserved transcription factor RfaH is recruited to a hairpin structure of the non-template DNA strand. *Elife*, **7**, e36349.
49. Meyer,O. and Schlegel,H.G. (1983) Biology of aerobic carbon monoxide-oxidizing bacteria. *Annu. Rev. Microbiol.*, **37**, 277–310.
50. Sambrook,J. and Russel,D.W. (2001) *Molecular Cloning: A Laboratory Manual Third Edition*. Cold Spring Harbor Press, NY.
51. Sprangers,R. and Kay,L.E. (2007) Quantitative dynamics and binding studies of the 20S proteasome by NMR. *Nature*, **445**, 618–622.
52. Drögemüller,J., Strauß,M., Schweimer,K., Jurk,M., Rösch,P. and Knauer,S.H. (2015) Determination of RNA polymerase binding surfaces of transcription factors by NMR spectroscopy. *Sci. Rep.*, **5**, 16428–16441.
53. Artsimovitch,I. and Landick,R. (2002) The transcriptional regulator RfaH stimulates RNA chain synthesis after recruitment to elongation complexes by the exposed nontemplate DNA strand. *Cell*, **109**, 193–203.
54. Hartl,M.J., Kretzschmar,B., Frohn,A., Nowrouzi,A., Rethwilm,A. and Wöhrl,B.M. (2008) AZT resistance of simian foamy virus reverse transcriptase is based on the excision of AZTMP in the presence of ATP. *Nucleic Acids Res.*, **36**, 1009–1016.
55. Yan,Y., Zhang,D., Zhou,P., Li,B. and Huang,S.-Y. (2017) HDOCK: a web server for protein-protein and protein-DNA/RNA docking based on a hybrid strategy. *Nucleic Acids Res.*, **45**, W365–W373.
56. Shi,J., Jin,Y., Bian,T., Li,K., Sun,Z., Cheng,Z., Jin,S. and Wu,W. (2015) SuhB is a novel ribosome associated protein that regulates expression of MexXY by modulating ribosome stalling in *Pseudomonas aeruginosa*. *Mol. Microbiol.*, **98**, 370–383.
57. Torres,M., Balada,J.-M., Zellars,M., Squires,C. and Squires,C.L. (2004) *In vivo* effect of NusB and NusG on rRNA transcription antitermination. *J. Bacteriol.*, **186**, 1304–1310.
58. Chen,L. and Roberts,M.F. (2000) Overexpression, purification, and analysis of complementation behavior of *E. coli* SuhB protein: comparison with bacterial and archaeal inositol monophosphatases. *Biochemistry*, **39**, 4145–4153.
59. Kozloff,L.M., Turner,M.A., Arellano,F. and Lute,M. (1991) Phosphatidylinositol, a phospholipid of ice-nucleating bacteria. *J. Bacteriol.*, **173**, 2053–2060.
60. Mooney,R.A., Davis,S.E., Peters,J.M., Rowland,J.L., Ansari,A.Z. and Landick,R. (2009) Regulator trafficking on bacterial transcription units *in vivo*. *Mol. Cell*, **33**, 97–108.
61. Schmidt,A., Kochanowski,K., Vedelaar,S., Ahrné,E., Volkmer,B., Callipo,L., Knoops,K., Bauer,M., Aebersold,R. and Heinemann,M. (2016) The quantitative and condition-dependent *Escherichia coli* proteome. *Nat. Biotechnol.*, **34**, 104–110.
62. Baniulyte,G., Singh,N., Benoit,C., Johnson,R., Ferguson,R., Paramo,M., Stringer,A.M., Scott,A., Lapierre,P. and Wade,J.T. (2017) Identification of regulatory targets for the bacterial Nus factor complex. *Nat. Commun.*, **8**, 2027.
63. Ptashne,M. (1988) How eukaryotic transcriptional activators work. *Nature*, **335**, 683–689.
64. Martchenko,M., Levitin,A. and Whiteway,M. (2007) Transcriptional activation domains of the Candida albicans Gcn4p and Gal4p homologs. *Eukaryotic Cell*, **6**, 291–301.
65. Ma,J. and Ptashne,M. (1987) Deletion analysis of GAL4 defines two transcriptional activating segments. *Cell*, **48**, 847–853.
66. Hope,I.A. and Struhl,K. (1986) Functional dissection of a eukaryotic transcriptional activator protein, GCN4 of yeast. *Cell*, **46**, 885–894.
67. Brzovic,P.S., Heikaus,C.C., Kisselev,L., Vernon,R., Herbig,E., Pacheco,D., Warfield,L., Littlefield,P., Baker,D., Klevit,R.E. *et al.* (2011) The acidic transcription activator Gcn4 binds the mediator subunit Gal11/Med15 using a simple protein interface forming a fuzzy complex. *Mol. Cell*, **44**, 942–953.

68. Uesugi,M., Nyanguile,O., Lu,H., Levine,A.J. and Verdine,G.L. (1997) Induced alpha helix in the VP16 activation domain upon binding to a human TAF. *Science*, **277**, 1310–1313.
69. Radhakrishnan,I., Pérez-Alvarado,G.C., Parker,D., Dyson,H.J., Montminy,M.R. and Wright,P.E. (1997) Solution structure of the KIX domain of CBP bound to the transactivation domain of CREB: a model for activator:coactivator interactions. *Cell*, **91**, 741–752.
70. Drysdale,C.M., Dueñas,E., Jackson,B.M., Reusser,U., Braus,G.H. and Hinnebusch,A.G. (1995) The transcriptional activator GCN4 contains multiple activation domains that are critically dependent on hydrophobic amino acids. *Mol. Cell Biol.*, **15**, 1220–1233.
71. Cress,W.D. and Triezenberg,S.J. (1991) Critical structural elements of the VP16 transcriptional activation domain. *Science*, **251**, 87–90.
72. Pufall,M.A. and Graves,B.J. (2002) Autoinhibitory domains: modular effectors of cellular regulation. *Annu. Rev. Cell Dev. Biol.*, **18**, 421–462.
73. Burmann,B.M., Knauer,S.H., Sevostyanova,A., Schweimer,K., Mooney,R.A., Landick,R., Artsimovitch,I. and Rösch,P. (2012) An α helix to β barrel domain switch transforms the transcription factor RfaH into a translation factor. *Cell*, **150**, 291–303.
74. Buetow,L. and Huang,D.T. (2016) Structural insights into the catalysis and regulation of E3 ubiquitin ligases. *Nat. Rev. Mol. Cell Biol.*, **17**, 626–642.
75. Au-Yeung,B.B., Shah,N.H., Shen,L. and Weiss,A. (2018) ZAP-70 in signaling, biology, and disease. *Annu. Rev. Immunol.*, **36**, 127–156.

Supplementary Data

SuhB is an integral part of the ribosomal antitermination complex and interacts with NusA

Benjamin Dudenhöffer[1], Hans Schneider[1], Kristian Schweimer[1], Stefan H Knauer[1,*]

[1] Biopolymers, University of Bayreuth, Universitätsstraße 30, 95447 Bayreuth, Germany

* To whom correspondence should be addressed. Tel: 0049 921 553868; Email: stefan.knauer@uni-bayreuth.de

Supplementary Table S 1: Oligonucleotides.

name	sequence 5´-3´	source
Fw_*suhB*	CATGCCATGGGAATGCATCCGATGCTGAACATC	Biolegio, Nijmegen, NL
Rv_*suhB*	CGCGGATCCTTAACGCTTCAGAGCGTCGC	
Fw_*s4*	CATATGGCAAGATATTTGGGTAAGC	Purimex, Grebenstein, D
Rv_*s4*	GGATCCTTACTTGGAGTAAAGCTCGACG	
Fw_*nusAΔar2*	GGAATTCCATATGAACAAAGAAATTTTGGCTGTAGTTG	Metabion, Steinkirchen, D
Rv_*nusAΔar2*	CCGCTCGAGTTAACCGAGGCTTTCCTGGGC	
AR2-D443C-FW	CTTGAAGGGGTAGATCGTTGTTTGGCATTCAAACTGGCCG	
AR2-D443C-RV	CGGCCAGTTTGAATGCCAAACAACGATCTACCCCTTCAAG	
Template_ *rrnG*-RNA	CCCACACAGATTGTCTGATAAATTGTTAAAGAGCAGTGCC GCTTCGCTTTTTCTCAGCGGCGCGGCCCTATAGTGAGTCG TATTA	
T-DNA_TAC	ATCCGTATCTTCGAGTGCCCACACAGATTGTCTCATAAAT TGTTAAAGAGCAGTGCCGC	
NT-DNA_TAC	GCGGCACTGCTCTTTAACAATTTATCAGACTTGTCCACGC TCGTCTCGAAGATACGGAT	
random RNA	UUUUUGAGUCUGCGGCGCGCG	

Supplementary Table S2: Interaction of NusA with SuhB. Normalized chemical shift changes of assigned [I,L,V]-NusA methyl groups upon addition of SuhB (molar ratio 1:5). Residues were defined as affected if $\Delta\delta_{norm} \geq 0.04$ (highlighted in grey).

NusA domain	amino acid number	$\Delta\delta_{norm}$
NTD	V9γ2	0.0219
	I43δ	0.0032
	L63δ1	0.0013
	L63δ2	0.0020
	V65γ1	0.0010
	I75δ	0.0002
	L87δ1	0.0014
	I97δ	0.0074
SKK	I150δ	0.0036
	V179γ1	0.0000
	V179γ2	0.0011
	I211δ	0.0036
	I221δ	0.0010
	I236δ	3.3561
	V238γ1	0.0022
	V262γ1	0.0032
AR1	I356δ	0.0295
	L363δ1	0.0040
	L363δ2	0.0020
	I365δ	0.0045
	V372γ1	0.0062
	L373δ1	0.0044
	L373δ2	0.0058
	V374γ1	0.0094
	L384δ1	0.0025
	L384δ2	0.0068
	L392δ2	0.0092
	I395δ	0.0050
	I417δ	0.0039
AR2	L444δ1	0.0032
	L444δ2	0.0036
	V453γ2	0.0042
	L456δ1	0.0027
	L459δ2	0.0069
	I464δ	0.0521

Supplementary Table S3: Interaction of NusA with NusG-NTD. Chemical shift changes of assigned [I,L,V]-NusA methyl groups upon addition of NusG-NTD (molar ratio 1:5). Residues were defined as affected if $\Delta\delta_{norm} \geq 0.04$ (highlighted in grey).

NusA domain	amino acid number	$\Delta\delta_{norm}$
NTD	V9γ2	0.0200
	I43δ	0.0049
	L63δ1	0.0050
	L63δ2	0.0066
	V65γ1	0.0042
	I75δ	0.0072
	L87δ1	0.0042
	I97δ	0.0055
SKK	I150δ	0.0055
	V179γ1	0.0063
	V179γ2	0.0062
	I211δ	0.0052
	I221δ	0.0043
	I236δ	3.3561
	V238γ1	0.0051
	V262γ1	0.0034
AR1	I356δ	0.0046
	L363δ1	0.0076
	L363δ2	0.0008
	I365δ	0.0017
	V372γ1	0.0065
	L373δ1	0.0080
	L373δ2	0.0003
	V374γ1	0.0082
	L384δ1	0.0055
	L384δ2	0.0010
	L392δ2	0.0049
	I395δ	0.0136
	I417δ	0.0070
AR2	L444δ1	0.0054
	L444δ2	0.0067
	V453γ2	0.0054
	L456δ1	0.0057
	L459δ2	0.0072
	I464δ	0.0081

Supplementary Table S4: Interaction of NusA with RNAP α-CTD. Normalized chemical shift changes of assigned [I,L,V]-NusA methyl groups upon addition of RNAP α-CTD (molar ratio 1:5). Residues were defined as affected if $\Delta\delta_{norm} \geq 0.04$ (highlighted in grey).

NusA domain	amino acid number	$\Delta\delta_{norm}$
NTD	V9γ2	0.0278
	I43δ	3.4673
	L63δ1	0.0062
	L63δ2	5.4665
	V65γ1	0.0105
	I75δ	3.3834
	L87δ1	0.0318
	I97δ	3.3739
SKK	I150δ	0.0060
	V179γ1	0.0030
	V179γ2	0.0050
	I211δ	0.0052
	I221δ	0.0044
	I236δ	0.0117
	V238γ1	0.0089
	V262γ1	0.0050
AR1	I356δ	0.0242
	L363δ1	0.0072
	L363δ2	0.0010
	I365δ	0.0038
	V372γ1	0.0091
	L373δ1	0.0040
	L373δ2	0.0011
	V374γ1	0.0178
	L384δ1	0.0063
	L384δ2	0.0050
	L392δ2	0.0027
	I395δ	0.0297
	I417δ	0.0072
AR2	L444δ1	0.0097
	L444δ2	0.0121
	V453γ2	0.0085
	L456δ1	0.0453
	L459δ2	0.0198
	I464δ	0.0574

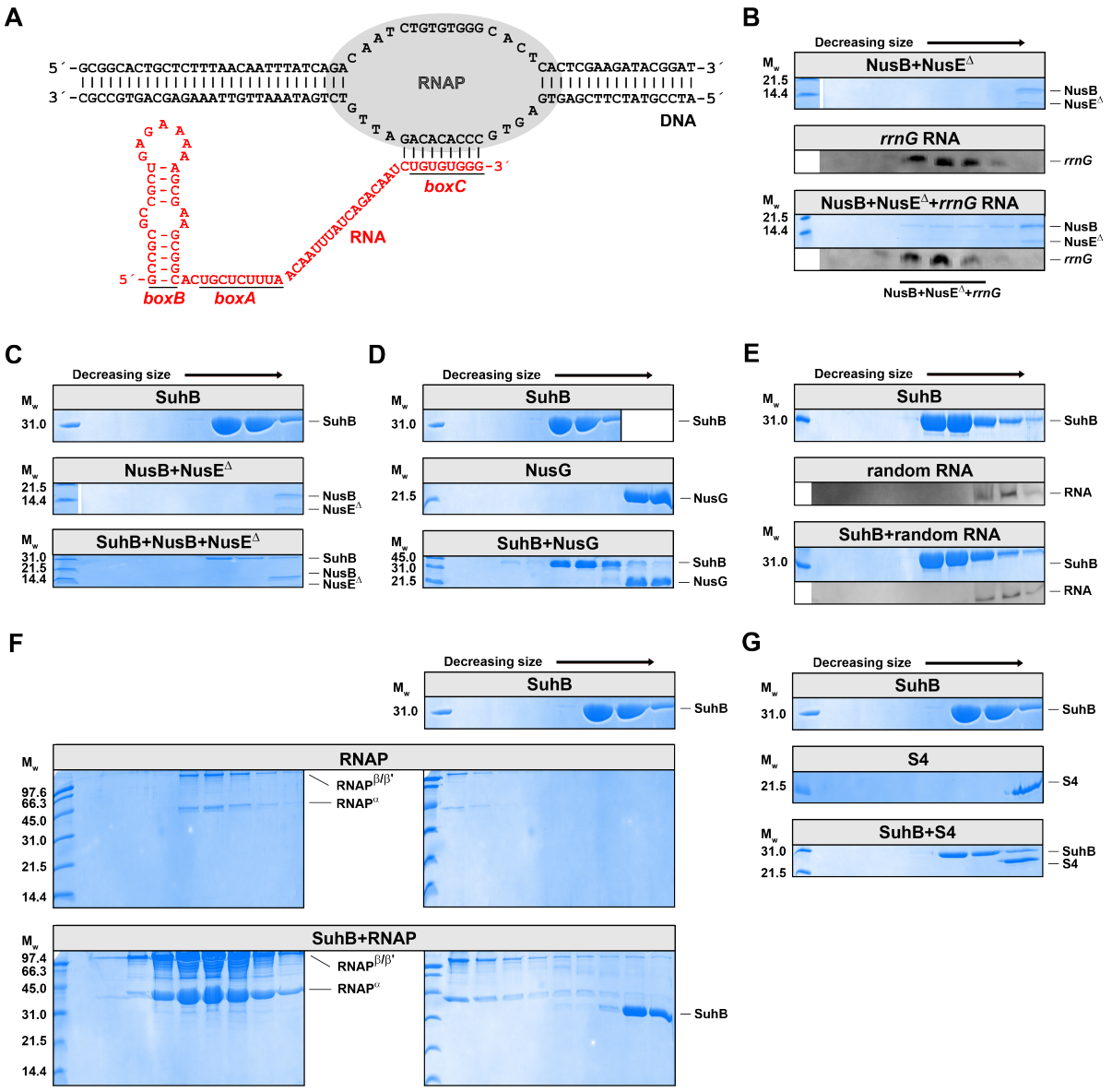

Supplementary Figure S1: Interaction studies. **(A)** Scheme of the *rrnG-EC*. For details on the assembly see Material and Methods. (**B-G**) Analyses of analytical size-exclusion chromatography runs by Coomassie-stained SDS-PAGE (proteins, in color) and Toluidine blue-stained urea-PAGE (RNA, in grayscale), monitoring interactions between NusE$^{\Delta}$/B and *rrnG* RNA **(B)**, SuhB and NusE$^{\Delta}$/B **(C)**, SuhB and NusG **(D)**, SuhB and a random RNA **(E)**, SuhB and RNAP **(F)**, and SuhB and S4 **(G)**. Mixtures loaded for each run are indicated in the boxes above the gels. The left lane shows the marker (SDS-PAGE standard low range, BioRad). Molecular weights (M_W) are indicated on the left, bands are identified on the right, and complexes formed are given below the gels. Gels are representative examples of at least two repetitions. When testing an interaction between SuhB and RNAP (panel F) a protein coeluted with the RNAP subunits whose M_W might correspond to the one of SuhB (left gel, bottom row), but analysis by peptide mass fingerprinting revealed that this protein is a degradation product of the RNAP β subunit.

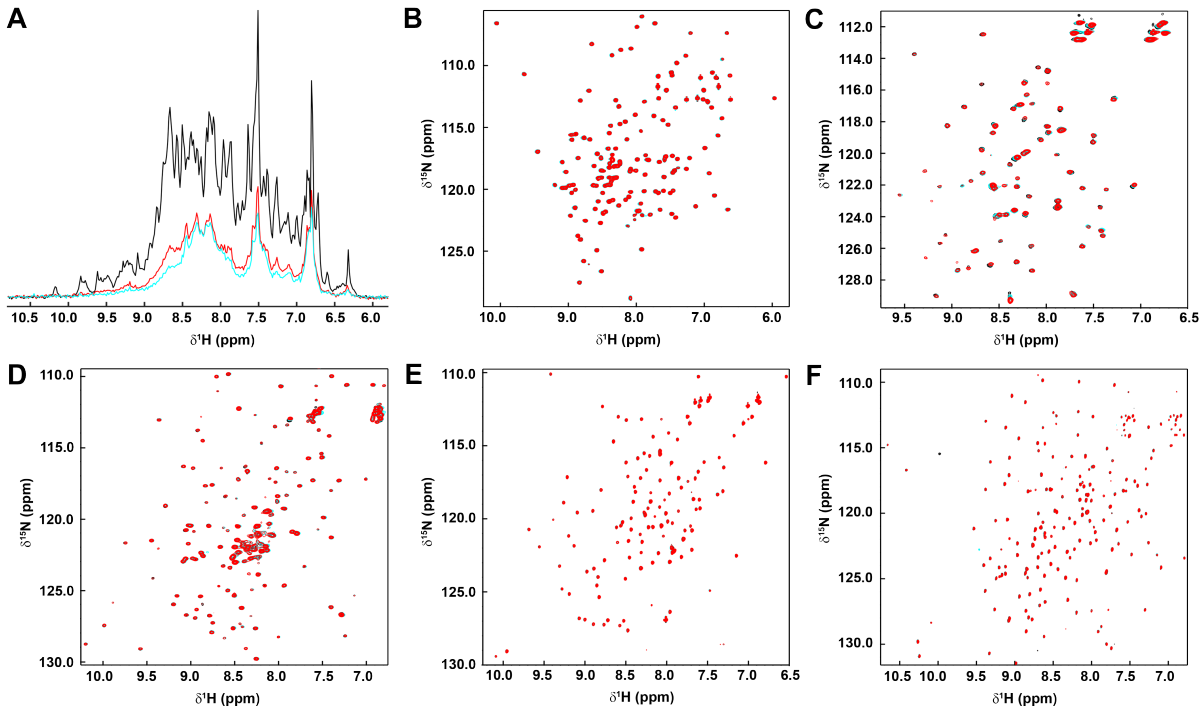

Supplementary Figure S2: SuhB interacts with NusA, but not with NusB, NusE$^{\Delta}$/B, or NusG. **(A)** 1D [^{1}H,^{15}N]-HSQC spectra of [^{2}H,^{15}N]-SuhB in the absence (black) and presence (molar ratio 1:1, cyan; molar ratio 1:2, red) of NusA (stock concentration 437 µM). **(B-D)** [^{1}H,^{15}N]-HSQC spectra of ^{15}N-NusB **(B)**, ^{15}N-NusE$^{\Delta}$/B **(C)**, and ^{15}N-NusG **(D)** in the absence (black) or presence (molar ratio 1:1, cyan; molar ratio 1:2, red) of SuhB (stock concentration of SuhB: 491 µM **(B)**, 470 µM **(C)**, 469 µM **(D)**). **(E,F)** [^{1}H,^{15}N]-HSQC spectra of ^{15}N-NusA-NTD **(E)** and [^{1}H,^{15}N]-BEST-TROSY spectra of ^{2}H,^{15}N-NusA-SKK **(F)** in the absence (black) or presence (molar ratio 1:1, cyan; molar ratio 1:2, red) of SuhB. Labelled proteins were initially present at 125 µM.

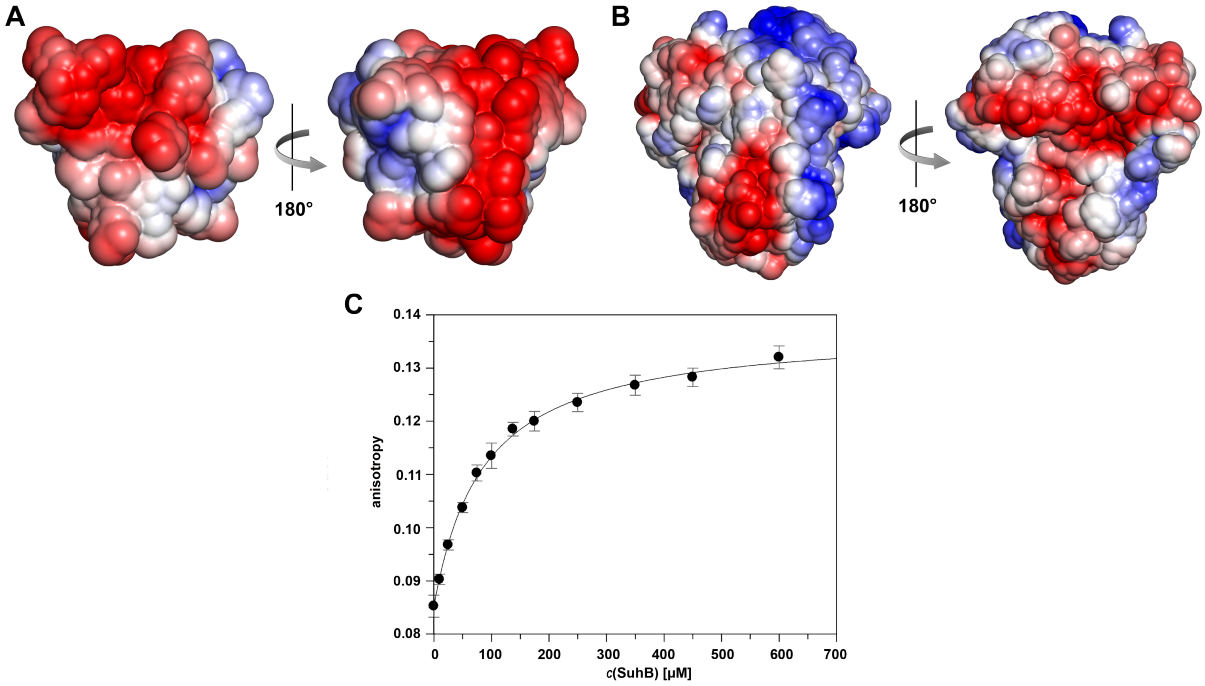

Supplementary Figure S3: SuhB:NusA-AR2 interaction. **(A,B)** Electrostatic surface potentials of NusA-AR2 **(A)** and SuhB **(B)** coloured from -3 kT/e^- (red) to +3 kT/e^- (blue). **(C)** Determination of SuhB:NusA-AR2^{D443C} binding affinity by fluorescence anisotropy measurements. 25 nM fluorescent labelled NusA-AR2^{D443C} was titrated with SuhB. For each titration step the mean value of four individual titrations is plotted against the SuhB concentration. The standard deviation is shown as bars. The curve represents the best fit to a two-component binding equation, yielding a K_D value of 83±4 µM.

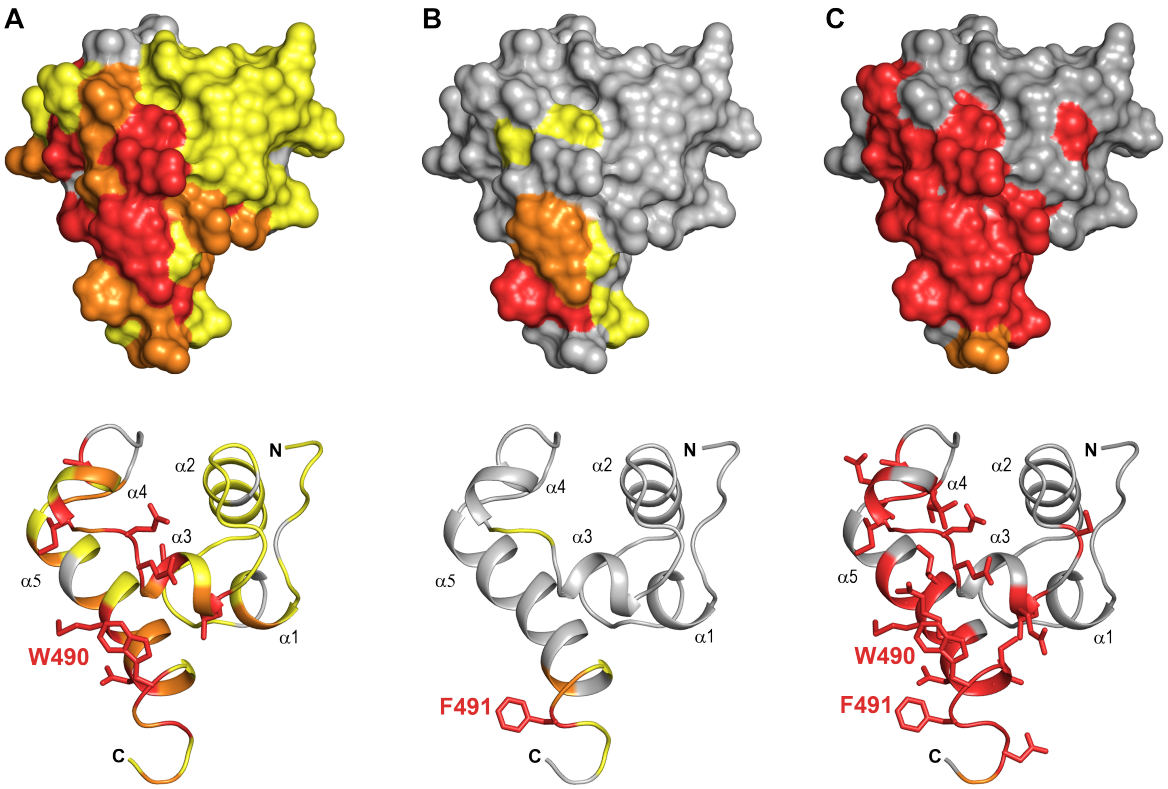

Supplementary Figure S4: Binding surfaces of SuhB **(A)**, NusG-NTD **(B)**, and αCTD **(C)** on NusA-AR2. NusA-AR2 (grey; PDB ID: 1WCN) is in surface (top) and ribbon (bottom) representation (PDB ID: 1WCN). Residues affected by binding as determined by [^{1}H,^{15}N]-HSQC titrations are colour-coded. Slightly affected, yellow; moderately affected, orange; Strongly affected, red. The side chains of strongly affected residues are depicted as sticks. Termini, secondary structure elements, and selected residues are labelled. Binding data for NusG-NTD and αCTD were taken from refs. (1) and (2), respectively.

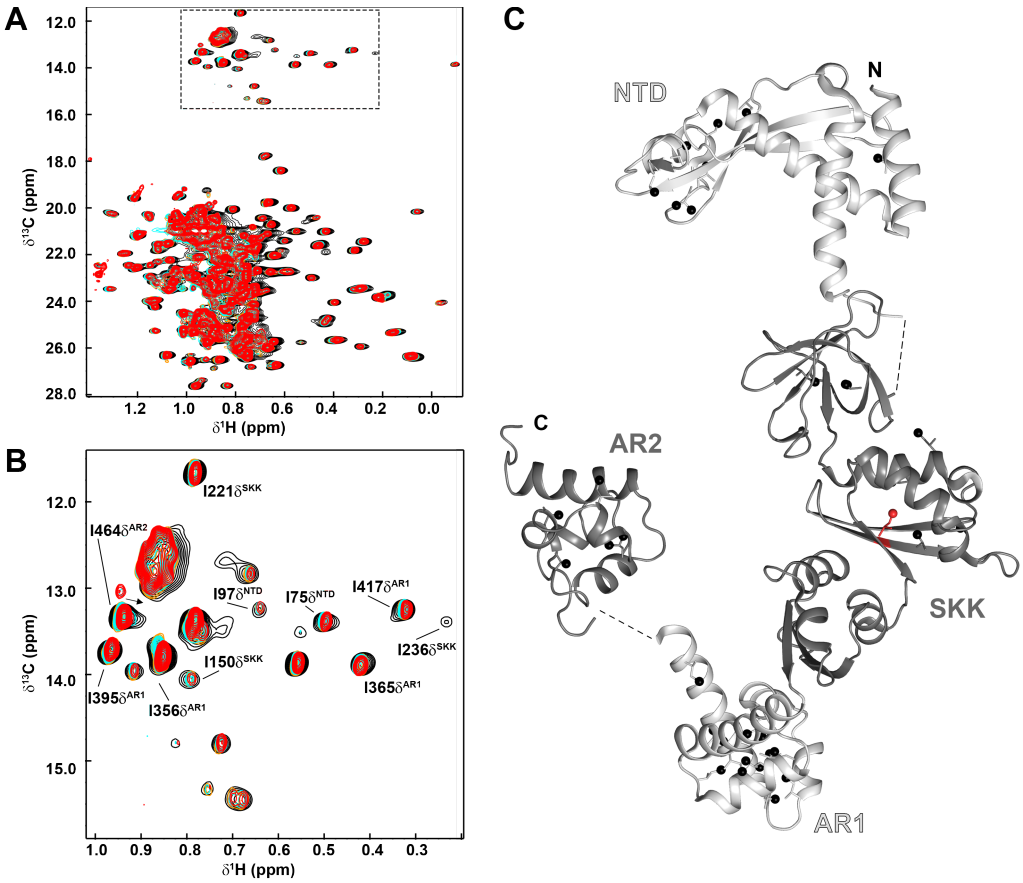

Supplementary Figure S5: NusG-NTD releases autoinhibition of NusA. **(A,B)** [^{1}H,^{13}C]-Methyl-TROSY spectra of the titration of 25 µM [I,L,V]-NusA with NusG-NTD. NusG-NTD was added in a molar ratio of 1:0, black; 1:0.5, orange; 1:1, cyan; 1:2, purple; 1:3, yellow; 1:5, red (concentration of NusG-NTD stock: 920 µM). The boxed region indicates the section as in **(B)**. Selected signals are labelled. **(C)** Structure of NusA in ribbon representation. Linker regions are indicated by dashed lines. Ile, Leu, and Val residues with assigned methyl groups are shown as sticks with carbon atoms of the methyl groups as black spheres. If a methyl group was affected upon addition of NusG-NTD ($\Delta\delta_{norm} \geq$ 0.04 ppm) the whole residue was coloured in red (see also **Supplementary Table S3**). PDB IDs: NusA-NTD: 2KWP, SKK-AR1: 5LM9, NusA-AR2: 1WCN.

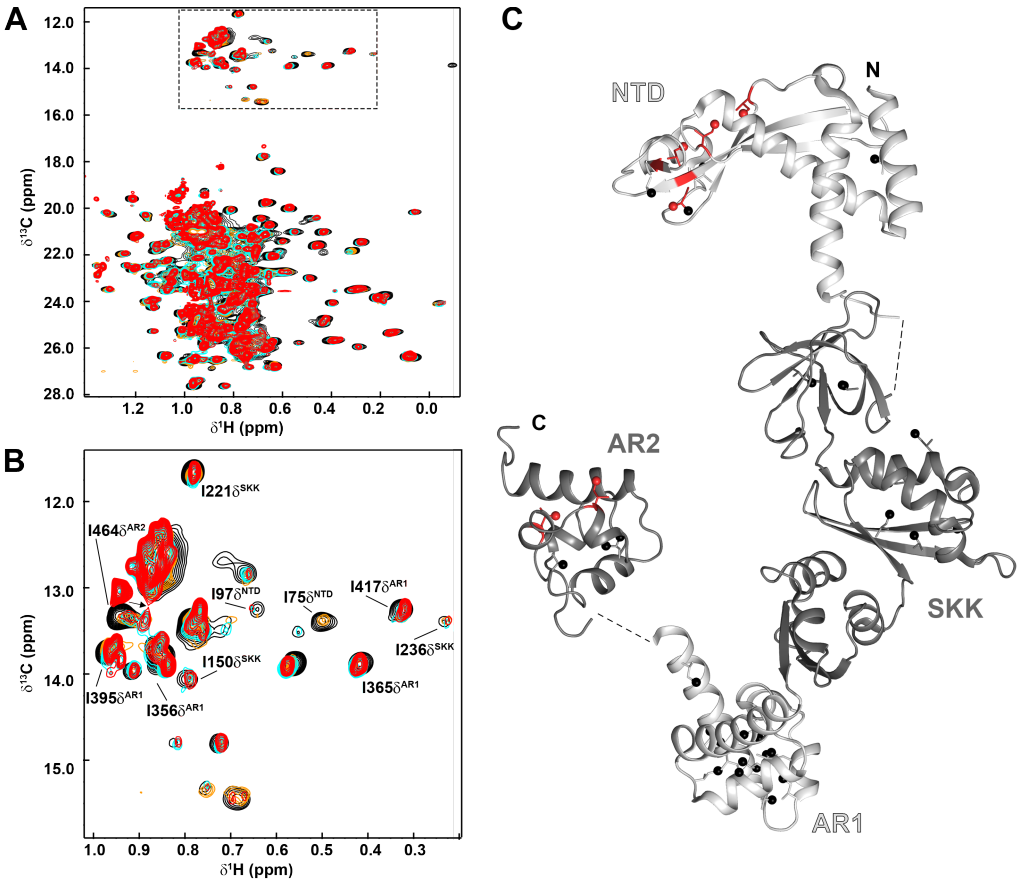

Supplementary Figure S6: αCTD releases autoinhibition of NusA. **(A,B)** [^{1}H,^{13}C]-Methyl-TROSY spectra of the titration of 25 µM [I,L,V]-NusA with αCTD. αCTD was added in a molar ratio of 1:0, black; 1:0.5, orange; 1:1, cyan; 1:2, purple; 1:3, yellow; 1:5, red (concentration of αCTD stock: 293 µM). The boxed region indicates the section as in **(B)**. Selected signals are labelled. **(C)** Structure of NusA in ribbon representation. Linker regions are indicated by dashed lines. Ile, Leu, and Val residues with assigned methyl groups are shown as sticks with carbon atoms of the methyl groups as black spheres. If a methyl group was affected upon addition of αCTD ($\Delta\delta_{norm} \geq 0.04$ ppm) the whole residue was coloured in red (see also **Supplementary Table S4**). PDB IDs: NusA-NTD: 2KWP, SKK-AR1: 5LM9, NusA-AR2: 1WCN.

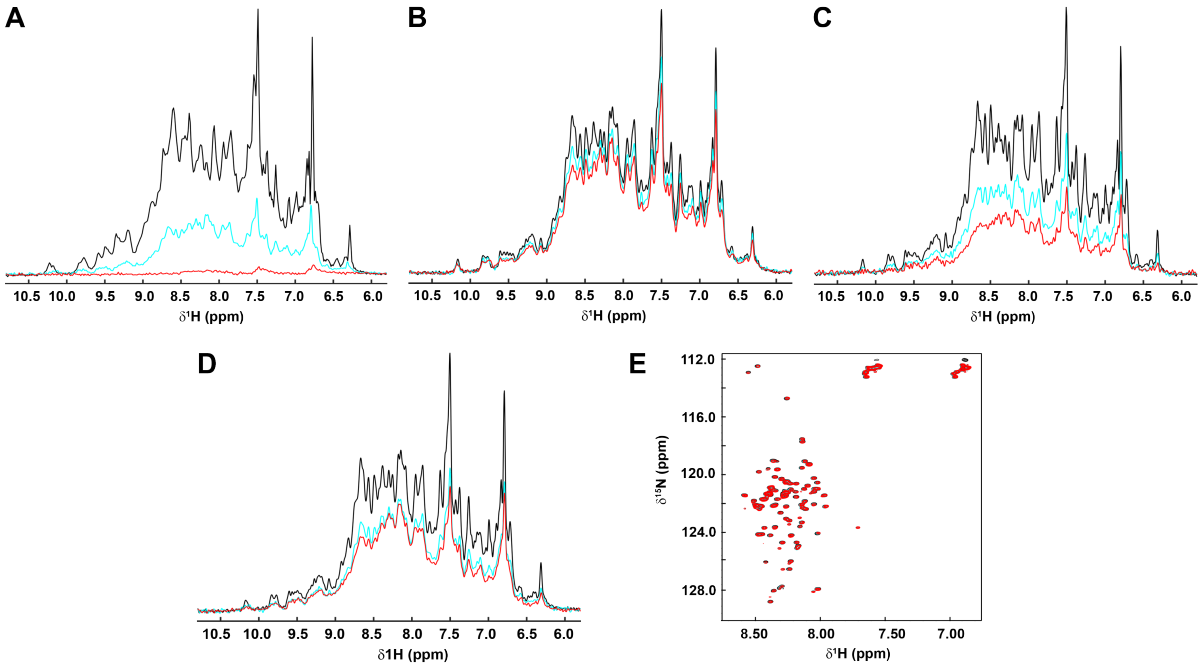

Supplementary Figure S7: SuhB binds to the β and β' subunit of RNAP. **(A)** 1D [^{1}H,^{15}N]-HSQC spectra of ^{2}H,^{15}N-SuhB in the absence (black, 50 µM ^{2}H,^{15}N-SuhB) and presence of RNAP (cyan, molar ratio 1:1, 31 µM ^{2}H,^{15}N-SuhB; red, molar ratio1:2, 18 µM ^{2}H,^{15}N-SuhB). **(B-D)** 1D [^{1}H,^{15}N]-HSQC spectra of 50 µM ^{2}H,^{15}N-SuhB in the absence (black) and presence of the RNAP α subunit **(B)**, the RNAP β subunit **(C)**, or the RNAP β' subunit **(D)** (molar ratio 1:1, cyan; 1:2, red). Stock concentrations: α subunit, 313 µM; β subunit, 98 µM; β' subunit, 225 µM. **(E)** 2D [^{1}H,^{15}N]-HSQC spectra of 125 µM ^{15}N-ω subunit in the absence (black) and presence of the SuhB (molar ratio 1:1, cyan; 1:2, red; stock concentration SuhB: 720 µM).

SUPPLEMENTARY REFERENCES

1. Strauß,M., Vitiello,C., Schweimer,K., Gottesman,M., Rösch,P. and Knauer,S.H. (2016) Transcription is regulated by NusA:NusG interaction. *Nucleic Acids Res.*, **44**, 5971–5982.

2. Schweimer,K., Prasch,S., Sujatha,P.S., Bubunenko,M., Gottesman,M.E. and Rösch,P. (2011) NusA interaction with the α subunit of E. coli RNA polymerase is via the UP element site and releases autoinhibition. *Structure*, **19**, 945–954.

7.2 Einzelarbeit B

Benjamin R. Dudenhoeffer, Jan Borggraefe, Kristian Schweimer und Stefan H. Knauer (2020): **NusA directly interacts with antitermination factor Q from phage λ.** *Scientific Reports* **10,** 6607-6621.

SCIENTIFIC REPORTS
nature research

OPEN

NusA directly interacts with antitermination factor Q from phage λ

Benjamin R. Dudenhoeffer[1], Jan Borggraefe[1,2,3], Kristian Schweimer[1] & Stefan H. Knauer[1*]

Antitermination (AT) is a ubiquitous principle in the regulation of bacterial transcription to suppress termination signals. In phage λ antiterminator protein Q controls the expression of the phage's late genes with loading of λQ onto the transcription elongation complex halted at a σ-dependent pause requiring a specific DNA element. The molecular basis of λQ-dependent AT and its dependence on N-utilization substance (Nus) A is so far only poorly understood. Here we used solution-state nuclear magnetic resonance spectroscopy to show that the solution structure of λQ is in agreement with the crystal structure of an N-terminally truncated variant and that the 60 residues at the N-terminus are unstructured. We also provide evidence that multidomain protein NusA interacts directly with λQ via its N-terminal domain (NTD) and the acidic repeat (AR) 2 domain, with the λQ:NusA-AR2 interaction being able to release NusA autoinhibition. The binding sites for NusA-NTD and NusA-AR2 on λQ overlap and the interactions are mutually exclusive with similar affinities, suggesting distinct roles during λQ-dependent AT, e.g. the λQ:NusA-NTD interaction might position NusA-NTD in a way to suppress termination, making NusA-NTD repositioning a general scheme in AT mechanisms.

Transcription of all cellular genomes is mediated by evolutionary related multisubunit RNA polymerases (RNAPs)[1]. RNA synthesis is a discontinuous process that underlies tight regulation by various transcription factors that bind to RNAP, affecting its processivity. In Gram-negative bacteria the core RNAP consists of five subunits (2 x α, β, β', ω). The flap region of the β subunit forms the outer wall of the RNA exit channel with the β flap tip helix (βFTH) at the top of this region being able to regulate the width of the channel, making it a key regulatory element[2–8].

Antitermination (AT) is a ubiquitous mechanism to suppress termination signals and is widely used in bacteria. AT has first been described for bacteriophage λ where it controls the expression of early and late genes, being thus essential for the life cycle of the phage[9]. Phage λ uses two AT mechanisms which involve either antiterminator protein N or antiterminator protein Q. In λN-dependent AT the intrinsically disordered protein N is recruited to elongating RNAP by an AT signal in the nascent RNA and forms a complex with RNAP and the *Escherichia coli* (*E. coli*) host factors N-utilization substances (Nus) A, B, E, and G[6,7]. In this transcription AT complex (TAC) λN repositions NusA and remodels the βFTH, enabling the TAC to read through termination signals by preventing the formation of pause/terminator hairpins[6,7].

In λQ-dependent AT protein λQ requires a λQ binding element (QBE) on the DNA for recruitment and is loaded onto RNAP halted at an adjacent sigma-dependent promoter-proximal pause site[10,11]. Recent cryo electron microscopy (EM) studies of the AT mechanism of protein Q from phage 21, Q21, revealed that two Q21 proteins engage with RNAP in a Q21-TAC, one of which forms a torus at the RNA exit channel, narrowing it to prevent the formation of pause/terminator hairpins[12,13]. Currently, over 15,000 lambdoid bacteriophage Q proteins have been identified, which can be grouped into three families (Q21 family: Pfam PF06530, λQ family: Pfam PF03589, and Q82 family: Pfam PF06323), and crystal structures of Q21 and an N-terminally truncated variant of λQ are available[12–14]. Although all Q proteins are encoded by genes located at equivalent positions in bacteriophage genomes and perform the same regulatory function they show neither significant amino acid sequence nor significant 3D structural similarity to each other, suggesting that the mechanism by which they mediate AT may be different.

[1]Biopolymers, University of Bayreuth, Universitätsstraße 30, 95447, Bayreuth, Germany. [2]Present address: Institute of Physical Biology, Heinrich-Heine-University, Universitätsstraße 1, 52428, Jülich, Germany. [3]Present address: Institute of Complex Systems, Forschungszentrum Jülich, Wilhelm-Johnen-Straße, 52428, Jülich, Germany. *email: stefan.knauer@uni-bayreuth.de

AT does not only play a role in the life cycle of bacteriophages but is necessary for the expression of certain bacterial genes[15,16]. In ribosomal AT, for example, RNAP pauses at an AT signal and a TAC is formed that contains Nus factors A, B, E, and G as well as further components such as ribosomal protein S4 and inositol monophosphatase SuhB[17–20]. If this TAC is only responsible for AT or also involved in posttranscriptional activities, e.g. RNA maturation, is yet unclear.

Thus, Nus factors are key players in transcription regulation with NusG being a representative of the only class of transcription factors that is conserved in all three kingdoms of life[21]. *E. coli* NusG consists of two flexibly connected domains, an N-terminal and a C-terminal domain (NTD, CTD), respectively (Supplementary Fig. 1a)[22]. NusG-NTD has a mixed α/β topology and binds to the β' clamp helices of RNAP, increasing its processivity, whereas NusG-CTD forms a five-stranded β-barrel that can interact with different binding partners (reviewed in[23]). For example, NusG-CTD is able to bind termination factor Rho, resulting in stimulation of Rho-dependent termination[24–26], or to ribosomal protein S10 so that NusG serves as physical linker between RNAP and the ribosome to couple transcription and translation[24]. S10 consists of one domain with mixed α/β topology and is a moonlighting protein, i.e. it is identical to transcription factor NusE, if it is not part of the ribosome (Supplementary Fig. 1b). In this case NusE forms a heterodimer with NusB (Supplementary Fig. 1b), an α-helical, one-domain protein. During λN-dependent AT the NusE:NusB complex recognizes specifically a *boxA* element on the RNA with both NusE and NusB making contacts to the RNA[27,28]. NusE is the active component in processive AT whereas NusB supports loading of NusE to the transcription machinery[27]. NusG-CTD can interact with NusE and thus anchors the NusE:NusB:*boxA* complex to the RNAP[6,7,24]. NusG-mediated tethering of NusE:NusB:*boxA* to the RNAP might also be important for ribosomal AT[17,18]. The multidomain protein NusA (Supplementary Fig. 1c) is highly conserved in bacteria and regulates pausing and termination[2,29], AT processes[30–32], and RNA folding[33]. NusA-NTD binds to the βFTH[2,6,7] and to the CTD of one of the RNAP α subunits (αCTD)[2], whereas the following three domains (S1, K homology (KH)1, KH2) form the compact RNA binding motif SKK[34]. In *E. coli* and other γ-proteobacteria NusA has two acidic repeat (AR) domains, AR1 and AR2, at its C-terminus[35]. NusA-AR1 interacts with λN[36–38], whereas NusA-AR2 serves as recruitment platform for various transcription factors such as the αCTD[39], NusG-NTD[40], and SuhB[17,18]. NusA is regulated via autoinhibition as NusA-AR2 binds to the KH1 domain, preventing RNA binding by NusA-SKK[39,41,42]. This autoinhibition may be released by RNAP αCTD to activate RNA binding by NusA[39], by SuhB during ribosomal AT[17,18] or by NusG-NTD, a process that might be play a role during NusG recruitment, in resynchronization of transcription:translation coupling or in modulation of termination efficiency[40].

Nus factors are involved in various AT mechanisms. It has been demonstrated that NusA is able to stimulate Q-dependent AT in phage 82[43] and it has been suggested that NusA promotes recruitment of Q in phage λ[32]. Here, we used solution-state nuclear magnetic resonance (NMR) spectroscopy to provide conclusive evidence that of all Nus factors only NusA interacts directly with λQ, establishing interactions *via* its NTD and AR2 domain. As NusA-NTD and λQ share binding sites on RNAP, the NusA-NTD:λQ interaction might be responsible for repositioning of NusA, stimulating λQ-mediated AT. We show that binding of λQ to NusA-AR2 releases autoinhibition of NusA, implying that NusA-AR2 is not only a versatile interaction platform for various transcription partners, but suggesting that NusA may be regarded as regulatory subunit of RNAP that substitutes the sigma factor.

Results

The solution structure of λQ. The 60 residues at the N-terminus of λQ are highly polar and are suggested to be disordered as, until now, only the crystal structure of a λQ variant lacking 38 residues at the N-terminus could be determined and even the electron density of this deletion variant was only interpretable starting at residue 62 (Fig. 1a)[14]. As the N-terminus, however, might have a functional role we used solution-state NMR spectroscopy to study the full length protein. The [^{1}H,^{15}N]-band-selective excitation short-transient transverse relaxation optimized spectroscopy (BEST-TROSY) spectrum of ^{15}N-labeled λQ showed good signal dispersion (Fig. 1b) and perfectly superimposes with the spectrum of a λQ deletion variant lacking 36 residues at the N-terminus ($\lambda Q^{\Delta 36}$). Additional signals in the spectrum of the full length protein are all located between 7.5 and 8.5 ppm in the proton dimension, typical for random coil structures, suggesting that the N-terminus is indeed disordered in solution (Fig. 1b). Using $\lambda Q^{\Delta 36}$ we assigned 75.4% of the amide backbone and 78.4% of the C^{α} backbone signals (Fig. 1a). Unassigned residues are especially located at the N-terminus, at the C-terminal end of helix α3 (aa 108–120) and in the center of helix α6 (aa 189–198). The chemical shift index (CSI) of C_{α} and C_{O} atoms is in perfect agreement with the crystal structure (Fig. 1c), demonstrating that the three-dimensional (3D) structures in solution and in the crystal are identical. Analytical gel filtration showed that protein solutions of λQ and $\lambda Q^{\Delta 36}$ were homogeneous, giving molecular weights of 30 kDa and 17 kDa for λQ and $\lambda Q^{\Delta 36}$, respectively (theoretical molecular mass: 23 kDa and 16 kDa), indicating that both proteins exist as monomers in solution (Supplementary Fig. 2a). Next, we determined the ^{15}N relaxation behavior of $\lambda Q^{\Delta 36}$ by NMR spectroscopy at 16.8 T magnetic field strength (Supplementary Fig. S2b) to characterize the overall tumbling of the protein. We obtained averaged ^{15}N relaxation rates of $0.84 \pm 0.06\,s^{-1}$ and $19.5 \pm 0.6\,s^{-1}$ for R_1 and R_2, respectively. Assuming isotropic tumbling, these rates correspond to a rotation correlation time τ_c of 14 ± 1 ns, which suggests a molecular weight of ~23 kDa. This result supports the conclusion that the protein is a monomer in solution. The fact that the experimentally determined molecular weights of λQ and $\lambda Q^{\Delta 36}$ are slightly larger than the theoretical values for the monomeric proteins might be attributed to the facts that (i) both have an unstructured N-terminus (60 and 30 amino acids, respectively) and (ii) both have an elongated shape, i.e. both do not behave like perfectly globular proteins.

λQ directly interacts with NusA. Nus factors are involved in both λN-dependent and ribosomal AT. They are part of huge nucleoprotein complexes that modify RNAP into a termination-resistant state, so-called TACs[6,7,17,18,20]. Efficient λQ-dependent AT requires at least NusA[44], which is thought to stabilize binding of

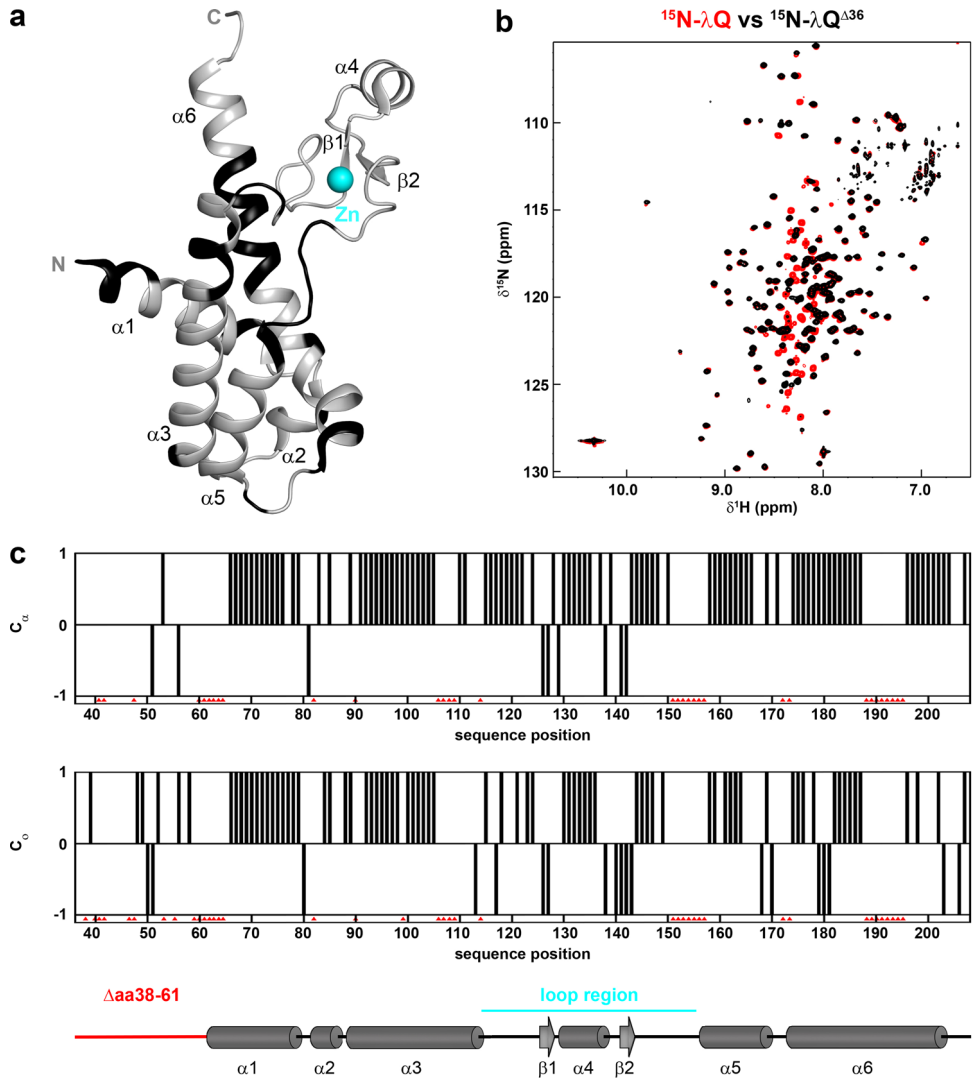

Figure 1. Structure of $\lambda Q^{\Delta 36}$. (**a**) Ribbon representation of the crystal structure of a λQ truncation variant lacking 38 residues at the N-terminus, electron density was only interpretable starting at residue 62 (PDB ID: 4MO1; gray). Termini and secondary structure elements are labeled. Unassigned amide backbone signals are shown in black, the Zn^{2+} is highlighted as cyan sphere. The PyMOL Molecular Graphics System (Version 1.7, Schrödinger, LLC.; https://pymol.org) was used for visualization. (**b**) Overlay of [^{1}H,^{15}N]-BEST-TROSY spectra of ^{15}N-λQ (red) and ^{15}N-$\lambda Q^{\Delta 36}$ (black). (**c**) Chemical shift index (CSI) for C_α and C_O of $\lambda Q^{\Delta 36}$ *vs*. secondary structure of the crystal structure (PDB ID: 4MO1). The missing residues due to non-interpretable electron density are indicated in red, the loop region is shown in cyan.

λQ to the TEC[32]. Thus, we used solution-state NMR spectroscopy to test if λQ directly interacts with any of the Nus factors. We titrated ^{15}N-labeled λQ with individual Nus factors and recorded one-dimensional (1D) [^{1}H,^{15}N]-heteronuclear single quantum coherence (HSQC) and two-dimensional (2D) [^{1}H,^{15}N]-BEST-TROSY spectra (Supplementary Fig. 3). For NusE we employed a protein variant which lacks the ribosome binding loop ($NusE^{\Delta}$), and which is in complex with NusB to increase solubility[27]. Only the presence of NusA (54.9 kDa) led to a significant change in the spectra of ^{15}N-λQ (Supplementary Fig. 3), namely the signal intensity of ^{15}N-λQ was significantly decreased upon addition of NusA (Supplementary Fig. 3a). Slower tumbling leads to increased transverse relaxation rates, which results in line broadening and thus ultimately in a decrease of signal intensity of ^{15}N-λQ signals. Consequently, the loss of ^{15}N-λQ signal intensity suggests a direct λQ:NusA interaction.

λQ binds to NusA-NTD. In order to identify the region of NusA that binds to λQ we carried out [^{1}H,^{15}N]-HSQC-based titrations of λQ and the individual domains of NusA with 1D and 2D spectra being recorded after each titration step. Titration of ^{15}N-λQ with NusA-NTD led to a significant change of the ^{15}N-λQ spectrum (Fig. 2a and Supplementary Fig. 4a), indicating complex formation. Likewise ^{15}N-NusA-NTD signals were substantially affected in the presence of λQ (Fig. 2b and Supplementary Fig. 4b). In both titrations the signal intensity of the labeled protein was decreased non-uniformly upon addition of the binding partner whereas chemical shift perturbations were only small, suggesting intermediate or slow chemical exchange on the NMR

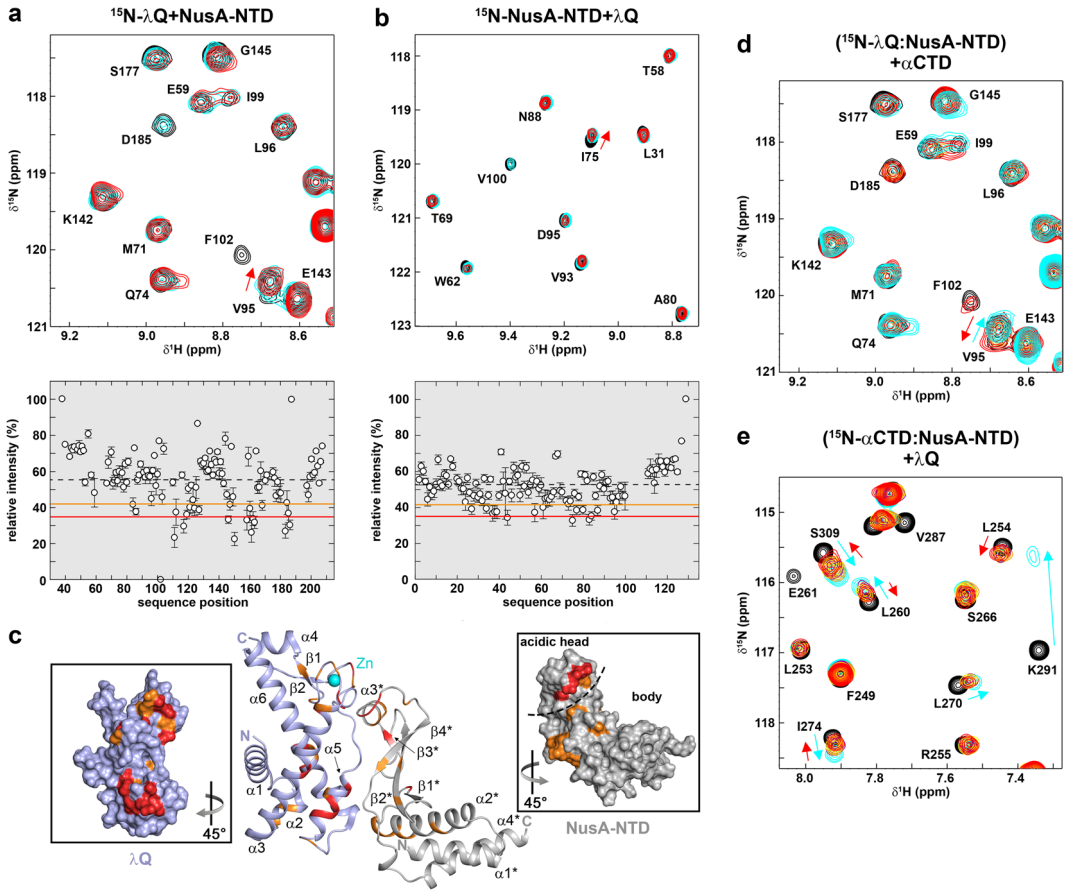

Figure 2. NusA interacts with λQ via its NTD. (a) (top) Section of [^{1}H,^{15}N]-BEST-TROSY spectra of the titration of 250 µM ^{15}N-λQ with NusA-NTD (molar ratios: 1:0, black; 1:1, cyan; 1:2 red). Selected signals are labeled. (bottom) Relative intensity of ^{15}N-λQ signals in the presence of one equivalent NusA-NTD. Orange and red lines indicate thresholds for moderately (1.0 σ of average relative signal intensity) and strongly (1.5 σ of average relative signal intensity) affected signals, respectively. The dashed line represents the mean relative intensity, error bars are given as black vertical lines. **(b)** (top) Section of [^{1}H,^{15}N]-HSQC spectra of the titration of 175 µM ^{15}N-NusA-NTD with λQ (molar ratios: 1:0, black; 1:1, cyan; 1:2 red). Selected signals are labeled. (bottom) Relative intensity of ^{15}N-NusA-NTD signals in the presence of one equivalent λQ with error bars. Thresholds as in (a). **(c)** Model of the λQ:NusA-NTD complex. The model was generated with the HADDOCK 2.2 server (https://haddock.science.uu.nl/services/HADDOCK2.2/) using affected residues as determined via NMR spectroscopy as restraints (see Supplementary Table 1). The model with the lowest HADDOCK and Z-score is depicted. λQ (PDB ID: 4MO1, lightblue) and NusA-NTD (PDB ID: 2KWP, gray) are shown in ribbon representation. Affected residues are colored (moderately affected residues, orange; strongly affected residues, red). Termini and secondary structure elements are labeled. Panels show the surface representations of λQ (left) and NusA-NTD (right) colored as in the complex. The PyMOL Molecular Graphics System (Version 1.7, Schrödinger, LLC.; https://pymol.org) was used for visualization. **(d)** αCTD detaches NusA-NTD from ^{15}N-λQ. Sections of [^{1}H,^{15}N]-BEST-TROSY spectra are shown. Molar ratios: ^{15}N-λQ:NusA-NTD: αCTD = 1:0:0, black; =1:2:0, cyan; 1:2:2, orange; 1:2:4, red. Initial concentration of ^{15}N-λQ: 250 µM. Selected signals are labeled, arrows indicate chemical shift changes upon addition of NusA-NTD (cyan) and αCTD (red). **(e)** λQ removes NusA-NTD from ^{15}N-αCTD. Sections of [^{1}H,^{15}N]-HSQC spectra are shown. Molar ratios: ^{15}N-αCTD:NusA-NTD:λQ = 1:0:0; black; =1:2:0; cyan; 1:2:2; orange; 1:2:4, purple; 1:2:6, yellow; 1:2:10, red. Initial concentration of ^{15}N-αCTD: 250 µM. Selected signals are labeled, arrows indicate chemical shift changes upon addition of NusA-NTD (cyan) and λQ (red).

time scale. Thus, in both titrations the change of signal intensity was analysed quantitatively by calculating the relative signal intensity of the ^{15}N-labeled protein in the presence of one equivalent of the non-labeled binding partner (for details see Material and Methods). In brief, we defined the relative intensity as ratio of the normalized remaining signal intensity of the ^{15}N-labeled protein in the presence of the binding partner to the normalized signal intensity of the free labeled protein. The relative intensity was plotted against the corresponding amino acid position (Fig. 2a,b) and thresholds at 1.5 σ and 1.0 σ of the mean relative signal intensity were used to identify strongly and moderately affected residues, respectively, which were then mapped onto the 3D structures of λQ and NusA-NTD (Fig. 2c). λQ residues affected by NusA-NTD binding form two continuous patches. The first patch involves residues located in α3 and α5, the second patch contains residues at C- and N-terminal parts of

the Zn-binding motif (Fig. 2c, left inset). NusA-NTD residues affected by binding of λQ are primarily located in the acidic head region and the upper part of the body region at the convex side of NusA-NTD. Due to insufficient long-term stability we did not record intermolecular nuclear Overhauser effect (NOE) interactions. Thus a docking model was generated based on the affected residues in both proteins and without allowing conformational rearrangements (Supplementary Fig. 4c-e). In the lowest energy model (Fig. 2c) the acidic head of NusA-NTD contacts the Zn-finger of λQ and the upper part of the NusA-NTD body interacts with the second patch of λQ, giving an overall interface area of 1050 Å^2.

We also checked if the unstructured N-terminus of λQ is involved in NusA-NTD binding by titrating ^{15}N-NusA-NTD with λQ$^{\Delta 36}$ and recorded a 2D [^{1}H,^{15}N]-HSQC spectrum after each titration step (Supplementary Fig. 5a). Like in the titration with full length λQ the intensity of ^{15}N-NusA-NTD signals was significantly decreased in the presence of λQ$^{\Delta 36}$, and the relative signal intensity in the equimolar titration step was plotted against the amino acid position of NusA-NTD (Supplementary Fig. 5b). Mapping of the affected residues onto the NusA-NTD structure (Supplementary Fig. 5c) resulted in the same binding site as identified in the titration with full length λQ, indicating that the N-terminus of λQ does not influence the interaction with NusA-NTD.

λQ and RNAPαCTD share binding sites on NusA-NTD. NusA-NTD contacts two regions of RNAP, the βFTH and the αCTD[2]. The λQ binding site is located on the convex side of NusA-NTD, overlapping with the binding site for RNAP αCTD[2], thus suggesting that binding of λQ and αCTD might be competitive. To test if the interactions of αCTD and λQ with NusA-NTD are mutual exclusive, we performed NMR-based competition experiments with [^{1}H,^{15}N]-HSQC spectra being recorded after each titration step. First, NusA-NTD was added in a two-fold molar excess to ^{15}N-Q, resulting in signal changes typical for ^{15}N-λQ:NusA-NTD complex formation (Fig. 2d and Supplementary Fig. 6a; see also Fig. 2a). Subsequent titration with αCTD reversed the signal changes (both chemical shift changes and loss of signal intensity), demonstrating that αCTD binds to NusA-NTD, detaching it from λQ. To confirm this finding we carried out a reverse experiment where NusA-NTD was added to ^{15}N-αCTD in a 1:2 molar ratio, leading to chemical shift perturbations that indicate complex formation. Addition of λQ reversed those changes, indicating that λQ removes NusA-NTD from αCTD by complexing it (Fig. 2e and Supplementary Fig. 6b). These results imply that the λQ:NusA-NTD and αCTD:NusA-NTD interactions are mutually exclusive and have similar affinities, which, in turn, suggests that both interactions are physiologically relevant. We excluded a direct αCTD:λQ interaction as the titration of ^{15}N-λQ with αCTD did not alter the spectra of ^{15}N-λQ (Supplementary Fig. 6c).

λQ does not interact with NusA-SKK and NusA-AR1. Having identified NusA-NTD as interaction partner of λQ we tested next if also NusA-SKK binds to it. We titrated ^{15}N-labeled λQ with NusA-SKK and *vice versa* and recorded 1D- and 2D-[^{1}H,^{15}N] correlation spectra after each titration step (Supplementary Fig. 7a,b). Even in the presence of a twofold molar excess of the unlabeled binding partner no significant changes were observable in the spectra of the labeled protein, excluding a direct NusA-SKK:λQ interaction. Using the same approach we asked if λQ binds to NusA-AR1, which contacts λN in λN-dependent AT[36–38], but again, no direct interaction could be detected (Supplementary Fig. 7c,d).

λQ binds to NusA-AR2. Finally, we tested if λQ interacts with NusA-AR2. Upon addition of NusA-AR2 to ^{15}N-λQ the 1D and 2D spectra of ^{15}N-λQ changed significantly (Fig. 3a and Supplementary Fig. 8a). As in the titration of ^{15}N-λQ with NusA-NTD, the intensity of ^{15}N-λQ signals decreased non-uniformly whereas only slight chemical shift perturbation were observable. Thus, we analyzed the change of signal intensity quantitatively. The relative intensity of ^{15}N-λQ signals in the presence of two equivalents NusA-AR2 was plotted against the amino acid sequence of λQ and affected residues were identified by using thresholds at 1.5 and 1.0 σ of the mean relative intensity (Fig. 3a). In contrast, the titration of ^{15}N-NusA-AR2 with λQ resulted in significant chemical shift perturbations and normalized chemical shift changes ($\Delta\delta_{norm}$) were plotted against the amino acid sequence of NusA-AR2 (Fig. 3b and Supplementary Fig. 8b). To visualize binding surfaces affected residues were mapped on the 3D structures of λQ and NusA-AR2 (Fig. 3c). λQ residues affected by NusA-AR2 binding are located opposite the Zn binding motif and the flexible arm, and strongly affected residues can be found predominantly in helices α3 and α5.

The λQ binding site of NusA-AR2 is located at the C-terminal part of the domain and comprises helix α5*, with W490 and F491 being strongly affected. These two residues are known to be responsible for the specific recognition of other transcription regulators such as αCTD[39], NusG-NTD[40], or SuhB[17,18]. As for the λQ:NusA-NTD complex, we did not record intermolecular NOE interactions due to insufficient long-term stability of λQ. Based on the identified binding surfaces a docking model of the λQ:NusA-AR2 complex was generated without allowing conformational rearrangements (Supplementary Fig. 8c-e). In the lowest energy model (Fig. 3c) helix α5* of NusA-AR2 packs against helices α3 and α5 of λQ so that W490 and F491 are central parts of the interface, which comprises a total area of 1230 Å^2. Finally, we determined the K_D for the λQ:NusA-AR2 complex by fluorescence anisotropy measurements using NusA-AR2^{D443C}, a NusA-AR2 variant where D443, located opposite the λQ binding site, is substituted by a Cys[18]. NusA-AR2^{D443C} was labeled site-specifically with fluorescein5-maleimide and titrated with λQ, giving a K_D of 268 ± 17 µM (Supplementary Fig. 8f). Repeating the HSQC-based titration of ^{15}N-NusA-NTD with λQ$^{\Delta 36}$ resulted in the same binding surface as determined for full length λQ (Supplementary Fig. 8g-i), suggesting that the unstructured N-terminus of λQ is not involved in NusA-AR2 binding. This finding was corroborated by fluorescence anisotropy measurements as the affinity of the NusA-AR2^{D443C}:λQ$^{\Delta 36}$ interactions was determined to be 271 ± 27 µM (Supplementary Fig. 8j).

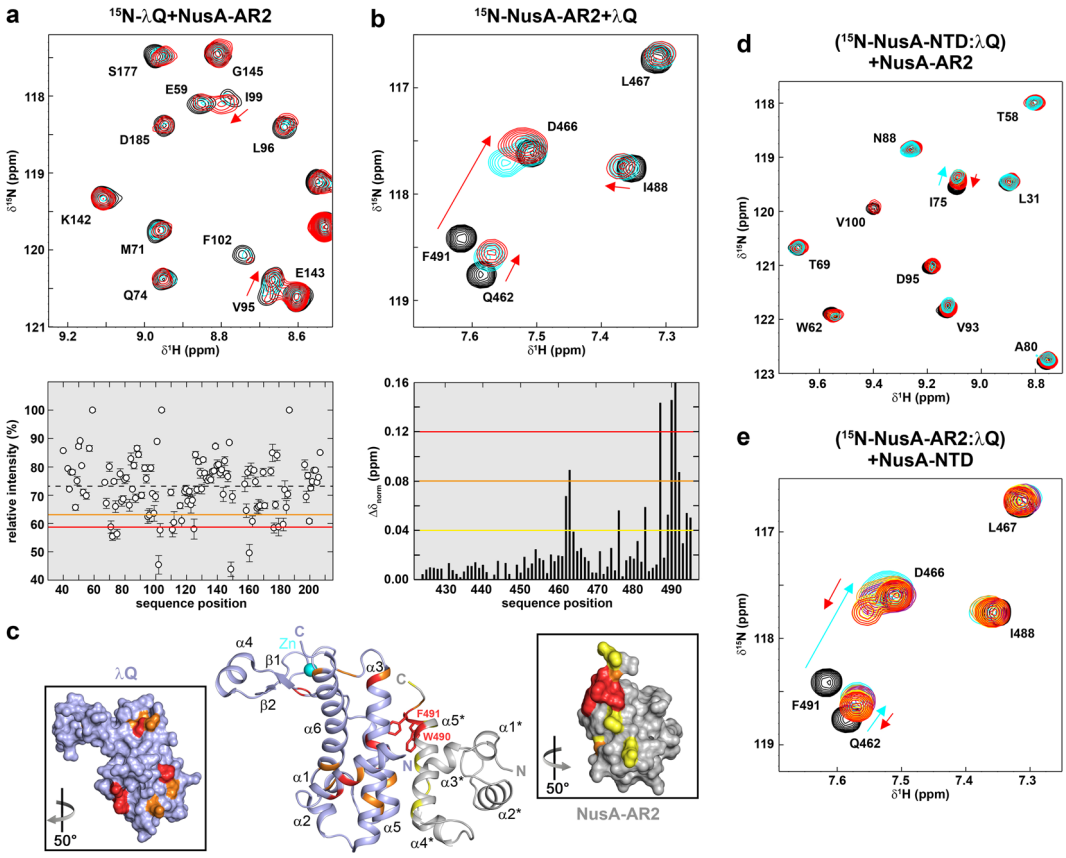

Figure 3. NusA interacts with λQ via its AR2 domain. (**a**) (top) Section of [^{1}H,^{15}N]-BEST-TROSY spectra of the titration of 250 µM ^{15}N-λQ with NusA-AR2. NusA-AR2 (molar ratios: 1:0, black; 1:1, cyan; 1:2 red). Selected signals are labeled. (bottom) Relative intensity of ^{15}N-λQ signals in the presence of two equivalents NusA-AR2. Error bars are given as black vertical lines. Orange and red lines indicate thresholds for moderately (1.0 σ of average relative signal intensity) and strongly (1.5 σ of average relative signal intensity) affected signals, respectively. The dashed line represents the mean relative intensity. **(b)** (top) Section of [^{1}H,^{15}N]-HSQC spectra of the titration of 250 µM ^{15}N-NusA-AR2 with λQ (molar ratios: 1:0, black; 1:1, cyan; 1:2 red). Selected signals are labeled. (bottom) Normalized chemical shift changes of ^{15}N-NusA-AR2 upon addition of two equivalents λQ. Yellow, orange, and red lines indicate thresholds for slightly (0.04 ppm $\leq \Delta\delta_{norm} <$ 0.08 ppm), moderately (0.08 ppm $\leq \Delta\delta_{norm} <$ 0.12 ppm) and strongly ($\Delta\delta_{norm} \geq$ 0.12 ppm) affected signals. **(c)** Model of the λQ:NusA-AR2 complex. The model was generated using the HADDOCK 2.2 server (https://haddock.science.uu.nl/services/HADDOCK2.2/) with the affected residues as determined by NMR spectroscopy as restraints (see Supplementary Table 1). The model with the lowest HADDOCK score is depicted. λQ (PDB ID: 4MO1, lightblue) and NusA-AR2 (PDB ID: 1WCN, gray) are in ribbon representation. Affected residues are colored (λQ: moderately affected residues, orange; strongly affected residues, red; NusA-AR2: slightly affected residues, yellow; moderately affected residues, orange; strongly affected residues, red). Termini and secondary structure elements are labeled. Panels show the surface representations of λQ (left) and NusA-AR2 (right) colored as in the complex. The PyMOL Molecular Graphics System (Version 1.7, Schrödinger, LLC.; https://pymol.org) was used for visualization. **(d)** NusA-AR2 removes λQ from ^{15}N-NusA-NTD. Sections of [^{1}H,^{15}N]-HSQC spectra are depicted. Molar ratios: ^{15}N-NusA-NTD:λQ:NusA-AR2 = 1:0:0, black; =1:2:0, cyan; 1:2:2, orange; 1:2:4, red. Initial concentration of ^{15}N-NusA-NTD: 250 µM. Selected signals are labeled, arrows indicate the chemical shift changes upon addition of λQ (cyan) and NusA-AR2 (red). **(e)** NusA-NTD detaches λQ from ^{15}N-NusA-AR2. Sections of [^{1}H,^{15}N]-HSQC spectra are shown. Molar ratios: ^{15}N-NusA-AR2:λQ:NusA-NTD = 1:0:0; black; =1:2:0; cyan; 1:2:2; orange; 1:2:4, purple; 1:2:6, yellow; 1:2:10, red. Initial concentration of ^{15}N-NusA-AR2: 250 µM. Selected signals are labeled, arrows show changes of chemical shifts upon addition of λQ (cyan) and NusA-NTD (red).

NusA-NTD and NusA-AR2 share binding sites on λQ. In summary, λQ is able to establish interactions with NusA-NTD and NusA-AR2 and comparison of their binding sites on λQ suggests that they are partially overlapping, involving residues located in helices α3 and α5. To test if binding of NusA-NTD and NusA-AR2 is indeed competitive, we carried out 2D [^{1}H,^{15}N]-HSQC-based competition experiments with spectra being recorded after each titration step. First, λQ was added in a two-fold molar excess to ^{15}N-NusA-NTD, resulting in changes of the ^{15}N-NusA-NTD spectrum typical for ^{15}N-NusA-NTD:λQ complex formation (Fig. 3d and Supplementary Fig. 9a). Subsequent titration with NusA-AR2 reversed those changes partially (Fig. 3d), demonstrating that NusA-AR2 complexes λQ, detaching it from NusA-NTD. To corroborate this finding we formed

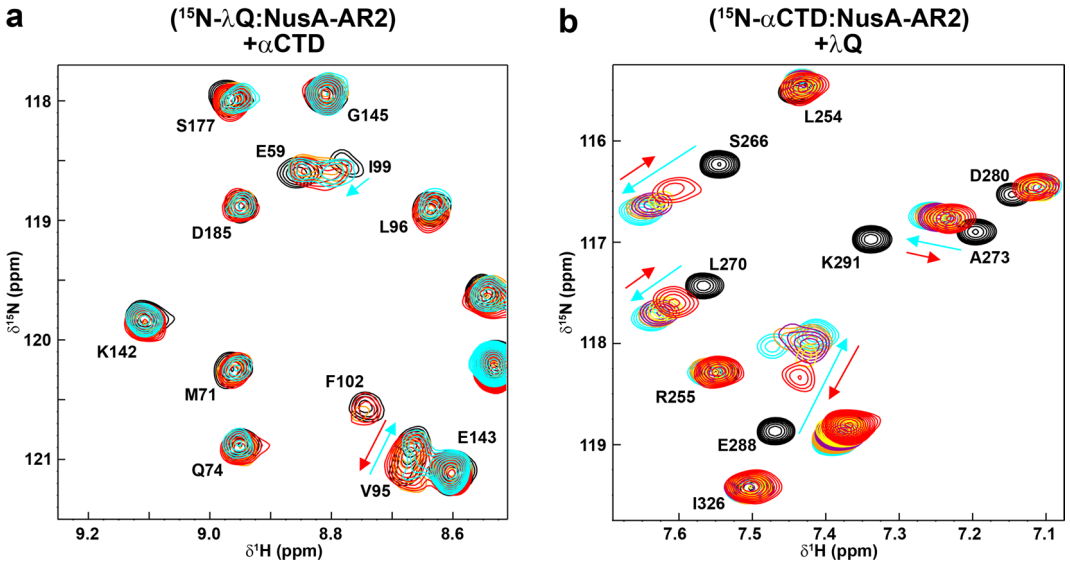

Figure 4. αCTD and λQ share binding sites on NusA-AR2. NMR-based competition experiments of λQ, αCTD, and NusA-AR2. **(a)** NusA-AR2 is detached from ^{15}N-λQ by αCTD. Sections of [^{1}H,^{15}N]-BEST-TROSY spectra are shown. Molar ratios: ^{15}N-λQ:NusA-AR2:αCTD = 1:0:0, black; =1:2:0, cyan; 1:2:2, orange; 1:2:4, red. Initial concentration of ^{15}N-λQ: 250 µM. Selected signals are labeled, arrows indicate chemical shift changes upon addition of NusA-AR2 (cyan) and αCTD (red). **(b)** λQ removes NusA-AR2 partially from ^{15}N-αCTD. Sections of [^{1}H,^{15}N]-HSQC spectra are depicted. Molar ratios: Molar ratios: ^{15}N-αCTD:NusA-AR2:λQ = 1:0:0; black; =1:2:0; cyan; 1:2:2; orange; 1:2:4, purple; 1:2:6, yellow; 1:2:10, red. Initial concentration of ^{15}N-αCTD: 250 µM. Selected signals are labeled and arrows show changes in chemical shifts upon addition of NusA-AR2 (cyan) and λQ (red).

a ^{15}N-NusA-AR2:λQ complex (molar ratio 1:2) leading to chemical shift perturbations of the ^{15}N-NusA-AR2 signals that confirm λQ binding (Fig. 3e and Supplementary Fig. 9b). Upon addition of NusA-NTD the chemical shifts shifted back towards their position in the spectrum of free ^{15}N-NusA-AR2 (Fig. 3e), showing that NusA-NTD binds to λQ while removing it from NusA-AR2. Thus, the λQ:NusA-NTD and the λQ:NusA-AR2 interactions are mutually exclusive with similar affinities.

λQ and RNAPαCTD share binding sites on NusA-AR2. In free NusA the AR2 domain binds to the KH1 domain of the SKK motif, preventing RNA binding by NusA-SKK and rendering NusA autoinhibited[39,41,42]. This autoinhibition can be released by the αCTD of RNAP as NusA-SKK and αCTD share binding sites on NusA-AR2[39]. NusA-AR2, however, can also bind to NusG-NTD, an interaction that might be involved in the regulation of Rho-dependent termination or in the recruitment of NusG[40], and to SuhB[17,18]. The NusA-AR2:SuhB complex formation is suggested to play a role in the transcriptional or posttranscriptional regulation of ribosomal AT. Interestingly, the binding sites for NusG-NTD, SuhB, and αCTD as well as λQ on NusA-AR2 all involve the C-terminal helix α5 and overlap. Moreover, it has been demonstrated that the interactions of NusA-AR2 with NusG-NTD, αCTD, and SuhB are competitive[18].

To show that also λQ competes with NusG-NTD, αCTD, and SuhB for NusA-AR2 binding we tested if the complexes λQ:NusA-AR2 and αCTD:NusA-AR2 are mutually exclusive by 2D NMR-based competition experiments with spectra being recorded after each titration step. First, NusA-AR2 was added in a twofold molar excess to ^{15}N-λQ, resulting in changes of the ^{15}N-λQ spectrum corresponding to ^{15}N-λQ:NusA-AR2 complex formation. Subsequent titration with the αCTD reversed both the chemical shift changes and the loss of signal intensity, showing that the αCTD detaches NusA-AR2 from λQ by binding to it (Fig. 4a and Supplementary Fig. 10a). To confirm this result we performed another competition experiment where λQ was titrated to a preformed ^{15}N-αCTD:NusA-AR2 complex (molar ratio 1:2). The addition of λQ reversed partially the chemical shift perturbations caused by the ^{15}N-αCTD:NusA-AR2 complex formation (Fig. 4b and Supplementary Fig. 10b), demonstrating that λQ can bind to NusA-AR2 in order to remove it from the αCTD. Together with previous data[18,40] this finding leads to the conclusion that the NusA-AR2 binding sites for αCTD, λQ, NusG-NTD, and SuhB largely overlap, rendering the interactions of these binding partners with NusA-AR2 competitive. Finally, the K_D value of the αCTD:NusA-AR2 interaction was determined by fluorescence anisotropy measurements using the NusA-AR2^{D443C} variant to be 8±1 µM (Supplementary Fig. 10c), in agreement with a previous report[39]. Thus, the affinity of the NusA-AR2^{D443C}:αCTD interaction is significantly higher than the one of the NusA-AR2^{D443C}:λQ interaction, which explains why λQ is able to detach NusA-AR2 only partially from the αCTD (Fig. 4).

λQ may release the autoinhibition of NusA. NusA-AR2 binding sites for αCTD, NusG-NTD and SuhB not only overlap, but all these factors are able to remove NusA-AR2 from NusA-SKK, releasing autoinhibition of NusA[18,39,41]. Thus, we explored if λQ has the same ability employing NMR-based displacement experiments.

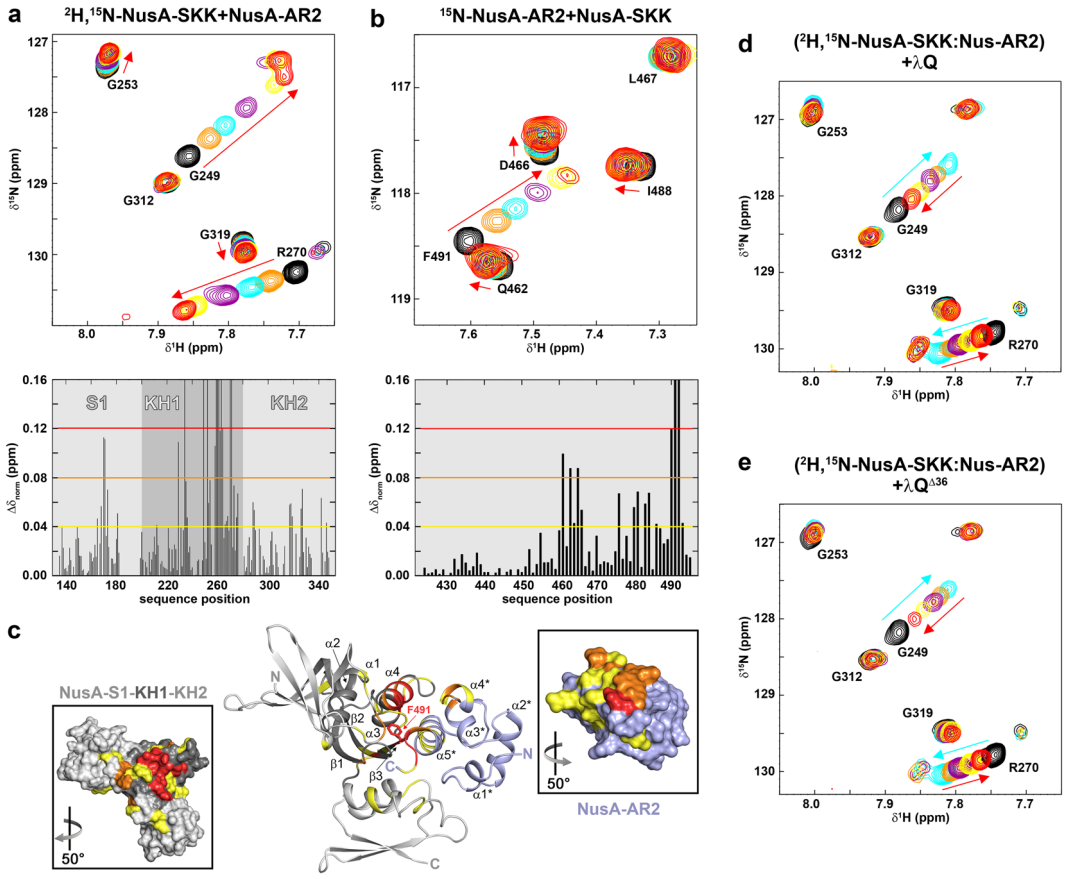

Figure 5. λQ releases autoinhibition of NusA. (**a**) (top) Sections of [^{1}H,^{15}N]-BEST-TROSY spectra of the titration of 300 µM ^{2}H,^{15}N-NusA-SKK with NusA-AR2 (molar ratios: 1:0, black; 1:0.5, orange; 1:1, cyan; 1:2 purple; 1:5 yellow; 1:7.5 red; stock concentration of NusA-AR2: 1.5 mM). Selected signals are labeled. (bottom) Normalized chemical shift perturbations of ^{2}H,^{15}N-NusA-SKK signals upon addition of 7.5 equivalents NusA-AR2. Yellow, orange, and red lines indicate thresholds for slightly (0.04 ppm $\leq \Delta\delta_{norm} <$ 0.08 ppm), moderately (0.08 ppm $\leq \Delta\delta_{norm} <$ 0.12 ppm) and strongly ($\Delta\delta_{norm} \geq$ 0.12 ppm) affected signals. **(b)** (top) Sections of [^{1}H,^{15}N]-HSQC spectra of the titration of 200 µM ^{15}N-NusA-AR2 with NusA-SKK (molar ratios: 1:0, black; 1:0.5, orange; 1:1, cyan; 1:2 purple; 1:5 yellow; 1:7.5 red; stock concentration of NusA-SKK: 500 µM). Selected signals are assigned. (bottom) Normalized chemical shift changes of ^{15}N-NusA-AR2 upon addition of 7.5 equivalents NusA-SKK. Thresholds as in **(b)**. **(c)** Model of the NusA-SKK:NusA-AR2 complex. The model was generated with the HADDOCK 2.2 server (https://haddock.science.uu.nl/services/HADDOCK2.2/) using affected residues as determined by NMR spectroscopy as restraints (see Supplementary Table 1). The model with the lowest HADDOCK score and Z-score is depicted. NusA-AR2 (PDB ID: 1WCN, lightblue) and NusA-SKK (PDB ID: 5LM9, gray) are in ribbon representation. Affected residues are colored (slightly affected residues, yellow; moderately affected residues, orange; strongly affected residues, red). Termini and secondary structure elements are labeled. Panels show the surface representations of NusA-AR2 (left) and NusA-SKK (right), colored as in the complex, whereby the KH1 domain is highlighted in dark gray. The PyMOL Molecular Graphics System (Version 1.7, Schrödinger, LLC.; https://pymol.org) was used for visualization. **(d)** λQ and **(e)** $\lambda Q^{\Delta 36}$ detach NusA-AR2 from ^{2}H,^{15}N-NusA-SKK. Sections of [^{1}H,^{15}N]-BEST-TROSY are shown. Molar ratios: ^{2}H,^{15}N-NusA-SKK: NusA-AR2:λQ/$\lambda Q^{\Delta 36}$ =1:0:0, black; =1:5:0, orange; =1:5:1, cyan; =1:5:2, purple; =1:5:5, yellow; =1:5:10, red. Initial concentration of ^{2}H,^{15}N-NusA-SKK: 175 µM. Selected signals are labeled and arrows indicate chemical shift changes upon addition of NusA-AR2 (cyan) and λQ/$\lambda Q^{\Delta 36}$ (red).

In control experiments we titrated ^{2}H,^{15}N-labeled NusA-SKK with NusA-AR2 and *vice versa* and recorded 1D and 2D [^{1}H,^{15}N] correlation spectra after each titration step to determine the chemical shift perturbations caused by NusA-AR2:NusA-SKK complex formation on both sides (Fig. 5a,b and Supplementary Fig. 11a,b). For both titrations normalized chemical shift perturbations were plotted against the amino acid sequence of the labeled protein (Fig. 5a,b) and mapped on the 3D structures (Fig. 5c). The identified binding surfaces were in agreement with previous data[39], i.e. the C-terminal part of NusA-AR2 is affected as well as the KH1 domain of NusA-SKK. Based on the normalized changes of the chemical shifts we estimated the affinity of the NusA-SKK:NusA-AR2 interaction to be <341 µM (Supplementary Fig. 11c). In an alternative approach we determined the K_D value by fluorescence anisotropy measurement employing the NusA-$AR2^{D443C}$ variant, yielding a slightly lower affinity (279 ± 17 µM; Supplementary Fig. 11d), similar to the one of the NusA-$AR2^{D443C}$:λQ interaction. As no structure of autoinhibited NusA is available we performed NMR-guided docking using the results of the HSQC titrations

and without allowing for conformational changes to obtain a model of the NusA-SKK:NusA-AR2 complex (Fig. 5c). NusA-AR2 packs tightly against the KH1 domain via its C-terminal helix with an interaction surface of 1230 Å^2, blocking the RNA binding site. Addition of λQ to a preformed ^{2}H,^{15}N-NusA-SKK:NusA-AR2 complex (molar ratio 1:2) led to a partial reversal of all signal shifts (Fig. 5d and Supplementary Fig. 11e). This finding is in agreement with the K_D values of the NusA-SKK:NusA-AR2 and NusA-AR2:λQ interactions and indicates that λQ binds to NusA-AR2 releasing NusA-SKK at the same time, thus being compatible with the release of NusA autoinhibition by λQ. However, one must bare in mind that isolated NusA domains were used in these experiments and that the affinity of NusA-AR2 for NusA-SKK might be higher in the full length protein due to an increased local concentration. Consequently, our results are in agreement with a λQ-induced release of autoinhibition of NusA, but not final prove. NMR-based approaches using the full length NusA protein failed due to stability issues. Repeating the competition experiment with λQ$^{\Delta 36}$ confirmed that the N-terminus is not required for this function of λQ (Fig. 5e and Supplementary Fig. 11f).

Discussion

Q-dependent AT is the second mechanism lambdoid phages use to suppress termination signals. N-mediated AT is the best studied AT mechanism by now whereas only little is known about AT relying on Q. Only recently, the structural basis for AT involving Q from bacteriophage 21 has been deciphered[12,13]. However, as mentioned before, Q proteins can be grouped into three families, Q21, Q82, and λQ, and these families show no significant amino acid sequence similarity and only very little similarity in the 3D structure (with structural information being available only for Q21 and a truncated version of λQ)[12–14]. Consequently, the molecular mechanisms they use to achieve AT might be completely different, despite the fact that all Q proteins seem to bind to or in the vicinity of the βFTH in order to affect pausing and termination[12,13,43,45]. One striking difference between Q21 and λQ is for example that the latter has a long N-terminal region with unknown function that has been suggested to be unstructured. Moreover, two distinct activities have been suggested for Q82, namely antipausing and RNA occlusion, which may both play a role in Q82 function[43]. Finally, it is known that Nus factors are involved in other AT mechanisms such as N-mediated and ribosomal AT[6,7,15,17,18]. At least NusA has been demonstrated to influence Q function in phages λ and 82, although the dependency of Q activity on NusA differs[32,43,44,46]. Thus, we set out to identify possible interactions of λQ with Nus factors.

Using solution-state NMR spectroscopy we assigned secondary structure elements of λQ$^{\Delta 36}$ and found that the solution structure is in good agreement with the crystal structure of an N-terminal truncation variant of λQ missing 38 amino acids (Fig. 1). Structural similarity to Q21 and region 4 of σ^{70} factor is limited to the helix-turn-helix (HTH) motif formed by helices α5 and α6[12,13,47,48], which might be involved in the recognition of the QBE[14]. Moreover, we confirmed that residues 1–66 are indeed unstructured (Fig. 1). It has been proposed that at least two molecules of λQ are involved in the AT process[11] and NMR spectroscopy and analytical SEC indicate that λQ and λQ$^{\Delta 36}$ exist as monomers in solution, suggesting that the N-terminus does not induce oligomerization. This implies several scenarios: (i) dimerization/oligomerization occurs upon DNA binding or loading to the paused TEC, similar to Q21[12,13], (ii) several Q proteins are involved in AT, but do not interact with each other, or (iii) λQ acts as monomer that contacts both suggested binding sites in the QBE on the DNA[11].

Q proteins bind to/near the βFTH of RNAP in order to exert their AT function[12,13,45] and Q21 has been shown to form a nozzle at the RNA exit channel through which the nascent RNA is guided, preventing the formation of pause or termination hairpins[12,13], i.e. AT can proceed without the need of any other factors. In contrast, Q82 is supposed to form a shield for the exiting RNA in a NusA-dependent manner[43] and also λQ-dependent AT is stimulated by NusA[32,44,46]. Thus, we asked if λQ makes direct interactions with any of the Nus factors and we show that λQ only interacts with NusA, contacting the NTD and the AR2 domain. In neither case the N-terminus of λQ is involved in the interaction so that its function remains elusive. Interestingly, the λQ binding sites for NusA-NTD and NusA-AR2 overlap so that NusA-NTD and NusA-AR2 binding are mutually exclusive (Fig. 6a,b), as confirmed by competition experiments, suggesting similar affinities and thus distinct roles for these complexes in λQ-dependent AT. Moreover, the NusA binding sites involve (at least partially) the HTH motif (Fig. 6c) so that NusA interaction might interfere with DNA binding and might thus be relevant only once λQ is loaded to the TEC, in agreement with the fact that NusA is usually recruited after the σ factor has left the TEC[49]. If more than one λQ molecule is loaded to the TEC, interactions with NusA-NTD, NusA-AR2 and DNA would be possible simultaneously.

The NusA-AR2:λQ interaction might have various regulatory roles. It could (i) stabilize the TAC, (ii) promote the engagement of λQ with the TAC, in agreement with a previous hypothesis[32], (iii) mediate NusA loading if NusA enters the TAC after λQ, (iv) alter the RNA binding properties of NusA by releasing autoinhibition, or (v) recruit further λQ molecules in the course of transcription, which might be necessary as the late gene region in phage λ comprises 26 kb, (vi) a combination of several of these possible functions.

During transcriptional pausing NusA-NTD interacts with βFTH and the αCTD, the latter interaction involving NusA-NTD helices α3 and parts of the preceding loop[2]. Thus the NusA-NTD:αCTD binding site overlaps with the NusA-NTD:λQ interaction surface and both interactions are mutually exclusive as demonstrated by NMR-based competition experiments (Fig. 2d,e), but λQ does not directly bind to αCTD (Supplementary Fig. 6c). Interestingly, the absence of the αCTD affects the ability of NusA to stimulate λQ-dependent AT[42], suggesting that the NusA-NTD:αCTD and NusA-NTD:λQ interactions have relevant roles in λQ-dependent AT.

NusA-NTD, λQ, and σ region 4 bind to the βFTH, competing for this binding site[2,45,50]. Thus, we hypothesize that upon loading λQ establishes contacts with the βFTH as σ region 4 has already been disengaged from its position in the initiation complex at this stage, as shown for Q21[12,13]. Our NMR data and a mutagenesis analysis[14] suggest that λQ, βFTH, and NusA-NTD cannot form a ternary complex as λQ binding sites for βFTH and NusA-NTD overlap, so that binding is competitive. In this case simultaneous contacts of λQ to the βFTH and NusA-NTD would only possible if more than one molecule λQ is present.

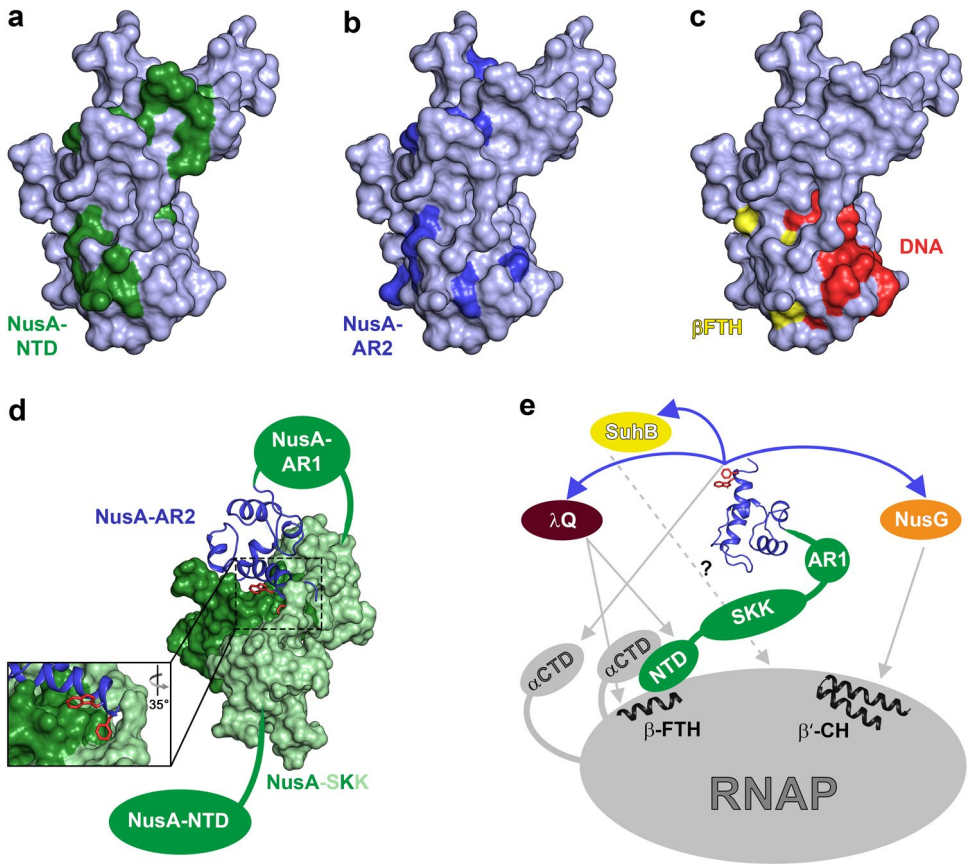

Figure 6. NusA functions during transcription regulation. **(a-c)** Interaction surfaces of λQ (λQ in surface representation, gray, PDB ID: 4MO1). Residues affected by NusA-NTD binding are colored in green (**a**; this study), NusA-AR2 binding in blue (**b**; this study), and βFTH and DNA binding in yellow and red, respectively (**c**; data taken from[14]). **(d)** Model of the autoinhibited state of NusA. NusA-AR2 (PDB ID: 1WCN, blue) is in ribbon, NusA-SKK (PDB ID: 5LM9, green) in surface representation, NusA-NTD and NusA-AR1 are depicted as green ellipsoids. The panel shows a magnification of the boxed region with W490 and F491 of NusA-AR2 as red sticks. **(e)** Scheme of possible roles of NusA. NusA-AR2 is shown in ribbon representation (PDB ID: 1WCN, blue) with W490 and F491 as red sticks, all other NusA domains and proteins are shown as ellipsoids and labeled. Selected RNAP binding sites are depicted in ribbon representation and labeled. Blue arrows indicate interactions of NusA-AR2 with other transcription factors, gray arrows show interactions with RNAP (the interaction of SuhB with RNAP requires further investigation and is displayed as dashed arrow). β' clamp helices, β'CH. The PyMOL Molecular Graphics System (Version 1.7, Schrödinger, LLC.; https://pymol.org) was used for visualization of protein structures.

Processive λN-mediated AT involves repositioning of NusA-NTD[6,7] and a similar mechanism has been suggested for ribosomal AT[17,18]. Although the structures of TACs and antiterminators, the time of antiterminator recruitment and the recruitment signals differ in Q-dependent, N-dependent, and ribosomal AT mechanisms[6,7,12,13,51] the repositioning of NusA-NTD might be a general scheme in AT. Thus, based on our findings we speculate that once recruited to the βFTH λQ may alter the usual NusA:RNAP and/or NusA:RNA contacts, which would finally result in a positioning of NusA-NTD in a way that may prevent the formation of pause and termination hairpins and thus enhances elongation, rendering Q-dependent AT, just like λN-dependent AT, processive[6,7].

NusA is a central transcriptional regulator and well conserved in bacteria. It is a multidomain protein, but only NusA from *E. coli* and some other γ-proteobacteria contains the two AR domains at the C-terminus[35]. In its isolated form, NusA is autoinhibited as NusA-AR2 binds to the KH1 domain of the SKK motif[39], preventing RNA binding by SKK (Fig. 6d). Regulation via autoinhibition is a common scheme in the regulation of all kinds of biochemical processes. In general, autoinhibition describes the negative regulation by intramolecular interactions of different regions of the polypeptide chain, that may even be coupled to conformational changes, and that inhibit the function of at least one of the regions[52,53]. Only under certain circumstances, e.g. the binding of a specific effector, autoinhibition is released and the protein/enzyme is activated. On NusA-AR2 NusA-SKK binding involves the same region as the interaction with λQ (Figs. 3c and 5c), SuhB[18], NusG-NTD[40], and αCTD[39]. Moreover, all known interaction partners of NusA-AR2 are able to release the autoinhibition of NusA and may thus serve as NusA activators. This activation may occur in binary complexes or when NusA is bound to RNAP via NusA-NTD.

NusA-AR1 and NusA-AR2 have nearly identical structures with 31.5% sequence identity and contain predominantly acidic residues, resulting in a very similar electrostatic potential surface[35]. Nevertheless, each AR domain is able to recognize specific targets. NusA-AR1 specifically binds to antiterminator protein N from phage λ[35,37], whereas several binding partners interact with NusA-AR2, e.g. λQ (Fig. 3), SuhB[17,18], NusG-NTD[40], and αCTD[39]. Interestingly, all these binding partners have overlapping binding sites on NusA-AR2, all involving helix α5, and all probably relying on a similar recognition mechanism based on the neighboring aromatic residues W490 and F491, located at the very C-terminus (Supplementary Fig. 12). A Leu (L414) and an Ala (A415) residue can be found at corresponding positions in NusA-AR1.

NusA is composed of several domains with the AR2 domain forming the C-terminus. As all domains are connected via flexible linkers, NusA has a high intramolecular flexibility, i.e. even when NusA is bound to RNAP via its NTD and the SKK motif to RNA during transcription, the AR2 domains can still move virtually independently. Thus, the AR2 domain may serve as flexible and versatile recruitment platform that allows the specific recruitment for various transcription factors in *E. coli* and other γ-proteobacteria (Fig. 6e), as suggested earlier[18]. Once bound to NusA-AR2 these regulators may stay at the AR2 domain or may be handed over to RNAP or other parts of the transcription machinery.

NusA has multiple, sometimes even opposing, functions, which are context- and regulator-dependent, ranging from pause-stimulation to AT. NusA is recruited early in transcription elongation[49] and its NTD occupies the same position as region 4 of the σ factor, i.e. it binds to the βFTH, which constitutes a part of the wall of the RNA exit channel[2]. By interacting with the βFTH NusA-NTD may affect the widening of the RNA exit channel, modulating the transcription speed[2,6,7]. Additionally, NusA-NTD is contacted by one of the αCTDs[2], suggesting that NusA-NTD would still be tethered to RNAP even if the NusA-NTD:βFTH contact was lost (e.g. if a λQ protein is bound to the βFTH). As discussed above, the AR2 domain is able to establish highly specific contacts to other transcription factors, allowing their specific recruitment to the RNAP and thus facilitate the modulation of RNAP activity. Taken together, the early recruitment of NusA, its tuneable function and its ability for the specific recruitment of various other transcription regulators not only underline the central role of NusA in transcription regulation, but imply that NusA may be regarded as auxiliary/additional RNAP subunit, similar to the σ factor, although not being encoded in the *rpo* operon.

Methods

Cloning and mutagenesis. The gene encoding λQ was amplified from the plasmid pUC57_lambdaq obtained from GenScript (Piscataway, NJ, USA; the gene was codon-optimized; additionally, an *Nco*I restriction site was introduced permitting the generation of a λQ deletion variant lacking 36 amino acids at the N-terminus (see below) without changing the amino acid sequence) by polymerase chain reaction using the primers Q-PciI-FW (5′-gc**acatgt**cccgcctggaatccgtggcaaaatttcac-3′; *Pci*I restriction site in bold) and Q-*Xho*I-RV (5′-g**ctcgag**tcagcgggtaacggcattcagg -3′; *Xho*I restriction site in bold; both primers were obtained from Metabion, Martinsried, Germany) and cloned into the pETGB1a expression vector (provided by Gunter Stier, EMBL Heidelberg, Germany) via *Pci*I and *Xho*I restriction sites, resulting in the recombinant plasmid pETGB1a_lambdaq. The gene coding for the Q variant lacking the 36 N-terminal residues, $\lambda Q^{\Delta 36}$, was obtained by restriction of pUC57_lambdaq with *Nco*I and *Xho*I and cloned into pETGB1a (pETGB1a_lambdaqdNΔ36). Both recombinant target proteins have a hexa-histidine tag, the B1 domain of streptococcal protein G (GB1), and a Tobacco Etch Virus (TEV) cleavage site at their N-termini.

Gene expression and protein purification. Production of NusA was carried out as described[40], as was production of NusA-NTD[54], NusA-SKK[55], NusA-AR1[37], NusA-AR2[40], NusA-AR2^{D443C} [18], NusB[28], NusE$^{\Delta}$:B[28], NusG[56], and αCTD[35].

Expression of *λq* was carried out in *E. coli* Rosetta (DE3) plysSRARE (Novagen, Madison, USA) harboring the plasmid pETGB1a_lambdaq. Lysogeny broth (LB) medium (supplemented with 34 μg/ml chloramphenicol and 30 μg/ml kanamycin) was inoculated with an overnight preculture to an optical density at 600 nm (OD_{600}) of 0.2 and incubated at 37 °C. When the culture reached an OD_{600} of 0.5 the temperature was decreased to 25 °C and overexpression was induced by addition of 0.2 mM Isopropyl β-D-1-thiogalactopyranoside (IPTG) at an OD_{600} of 0.7. Four hours after induction cells were harvested by centrifugation (6,000 × *g*, 10 min, 4 °C), resuspended in buffer Q-A (50 mM Tris(hydroxymethyl)aminomethane (Tris)/HCl, pH 7.4, 250 mM NaCl, 5 mM Dithiothreitol (DTT)), and lyzed using a microfluidizer (Microfluidics, Newton, USA). The lysate was cleared by centrifugation (75,000 × *g*, 30 min, 4 °C) and the crude extract was filtrated (0.45 μm filter) before being applied to a 5 ml HisTrap HP column (GE Healthcare, Chalfont St Giles, UK) loaded with Zn^{2+} instead of Ni^{2+}-Ions. Upon washing with buffer Q-A elution was carried out via a step gradient with increasing imidazole concentrations (10 mM–500 mM in buffer Q-A). Fractions that contained His_6-Gb1-λQ were combined and dialyzed against buffer Q-A (molecular weight cut-off (MWCO) 3,500 Da) at 4 °C overnight in the presence of TEV protease. The dialysate was loaded on a 5 ml HisTrap HP column (loaded with Zn^{2+}) coupled to a 5 ml Heparin HP column (GE Healthcare, Munich, Germany) and the columns were washed with buffer Q-A. Subsequently, the HisTrap HP chelating column was removed and the Heparin HP column was eluted using a constant gradient from 250 mM to 1 M NaCl in buffer Q-A. Fractions that contained λQ protein were combined and dialyzed against buffer Q-B (50 mM 3-(*N*-morpholino)propanesulfonic acid (MOPS) buffer, pH 6.5, 300 mM NaCl, 150 mM D-Glucose, 5 mM DTT; MWCO 3,500 Da) at 4 °C. The protein was polished by a gel filtration step using a Superdex75 10/600 column (GE Healthcare, Munich, Germany) and buffer Q-B. Fractions containing pure λQ were concentrated by ultrafiltration (MWCO 3,000 Da), shock frozen in liquid nitrogen, and stored at −80 °C. The production of $\lambda Q^{\Delta 36}$ was carried out analogously.

Analytical gel filtration of λQ and λQΔ[36]. Analytical gel filtration was carried out using a Superdex 75 10/300 GL column (GE Healthcare, Munich, Germany; 20 mM Tris/HCl (pH 7.5), 150 mM NaCl, 5% (v/v) glycerol). In order to estimate the molecular weights of λQ and $\lambda Q^{\Delta 36}$ a standard curve was generated using aprotinin (6.5 kDa; Sigma-Aldrich, Darmstadt, Germany), ribonuclease (13.7 kDa; GE Healthcare, Munich, Germany), carbonic anhydrase (29.0 kDa; GE Healthcare, Munich, Germany), ovalbumin (43 kDa; GE Healthcare, Munich, Germany), and albumin (66.0 kDa; Sigma-Aldrich, Darmstadt, Germany). 250 µg protein were applied per run.

Quality control of recombinant proteins. The quality of proteins used in this study was assessed based on the guidelines established by ARBRE-MOBIEU and P4EU (https://arbre-mobieu.eu/guidelines-on-protein-quality-control/). Sodium dodecyl sulfate polyacrylamide gel electrophoresis (SDS-PAGE) was used to check the purity of proteins. UV/visible spectra from 220–340 nm were recorded on a Nanodrop ND-100 spectrometer (PEQLAB, Erlangen, Germany) to ensure the absence of nucleic acids and aggregation. In order to determine concentrations the absorbance at 280 nm was measured in a 10 mm quartz cuvette (Hellma, Müllheim, Germany) on a Biospectrometer basic (Eppendorf, Hamburg, Germany). Identity was confirmed by peptide mass fingerprinting (Department of Biochemistry, University of Bayreuth, Germany) and homogeneity was ensured by analytical gel filtration using a Superdex 75 or a Superdex 200 10/300 GL column (GE Healthcare, Munich, Germany). Circular dichroism (CD) spectroscopy (1 mm quartz cuvette; J-1100, JASCO, Pfungstadt, Germany) was performed to assess the folding state (the folding state of unlabeled λQ and $\lambda Q^{\Delta 36}$ was additionally checked by recording one dimensional ^{1}H-NMR spectra).

Isotopic labeling of proteins. Isotopic labeling was essentially based on published protocols[54]. To produce uniformly ^{15}N- or ^{15}N,^{13}C-labeled proteins *E. coli* cells were grown in minimal medium M9[57,58] containing $(^{15}NH_4)_2SO_4$ (CortecNet, Voisins-Le-Bretonneux, France) or $(^{15}NH_4)_2SO_4$ and ^{13}C-glucose (Campro Scientific, Berlin, Germany) as sole source for nitrogen or carbon, respectively. For expression of *λq* and $\lambda q^{\Delta 36}$ Fe(III) citrate and the trace element solution were omitted, but $ZnCl_2$ was added to a final concentration of 4 $^{mg}/_{ml}$. Deuterated proteins were produced by growing *E. coli* cells in M9 medium[57,58] which was prepared with stepwise increasing amounts of D_2O (25% (v/v), 50% (v/v), 99.9% (v/v) D_2O; Eurisotop, Saint-Aubin, France). Expression and purification protocols were the same as for proteins produced in LB medium.

NMR spectroscopy. NMR experiments were performed at 298 K on Bruker *Avance* 700 MHz, Bruker *Ascend Aeon* 900 MHz, and Bruker *Ascend Aeon* 1 000 MHz spectrometers, all being equipped with cryogenically cooled inverse triple resonance probes. The experimental setup and data analysis was done essentially as described[18]. Samples contained 10% (v/v) D_2O for locking and were in 3 mm tubes with an initial volume of 250 µl, if not stated otherwise. In-house routines were used for data conversion and processing, MatLab (The MathWorks, Inc., Version 7.1.0.183) was used for visualization and analysis of one-dimensional (1D) spectra and NMRViewJ (One Moon Scientific, Inc., Westfield, NJ, USA) to visualize and analyze two-dimensional (2D) and three-dimensional (3D) spectra. Assignments for the backbone amide resonances of NusA-AR2[35], NusA-AR1[59], NusA-SKK[39], αCTD[39], and NusA-NTD[54] were taken from previous studies.

For resonance assignment of the $\lambda Q^{\Delta 36}$ backbone BEST-TROSY-based triple resonance experiments[60–62] were recorded using 5 mm tubes (500 µl sample volume) with the ^{2}H,^{13}C,^{15}N-labeled protein (270 µM) being in 25 mM MES (pH 7.0), 100 mM NaCl, 5 mM DTT. ^{15}N-longitudinal and transverse relaxation rates of $\lambda Q^{\Delta 36}$ were recorded with a ^{15}N-labeled sample at 298 K and 700.2 MHz ^{1}H frequency using standard methods[63]. Relaxation delays were fitted to a monoexponential decay by NMRViewJ (One Moon Scientific, Inc., Westfield, NJ, USA). The rotation correlation time was determined using the TENSOR 2 package[64] assuming an isotropic model for molecular tumbling. Only residues located in rigid regions were used in the analysis. The error of R_1 and R_2 was set to 5% and 8%, respectively, according to ref. [65].

For interaction studies and competition experiments proteins were in 50 mM MOPS, pH 6.5, 300 mM NaCl, 150 mM D-Glucose, 5 mM DTT (exception: 5 mm tubes were used to study the interaction of NusA-SKK with NusA-AR2 with proteins being in 50 mM MOPS, pH 6.5, 100 mM NaCl, 150 mM D-Glucose, 5 mM DTT). Either [^{1}H,^{15}N]-HSQC or [^{1}H,^{15}N]-BEST-TROSY experiments were used to record [^{1}H,^{15}N] correlation spectra. To compare 1D spectra we normalized them by receiver gain, length of the 90° proton pulse, number of scans, and protein concentration.

[^{1}H,^{15}N] correlation-based titrations (either HSQC or BEST-TROSY) were analyzed quantitatively by calculating either changes in intensity or changes in chemical shifts. If chemical shift changes were in the fast regime of chemical exchange we calculated the normalized chemical shift perturbation ($\Delta\delta_{norm}$) according to Eq. (1).

$$\Delta\delta_{\mathrm{norm}} = \sqrt{(\Delta\delta^{1}H)^2 + [0.1 \cdot (\Delta\delta^{15}N)]^2} \tag{1}$$

with Δδ being the resonance frequency difference in ppm.

Plotting of $\Delta\delta_{norm}$ against the amino acid position of the labeled protein and introduction of thresholds at 0.04 ppm, 0.08 ppm, and 0.12 ppm allowed the identification of slightly, moderately, and strongly affected residues. In order to determine dissociation constants (K_D) from these titrations we analyzed the normalized chemical shift changes (in Hz) and fitted a two-state model (Eq. 2) to the chemical shift change of amide protons showing fast exchange in the chemical shift timescale.

$$\Delta\nu = \Delta\nu_{End} \cdot \frac{[P]_0 \cdot r + [P]_0 + K_D - \sqrt{(K_D + [P]_0 + [P]_0 \cdot r)^2 - 4 \cdot ([P]_0)^2 \cdot r}}{2 \cdot [P]_0} \tag{2}$$

with $\Delta\nu$ being the normalized resonance frequency difference (Hz), $\Delta\nu_{End}$ the normalized resonance frequency difference between free and fully bound protein (Hz), r the ratio of unlabeled to labeled protein, and $[P]_0$ the total concentration of ^{15}N-labeled protein (the decrease of $[P]_0$ due to dilution was taken into account during fitting). Fitting was done using MatLab (The MathWorks, Inc., Version 7.1.0.183) with K_D and $\Delta\nu_{End}$ being fitting parameters.

If the system was in slow or intermediate chemical exchange the signal intensities were analyzed quantitatively as described[66]. In brief, signal intensities were normalized by receiver gain, length of the 90° proton pulse, number of scans, and protein concentration. In order to eliminate an intensity decrease due to slight precipitation signals within one spectrum were normalized to the most intense signal. Subsequently, we calculated the relative signal intensity in each titration step, i.e. the ratio of the remaining, normalized signal intensity of the spectrum of the respective titration step to the normalized signal intensity of the spectrum of the free, labeled protein. The error was calculated based on the standard deviation of the noise level applying error propagation. Then, we calculated the mean value of all relative signal intensities in each titration step and residues with relative signal intensities below thresholds at 1 and 1.5 σ of the mean value were classified as moderately or strongly affected, respectively.

Fluorescence anisotropy measurements. Fluorescence anisotropy measurements were performed as described[18]. Site-specific labeling of NusA-AR2^{D443C} with fluorescein-5-maleimide (ThermoFisher Scientific, Waltham, USA) was done according to the manufacturer's protocol, i.e. after incubation of 25 µM of NusA-AR2^{D443C} with 750 µM fluorescein-5-maleimide in labeling buffer (20 mM Na phosphate, pH 7.0, 150 mM NaCl) at 4 °C overnight the solution was loaded on a PD MiniTrap Sephadex G-25 gravity column (GE Healthcare, Munich, Germany) equilibrated with fluorescence buffer (50 mM Na-P, pH 6.5, 100 mM NaCl, 150 mM glucose, 5 mM DTT, 0.05% (v/v) Tween). Elution was carried out with fluorescence buffer. The protein concentration and the degree of labeling were determined by UV/vis spectroscopy on a Nanodrop ND-1000 spectrometer (PEQLAB, Erlangen, Germany) according to the manufacturer's protocol.

For each titration step individual 100 µl samples were prepared with each sample containing 25 nM labeled NusA-AR2^{D443C} and increasing concentrations of unlabeled protein. All proteins were in fluorescence buffer and measurements were done in black, sterile 96-well microtiter plates (Brand, Wertheim, Germany) at 25 °C in a Synergy 2 microplate reader (BioTek, Winooski, USA). Four independent replicates were prepared per titration step and the anisotropy values were averaged. Finally, the mean anisotropy values were plotted against the titrant concentration and anisotropy data was fitted to a two-state binding model (Eq. 3) using GraFit 5.0 (Erithacus Software; http://www.erithacus.com/grafit/index.html).

$$A = \frac{A_S + \left[\text{complex}\right]/[S]_0 \cdot \left(R \cdot A_{\text{complex}} - A_S\right)}{1 - [\text{complex}]/[S]_0 + R \cdot [\text{complex}]/[S]_0} \tag{3}$$

with

$$[\text{complex}] = \frac{K_D + [P]_0 + [S]_0 - \sqrt{(K_D + [P]_0 + [S]_0)^2 - 4 \cdot [S] \cdot [P]_0}}{2} \tag{4}$$

where A is the measured anisotropy, A_S the anisotropy of labeled NusA-AR2^{D443C}, $A_{complex}$ the anisotropy of the complex, [complex] the concentration of the complex, $[S]_0$ and $[P]_0$ the total concentrations of labeled NusA-AR2^{D443C} and the titrant, respectively, K_D the dissociation constant, and R the ratio of the fluorescence intensities of fully bound and free substrate at 520 nm.

Docking. The complexes λQ:NusA-NTD, λQ:NusA-AR2, and NusA-AR2:NusA-SKK were modeled with the HADDOCK 2.2 server (https://haddock.science.uu.nl/services/HADDOCK2.2/)[67] using H-N correlation data from NMR titrations as restraints (Supplementary Table 1). The size of interaction interfaces was calculated via the "Protein interfaces, surfaces and assemblies" service PISA at the European Bioinformatics Institute (http://www.ebi.ac.uk/pdbe/prot_int/pstart.html[68].

Visualization of protein structures. The PyMOL Molecular Graphics System (Version 1.7, Schrödinger, LLC.; https://pymol.org) was used for graphical representations of protein structures.

Data Availability

The chemical shift assignment of λQ$^{\Delta 36}$ were deposited in the Biological Magnetic Resonance Data Bank under the accession code 28043. We generated models of the λQ:NusA-NTD, the λQ:NusA-AR2, and the NusA-SKK:NusA-AR2 complex. Coordinates for λQ, NusA-NTD, NusA-SKK, and NusA-AR2 are available in the Protein Data Bank (PDB; 4MO1, 2KWP, 5LM9, 1WCN), the coordinates of the best complex models are provided as Supplementary data. Other data and materials are available from the corresponding author upon reasonable request.

Received: 20 November 2019; Accepted: 27 March 2020;
Published online: 20 April 2020

References

1. Werner, F. & Grohmann, D. Evolution of multisubunit RNA polymerases in the three domains of life. *Nat. Rev. Microbiol.* **9**, 85–98 (2011).
2. Guo, X. *et al.* Structural Basis for NusA Stabilized Transcriptional Pausing. *Mol. Cell* **69**, 816–827.e4 (2018).

3. Ha, K. S., Toulokhonov, I., Vassylyev, D. G. & Landick, R. The NusA N-terminal domain is necessary and sufficient for enhancement of transcriptional pausing via interaction with the RNA exit channel of RNA polymerase. *J. Mol. Biol.* **401**, 708–725 (2010).
4. Ma, C. *et al*. RNA polymerase-induced remodelling of NusA produces a pause enhancement complex. *Nucleic Acids Res.* **43**, 2829–2840 (2015).
5. Geszvain, K., Gruber, T. M., Mooney, R. A., Gross, C. A. & Landick, R. A hydrophobic patch on the flap-tip helix of *E.coli* RNA polymerase mediates sigma(70) region 4 function. *J. Mol. Biol.* **343**, 569–587 (2004).
6. Said, N. *et al*. Structural basis for λN-dependent processive transcription antitermination. *Nat. Microbiol.* **2**, 17062 (2017).
7. Krupp, F. *et al*. Structural Basis for the Action of an All-Purpose Transcription Anti-termination Factor. *Mol. Cell* **74**, 143–157.e5 (2019).
8. Kang, J. Y. *et al*. RNA Polymerase Accommodates a Pause RNA Hairpin by Global Conformational Rearrangements that Prolong Pausing. *Mol. Cell* **69**, 802–815.e1 (2018).
9. Gottesman, M. E. & Weisberg, R. A. Little lambda, who made thee? *Microbiol. Mol. Biol. Rev.* **68**, 796–813 (2004).
10. Strobel, E. J. & Roberts, J. W. Regulation of promoter-proximal transcription elongation: enhanced DNA scrunching drives λQ antiterminator-dependent escape from a σ70-dependent pause. *Nucleic Acids Res.* **42**, 5097–5108 (2014).
11. Guo, J. & Roberts, J. W. DNA binding regions of Q proteins of phages lambda and phi80. *J. Bacteriol.* **186**, 3599–3608 (2004).
12. Shi, J. *et al*. Structural basis of Q-dependent transcription antitermination. *Nat. Commun.* **10**, 2925 (2019).
13. Yin, Z., Kaelber, J. T. & Ebright, R. H. Structural basis of Q-dependent antitermination. *Proc. Natl. Acad. Sci. USA* **116**, 18384–18390 (2019).
14. Vorobiev, S. M. *et al*. Structure of the DNA-binding and RNA-polymerase-binding region of transcription antitermination factor λQ. *Structure* **22**, 488–495 (2014).
15. Squires, C. L., Greenblatt, J., Li, J., Condon, C. & Squires, C. L. Ribosomal RNA antitermination *in vitro*: requirement for Nus factors and one or more unidentified cellular components. *Proc. Natl. Acad. Sci. USA* **90**, 970–974 (1993).
16. Baniulyte, G. *et al*. Identification of regulatory targets for the bacterial Nus factor complex. *Nat. Commun.* **8**, 2027 (2017).
17. Huang, Y.-H., Said, N., Loll, B. & Wahl, M. C. Structural basis for the function of SuhB as a transcription factor in ribosomal RNA synthesis. *Nucleic Acids Res.* **47**, 6488–6503 (2019).
18. Dudenhoeffer, B. R., Schneider, H., Schweimer, K. & Knauer, S. H. SuhB is an integral part of the ribosomal antitermination complex and interacts with NusA. *Nucleic Acids Res.* **47**, 6504–6518 (2019).
19. Torres, M., Condon, C., Balada, J. M., Squires, C. & Squires, C. L. Ribosomal protein S4 is a transcription factor with properties remarkably similar to NusA, a protein involved in both non-ribosomal and ribosomal RNA antitermination. *EMBO J.* **20**, 3811–3820 (2001).
20. Singh, N. *et al*. SuhB Associates with Nus Factors To Facilitate 30S Ribosome Biogenesis in *Escherichia coli*. *MBio* **7**, e00114 (2016).
21. Werner, F. A nexus for gene expression-molecular mechanisms of Spt5 and NusG in the three domains of life. *J. Mol. Biol.* **417**, 13–27 (2012).
22. Mooney, R. A., Schweimer, K., Rösch, P., Gottesman, M. & Landick, R. Two structurally independent domains of *E. coli* NusG create regulatory plasticity via distinct interactions with RNA polymerase and regulators. *J. Mol. Biol.* **391**, 341–358 (2009).
23. Artsimovitch, I. & Knauer, S. H. Ancient Transcription Factors in the News. *MBio* **10**, e01547–18 (2019).
24. Burmann, B. M. *et al*. A NusE:NusG complex links transcription and translation. *Science* **328**, 501–504 (2010).
25. Mitra, P., Ghosh, G., Hafeezunnisa, M. & Sen, R. Rho Protein: Roles and Mechanisms. *Annu. Rev. Microbiol.* **71**, 687–709 (2017).
26. Lawson, M. R. *et al*. Mechanism for the regulated control of transcription by a universal adapter protein. *Mol. Cell* **71**, 1–12 (2018).
27. Luo, X. *et al*. Structural and functional analysis of the *E. coli* NusB-S10 transcription antitermination complex. *Mol. Cell* **32**, 791–802 (2008).
28. Burmann, B. M., Luo, X., Rösch, P., Wahl, M. C. & Gottesman, M. E. Fine tuning of the *E. coli* NusB:NusE complex affinity to *BoxA* RNA is required for processive antitermination. *Nucleic Acids Res.* **38**, 314–326 (2010).
29. Artsimovitch, I. & Landick, R. Pausing by bacterial RNA polymerase is mediated by mechanistically distinct classes of signals. *Proc. Natl. Acad. Sci. USA* **97**, 7090–7095 (2000).
30. Friedman, D. I. & Baron, L. S. Genetic characterization of a bacterial locus involved in the activity of the N function of phage lambda. *Virology* **58**, 141–148 (1974).
31. Vogel, U. & Jensen, K. F. NusA is required for ribosomal antitermination and for modulation of the transcription elongation rate of both antiterminated RNA and mRNA. *J. Biol. Chem.* **272**, 12265–12271 (1997).
32. Yarnell, W. S. & Roberts, J. W. The phage lambda gene Q transcription antiterminator binds DNA in the late gene promoter as it modifies RNA polymerase. *Cell* **69**, 1181–1189 (1992).
33. Pan, T., Artsimovitch, I., Fang, X. W., Landick, R. & Sosnick, T. R. Folding of a large ribozyme during transcription and the effect of the elongation factor NusA. *Proc. Natl. Acad. Sci. USA* **96**, 9545–9550 (1999).
34. Worbs, M., Bourenkov, G. P., Bartunik, H. D., Huber, R. & Wahl, M. C. An extended RNA binding surface through arrayed S1 and KH domains in transcription factor NusA. *Mol. Cell* **7**, 1177–1189 (2001).
35. Eisenmann, A., Schwarz, S., Prasch, S., Schweimer, K. & Rösch, P. The *E. coli* NusA carboxy-terminal domains are structurally similar and show specific RNAP- and lambdaN interaction. *Protein Sci.* **14**, 2018–2029 (2005).
36. Mah, T. F., Li, J., Davidson, A. R. & Greenblatt, J. Functional importance of regions in *Escherichia coli* elongation factor NusA that interact with RNA polymerase, the bacteriophage lambda N protein and RNA. *Mol. Microbiol.* **34**, 523–537 (1999).
37. Prasch, S. *et al*. Interaction of the intrinsically unstructured phage lambda N Protein with *Escherichia coli* NusA. *Biochemistry* **45**, 4542–4549 (2006).
38. Bonin, I. *et al*. Structural basis for the interaction of *Escherichia coli* NusA with protein N of phage lambda. *Proc. Natl. Acad. Sci. USA* **101**, 13762–13767 (2004).
39. Schweimer, K. *et al*. NusA interaction with the α subunit of *E. coli* RNA polymerase is via the UP element site and releases autoinhibition. *Structure* **19**, 945–954 (2011).
40. Strauß, M. *et al*. Transcription is regulated by NusA:NusG interaction. *Nucleic Acids Res.* **44**, 5971–5982 (2016).
41. Mah, T. F., Kuznedelov, K., Mushegian, A., Severinov, K. & Greenblatt, J. The alpha subunit of *E. coli* RNA polymerase activates RNA binding by NusA. *Genes Dev.* **14**, 2664–2675 (2000).
42. Liu, K., Zhang, Y., Severinov, K., Das, A. & Hanna, M. M. Role of *Escherichia coli* RNA polymerase alpha subunit in modulation of pausing, termination and anti-termination by the transcription elongation factor NusA. *EMBO J.* **15**, 150–161 (1996).
43. Shankar, S., Hatoum, A. & Roberts, J. W. A transcription antiterminator constructs a NusA-dependent shield to the emerging transcript. *Mol. Cell* **27**, 914–927 (2007).
44. Yang, X. J., Goliger, J. A. & Roberts, J. W. Specificity and mechanism of antitermination by Q proteins of bacteriophages lambda and 82. *J. Mol. Biol.* **210**, 453–460 (1989).
45. Deighan, P., Diez, C. M., Leibman, M., Hochschild, A. & Nickels, B. E. The bacteriophage lambda Q antiterminator protein contacts the beta-flap domain of RNA polymerase. *Proc. Natl. Acad. Sci. USA* **105**, 15305–15310 (2008).
46. Grayhack, E. J., Yang, X. J., Lau, L. F. & Roberts, J. W. Phage lambda gene Q antiterminator recognizes RNA polymerase near the promoter and accelerates it through a pause site. *Cell* **42**, 259–269 (1985).
47. Campbell, E. A. *et al*. Crystal structure of *Escherichia coli* sigmaE with the cytoplasmic domain of its anti-sigma RseA. *Mol. Cell* **11**, 1067–1078 (2003).
48. Campbell, E. A. *et al*. Structure of the bacterial RNA polymerase promoter specificity sigma subunit. *Mol. Cell* **9**, 527–539 (2002).

49. Mooney, R. A. *et al*. Regulator trafficking on bacterial transcription units *in vivo*. *Mol. Cell* **33**, 97–108 (2009).
50. Kuznedelov, K. *et al*. A role for interaction of the RNA polymerase flap domain with the sigma subunit in promoter recognition. *Science* **295**, 855–857 (2002).
51. Kang, J. Y. *et al*. Structural basis of transcription arrest by coliphage HK022 Nun in an *Escherichia coli* RNA polymerase elongation complex. *Elife* **6**, e25478 (2017).
52. Burmann, B. M. *et al*. An α helix to β barrel domain switch transforms the transcription factor RfaH into a translation factor. *Cell* **150**, 291–303 (2012).
53. Zuber, P. K., Schweimer, K., Rösch, P., Artsimovitch, I. & Knauer, S. H. Reversible fold-switching controls the functional cycle of the antitermination factor RfaH. *Nat. Commun.* **10**, 702 (2019).
54. Drögemüller, J. *et al*. Exploring RNA polymerase regulation by NMR spectroscopy. *Sci. Rep.* **5**, 10825 (2015).
55. Prasch, S. *et al*. RNA-binding specificity of *E. coli* NusA. *Nucleic Acids Res.* **37**, 4736–4742 (2009).
56. Burmann, B. M., Scheckenhofer, U., Schweimer, K. & Rösch, P. Domain interactions of the transcription-translation coupling factor *Escherichia coli* NusG are intermolecular and transient. *Biochem. J.* **435**, 783–789 (2011).
57. Sambrook, J. & Russel, D. W. Molecular Cloning: A Laboratory Manual. vol. 3 (Cold Spring Harbor Press, 2001).
58. Meyer, O. & Schlegel, H. G. Biology of aerobic carbon monoxide-oxidizing bacteria. *Annu. Rev. Microbiol.* **37**, 277–310 (1983).
59. Eisenmann, A., Schwarz, S., Rösch, P. & Schweimer, K. Sequence-specific ^{1}H, ^{13}C, ^{15}N resonance assignments and secondary structure of the carboxyterminal domain of the *E. coli* transcription factor NusA. *J Biomol NMR* **28**, 193–194 (2004).
60. Favier, A. & Brutscher, B. Recovering lost magnetization: polarization enhancement in biomolecular NMR. *J. Biomol. NMR* **49**, 9–15 (2011).
61. Bax, A. & Grzesiek, A. Methodological advances in protein NMR. *Acc. Chem. Res.* **26**, 131–138 (1993).
62. Sattler, M., Schleucher, J. & Griesinger, C. Heteronuclear multidimensional NMR experiments for the structure determination of proteins in solution employing pulsed field gradients. *Prog. Nucl. Magn. Reson. Spectrosc.* **34**, 93–158 (1999).
63. Kay, L. E., Torchia, D. A. & Bax, A. Backbone dynamics of proteins as studied by nitrogen-15 inverse detected heteronuclear NMR spectroscopy: application to staphylococcal nuclease. *Biochemistry* **28**, 8972–8979 (1989).
64. Dosset, P., Hus, J.-C., Blackledge, M. & Marion, D. Efficient analysis of macromolecular rotational diffusion from heteronuclear relaxation data. *J. Biomo.l NMR* **16**, 23–28 (2000).
65. Rossi, P. *et al*. A microscale protein NMR sample screening pipeline. *J. Biomol. NMR* **46**, 11–22 (2010).
66. Drögemüller, J. *et al*. Determination of RNA polymerase binding surfaces of transcription factors by NMR spectroscopy. *Sci. Rep.* **5**, 16428–16441 (2015).
67. de Vries, S. J., van Dijk, M. & Bonvin, A. M. J. J. The HADDOCK web server for data-driven biomolecular docking. *Nat. Protoc.* **5**, 883–897 (2010).
68. Krissinel, E. & Henrick, K. Inference of macromolecular assemblies from crystalline state. *J. Mol. Biol.* **372**, 774–797 (2007).

Acknowledgements

We thank Ramona Heissmann, Ulrike Persau, and Andrea Hager for excellent technical assistance and the Northern Bavarian NMR Centre (NBNC) for access to the NMR spectrometers. This work was supported by the German Research Foundation (Ro617/21–1 to Paul Rösch). The open access charge was funded by German Research Foundation and the University of Bayreuth in the funding program open access publication.

Author contributions

S.H.K. supervised the project. The experiments were designed by S.H.K., K.S., and B.R.D. J.B., B.R.D., and K.S. made the assignment of $\lambda Q^{\Delta 36}$ (the corresponding NMR experiments were carried out by K.S.). All interactions studies and competition experiments were performed by B.R.D., and data was analyzed and evaluated by B.R.D. and S.H.K. B.R.D. and S.H.K. carried out the docking runs and S.H.K. and B.R.D. wrote the manuscript with input from all authors.

Competing interests

The authors declare no competing interests.

Additional information

Supplementary information is available for this paper at https://doi.org/10.1038/s41598-020-63523-5.

Correspondence and requests for materials should be addressed to S.H.K.

Reprints and permissions information is available at www.nature.com/reprints.

Publisher's note Springer Nature remains neutral with regard to jurisdictional claims in published maps and institutional affiliations.

Supplementary Information

NusA directly interacts with antitermination factor Q from phage λ

Benjamin R. Dudenhoeffer[1], Jan Borggräfe[1,2], Kristian Schweimer[1], Stefan H. Knauer[1,*]

[1]Biopolymers, University of Bayreuth, Universitätsstraße 30, 95447 Bayreuth, Germany

[2]Current address:

Institute of Physical Biology, Heinrich-Heine-University, Univeristätsstraße 1, 40225 Düsseldorf, Germany

Institute of Complex Systems, Forschungszentrum Jülich, Wilhelm-Johnen-Straße, 52428 Jülich, Germany

*Correspondence to: stefan.knauer@uni-bayreuth.de

Supplementary Table 1: Structures and active residues used in docking to model the complexes λQ:NusA-NTD, λQ:NusA-AR2, and NusA-AR2:NusA-SKK.

complex	**Input structures**	**Active residues**
λQ:NusA-NTD	λQ: 4MOI, chain A NusA-NTD: 2KWP, model 1	λQ: 84, 86, 102, 111, 112, 117, 119, 121, 124, 127, 146, 147, 150, 158, 160, 161, 162, 163, 168, 183, 185, 186 NusA-NTD: 27, 34, 37, 38, 39, 44, 57, 61, 73, 75, 77, 80, 83, 84, 87, 95
λQ:NusA-AR2	λQ: 4MOI, chain A NusA-AR2: 1WCN, model 1	λQ: 71, 72, 75, 95, 96, 102, 103, 111, 112, 117, 125, 149, 161, 163, 177, 180, 183, 200 NusA-AR2: 462, 463, 476, 483, 487, 489, 490, 491, 492, 494, 495
NusA-AR2:NusA-SKK	NusA-AR2: 1WCN, model 1 NusA-SKK: 5LM9 (the structure also includes NusA-AR1)	NusA-AR2: 461, 463, 464, 465, 466, 476, 480, 482, 483, 484, 486, 490, 491, 492, 493 NusA-SKK: 165, 168, 170, 171, 173, 181, 212, 229, 234, 235, 236, 249, 252, 253, 254, 258, 259, 260, 261, 262, 263, 264, 266, 267, 268, 270, 271, 273, 275, 276, 288, 289, 317, 318, 319, 326, 327, 342, 346

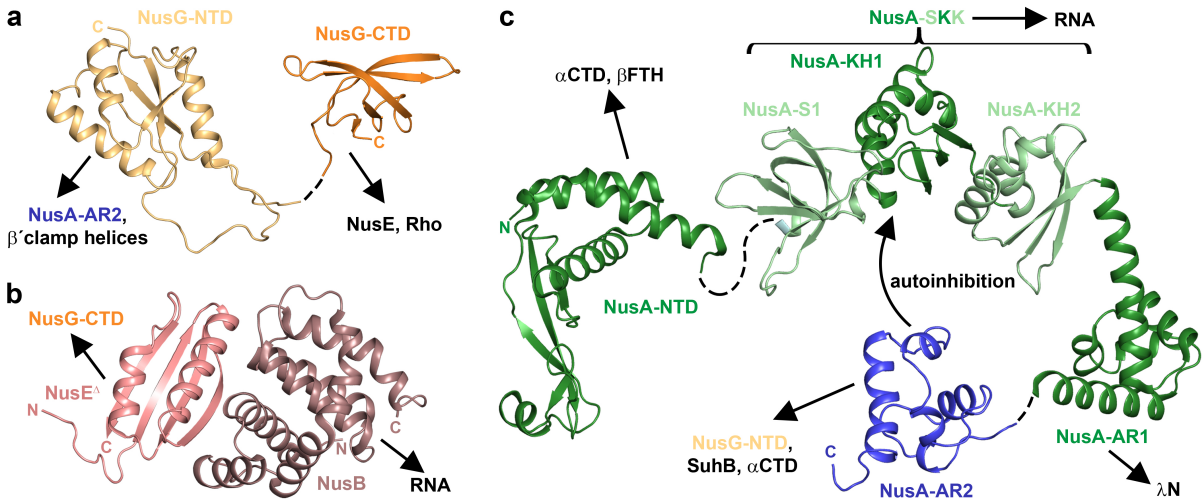

Supplementary Figure 1: Structures of Nus factors. The structures of NusG **(a)**, the NusB:NusE$^{\Delta}$ complex **(b)**, and NusA **(c)** are shown in ribbon representation, domains are color-coded, and flexible linkers are depicted as dashed lines. Termini are labeled and interaction partners are indicated. PDB IDs: NusG-NTD, 2K06; NusG-CTD, 2JVV; NusB:NusE$^{\Delta}$, 3D3B; NusA-NTD, 2KWP; NusA-SKK-AR1, 5LM9; NusA-AR2, 1WCN. The PyMOL Molecular Graphics System (Version 1.7, Schrödinger, LLC.; https://pymol.org) was used for visualization.

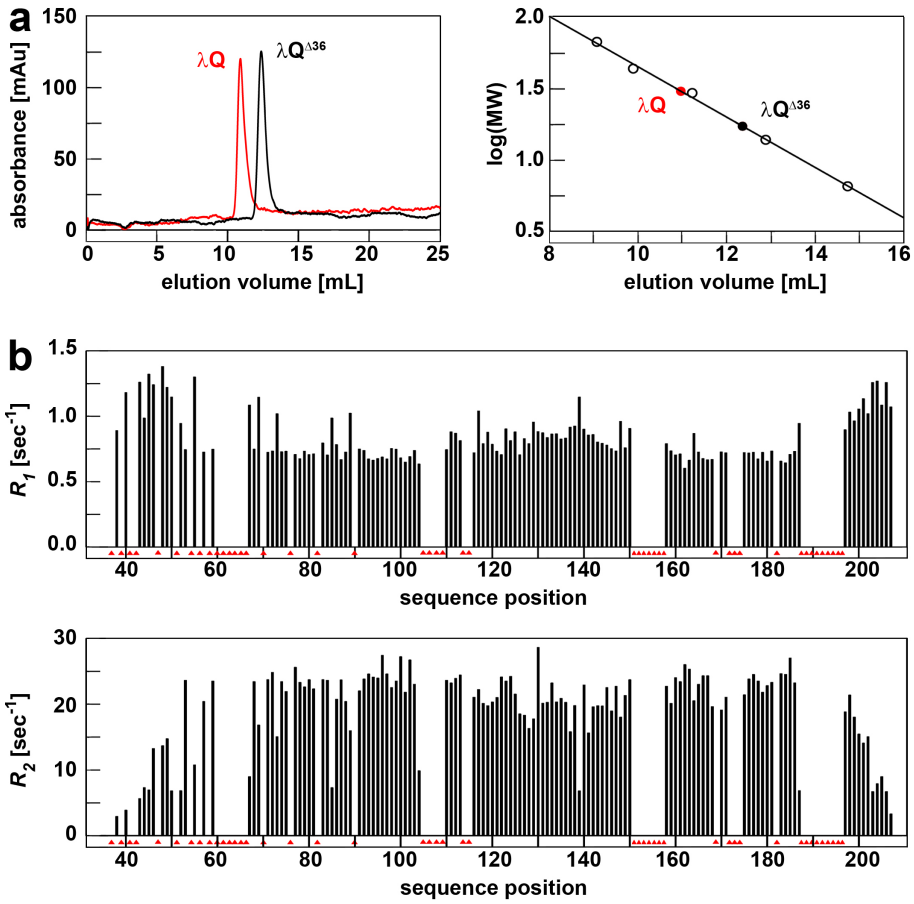

Supplementary Figure 2: Characterization of λQ and λQ$^{\Delta 36}$. (a) Analytical gel filtration using a Superdex 75 10/300 GL column. (Left) Chromatograms of λQ and λQ$^{\Delta 36}$. (Right) Standard curve generated with aprotinin, ribonuclease, carbonic anhydrase, ovalbumin, and albumin (empty black circles). The molecular weights of λQ (black filled circle) and λQ$^{\Delta 36}$ (red filled circle) were determined as 30 kDa and 17 kDa, respectively. **(b)** Determination of relaxation rates R_1 (top) and R_2 (bottom) of ^{15}N-λQ$^{\Delta 36}$. Red triangles mark residues for which no relaxation rates could be determined.

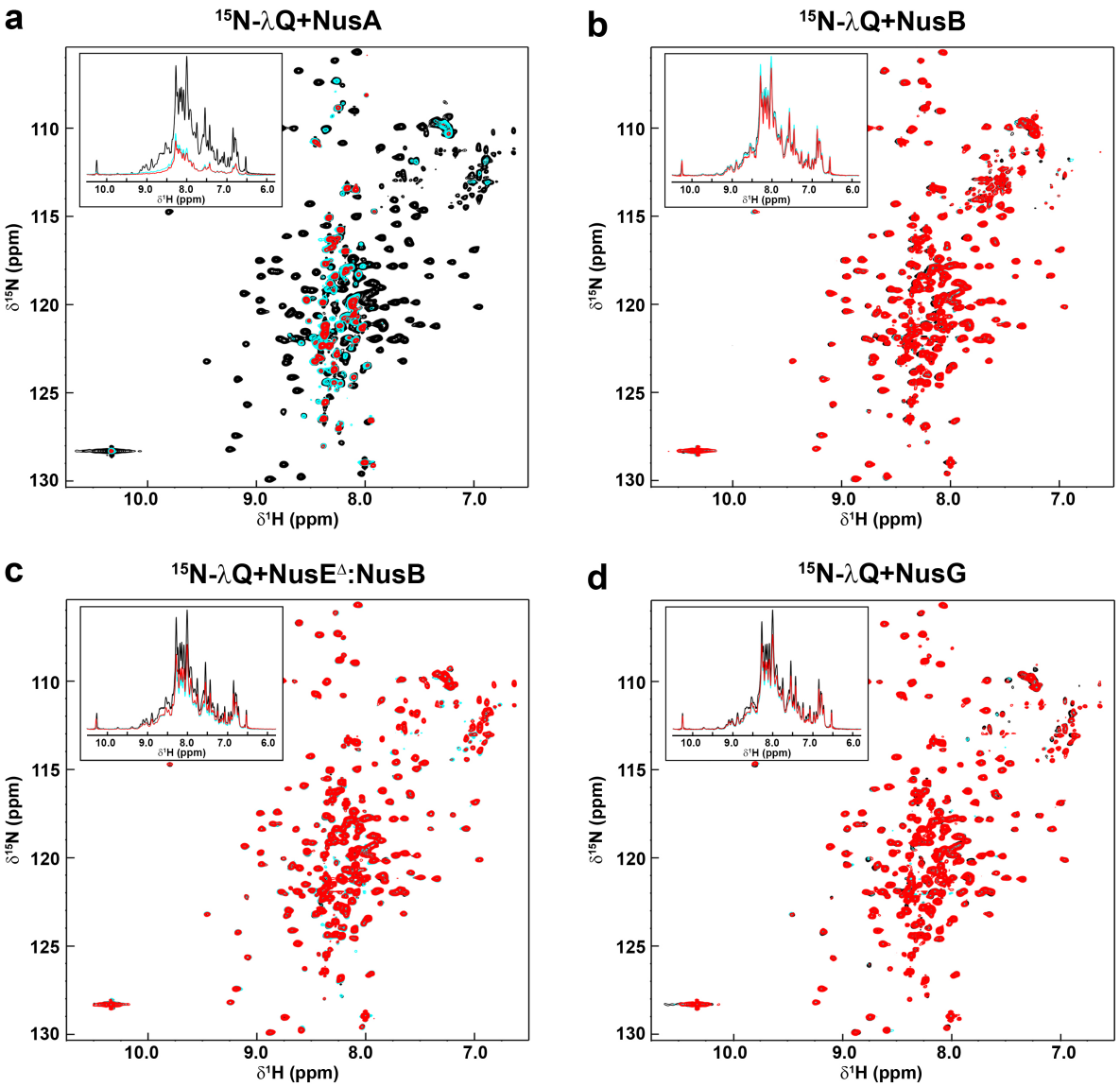

Supplementary Figure 3: λQ interacts with NusA, but not with NusB, NusE$^{\Delta}$, or NusG. 2D [^{1}H,^{15}N]-BEST-TROSY spectra of 125 µM ^{15}N-λQ in the absence (black) and presence (molar ratio 1:1, cyan; 1:2, red) of NusA **(a),** NusB **(b)**, NusB:NusE$^{\Delta}$ **(c)**, and NusG **(d)**. Corresponding 1D [^{1}H,^{15}N]-HSQC spectra are shown as insets.

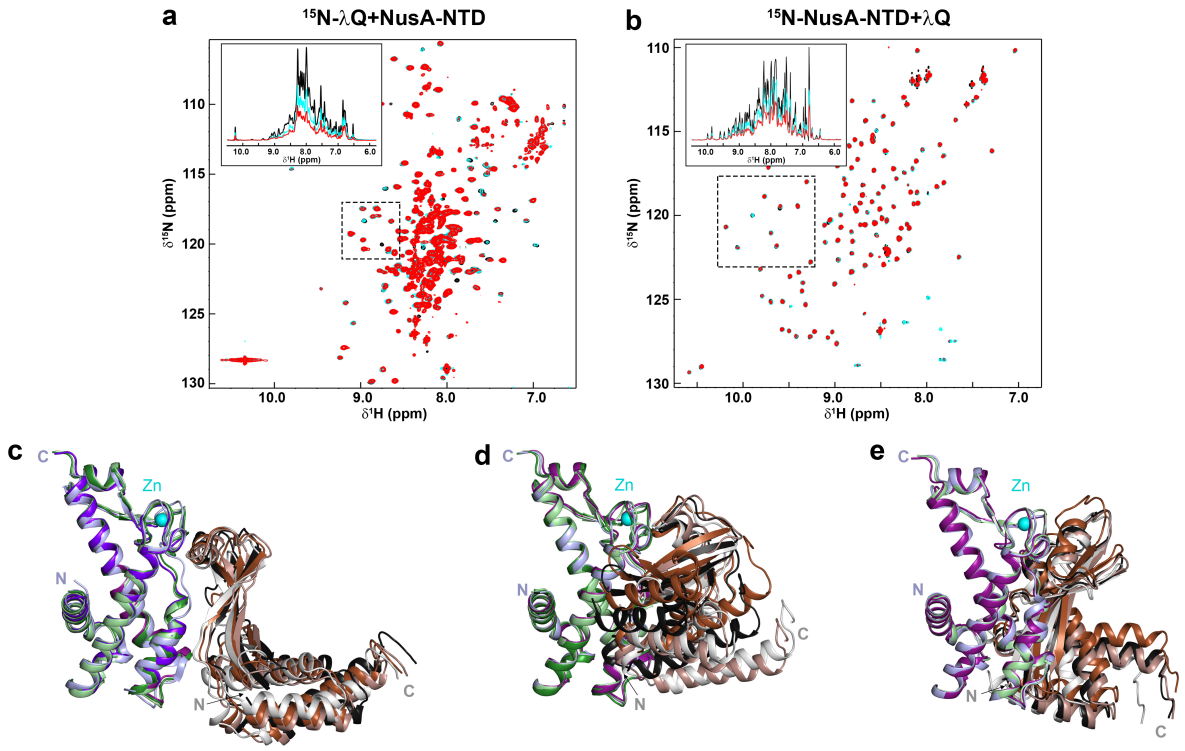

Supplementary Figure 4: λQ directly interacts with NusA-NTD. **(a)** 2D [^{1}H,^{15}N]-BEST-TROSY spectra of the titration of 250 µM ^{15}N-λQ with NusA-NTD (molar ratios: 1:0, black; 1:1, cyan; 1:2 red). The dashed box indicates the section shown in Fig. 2a. Corresponding 1D [^{1}H,^{15}N]-HSQC spectra are shown as inset. **(b)** 1D and 2D [^{1}H,^{15}N]-HSQC spectra of the titration of 175 µM ^{15}N-NusA-NTD with λQ (molar ratios: 1:0, black; 1:1, cyan; 1:2). The dashed box in **(b)** indicate the sections shown in Fig. 2b. **(c-e)** Models of the λQ:NusA-NTD complex. The models were generated with by docking (HADDOCK 2.2 server (https://haddock.science.uu.nl/services/HADDOCK2.2/) using the affected residues as restraints. The three clusters with the lowest Z and HADDOCK scores are shown (increasing values from **(c)** to **(e)**) with each cluster having three superimposed structures. The proteins are depicted in ribbon representation, the Zn^{2+} ion is shown as cyan sphere. PDB IDs: λQ, 4MOI; NusA-NTD, 2KWP. The PyMOL Molecular Graphics System (Version 1.7, Schrödinger, LLC.; https://pymol.org) was used for visualization.

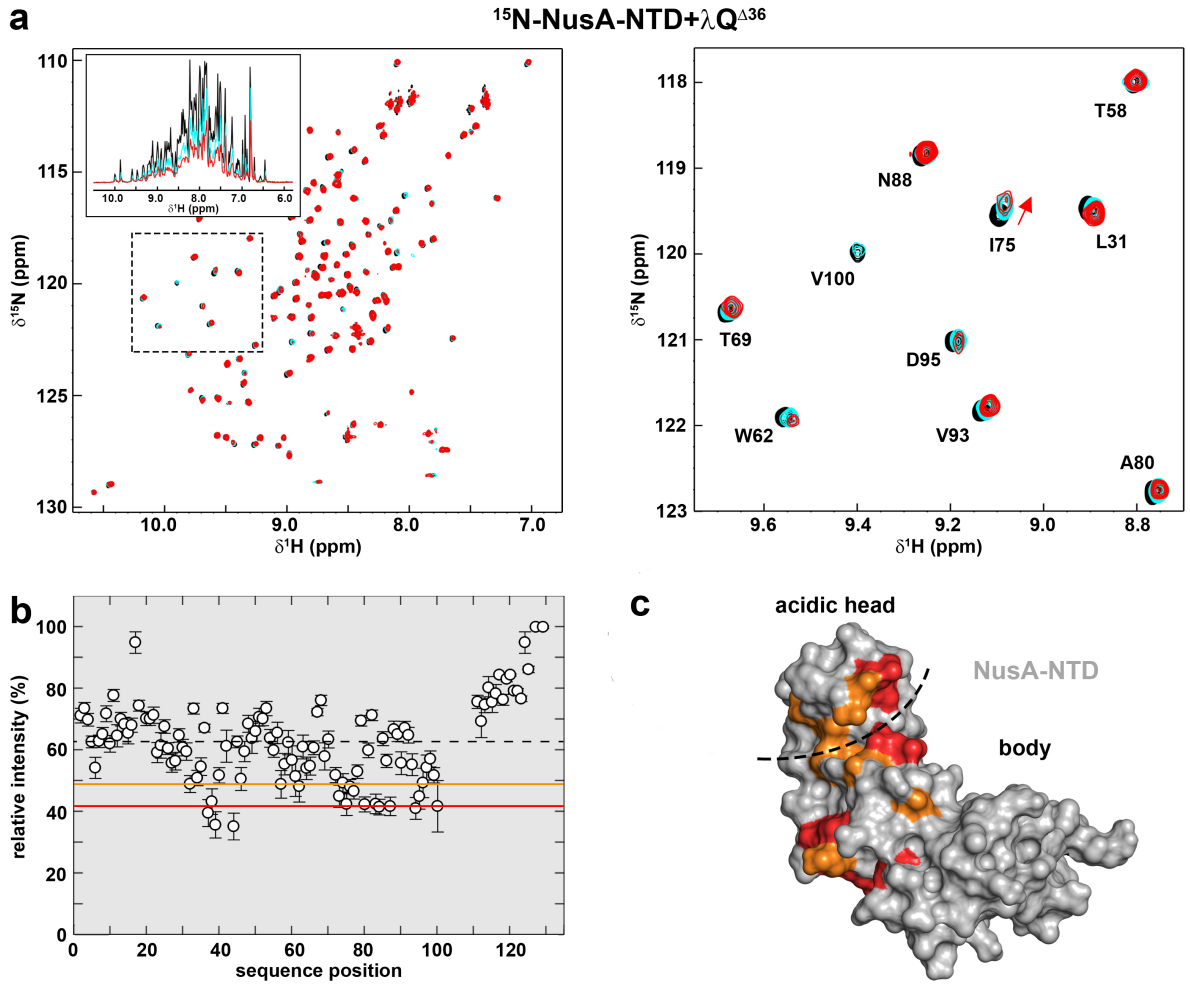

Supplementary Figure S5: $\lambda Q^{\Delta 36}$ directly interacts with NusA-NTD. **(a)** 1D and 2D [^{1}H,^{15}N]-HSQC spectra of the titration of 175 µM ^{15}N-NusA-NTD with $\lambda Q^{\Delta 36}$ (molar ratios: 1:0, black; 1:1, cyan; 1:2). The dashed box in **(a)** indicate the section marks the section shown on the right. **(b)** Relative intensity of NusA-NTD signals in the presence of one equivalent $\lambda Q^{\Delta 36}$. Orange and red lines indicate thresholds for moderately (1.0 σ of average relative signal intensity) and strongly (1.5 σ of average relative signal intensity) affected signals, respectively. Error bars are given as black vertical lines. **(c)** Mapping of the affected residues on NusA-NTD (PDB ID: 2KWP, gray in surface representation). Moderately affected residues, orange; strongly affected residues, red. The PyMOL Molecular Graphics System (Version 1.7, Schrödinger, LLC.; https://pymol.org) was used for visualization.

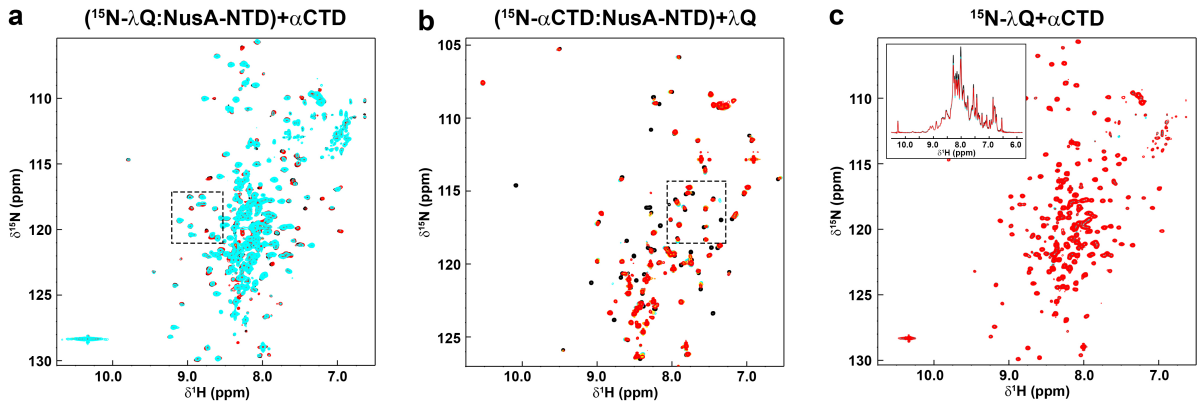

Supplementary Figure 6: The αCTD of RNAP and λQ share binding sites on NusA-NTD. (a) αCTD detaches NusA-NTD from ^{15}N-λQ. 2D [^{1}H,^{15}N]-BEST-TROSY spectra are shown. Molar ratios: ^{15}N-λQ:NusA-NTD:αCTD = 1:0:0, black; =1:2:0, cyan; 1:2:2, orange; 1:2:4, red. Initial concentration of ^{15}N-λQ: 250 µM. The dashed box indicates the section shown in Fig. 2d. **(b)** NusA-NTD is removed from ^{15}N-αCTD by λQ. 2D [^{1}H,^{15}N]-HSQC spectra are depicted. Molar ratios: ^{15}N-αCTD:NusA-NTD:λQ = 1:0:0; black; =1:2:0; cyan; 1:2:2; orange; 1:2:4, purple; 1:2:6, yellow; 1:2:10, red. Initial concentration of ^{15}N-αCTD: 250 µM. The dashed box corresponds to the section shown in Fig. 2e. **(c)** [^{1}H,^{15}N]-BEST-TROSY spectra of the titration of 125 µM ^{15}N-λQ with αCTD (molar ratios: 1:0, black; 1:1, cyan; 1:2, red). The inset shows corresponding 1D [^{1}H,^{15}N]-HSQC spectra.

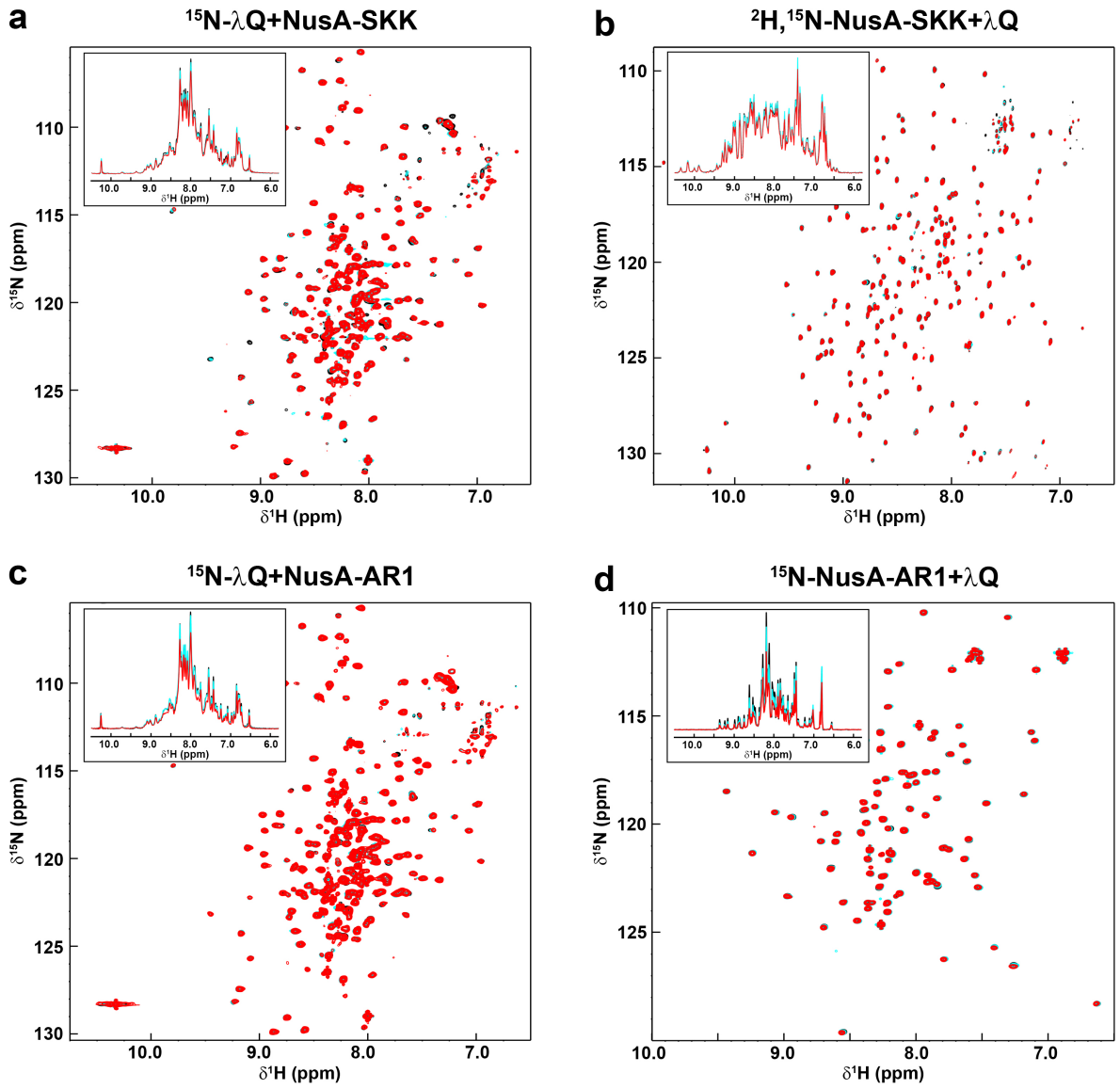

Supplementary Figure 7: λQ interacts with neither NusA-SKK nor NusA-AR1. (a) 1D [^{1}H,^{15}N]-HSQC and 2D [^{1}H,^{15}N]-BEST-TROSY spectra of the titration of 125 µM ^{15}N-λQ with NusA-SKK (molar ratios: 1:0, black; 1:1, cyan; 1:2). **(b)** 1D [^{1}H,^{15}N]-HSQC and 2D [^{1}H,^{15}N]-BEST-TROSY spectra of the titration of 125 µM ^{2}H,^{15}N-NusA-SKK with λQ (molar ratios: 1:0, black; 1:1, cyan; 1:2 red). **(c)** 1D [^{1}H,^{15}N]-HSQC and 2D [^{1}H,^{15}N]-BEST-TROSY spectra of the titration of 175 µM ^{15}N-λQ with NusA-AR1 (molar ratios: 1:0, black; 1:1, cyan; 1:2 red). **(d)** 1D and 2D [^{1}H,^{15}N]-HSQC spectra of the titration of 125 µM ^{15}N-NusA-AR1 with λQ (molar ratios: 1:0, black; 1:1, cyan; 1:2 red).

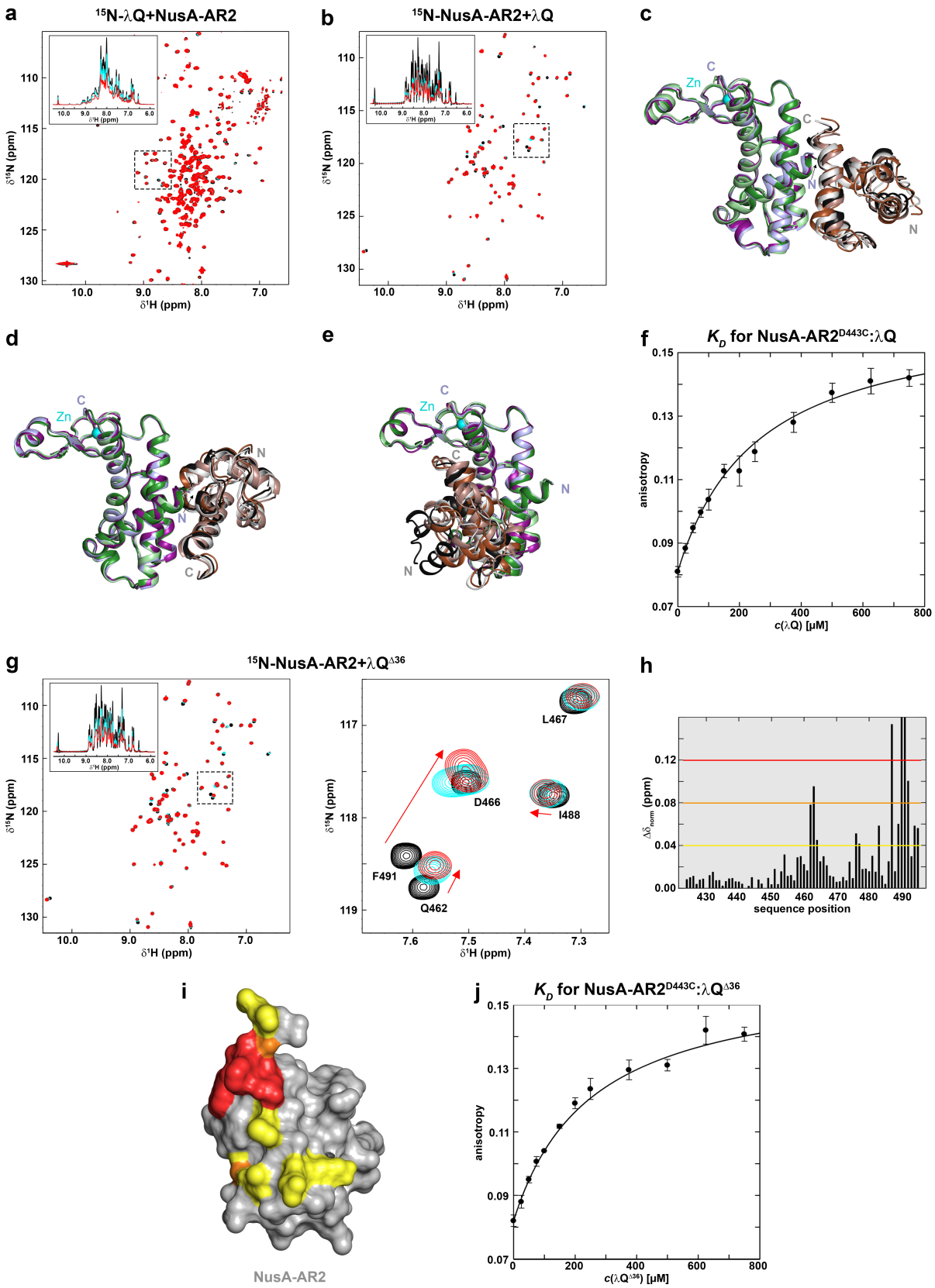

Supplementary Figure 8: λQ interacts directly with NusA-AR2. (a) 1D [^{1}H,^{15}N]-HSQC and 2D [^{1}H,^{15}N]-BEST-TROSY spectra of the titration of 250 µM ^{15}N-λQ with NusA-AR2

(molar ratios: 1:0, black; 1:1, cyan; 1:2 red). The dashed box indicates the section shown in Fig. 3a. **(b)** 1D and 2D [^{1}H,^{15}N]-HSQC spectra of the titration of 250 µM ^{15}N-NusA-AR2 with λQ (molar ratios: 1:0, black; 1:1, cyan; 1:2 red). The dashed box marks the section depicted in Fig. 3b. **(c-e)** Models of the λQ:NusA-AR2 complex. The models were generated by docking using the affected residues as restraints (the HADDOCK 2.2 server (https://haddock.science.uu.nl/services/HADDOCK2.2/). The three clusters with the lowest Z and HADDOCK scores are shown (increasing values from **(c)** to **(e)**) with each cluster comprising three superimposed structures. The proteins are depicted in ribbon representation, the Zn^{2+} ion as cyan sphere. PDB IDs: λQ, 4MOI;NusA-AR2, 1WCN. The PyMOL Molecular Graphics System (Version 1.7, Schrödinger, LLC.; https://pymol.org) was used for visualization. **(f)** Determination of the K_D of the λQ:NusA-AR2^{D443C} interaction by fluorescence anisotropy measurements. The standard deviation is shown as vertical bars. The curve represents the best fit to a two-component binding equation, yielding a K_D value of 268±17 µM. Fitting was performed with GraFit 5.0 (Erithacus Software; http://www.erithacus.com/grafit/index.html). **(g)** 1D and 2D [^{1}H,^{15}N]-HSQC spectra of the titration of 250 µM ^{15}N-NusA-AR2 with λQ$^{\Delta 36}$ (molar ratios: 1:0, black; 1:1, cyan; 1:2 red). The dashed box indicates the section shown on the right. Selected signals are assigned, arrows indicating chemical shift changes during the titration. **(h)** Normalized chemical shift changes of NusA-AR2 upon the addition of two equivalents λQ$^{\Delta 36}$. Yellow, orange, and red lines indicate thresholds for slightly (0.04 ppm ≤ $\Delta\delta_{norm}$ < 0.08 ppm), moderately (0.08 ppm ≤ $\Delta\delta_{norm}$ < 0.12 ppm) and strongly ($\Delta\delta_{norm}$ ≥ 0.12 ppm) affected signals, respectively. **(i)** Mapping of the affected residues from **(h)** on the structure of NusA-AR2 (PDB ID: 1WCN, gray, in surface representation). Slightly affected residues, yellow; Moderately affected residues, orange; strongly affected residues, red. The PyMOL Molecular Graphics System (Version 1.7, Schrödinger, LLC.; https://pymol.org) was used for visualization. **(j)** Determination of the affinity of the λQ$^{\Delta 36}$:NusA-AR2^{D443C} interaction by fluorescence

anisotropy measurements. Representation as in **(f)**. The curve represents the best fit to a two-component binding equation, yielding a K_D value of 268±17 μM. Fitting was performed with GraFit 5.0 (Erithacus Software; http://www.erithacus.com/grafit/index.html).

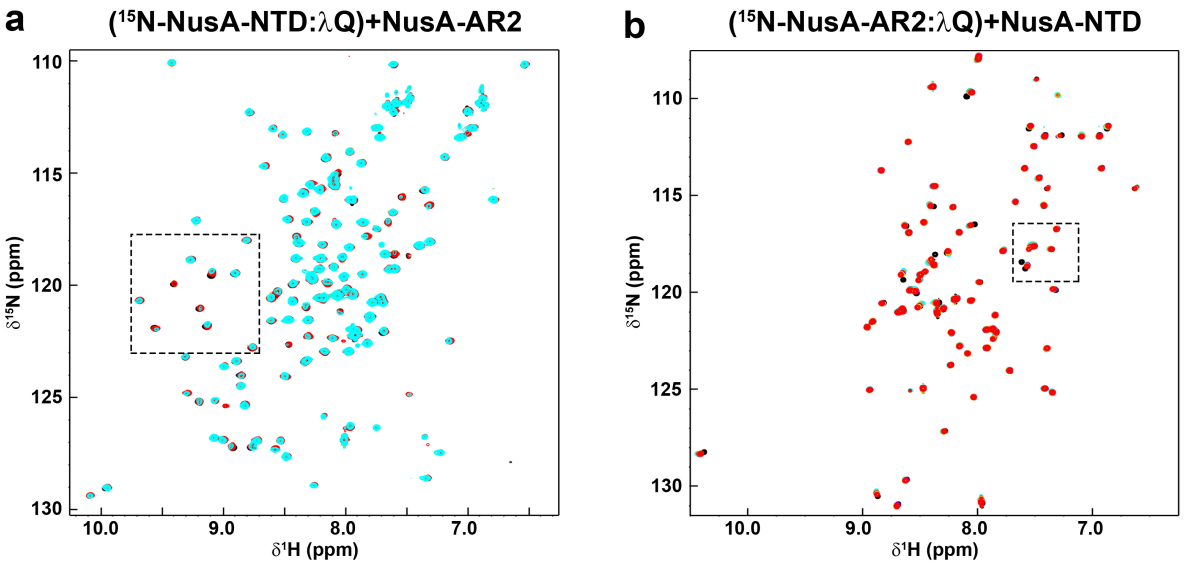

Supplementary Figure 9: NMR-based competition experiments of λQ, NusA-NTD and NusA-AR2. (a) NusA-AR2 detaches λQ from ^{15}N-NusA-NTD. 2D [^{1}H,^{15}N]-HSQC spectra are shown, dashed boxes indicate the sections shown in Fig. 3d. Molar ratios: ^{15}N-NusA-NTD:λQ:NusA-AR2 = 1:0:0, black; =1:2:0, cyan; 1:2:2, orange; 1:2:4, red. Initial concentration of ^{15}N-NusA-NTD: 250 µM. **(b)** λQ is removed from ^{15}N-NusA-AR2 by NusA-NTD. 2D [^{1}H,^{15}N]-HSQC spectra are depicted with the dashed box marking the region shown in Fig. 3e. Molar ratios: ^{15}N-NusA-AR2:λQ:NusA-NTD = 1:0:0; black; =1:2:0; cyan; 1:2:2; orange; 1:2:4, purple; 1:2:6, yellow; 1:2:10, red. Initial concentration of ^{15}N-NusA-AR2: 250 µM.

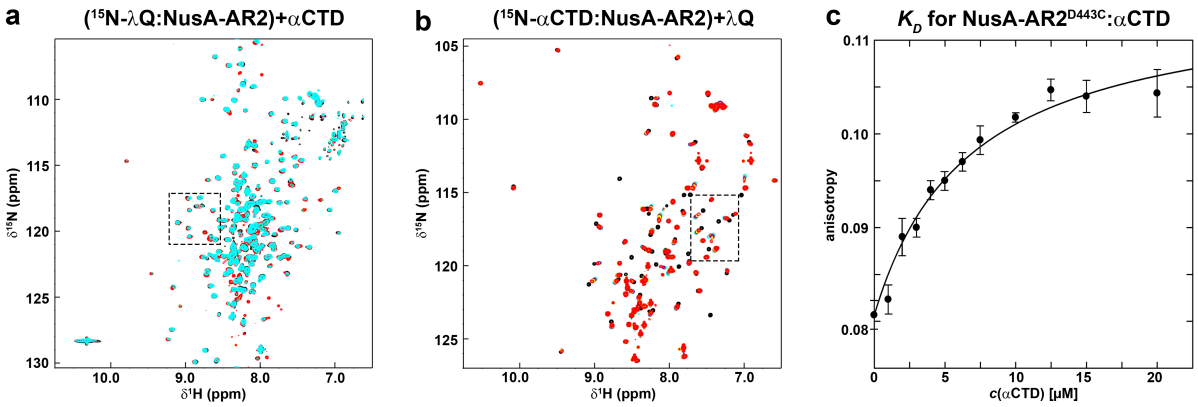

Supplementary Figure 10: The αCTD and λQ share binding sites on NusA-AR2. (a) Removal of NusA-AR2 from ^{15}N-λQ by αCTD. 2D [^{1}H,^{15}N]-BEST-TROSY spectra are shown, the dashed box indicates the region shown in Fig. 4a. Molar ratios: ^{15}N-λQ:NusA-AR2:αCTD = 1:0:0, black; =1:2:0, cyan; 1:2:2, orange; 1:2:4, red. Initial concentration of ^{15}N-λQ: 250 µM. **(b)** λQ detaches NusA-AR2 from ^{15}N-αCTD. 2D [^{1}H,^{15}N]-HSQC spectra are depicted, the dashed box marks the section magnified in Fig. 4b. Molar ratios: ^{15}N-αCTD:NusA-AR2:λQ = 1:0:0; black; =1:2:0; cyan; 1:2:2; orange; 1:2:4, purple; 1:2:6, yellow; 1:2:10, red. Initial concentration of ^{15}N-αCTD: 250 µM. **(c)** Determination of the affinity of the αCTD:NusA-AR2^{D443C} interaction by fluorescence anisotropy measurements. The standard deviation is shown as bars. The curve represents the best fit to a two-component binding equation, yielding a K_D value of 8±1 µM. Fitting was performed with GraFit 5.0 (Erithacus Software; http://www.erithacus.com/grafit/index.html).

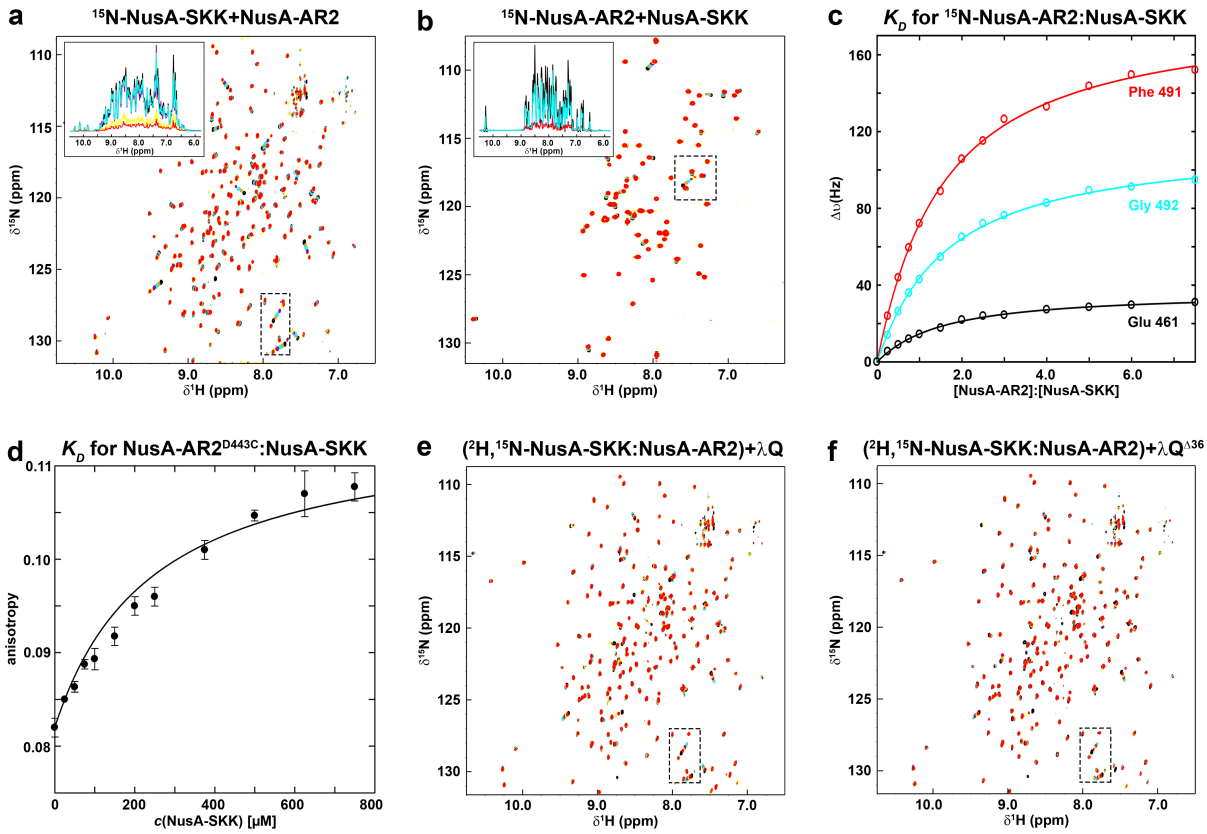

Supplementary Figure 11: NusA autoinhibition can be released by λQ. (a) 1D [^{1}H,^{15}N]-HSQC and 2D [^{1}H,^{15}N]-BEST-TROSY spectra of the titration of 300 µM ^{2}H,^{15}N-NusA-SKK with NusA-AR2 (molar ratios: 1:0, black; 1:0.5, orange; 1:1, cyan; 1:2 purple; 1:5 yellow; 1:7.5 red; concentration of NusA-AR2 stock: 1.5 mM). The dashed box marks the section shown in Fig. 5a. **(b)** 1D and 2D [^{1}H,^{15}N]-HSQC spectra of the titration of 200 µM ^{15}N-NusA-AR2 with NusA-SKK (molar ratios: 1:0, black; 1:0.5, orange; 1:1, cyan; 1:2 purple; 1:5 yellow; 1:7.5 red; concentration of NusA-SKK stock: 500 µM). The dashed box corresponds to the region shown in Fig. 5b. **(c)** Determination of the affinity of the NusA-AR2:NusA-SKK interaction based on the titration of ^{15}N-NusA-AR2 with NusA-SKK. Titration curves for selected residues of ^{15}N-NusA-AR2 are shown. The individual curves representing the best fit to a two-component binding equation, yielding an average K_D value of <341 µM. **(d)** Determination of the K_D of the NusA-SKK:NusA-AR2^{D443C} interaction by fluorescence anisotropy measurements. 25 nM fluorescent labeled NusA-AR2^{D443C} was titrated with NusA-SKK. For each titration step the mean value of four individual titrations is plotted against the

NusA-SKK concentration. The standard deviation is shown as bars. The curve represents the best fit to a two-component binding equation, yielding a K_D value of 279±17 μM. **(e)** λQ removes NusA-AR2 from $^{2}H,^{15}N$-NusA-SKK. 2D [$^{1}H,^{15}N$]-BEST-TROSY spectra are shown and the dashed box indicates the section shown in Fig. 5d. Molar ratios: $^{2}H,^{15}N$-NusA-SKK:NusA-AR2:λQ =1:0, black; =1:5, orange; =1:5:1, cyan; =1:5:2, purple; =1:5:5, yellow; =1:5:10, red. Initial concentration of $^{2}H,^{15}N$-NusA-SKK: 175 μM. **(f)** $\lambda Q^{\Delta 36}$ detaches NusA-AR2 from $^{2}H,^{15}N$-NusA-SKK. 2D [$^{1}H,^{15}N$]-BEST-TROSY spectra are depicted, the dashed box marks the region shown in Fig. 5e. Molar ratios: $^{2}H,^{15}N$-NusA-SKK:NusA-AR2:$\lambda Q^{\Delta 36}$ =1:0, black; =1:5, orange; =1:5:1, cyan; =1:5:2, purple; =1:5:5, yellow; =1:5:10, red. Initial concentration of $^{2}H,^{15}N$-NusA-SKK: 175 μM.

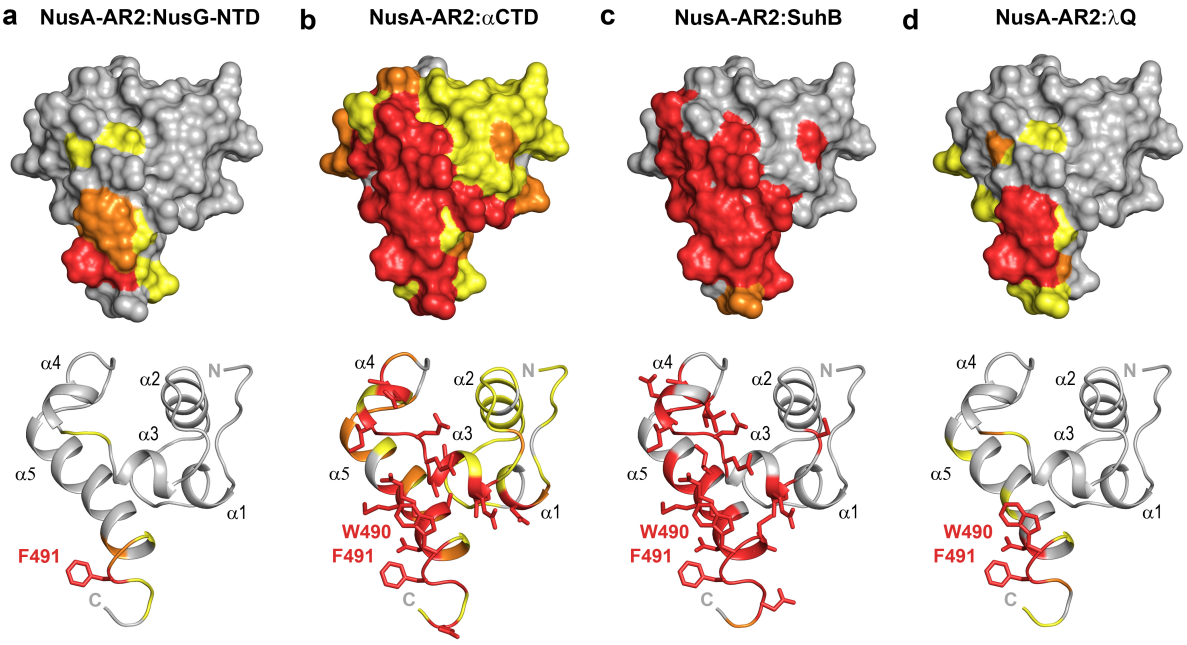

Supplementary Figure 12: NusA-AR2 interacts with various interaction partners. NusA-AR2 binding surfaces of NusG-NTD **(a)**, αCTD **(b)**, SuhB **(c)** and λQ **(d)** are shown. NusA-AR2 (gray; PDB ID: 1WCN) is in surface (top) and ribbon (bottom) representation. Residues affected by binding as determined by [^{1}H,^{15}N]-HSQC titrations are color-coded (slightly affected, yellow; moderately affected, orange; strongly affected, red). The side chains of strongly affected residues are depicted as sticks. Termini, secondary structure elements, and selected residues are labeled. Binding data for NusG-NTD, SuhB and αCTD were taken from references [1–3]. The PyMOL Molecular Graphics System (Version 1.7, Schrödinger, LLC.; https://pymol.org) was used for visualization.

Supplementary References

1. Dudenhoeffer, B. R., Schneider, H., Schweimer, K. & Knauer, S. H. SuhB is an integral part of the ribosomal antitermination complex and interacts with NusA. *Nucleic Acids Res*. **47**, 6504–6518 (2019).

2. Schweimer, K. *et al.* NusA interaction with the α subunit of E. coli RNA polymerase is via the UP element site and releases autoinhibition. *Structure* **19**, 945–954 (2011).

3. Strauß, M. *et al.* Transcription is regulated by NusA:NusG interaction. *Nucleic Acids Res.* **44**, 5971–5982 (2016).

7.3 Einzelarbeit C

Benjamin R. Dudenhoeffer, Marlon Wörner, Jan Bodenschlägel, Kristian Schweimer und Stefan H. Knauer: **Antitermination factor λQ mediates NusA-NTD rearrangement on RNAP βflap.** Manuskript.

Antitermination factor λQ mediates NusA-NTD rearrangement on RNAP βflap

Benjamin R. Dudenhoeffer[1], Marlon Wörner[1], Jan Bodenschlägel[1], Kristian Schweimer[1], Stefan H. Knauer[1,*]

[1]Biochemistry IV - Biopolymers, University of Bayreuth, Universitätsstraße 30, 95447 Bayreuth, Germany

*To whom correspondence should be addressed. Tel: +49 921 553868; Email: stefan.knauer@uni-bayreuth.de

ABSTRACT

A common mechanism of transcription regulation is antitermination (AT) where termination signals are suppressed. Phage λ uses AT to regulate the expression of its late genes in *Escherichia coli*. In this process AT protein λQ binds to RNA polymerase (RNAP) and AT efficiency is enhanced by N-utilization substance (Nus) factor A. Here we used solution-state nuclear magnetic resonance spectroscopy to decipher the molecular basis of λQ-dependent AT and the role of NusA. We provide structural evidence that λQ directly interacts with the flap tip helix (FTH) of RNAP, and that it competes with both the σ^{70} factor and the N-terminal domain (NTD) of NusA for binding to the FTH. Our results indicate that λQ-dependent displacement of σ^{70} from the FTH may destabilize the holo RNAP to promote pause escape, and that λQ may induce a rearrangement of NusA-NTD on RNAP, suggesting that NusA-repositioning is a general scheme in AT.

INTRODUCTION

The central enzyme of transcription is RNA polymerase (RNAPs), which catalyzes the synthesis of RNA based on a DNA template in a transcription cycle consisting of initiation, elongation, and termination. All cellular genomes are transcribed by multisubunit RNAPs that are conserved in all domains of life with RNAPs from Gram negative bacteria being the simplest representatives, comprising five subunits (2xα,β,β´,ω) [1,2]. Bacterial RNAPs have to bind σ factor as only the resulting holoenzyme is capable of promoter-specific initiation. In *Escherichia coli* (*E. coli*) σ^{70} is responsible for the recognition of housekeeping gene promoters[3]. It consists of 4 conserved sequence regions (σ^{70}_{R1-4}) that can be divided into subregions 1.1, 1.2, 2.1, 2.2, 2.3, 2.4, 3.0, 3.1, 3.2, 4.2, and 4.2 and which fold into four structural domains ($\sigma^{70}_{1.1}$, σ^{70}_{2}, σ^{70}_{3}, σ^{70}_{4}) connected by flexible linkers. Additionally, a non-conserved region (σ^{70}_{NCR}) is located between $\sigma^{70}_{R1.2}$ and $\sigma^{70}_{R2.1}$ [4,5]. In the holoenzyme σ^{70} establishes various contacts with the RNAP, e.g. $\sigma^{70}_{R1.2}$, $\sigma^{70}_{R2.1}$, and $\sigma^{70}_{R2.2}$ interact with the clamp helices of the RNAP β´ subunit (β´ CH) [6] and $\sigma^{70}_{R4.1}$ and $\sigma^{70}_{R4.2}$ bind to the flap-tip helix (FTH) of the flap domain of the RNAP β subunit [7,8]. Specific promoter recognition by σ^{70} requires two conserved sequence elements, the -35 and the -10 elements with the numbers accounting for their position relative to the transcription start site [9]. Upon transition to elongation RNAP forms a stable complex with the nucleic acids, the so-called transcription elongation complex (TEC), and the σ^{70} factor usually dissociates [10]. Termination of transcription either occurs intrinsically by RNA hairpin formation or is mediated by termination factor ρ [11].

Antitermination (AT), the suppression of termination signals, is a widespread process and was first discovered in bacteriophage λ[12], where two distinct mechanisms exist, involving either AT protein λN or AT protein λQ: λN-mediated AT is required for switching from early to delayed early gene expression during the lytic life cycle of λ phage[13], whereas λQ controls the expression of the phage's late gene operon necessary for packing and lysis [14]. In λN-mediated AT, phage protein λN binds to a N-utilization (*nut*) sequence on the nascent RNA and, together with host proteins N utilization substances (Nus) A, B, E, and G, alters the TEC into a termination resistant state by forming a transcription AT complex (TAC) [15,16]. In λQ mediated-AT, phage protein λQ requires two *cis*-acting elements within the phage's late gene promotor $P_{R'}$: a σ^{70}-dependent pause sequence following transcription initiation (at +16 nucleotides (nt)) [17–19] and a subsequent λQ binding element (QBE) [20] to alter the TEC into a TAC. At position +13 of a λQ-controlled operon, RNAP is anchored to the DNA and further transcription to the σ^{70}-dependent pause site at +16 leads to formation of a scrunched complex [21], providing a substrate for λQ binding [17]. At the pause site σ^{70}_{R2} binds to the pause inducing -10-like sequence [17,18] and σ^{70}_{R4} to the -35 like element [19]. In related phage 21 two Q^{21} proteins interact with two distinct elements of the QBE

and are simultaneously interacting with the RNAP holoenzyme. One Q^{21} binds to the FTH of RNAP, leading to the disengagement of σ^{70}_{R4} from FTH and weakening of σ^{70} binding on RNAP, whereas the second Q^{21} protein forms a torus by interacting with the RNA exit channel, forcing the nascent RNA through the torus, preventing pausing and formation of terminator hairpins [22,23]. A second pause-inducing element (called EPS) is located directly downstream of the -10-like pause sequence [24] and determines the frequency at which pause escape occurs. Pause escape involves disengagement of σ^{70}, driven by λQ-induced destabilization of the σ^{70}:RNAP interaction [22,23], and DNA scrunching [21]. Afterwards λQ becomes a stable component of the TEC [22,23] throughout the entire late operon of 26 kb [25], inhibiting pausing and allowing read-through of multiple intrinsic and ρ-dependent termination sites [14,26]. Despite λQs ability to be sufficient to mediate AT in phage late gene operon alone [25] NusA stimulates the AT function of λQ substantially [17] and, as sole of all Nus factors, directly interacts with λQ [27].

NusA is a multidomain protein and a versatile regulator of transcription. It is involved in RNA folding [28], transcriptional pausing associated with nascent RNA hairpins [29], and intrinsic [30,31] as well as ρ-dependent termination [32,33]. The N-terminal domain (NTD) is followed by the domains S1, K homology (KH) 1, and KH2, which form the compact RNA binding motif SKK, and, in *E. coli* and other γ-proteobacteria, by two acidic repeat (AR) domains, AR1 and AR2.

NusA-NTD interacts with the FTH of the β subunit and may simultaneously be contacted by the CTD of one of the α subunits (αCTD). The SKK motif recognizes specifically the spacer region of *nut* sites, an interaction important in AT processes. AR1 and AR2 exhibit similar topology and polarity, but have distinct interaction partners: NusA-AR1 solely interacts with phage protein λN during λN-dependent AT [34], whereas NusA-AR2 binds to the NusA-KH1 domain, preventing RNA binding of SKK and thus autoinhibiting NusA [35–37]. Upon interaction of NusA-AR2 with the αCTD, NusA autoinhibition is released and αCTD is hindered from reattaching to the upstream promoter [36,38]. Moreover, NusA-AR2 serves as recruitment platform for various transcriptional regulators, such as NusG [39], ribosomal AT protein SuhB [40,41] and λQ [27].

NusA's effect on transcription strongly depends on its global conformation, which, in turn, is determined by the mode how NusA-NTD interacts with the FTH. For example, during NusA-stimulated pause enhancement, NusA-NTD contacts the FTH and the αCTD. In contrast, NusA may enhance λN-dependent AT. Here, protein λN repositions NusA-NTD by disrupting the NusA-NTD:αCTD interaction, allowing a 45 ° rotation around the helix connecting NusA-NTD and NusA-SKK. Consequently, NusA-NTD and λN form a tripod shaped complex, which engages with the FTH, stimulating λN-dependent AT [15,16].

As mentioned above, NusA can also enhance λQ-dependent AT substantially [17]. Interestingly, λQ specifically contacts two domains of NusA: NusA-NTD and NusA-AR2. The NusA-AR2:λQ interaction has been suggested to be involved in the recruitment mechanism of λQ, whereas the function of λQ:NusA-NTD interaction remains elusive. The fact that NusA-mediated stimulation of λN-dependent AT relies on repositioning of NusA-NTD suggests that also λQ-mediated AT may require another binding mode of NusA-NTD. Here, we used solution state nuclear magnetic resonance (NMR) spectroscopy to study how the interplay of NusA-NTD with the αCTD and the FTH is affected by the presence of λQ. We identify the λQ:FTH interface and demonstrate that λQ and NusA-NTD compete for binding to the FTH and do not form a ternary complex. Our results also indicate that λQ repositions NusA-NTD on the RNAP, which might be a key step in transforming NusA from a termination-enhancing to an AT-stimulating factor. Furthermore, our analysis reveals that λQ is able to displace σ^{70} from the FTH, destabilizing the RNAP holoenzyme, without the need of additional energy provided by DNA scrunching. Thus, λQ might be the crucial factor for escaping of the TEC from the σ^{70}-dependent pausing site.

MATERIAL AND METHODS

Cloning. The gene encoding the βflap construct lacking the i9 region from *E. coli* RNAP β-UE (amino acids 829-938 and 1039-1060) was provided by GenScript (Piscataway, NJ, USA) in vector pUC57. The gene was amplified using polymerase chain reaction (primers: 5´-catgccatgggaaccaccatccacattcagg-3´ and 5´-cgggatccttagatacggcgttttaccgcc-3´; Metabion, Martinsried, Germany) and cloned into a pETGB1a expression vector (provided by Gunter Stier, EMBL Heidelberg, Germany) *via Nco*I and *BamH*I restriction sites. The recombinant plasmid pETGB1a_betaflap allowed the expression of *βflap,* resulting in a fusion protein with a hexa-histidine tag, a B1 domain of streptococcal protein G (GB1) solubility tag and a Tobacco Etch Virus (TEV) cleavage site at its N-terminus.

Gene expression and protein purification. Production of NusA-NTD [42], αCTD [43], RNAP [44], σ^{70} [45], λQ, and $\lambda Q^{\Delta 36}$, [27] was carried out as previously described. RNAP lacking αCTD ($RNAP^{\Delta\alpha CTD}$; amino acids 1-235 of the α-UE are missing) was produced as RNAP.

βflap expression was done in Lysogeny broth (LB) medium (supplemented with 30 µg/ml kanamycin) using *E. coli* BL21 (λ DE3) cells (Novagen, Madison, USA) harboring pETGBqa_betaflap. LB medium was inoculated by an overnight preculture grown at 37 °C to an optical density at 600 nm (OD_{600}) of 0.2. After reaching an OD_{600} of 0.5 the temperature was reduced to 16 °C and at an OD_{600} of 0.7 expression was induced by addition of 0.1 mM Isopropyl β-D-1-thiogalactopyranoside (IPTG). Cells were harvested after overnight growth by centrifugation (6,000 x *g*, 10 min, 4 °C) and resuspended in buffer A (20 mM Tris(hydroxymethyl)aminomethane (Tris)/HCl, pH 7.4, 150 mM NaCl, 5 %(v/v) glycerol, 1 mM Dithiothreitol (DTT); ~4 ml per g cells) before being lysed by a microfluidizer (Microfluidics, Newton, USA). The lysate was cleared from debris by centrifugation (13 000 x *g*, 30 min, 4 °C) and subsequent filtration (0.45 µm filter). Afterwards, the crude extract was applied to a 5 ml HisTrap HP column (GE Healthcare, Chalfont St Giles, UK) equilibrated with buffer A. After washing with 20 column volumes buffer A His_6-Gb1-βflap was eluted *via* a step gradient with increasing imidazole concentrations (50 mM - 1 M in buffer A). Target protein containing fractions were combined and the protein was cleaved by TEV protease during overnight dialysis against 4 l buffer A (molecular weight cut-off (MWCO) 3,500 Da) at 4 °C. For removal of the cleaved His_6-Gb1 tag the dialysate was applied to a 5 ml HisTrap HP column equilibrated. The column was washed with buffer A and elution was carried out with a step gradient with increasing imidazole concentrations (50 mM - 1 M in buffer A). βflap containing fractions were combined and after dialysis overnight against buffer C (50 mM 3-(*N*-morpholino)

propanesulfonic acid (MOPS) buffer, pH 6.5, 300 mM NaCl, 150 mM D-Glucose, 5 mM DTT) (MWCO 3 500 Da) at 4 °C, concentrated by ultrafiltration (MWCO 3,000 Da), shock frozen in liquid nitrogen, and stored at -80 °C.

Quality control of proteins. Quality of proteins used in this study was checked according to guidelines established by ARBRE-MOBIEU and P4EU (https://arbre-mobieu.eu/guidelines-on-protein-quality-control/). In brief, sodium dodecyl sulfate polyacrylamide gel electrophoresis (SDS-PAGE) was used for checking protein purity, UV/vis spectroscopy from 220-400 nm (Nanodrop ND-100 spectrometer, PEQLAB, Erlangen, Germany) for checking the absence of nucleic acids and aggregates, analytical gel filtration (Superdex 75 or a Superdex 200 10/300 GL column, GE Healthcare, Munich, Germany) for checking protein homogeneity, and circular dichroism (CD) spectroscopy from 190-240 nm (1 mm quartz cuvette; J-1100, JASCO, Pfungstadt, Germany) for checking the folding state. In case of unlabelled *βflap* additionally one dimensional ^{1}H-NMR spectra were recorded to assess its folding state. Protein concentrations were determined by measuring the absorbance at 280 nm (10 mm quartz cuvette, Hellma, Müllheim, Germany) on a Biospectrometer basic (Eppendorf, Hamburg, Germany). Identity was confirmed by peptide mass fingerprinting (Department of Biochemistry, University of Bayreuth, Germany).

Isotopic labelling of proteins. Protein labelling was done by growing *E. coli* cells in M9 medium [46,47]. For uniform ^{15}N-labelling $(^{15}NH_4)_2SO_4$ (CortecNet, Voisins-Le-Bretonneux, France) was added as sole nitrogen source. For perdeuteration of proteins M9 medium was prepared with 99.9 % (v/v) D_2O; Eurisotop, Saint-Aubin, France) and d_7-glucose as carbon source. βflap was perdeuterated and ^{13}C,^{15}N-labelled for NMR backbone assignment; here ^{13}C,d_7-glucose was used as carbon source. Production of site-specific [^{1}H,^{13}C]-labelled Ile, Leu, and Val methyl groups ([I,L,V]-labelling) in perdeuterated NusA-NTD is based on published protocols [48]. In brief, *E. coli* cells were grown as described for the production of perdeuterated proteins, but 1 h before induction 60 mg/l 2-keto-3-d_3-4-^{13}C-butyrate and 100 mg/l 2-keto-3-methyl-d_3-3-d_1-4-^{13}C-butyrate (both from Eurisotop, St. Aubin Cedex, France) were added. Expression and purification protocols of labelled proteins were the same as for unlabelled proteins.

NMR experiments. NMR experiments were conducted at 298 K on Bruker *Avance* 700 MHz, Bruker *Ascend Aeon* 900 MHz, and Bruker *Ascend Aeon* 1 000 MHz spectrometers, all being

equipped with cryogenically cooled inverse triple resonance probes. Apodization, Forurier transformation, phase correction and baseline correction was done by in-house routines. Two dimensional (2D) and three dimensional (3D) spectra were visualised and analysed by NMRViewJ (One Moon Scientific, Inc., Westfield, NJ, USA), one dimensional (1D) spectra were plotted with MatLab (The MathWorks, Inc., Version 7.1.0.183).

Standard double and triple resonance experiments and a sample of 500 µl (5 mm tube) 260 µM $^{2}H,^{13}C,^{15}N$-βflap in 10 mM K-P (pH 7.0), 50 mM KCl, 1 mM DTT at 298 K [49,50] were used for resonance assignment of the βflap backbone. Backbone amide resonance assignments of αCTD [36], NusA-NTD [42], and λQ [27] were taken from previous studies.

Interaction studies of NusA-NTD:βFlap and NusA-NTD:αCTD were performed in 5 mm tubes with an initial sample volume of 500 µl. The proteins were in 50 mM Na-P, pH 6.5, 100 mM NaCl, 150 mM D-Glucose, 5 mM DTT. All other NMR titrations/interaction studies were done in 3 mm NMR tubes with an initial sample volume of 200 µl using 50 mM MOPS, pH 6.5, 300 mM NaCl, 150 mM D-Glucose, 5 mM DTT (exception: for experiments involving σ^{70} proteins were in 50 mM MOPS, pH 6.5, 500 mM NaCl, 150 mM D-Glucose, 5 mM DTT). All samples contained 10 % (v/v) D_2O for locking. For titrations with with ILV-labelled NusA-NTD the buffer was prepared with 99.9 % (v/v) D_2O.

In order to compare 1D spectra and signal intensities of 2D spectra the intensities were normalized by protein concentration, number of scans, length of the 90° proton pulse, and receiver gain.

If the system was in slow and/or intermediate exchange on the NMR time scale (experiments involving ILV-labelled NusA-NTD and ^{15}N-λQ:βflap) the signal intensities of 2D spectra were analysed quantitatively by calculating relative intensities as described [40,51]. In brief, for each titration step the intensities were first normalized by the 90° proton pulse, receiver gain, concentration, and number of scans. Afterwards, the normalized intensities of a certain titration step were divided by the normalized intensities of the free, labelled protein. In order to identify affected residues the mean relative signal intensity was calculated in a titration step and thresholds were defined at 1.25 and 2 σ of the mean value for the ^{15}N-λQ:βflap interaction and 0.5 and 1 σ for all studies involving ILV-NusA-NTD. Residues with relative signal intensities below these thresholds were classified as moderately or strongly affected, respectively.

If the system was in the fast regime on the chemical shift timescale normalized chemical shift changes ($\Delta\delta_{norm}$) were calculated according to equation (1) for [$^{1}H,^{15}N$] correlation spectra, with $\Delta\delta$ being the resonance frequency difference in ppm.

$$\Delta\delta_{\text{norm}} = \sqrt{\left(\Delta\delta\ ^{1}\text{H}\right)^2 + \left[0.1 \cdot \left(\Delta\delta^{15}\text{N}\right)\right]^2} \qquad (1)$$

Residues were classified as slightly, moderately, and strongly affected, if $0.04\ \text{ppm} \leq \Delta\delta_{\text{norm}} < 0.08\ \text{ppm}$, $0.08 \leq \Delta\delta_{\text{norm}} < 0.12\ \text{ppm}$, and $\Delta\delta_{\text{norm}} \geq 0.12\ \text{ppm}$, respectively.

Both NusA-NTD:βflap and NusA-NTD:αCTD [^{1}H,^{15}N]-HSQC titrations allowed the calculation of dissociation constants (K_D). Data was fitted to a two-state binding equation (2).

$$\Delta\nu = \Delta\nu_{End} * \frac{[P]_0 * r + [P]_0 + K_D - \sqrt{(K_D + [P]_0 + [P]_0 * r)^2 - 4 * ([P]_0)^2 * r}}{2 * [P]_0} \qquad (2)$$

$\Delta\nu$ is the normalized resonance frequency difference in [Hz], $\Delta\nu_{end}$ is the normalized resonance frequency difference between free and bound protein in [Hz], r is the ratio of protein to labeled protein and $[P]_0$ total concentration of ^{15}N labeled protein; reduction of $[P]_0$ due to dilution was taken into account for fitting. Fitting was done with MatLab (The MathWorks, Inc., Version 7.1.0.183) and K_D and $\Delta\nu_{end}$ were used as fitting parameters.

Programs. Protein structures were visualised with PyMOL Molecular Graphics System (Version 1.7, Schrödinger, LLC.).

RESULTS

The solution structure of the βflap construct βflap$^{\Delta}$

The flap region of the RNAP β subunit forms the wall of the RNA exit channel with an α helix at the tip called βflap tip Helix (FTH), which functions as lid and regulates the width of the channel. Consequently, the FTH is a central element of transcription regulation. The FTH interacts, on the one hand, with the nascent RNA, enhancing pausing and intrinsic termination efficiency [52,53], and, on the other hand, with transcription factors such as σ^{70} [7,8], NusA [15,16,29,30,42,54] and phage λ AT proteins λN [15,16] and λQ [55], which regulate transcription in various, sometimes opposing, ways. Due to its high mobility [54] no interpretable electron density is available for the FTH in many RNAP structures [56–58].

Thus, we decided to study the βflap region by solution state NMR spectroscopy and generated a construct termed *βflap$^{\Delta}$* that is suitable for this technique. It comprises amino acids 829-1060 of the β subunit, but the 99 amino acid long i9 helices, which extend deep into the interior of the RNAP, were deleted, resulting in a 136 amino acid protein (residues 829-938 and 1039-1060 of β-subunit; Fig. 1A, inset). We assigned 92.9 % of the amide backbone signals and 96.2 % of the C^{α} backbone signals of βflap$^{\Delta}$ (Fig. 1A). Unassigned residues are mainly located in unstructured areas. The chemical shift index (CSI) of C_{α} and C_O atoms of βflap$^{\Delta}$ is in perfect agreement with the corresponding region in the crystal structure of RNAP (Fig. 1B), confirming that our construct is correctly folded, i.e. it consists of a short α-helix (α1) and a four-stranded antiparallel β-sheet (β1- β4) with the FTH being inserted between strands β2 and β3 via long flexible arms. Moreover, it is important to note that the FTH (residues 897-906) is a well-defined α-helix and that interactions of the FTH can thus be perfectly studied by NMR spectroscopy. We also determined the ^{15}N relaxation behavior of βflap$^{\Delta}$ at 16.8 T magnetic field strength to characterize the overall tumbling of the protein and the flexibility of the FTH (Fig. 1C,D). The FTH and the neighbouring regions (amino acids 892-912) have increased R_1 and decreased R_2 values, confirming that the FTH is highly mobile and that this flexibility is conferred by the adjacent unstructured arm regions, in agreement with findings for the FTH from *Bacillus subtilis* RNAP [54]. Excluding the FTH and flexible loops, we obtained averaged ^{15}N relaxation rates R_1 and R_2 of 0.94 s^{-1} and 17.67 s^{-1}, respectively, which correspond to a rotation correlation time of 11 ns assuming anisotropic tumbling and an elongated shape.

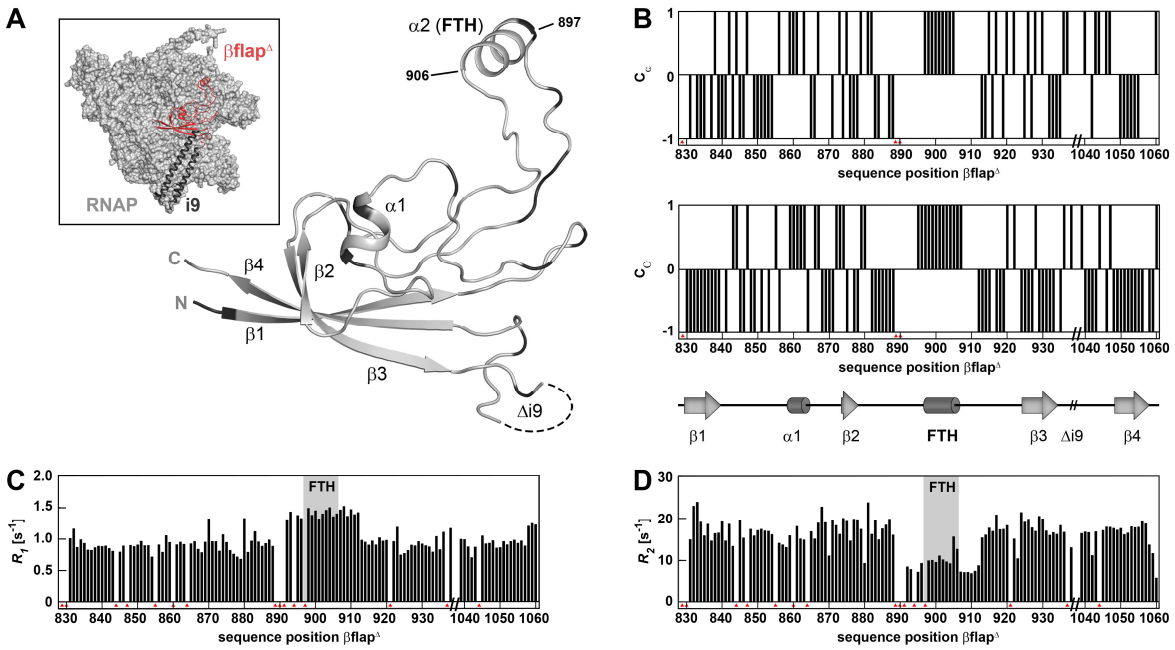

Figure 1: Structure of βflap$^{\Delta}$ in solution. (A) Crystal structure of βflap$^{\Delta}$ in ribbon representation (grey), coordinates taken from the crystal structure of *E. coli* core RNAP (PDB ID: 4KMU). Termini and secondary structure elements are labelled. Sequence position of the βflap tip helix (FTH) is marked by amino acid numbers, the position of the βi9 helices is indicated. Amine backbone signals assigned by NMR spectroscopy are shown in grey, unassigned amine backbone signals are in black. The inset shows RNAP in surface representation (grey) with βflap$^{\Delta}$ and the i9 helices in ribbon representation coloured in red and dark grey, respectively. **(B)** Chemical shift index (CSI) for C_α and C_O of βflap$^{\Delta}$ versus sequence position. Secondary structure elements from (A) are shown below. Red triangles mark unassigned residues. **(C)** R_1 and **(D)** R_2 versus sequence position of βflap$^{\Delta}$. Red triangles mark residues the rates of which could not be determined. The position of the FTH is indicated in grey.

NusA-NTD binding on RNAP-βflap

In order to test the functionality of βflap$^{\Delta}$ we studied its interaction with a known binding partner, NusA-NTD, by NMR spectroscopy [30,42,54]. First, ^{15}N-NusA-NTD was titrated with βflap$^{\Delta}$ and one-dimensional (1D) and two-dimensional (2D) [^{1}H,^{15}N] heteronuclear single quantum coherence (HSQC) spectra were recorded after each titration step (Fig. 2A). Addition of βflap$^{\Delta}$ led to significant chemical shift perturbations of ^{15}N-NusA-NTD, indicating fast chemical exchange on the NMR timescale. Normalized chemical shift changes ($\Delta\delta_{norm}$) were plotted against the amino acid sequence of NusA-NTD to identify affected residues, which were, subsequently, mapped on the structure of NusA-NTD. Residues affected by βflap binding are located in helices α1, α2, and α4, and form a continuous interaction surface at the bottom part of the NusA-NTD body, in agreement with previous reports that found that these helices together with residues from the hydrophobic core create a hydrophobic binding pocket for the FTH [29,54]. Next, we performed the reverse titration and added NusA-NTD to ^{15}N-βflap$^{\Delta}$ (Fig. 2B).

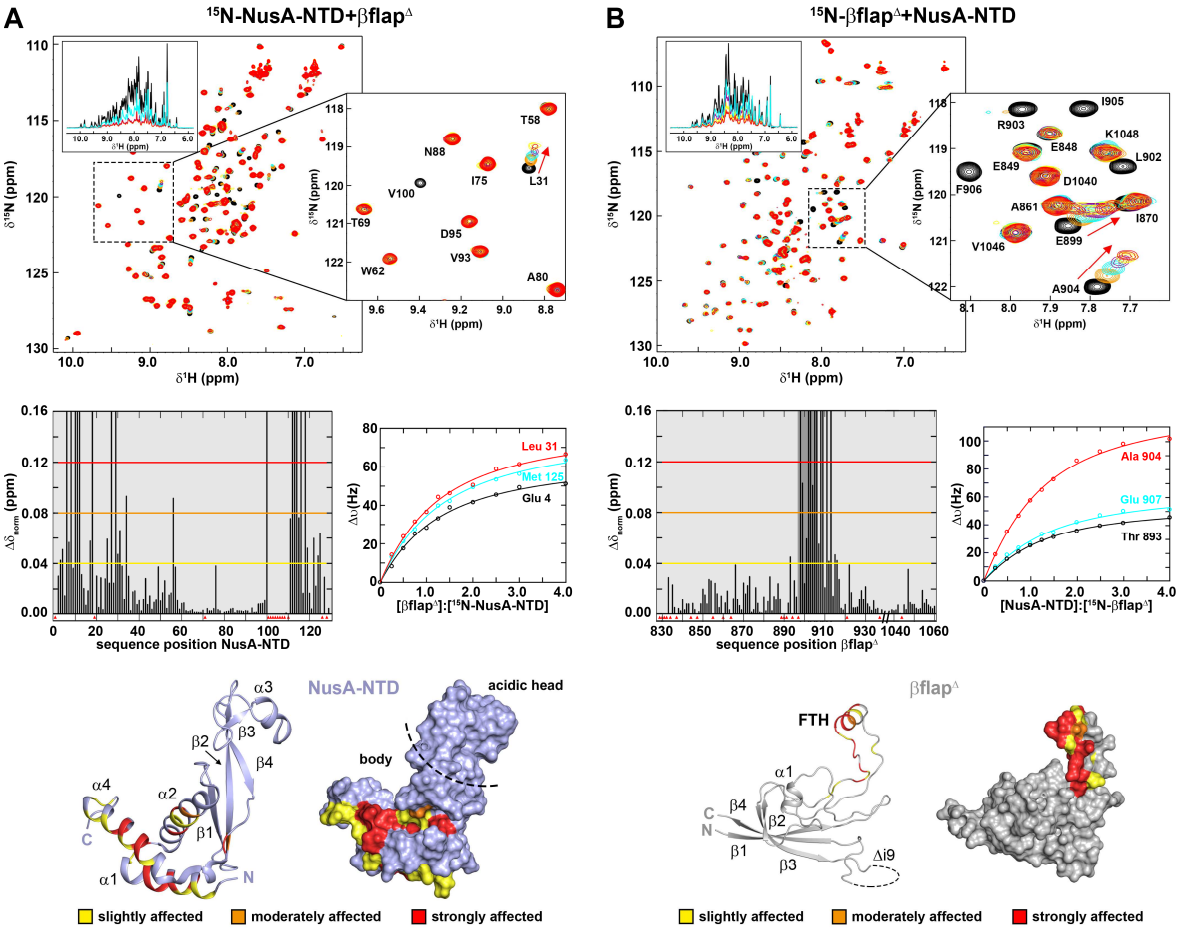

Figure 2: NusA-NTD interacts with βflap$^{\Delta}$. **(A)** Titration of ^{15}N-NusA-NTD with βflap$^{\Delta}$. **(top)** 2D [^{1}H,^{15}N]-HSQC spectra of the titration. Molar ratios: 1:0, black; 1:0.5, orange; 1:1, cyan; 1:2, purple; 1:3, yellow, 1:4, red (concentration of ^{15}N-NusA-NTD: 200 µM; concentration of βflap$^{\Delta}$ stock: 400 µM). The panel on the right side shows a magnification of the boxed region. Selected signals are labelled, arrows indicate changes of chemical shifts. The inset shows the 1D [^{1}H,^{15}N]-HSQC spectra of certain titration steps. **(middle, left)** Normalized chemical shift changes of ^{15}N-NusA-NTD versus sequence position. Thresholds for slightly (0.04 ppm ≤ $\Delta\delta_{norm}$ < 0.08 ppm), moderately (0.08 ppm ≤ $\Delta\delta_{norm}$ < 0.12 ppm), and strongly ($\Delta\delta_{norm}$ ≥ 0.12 ppm) affected residues are indicated by a yellow, orange, and red line. Unassigned residues are marked as red triangles. **(middle, right)** Titration curves of selected residues of ^{15}N-NusA-NTD. The individual curves represent the best fit to a two-component, 1:1 binding equation, yielding an average K_D value of 197 ± 47 µM. **(bottom)** Mapping of affected residues on the structure of NusA-NTD (PDB ID: 2KWP; light blue) in ribbon (left) and surface (right) representation. The colour code is indicated. Termini and secondary structure elements are labelled, the body and acidic head region are indicated. **(B)** Titration of ^{15}N-βflap$^{\Delta}$ with NusA-NTD **(top)** 2D [^{1}H,^{15}N]-HSQC spectra of the titration. Molar ratios: 1:0, black; 1:0.5, orange; 1:1, cyan; 1:2, purple; 1:3, yellow, 1:4, red (concentration of ^{15}N-βflap$^{\Delta}$: 200 µM; concentration of NusA-NTD stock: 1 mM). The right panel shows a magnification of the boxed region. Selected signals are labelled, chemical shift perturbations are indicated by arrows. The inset shows selected 1D [^{1}H,^{15}N]-HSQC spectra. **(middle, left)** Normalized chemical shift changes of ^{15}N-βflap$^{\Delta}$ versus sequence position. Representation as in (A). **(middle, right)** NMR titration curve for selected residues of ^{15}N-βflap$^{\Delta}$. The binding curves were fitted to a two-component 1:1 binding equation, yielding a K_D value of 163 ± 22 µM. **(bottom)** Mapping of the affected residues from on the structure of βflap$^{\Delta}$ (PDB ID: 4KMU; grey). Representation and colour code as in (A).

Again, the system was in fast chemical exchange so that we calculated $\Delta\delta_{norm}$ and plotted it against the amino acid sequence of βflap$^{\Delta}$. Mapping of affected residues on the structure of βflap$^{\Delta}$ reveals that only the FTH and residues in the adjacent flexible arms are involved in the interaction with strongly affected residues being found in the FTH (E898, L902, R903, I905, F906) and the C-terminal arm, in perfect agreement with previous studies [8,15,16,54]. As both systems were in fast chemical exchange K_D values could be determined for both interactions using a two-state binding model, yielding 197±47 µM for the ^{15}N-NusA-NTD:βflap and 163±22 µM for the ^{15}N-βflap:NusA-NTD interaction, respectively.

Overall, we conclude that our βflap construct is fully functional and perfectly suited to study the interplay of the FTH with NusA-NTD and λQ.

NusA-NTD contacts FTH and αCTD simultaneously

During *his* operon-mediated TEC pausing NusA-NTD interacts not only with the FTH but also contacts the αCTD with both interactions being necessary for enhancement of transcriptional pausing [29,30]. Thus, we set out to follow the assembly of the ternary NusA-NTD:βflap$^{\Delta}$:αCTD complex by NMR spectroscopy. This, however, required first the determination of the αCTD interaction surface of NusA-NTD and *vice versa*, which was accomplished by titrating either ^{15}N-NusA-NTD with αCTD or ^{15}N-αCTD with NusA-NTD and recording [^{1}H,^{15}N]-HSQC spectra after each titration step (Supplementary Fig. S1). αCTD binding affects primarily the acidic head region and the adjacent strands β2 and β4 of NusA-NTD, whereas NusA-NTD contacts αCTD helices α1, α3, and α4, all data being in agreement with a previous report [29]. Affinities were determined as 27±9 µM for the ^{15}N-NusA-NTD:αCTD and 23±6 µM for the ^{15}N-αCTD:NusA-NTD interaction. To check that βflap$^{\Delta}$ does not bind to αCTD we performed NMR titrations of ^{15}N-βflap$^{\Delta}$ with αCTD and *vice versa* (Supplementary Figure S2A,B). Even addition of a two-fold excess of the unlabelled component did not change the [^{1}H,^{15}N]-HSQC spectra of ^{15}N-labelled protein, ruling out complex formation.

In order to assemble the ternary NusA-NTD:βflap$^{\Delta}$:αCTD complex as observed in the *his*-paused TEC, we titrated ^{2}H,^{15}N-NusA-NTD with αCTD and then added βflap$^{\Delta}$ (Fig. 3A, Supplementary Fig. S2C). The presence of αCTD led to the changes of the ^{2}H,^{15}N-NusA-NTD spectrum indicating complex formation (Supplementary Fig. S1A). The subsequent addition of βflap$^{\Delta}$ resulted in chemical shift perturbations typical for the ^{2}H,^{15}N-NusA-NTD:βflap$^{\Delta}$ interaction (Fig. 2A). Strikingly ^{2}H,^{15}N-NusA-NTD signals shifting upon αCTD binding were not affected by the presence of βflap$^{\Delta}$ and *vice versa*, indicating that the binding sites on NusA-NTD are distinct and not overlapping. To complement our findings we asked if this ternary complex can

also occur with complete RNAP, but under non-pausing conditions. Thus, we tested the assembly of this complex using RNAP instead of βflap$^{\Delta}$. Due to the huge molecular mass of RNAP we utilized ^{1}H,^{13}C-labelled methyl groups of Ile, Leu and Val as NMR-active probes in deuterated NusA-NTD and carried out transverse relaxation optimized spectroscopy (TROSY)-based titrations with RNAP (Fig. 3B) and an RNAP variant lacking the αCTD (RNAP$^{\Delta\alpha CTD}$) (Fig. 3C). In both cases signal intensity decreased non-uniformly which may be attributed to a combination of several effects: (i) the increase in molecular mass due to complex formation led to a general decrease in signal intensity, (ii) signal intensity of NusA-NTD methyl groups in the RNAP binding site is decreased more strongly than that of methyl groups located elsewhere due to dipol:dipol interactions with protons of RNAP, (iii) chemical exchange processes may affect signal intensity. The loss of signal intensity was analysed quantitatively by calculating relative intensities in each titration step (see Material and Methods), which was then plotted against the amino acid sequence of NusA-NTD (Figure 3B,C). The mean relative intensity was calculated and thresholds at 0.5 σ and 1.0 σ below the mean relative single intensity were introduced to identify moderately and strongly affected residues, respectively. These were mapped on the structure of NusA-NTD and, due to the low number of ILV probes, the binding sites were graphically extended by highlighting 2 amino acids on either side of an affected ILV residue (if they were not unaffected ILV residues themselves; Fig. 3B,C and Supplementary Fig. S2 D,E). Binding of RNAP affects residues both in the acidic head and in the body, whereas RNAP$^{\Delta\alpha CTD}$ contacts NusA-NTD only at its body, corroborating our findings using βflap$^{\Delta}$ and αCTD. Finally, the binding sites identified by [^{1}H,^{15}N]-based titrations are in perfect agreement with the interaction surfaces observed in the *his*-paused TEC [29], confirming that our βflap$^{\Delta}$ construct is perfectly suitable to study the FTH on a molecular level. Moreover, our results demonstrate that NusA-NTD contacts the FTH and the αCTD simultaneously in isolated RNAP, suggesting that these interactions are not only required to mediate NusA-enhanced pausing, but represent the normal binding mode of NusA-NTD.

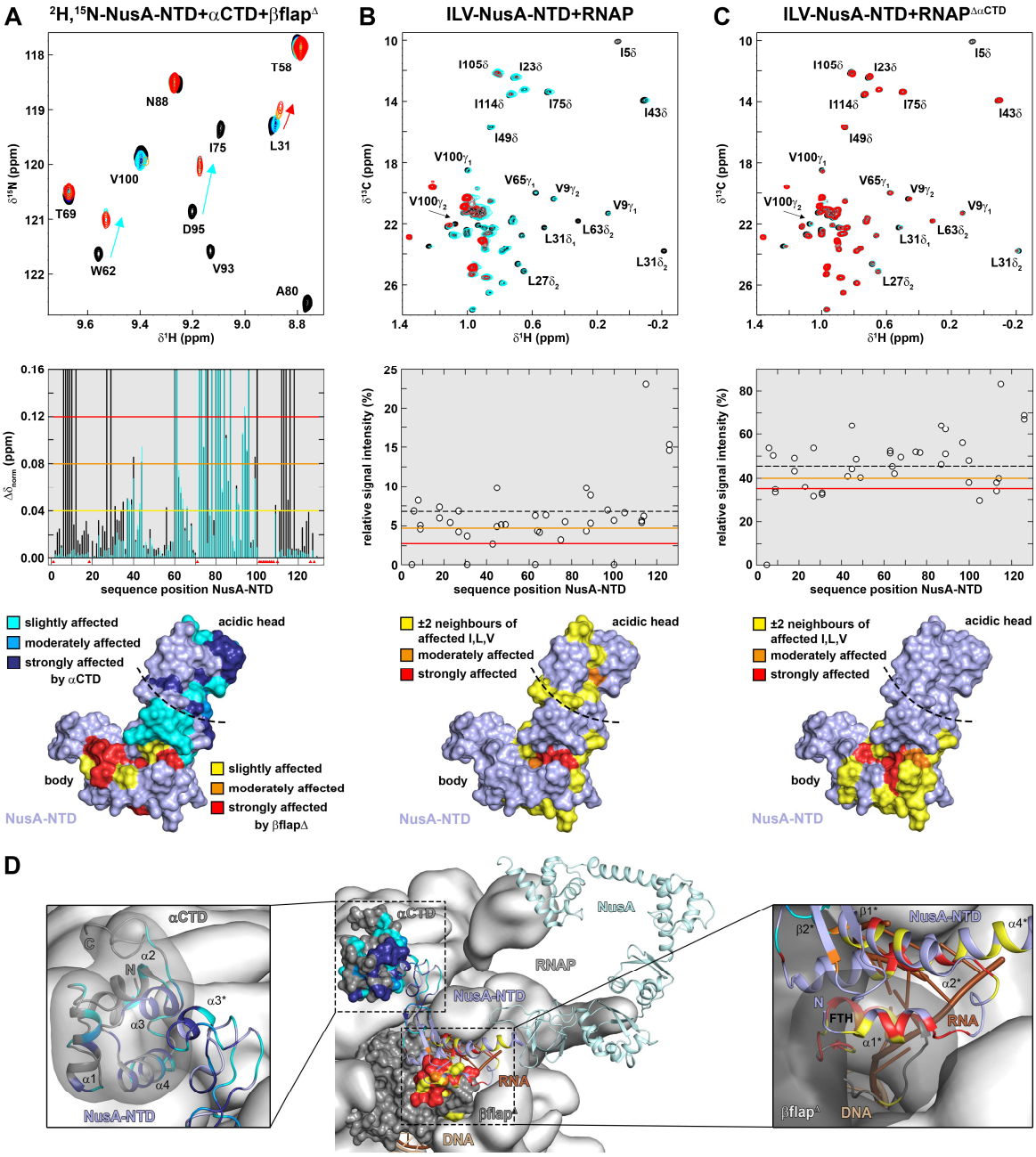

Figure 3: NusA-NTD interacts with αCTD and βflap simultaneously. (A) Titration of 250 µM $^{2}H,^{15}N$-NusA-NTD with αCTD and βflap$^{\Delta}$. **(top)** Section of 2D [$^{1}H,^{15}N$]-HSQC spectra. Molar ratio of $^{2}H,^{15}N$-NusA-NTD:αCTD:βflap$^{\Delta}$ = 1:0:0, black; = 1:1:0, blue; = 1:2:0, cyan; = 1:2:1, orange; = 1:2:2, red. Selected signals are assigned. Cyan and red arrows indicate chemical shift changes upon addition of αCTD and βflap$^{\Delta}$, respectively. **(middle)** HSQC-derived normalized chemical shift changes of $^{2}H,^{15}N$-NusA-NTD in the presence of 2 equivalents αCTD (black) and after addition of 2 equivalents βflap to the $^{2}H,^{15}N$-NusA-NTD:αCTD complex (cyan). Thresholds for slightly (0.04 ppm ≤ $\Delta\delta_{norm}$ < 0.08 ppm), moderately (0.08 ppm ≤ $\Delta\delta_{norm}$ < 0.12 ppm), and strongly ($\Delta\delta_{norm}$ ≥ 0.12 ppm) affected residues are indicated yellow, orange, and red horizontal lines. Unassigned residues are marked as red triangles. **(bottom)** Mapping of affected residues on the structure of NusA-NTD (PDB ID: 2KWP; light blue, surface representation). The acidic head is separated from the body region by a dashed line. The colour code is indicated. **(B,C)** Interaction of ILV-NusA-NTD with RNAP **(B)** and RNAP$^{\Delta\alpha CTD}$ **(C)**. **(top)** 2D [$^{1}H,^{13}C$]-Methyl-TROSY spectra of ILV-NusA-NTD in the absence (black, 75 µM ILV-NusA-NTD) and presence of RNAP/ RNAP$^{\Delta\alpha CTD}$ (cyan,

molar ratio 1:1, 38 µM / 19 µM ILV-NusA-NTD; red, molar ratio 1:2, 20 µM / 12 µM ILV-NusA-NTD). Selected signals are labelled. **(middle)** Relative intensities of ILV-NusA-NTD methyl group signals in the presence of one equivalent of RNAP / RNAP$^{\Delta\alpha CTD}$ versus sequence position of NusA-NTD. The dashed line indicates the average relative signal intensity, orange and red lines mark the thresholds for moderately (0.5 σ of average relative signal intensity) and strongly (1.0 σ of average relative signal intensity) affected signals. **(bottom)** Mapping of affected residues on the structure of NusA-NTD (PDB ID: 2KWP; light blue, surface representation). For graphical illustration of the interaction site the complete amino acid is coloured (the colour code is indicated). The acidic head and body regions are separated by a dashed line. **(D)** Cryo-EM structure of paused TEC with bound NusA (PDB ID: 6FLQ). RNAP is shown in surface representation (grey) with αCTD and βflap$^{\Delta}$ highlighted in dark grey. NusA (light blue, NusA-NTD; cyan, NusA-SKK-AR1-AR2) and nucleic acids are shown in ribbon representation (brown, RNA; wheat, DNA). NusA-NTD residues affected by αCTD binding (see also Fig. S1) and interaction with βflap$^{\Delta}$ (see also Fig. 2) are highlighted. Panels show details of the boxed regions. Termini and secondary structure elements are labelled.

λQ:FTH binding surface

The FTH is not only the anchor point for NusA-NTD, but also for phage λ AT proteins λN [15,16] and λQ [55]. Although cryoEM structures of Q-modified TECs are available for phage 21 [22,23], the molecular basis of λQ binding to RNAP FTH is not well understood. Thus, we carried out a [^{1}H,^{15}N]-HSQC-based titration where we added βflap$^{\Delta}$ to ^{15}N-λQ. Only minor changes in chemical shifts were observable, but a non-uniform decrease in signal intensity (Fig. 4A and Supplementary Fig. S3A). Relative intensities of ^{15}N-λQ signals in the presence of two equivalents of βflap$^{\Delta}$ were plotted against the amino acid sequence of λQ and affected residues were mapped on the structure of λQ (Fig. 4A). A continuous binding surface is not observable, but residues strongly affected by βflap$^{\Delta}$ binding are located in helices α1 (N68, M71, H75, V77), α3 (L99, F102, A112), and α5 (A160) and form a hydrophobic cluster. Helices α3 and α5 being involved in the interaction with βflap$^{\Delta}$ is in agreement with data obtained from a bacterial two-hybrid approach [55]. The N-terminus of λQ, i.e. amino acids 1-67, is unstructured [27]. Residues 38-67 are not affected by βflap$^{\Delta}$ binding and, although not assigned, signals corresponding to amino acids 1-37 are located between 7.5 and 8.5 ppm in the proton dimension and their intensity is not decreased. Thus, we conclude that the λQ N-terminus is not involved in binding to βflap$^{\Delta}$.

In order to determine the λQ binding site on βflap$^{\Delta}$ we titrated ^{15}N-βflap$^{\Delta}$ with λQ (Fig. 4B and Supplementary Fig. S3B), resulting in significant perturbations of ^{15}N-βflap$^{\Delta}$ chemical shifts. Plotting of $\Delta\delta_{norm}$ against the amino acid sequence of βflap$^{\Delta}$ identified three residues that are significantly affected by λQ binding (L901, L902, F906) and highlighting them on the structure of βflap$^{\Delta}$ shows that all are located on one side of the FTH, in agreement with a previous report [55]. Repeating the titration with a λQ variant lacking 36 amino acids at the N-terminus (λQ$^{\Delta 36}$, [27]) resulted in the same binding site on βflap$^{\Delta}$, confirming that the N-terminus of λQ is not involved

in binding to the FTH. In summary, our findings suggest that the FTH recognizes λQ via hydrophobic interactions.

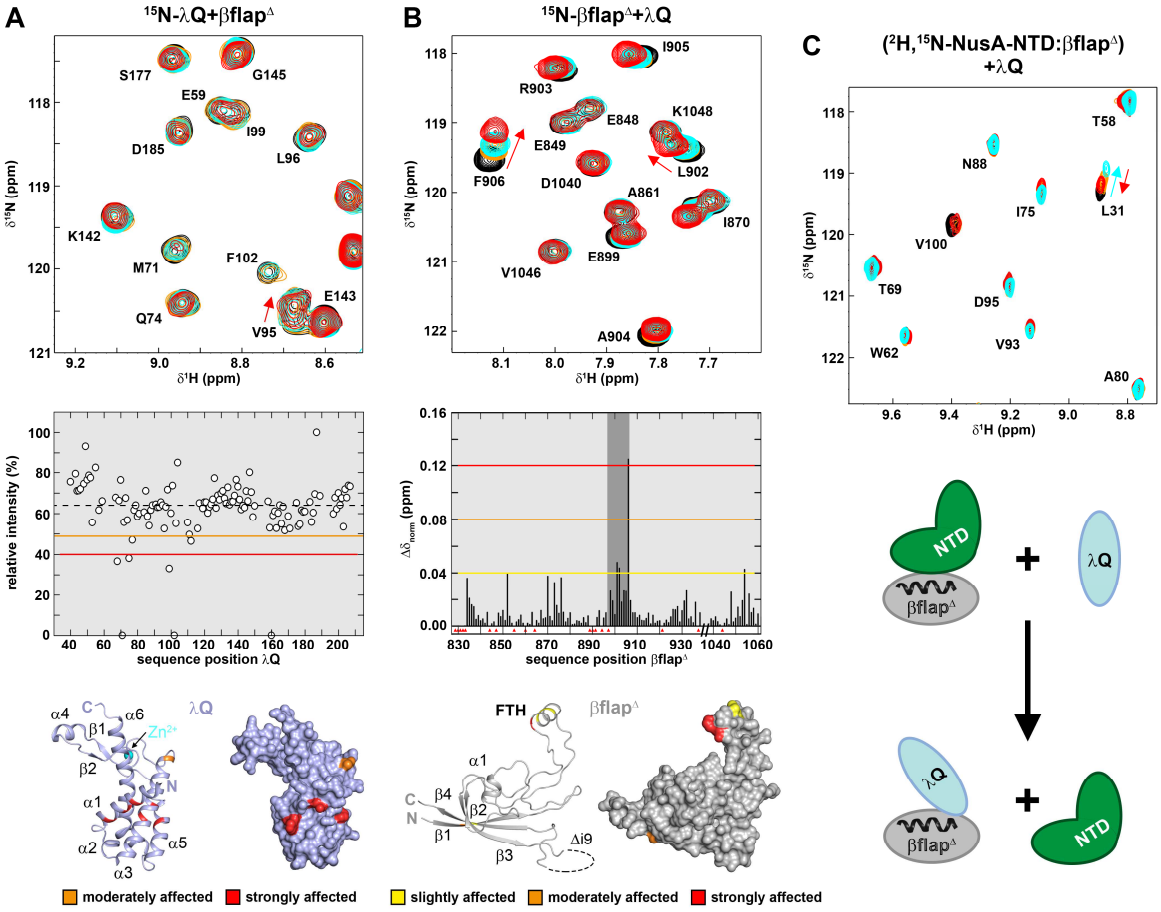

Figure 4: : λQ binds to FTH and disrupts the NusA-NTD:βflap$^{\Delta}$ interaction. (A) Titration of ^{15}N-λQ with βflap$^{\Delta}$. **(top)** Section of 2D [^{1}H,^{15}N]-BEST-TROSY spectra of the titration (concentration of ^{15}N-λQ : 175 µM). Molar ratios: 1:0, black; 1:0.5, orange; 1:1, cyan; 1:2 red. Selected signals are labelled. Arrows indicate chemical shift changes. **(middle)** Relative intensities of ^{15}N-λQ signals in the presence of 2 equivalents of βflap$^{\Delta}$. The dashed line marks the average relative signal intensity, orange and red lines indicate thresholds for moderately (1.25 σ of average relative signal intensity) and strongly (2.0 σ of average relative signal intensity) affected signals. **(bottom)** Mapping of affected residues from on the structure of λQ (PDB ID: 4MO1; light blue, left: ribbon representation; right: surface representation). The colour code is indicated. Termini and secondary structure elements are labelled. **(B)** Titration of ^{15}N-βflap$^{\Delta}$ with λQ. **(top)** Section of 2D [^{1}H,^{15}N]-HSQC spectra of the titration (concentration of ^{15}N-βflap$^{\Delta}$: 175 µM). Molar ratios: 1:0, black; 1:0.5, orange; 1:1, cyan; 1:2 red. Selected signals are labelled and chemical shift perturbations are indicated by arrows. **(middle)** Normalized chemical shift changes of ^{15}N-βflap$^{\Delta}$ in the presence of 2 equivalents λQ. Thresholds for slightly (0.04 ppm ≤ $\Delta\delta_{norm}$ < 0.08 ppm), moderately (0.08 ppm ≤ $\Delta\delta_{norm}$ < 0.12 ppm), and strongly ($\Delta\delta_{norm}$ ≥ 0.12 ppm) affected residues are indicated by yellow, orange, and red lines. Unassigned residues are indicated by red triangles. **(bottom)** Mapping of the affected residues from on the structure of βflap$^{\Delta}$ (PDB ID: 4KMU; grey) in ribbon (left) and surface (right) representation. The colour code is indicated. Termini and secondary structure elements are labelled. **(C)** λQ displaces NusA-NTD from βflap$^{\Delta}$. **(top)** Section of the 2D [^{1}H,^{15}N]-HSQC spectra of a competition experiment of ^{2}H,^{15}N-NusA-NTD with βflap$^{\Delta}$ and λQ (initial concentration of ^{2}H,^{15}N-NusA-NTD: 250 µM). Molar ratios: 1:0:0, black; 1:2:0, cyan; 1:2:2, orange; 1:2:4, red. Selected signals are labelled. Arrows indicate changes of ^{2}H,^{15}N-NusA-NTD chemical shifts upon addition of βflap (cyan) and λQ (red), respectively. **(bottom)** Scheme of the displacement experiment.

λQ and NusA-NTD compete for FTH binding

The binding mode of NusA to RNAP determines the effect NusA exerts on transcription. Binding of NusA-NTD to both FTH and αCTD leads to an enhancement of transcriptional pausing and intrinsic termination [29,30]. During λN-dependent AT, λN disrupts the αCTD:NusA-NTD interaction and forms a tripod shaped complex with NusA-NTD that binds to the FTH so that both NusA-NTD and λN establish contacts to the FTH, remodeling it [16]. AT the same time NusA-NTD is repositioned, allowing the TEC to read through pausing and termination signals [15,16,29].

In λQ-mediated AT λQ binds to the FTH and is able to interact with NusA-NTD with the ladder binding site overlapping with the αCTD:NusA-NTD interaction surface [27]. Thus, we asked how λQ affects the mode of NusA-NTD binding. First we tested if NusA-NTD, λQ and the FTH can form a ternary complex, maybe similar to the complex involved in λN-mediated AT, carrying out [^{1}H,^{15}N]-HSQC-based competition experiments. Addition of βflap$^{\Delta}$ to ^{2}H,^{15}N-NusA-NTD resulted in changes of the ^{2}H,^{15}N-NusA-NTD spectrum indicating complex formation (Fig. 4C and Supplementary Fig. S4A). Subsequent titration with λQ reversed these changes, implying that λQ displaces βflap$^{\Delta}$ from NusA-NTD and that no ternary NusA-NTD:λQ:FTH complex is formed. In a follow-up titration, we studied how the presence of λQ affects the ternary αCTD:NusA-NTD:βflap$^{\Delta}$ complex (Fig. 5A and Supplementary Fig. S4B). We added αCTD and βflap$^{\Delta}$ subsequently to ^{2}H,^{15}N-NusA-NTD (molar ratio 1:1:1) leading to changes in the ^{2}H,^{15}N-NusA-NTD spectrum confirming the formation of the ternary complex (see also Fig. 3). Strikingly, the addition of λQ partly reversed those changes caused by ^{2}H,^{15}N-NusA-NTD:βflap$^{\Delta}$ binding (e.g. L32 and V100), whereas chemical shift perturbations due to ^{2}H,^{15}N-NusA-NTD:αCTD binding were not affected. This finding indicates that λQ displaces βflap$^{\Delta}$ from NusA-NTD, in agreement with our previous experiment, whereas the αCTD:NusA-NTD interaction remains unaffected, indicating that the affinity of λQ for FTH is higher than for NusA-NTD. To corroborate our results in a more native environment we assessed how λQ affects the binding mode of NusA-NTD on complete RNAP using ILV-NusA-NTD (Fig. 5B). Addition of RNAP to ILV-NusA-NTD in a molar ration of 1:1 resulted in a non-uniform decrease of intensity of NusA-NTD methyl group signals due to complex formation as shown before (Fig. 3B). When this complex was titrated with λQ the intensity of some signals increased. To analyze the effect of λQ quantitatively, we calculated the difference of relative intensities of ILV-NusA-NTD signals in the ILV-NTD:RNAP: λQ complex (1:1:1) and in the ILV-NusA-NTD:RNAP complex (1:1) and mapped it against the amino acid sequence position of NusA-NTD. Next, we introduced thresholds at 0.5 σ and 1.0 σ of the mean relative intensity change to identify moderately and strongly affected residues, respectively.

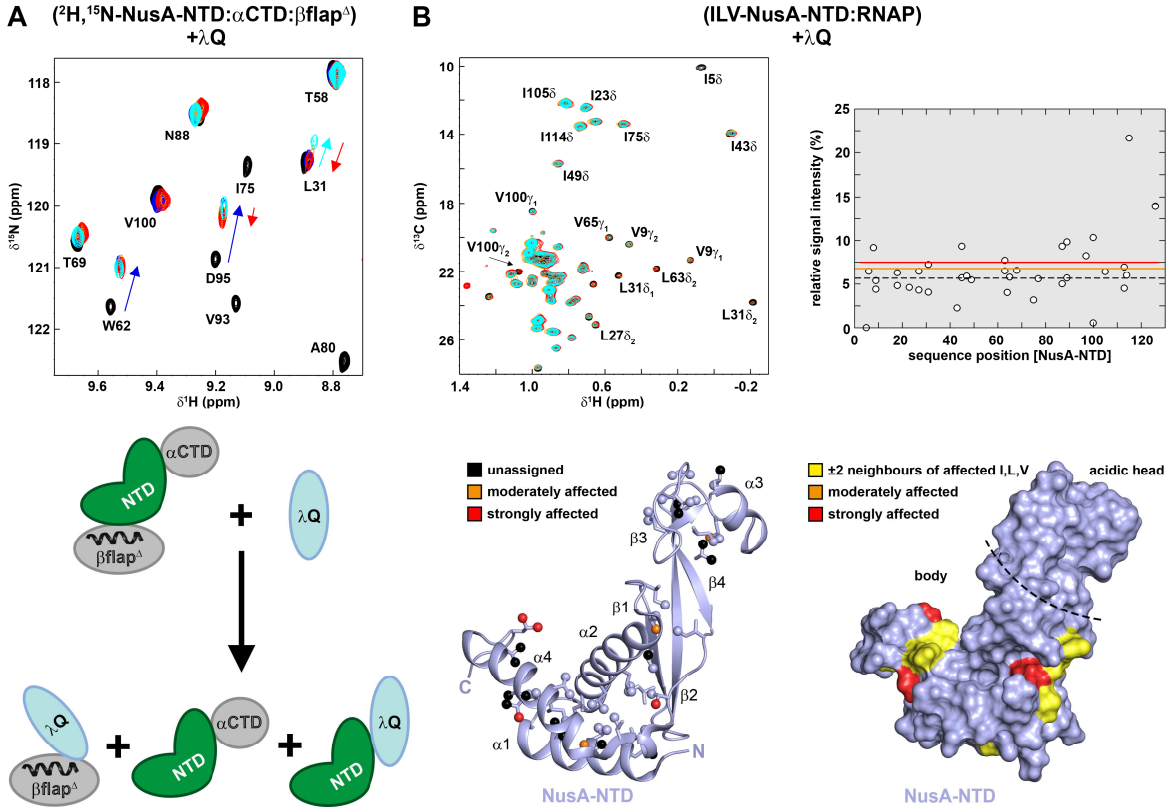

Figure 5: In the presence of λQ NusA-NTD interacts only with the αCTD. (A) λQ disrupts the NusA-NTD:βflap$^{\Delta}$ interaction in a NusA-NTD:βflap$^{\Delta}$:αCTD complex. **(top)** A section of the 2D [^{1}H,^{15}N]-HSQC spectra of a competition experiment where λQ is added to a preformed ^{2}H,^{15}N-NusA-NTD:βflap$^{\Delta}$:αCTD ternary complex (initial concentration of ^{2}H,^{15}N-NusA-NTD: 250 µM). Molar ratios: ^{2}H,^{15}N-NusA-NTD:αCTD:βflap$^{\Delta}$:λQ = 1:0:0:0, black; = 1:2:0:0, cyan; = 1:2:2:0, blue; = 1:2:2:1, orange; = 1:2:2:2, red. Selected signals are labelled. Arrows show the chemical shift changes of ^{2}H,^{15}N-NusA-NTD upon addition of αCTD (cyan), βflap (dark blue) and λQ (red). **(bottom)** Scheme of the competition experiment. **(B)** Titration of ILV-NusA-NTD with RNAP and λQ. **(top, left)** 2D [^{1}H,^{13}C]-methyl TROSY spectra of ILV-NusA-NTD in the absence (black, 75 µM) and presence (cyan, molar ratio 1:1, 40 µM ILV-NusA-NTD) of RNAP, and upon subsequent addition of λQ (orange, molar ratio 1:1:0.5, 37 µM ILV-NusA-NTD; red, molar ratio 1:1:1, 34 µM ILV-NusA-NTD). Selected signals are labelled. **(top, right)** Intensities of ILV-NusA-NTD methyl group signals in the presence of RNAP and λQ (molar ratio 1:1:1) relative to intensities of ILV-NusA-NTD methyl group signals in the ILV-NusA-NTD:RNAP complex (molar ratio 1:1) versus sequence position of NusA-NTD. The dashed line represents the average relative signal intensity, orange and red lines indicate thresholds for moderately (0.5 σ higher as average relative signal intensity increase) and strongly (1.0 σ higher as average relative signal intensity increase) affected signals upon λQ addition to the ILV-NusA-NTD:RNAP complex. **(bottom)** Mapping of the affected residues on the structure of NusA-NTD (PDB ID: 2KWP; light blue). (left) ribbon representation of NusA-NTD. Ile, Val, and Leu residues are shown as sticks with carbon atoms of terminal methyl groups as spheres. The colour code is indicated. Termini and secondary structure elements are labelled. (right) NusA-NTD in surface representation. The colour code is indicated; the complete amino acid is coloured for graphical illustration of the interaction site. The acidic head of NusA-NTD is separated by a dashed line from the body region.

Mapping of these residues on the NusA-NTD-structure reveals that mainly helices α1 and α4 as well as adjacent loops are affected. Due to the low number of NMR active probes affected

regions were graphically extended by highlighting directly neighbouring residues. The resulting binding surfaces clearly shows that the presence of λQ affects only the body of NusA-NTD and thus the FTH binding site (see also Fig. 3B,C). From these results we conclude that λQ disrupts NusA-NTD:FTH binding, while the interaction of NusA-NTD:αCTD interaction is maintained.

λQ is able to displace σ^{70} from RNAP

Two factors have been suggested to be required to release σ^{70} from RNAP at the σ^{70}-dependent pause in phage λ's late promoter p_R': (i) λQ-mediated destabilization of the σ^{70}:RNAP interaction, similar to Q[21,22,23] and (ii) DNA scrunching [21], with the ladder being the driving force. As σ^{70}_{R4} [8], NusA-NTD [29,30,42,54], and λQ [55] (Fig. 4B) share the FTH as binding site we asked if NusA-NTD and/or λQ could stimulate release of σ^{70} from the FTH by performing [^{1}H,^{15}N]-HSQC-based competition experiments using βflap$^{\Delta}$.

Addition of one equivalent σ^{70} to ^{15}N-βflap$^{\Delta}$ led to a significant intensity decrease of ^{15}N-βflap$^{\Delta}$ signals (Fig. 6A and Supplementary Fig. S5A). σ^{70} has a molecular mass of ~70 kDa and thus a high transverse relaxation rate, which strongly affects the relaxation behavior of ^{15}N-βflap upon complex formation, resulting in severe line broadening of ^{15}N-βflap signals. Hence, the intensity decrease of ^{15}N-βflap$^{\Delta}$ signals in the presence of σ^{70} implies binding. Subsequent addition of a twofold molar excess of λQ recovered most ^{15}N-βflap$^{\Delta}$ signals completely. Additionally, the final spectrum shows chemical shift changes of some signals as compared to the spectrum of free ^{15}N-βflap$^{\Delta}$, which can be attributed to λQ:FTH binding (e.g. R903, I905, F906; see also Fig. 2B). These findings suggest that λQ displaces σ^{70} from the FTH. Notably, reporter assays suggest that σ^{70}_{R4} directly interacts with λQ [59]. Titration of ^{15}N-λQ with σ^{70} confirms this hypothesis as ^{15}N-λQ signal intensity is dramatically diminished in the presence of σ^{70} due to an increase in molecular mass upon complex formation (Supplementary Fig. S5B). As, however, in the competition experiment the intensity of ^{15}N-βflap$^{\Delta}$ signals in the initial and final spectrum is nearly identical, we exclude the formation of a ternary FTH:λQ:σ^{70} complex. In contrast to λQ, NusA-NTD neither releases σ^{70} from the FTH (Supplementary Fig. S5C) nor binds to σ^{70} (Supplementary Fig. S5D).

As σ^{70} interacts with RNAP not only via σ^{70}_{R4}, but also via four other discrete sets of contacts [60-63], we repeated the competition experiment using complete RNAP, recording 1D [^{1}H,^{15}N]-HSQC spectra. Addition of RNAP (~400 kDa) to ^{15}N-σ^{70} decreased the intensity of ^{15}N-σ^{70} signals significantly, suggesting formation of the holoenzyme (Fig. 6B). Subsequently, we added λQ and ~75 % of ^{15}N-σ^{70} signal intensity could be recovered, implying (partial) release of σ^{70}, in agreement with our previous finding that disrupts the σ^{70}_{R4}:FTH interaction. Although we cannot

determine if σ^{70} is completely released or still remains attached to RNAP by some of its other interactions, λQ obviously weakens the holo RNAP complex and may thus escape from the σ^{70}-dependent pause. In contrast to λQ, NusA-NTD influences the stability of holo RNAP only marginally, even in high molar excess (Supplementary Fig. S5E).

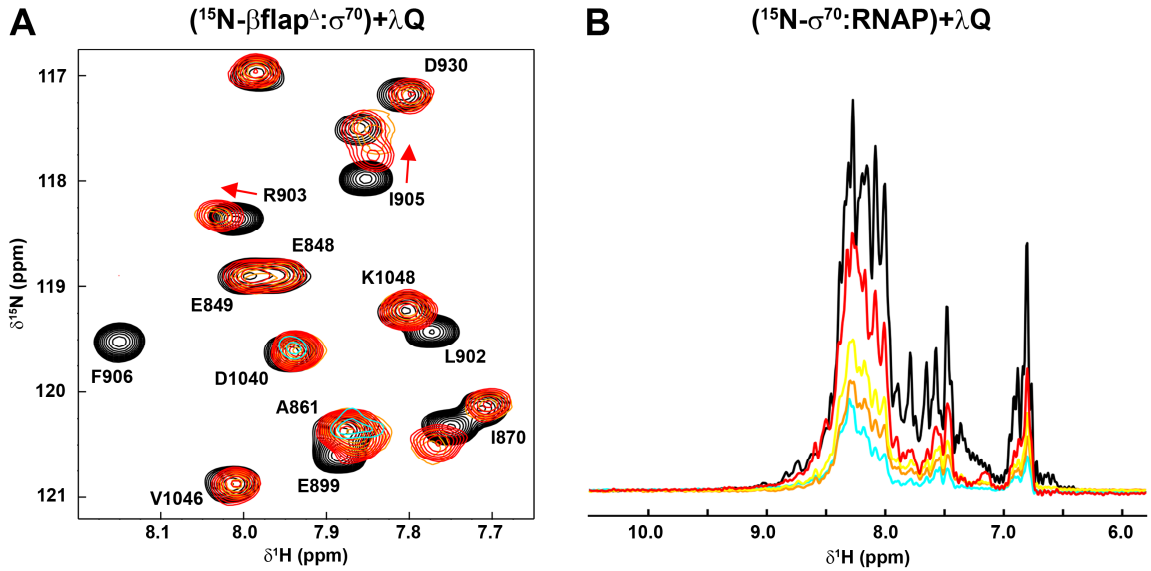

Figure 6: λQ destabilizes σ^{70}:RNAP interactions. **(A)** λQ displaces σ^{70} from $\beta flap^{\Delta}$. Section of 2D [^{1}H,^{15}N]-HSQC spectra of ^{15}N-$\beta flap^{\Delta}$ in the absence and presence of σ^{70} and upon subsequent titration with λQ (initial concentration of ^{15}N-$\beta flap^{\Delta}$: 200 µM). Molar ratios of ^{15}N-$\beta flap^{\Delta}$:σ^{70}:λQ = 1:0:0, black; = 1:1:0, cyan; = 1:1:1, orange; = 1:1:2 red. Selected signals are labelled. Arrows indicate differences of chemical shifts of ^{15}N-$\beta flap^{\Delta}$ in its free form and in the presence of σ^{70} and λQ (1:1:1). **(B)** Titration of a ^{15}N-σ^{70}:RNAP complex with λQ. 1D [^{1}H,^{15}N]-HSQC spectra of ^{15}N-σ^{70} in the absence (black, 40 µM ^{15}N-σ^{70}) and presence of RNAP (cyan, molar ratio 1:1, 40 µM ^{15}N-σ^{70}) and upon subsequent titration with λQ (molar ratio = 1:1:1, orange; = 1:1:2, yellow; = 1:1:5, red).

DISCUSSION

Transcription is a highly regulated process with numerous transcription factors directly contacting RNAP, with Nus factors being a conserved class of transcription factors involved in the regulation of housekeeping genes in bacteria (reviewed in [64]). A central regulatory element of RNAP is the FTH, an α-helix that forms the lid of the RNA exit channel, regulating its width. During transcription initiation σ^{70} makes extensive contacts with the RNAP, one being for example the σ^{70}_{R4}:FTH interaction, rendering the holoenzyme capable of specific promoter recognition [7,8]. Simultaneous binding of NusA-NTD to the FTH and the αCTD during transcription elongation enhances TEC pausing and termination efficiency [29,30]. In λN-dependent AT protein λN forms a complex with NusA-NTD, which repositions NusA-NTD and interacts with the FTH, transforming the TEC into a TAC that suppresses termination signals [15,16].

The second AT mechanism in phage λ, λQ-dependent AT, is only poorly understood. Nowadays, more than 15,000 Q proteins are known which can be classified into three families: λQ family, Q21 family, and Q82 family. Cryo EM studies of Q21-mediated AT showed that two Q21 molecules bind to RNAP resulting in a Q21-TAC, where one Q21 protein binds to the FTH while the other forms a torus at the RNA exit channel through which the RNA is threated, preventing pause / termination hairpin formation [22,23]. Strikingly, Q proteins do not show any significant similarity in their amino acid sequence composition or their three-dimensional structure, although they are all encoded by genes at equivalent positions in the genome and fulfill the same function. For example, as compared to Q21 λQ possesses a 67 amino acid long N-terminus that is unstructured and has an unknown function [27]. Thus, the molecular basis of how Q proteins accomplish their regulatory role might be significantly different.

Bacterial two-hybrid approaches suggest that λQ also interacts with the FTH [55]. Moreover, λQ establishes contacts with σ^{70} [59,65] and NusA-NTD [27], with the ladder interaction being relevant as, although λQ is able to perform its AT function on its own, NusA can enhance λQ-dependent AT substantially [17]. Thus, we assessed the molecular basis of the λQ:FTH interaction and if λQ-dependent AT also involves repositioning of NusA-NTD, reminiscent of λN-mediated AT.

As the FTH is a highly mobile element we decided to study its interactions via solution state NMR spectroscopy. Hence, we first generated a construct of the RNAP βflap region, $\beta flap^{\Delta}$ (Fig. 1A), suitable for NMR studies. The solution structure of $\beta flap^{\Delta}$ shows that the FTH is a well-defined α-helix, even in the absence of binding partners, in agreement with a previous study for *B. subtilis* βflap [54]. This implies that the lack of electron density for the FTH in most RNAP/transcription complex structures without an FTH binding partner is due to its high mobility and not due to the FTH being disordered as postulated [56]. The relaxation behavior

further demonstrates that not only the FTH is flexible as seen for *B. subtilis* βflap region [54], but also the flanking unstructured arm regions (Fig. 1C,D), explaining how the FTH is able to undergo large conformational rearrangements, as observed, for example, in Q21-dependent AT, where the arms can translocate the FTH up to 42 Å [22,23].

To ensure that our βflap$^{\Delta}$ construct is functional we probed its ability to interact with a known binding partner, NusA-NTD. Our experiments reveal that the NusA-NTD:βflap$^{\Delta}$ interface is located on the body of NusA-NTD and on the FTH of βflap (Fig. 2), in agreement with previous findings [15,16,29,42]. Earlier studies have shown that the NusA-NTD body, consisting of helices α1, α2, and α4, rearranges to form a hydrophobic pocket, which is able to recognize and accommodate the hydrophobic side of the FTH [29,54]. In *B. subtilis* I56 has been postulated to mediate this conformational rearrangement [54]. Interestingly, the corresponding residue in *E. coli* NusA-NTD, F56, which is located in strand β2 and thus in the interior of the protein, is also affected by βflap$^{\Delta}$ binding, suggesting that the rearrangement in *E. coli* NusA-NTD may be mediated by this residue. Overall, these findings demonstrate that βflap$^{\Delta}$ is an ideal model construct to study the functions of the FTH.

NusA-NTD not only binds to the FTH, but can simultaneously contact the αCTD during transcriptional pausing as observed in cryo EM structure [29]. In order to study the effects of λQ on NusA-NTD, we confirmed that the αCTD binding site is located at the acidic head of NusA-NTD and does not overlap with the FTH binding site. We show that concurrent binding can easily be followed be NMR spectroscopy in the context of both βflap$^{\Delta}$ and core RNAP (Fig. 3). As we used isolated RNAP, we suggest that this binding mode does not only occur during pausing but may be the "normal" binding mode of NusA-NTD during elongation and may be relevant for other regulatory functions such as transcription:translation coupling. Interestingly, the affinity of NusA-NTD is nearly one order of magnitude higher for the αCTD (25 μM) than for the FTH (180 μM). Hence, we hypothesize that the NusA-NTD:FTH interaction might be (temporarily) lost to allow NusA-NTD rearrangement/repositioning, while the NusA-NTD:αCTD interaction stays intact ensuring fast rebinding of the NusA-NTD to the FTH.

Having established βflap$^{\Delta}$ as test construct and assessed the binding mode of NusA-NTD we studied the molecular basis of λQ binding to the FTH. We demonstrate that the FTH contacts a small hydrophobic cluster at the concave side of λQ involving residues in helices α1, α3, and α5 (Fig. 4), in agreement with the results of a bacterial two-hybrid approach [55]. The long N-terminus of λQ is unstructured and not involved in FTH binding and there is no indication for

oligomerization or structural rearrangements of λQ upon FTH binding. However, λQ establishes further interactions, e.g. with the QBE [20] and σ^{70}_{R4} [65], which might alter λQ's conformation.

The FTH contacts λQ via hydrophobic residues located on one side of the helix (L901, L902, F906). These residues are also involved in binding to Q21 [22,23], NusA-NTD [29], and σ^{70}_{R4} [8], suggesting that in all cases the recognition relies primarily on hydrophobic interactions whereas F906 might ensure specificity. Overall, the binding mode of λQ and Q21 to the FTH is similar, but we cannot conclude if the mode of action of λQ is similar to that of Q21, which forms a torus for the RNA to suppress termination [22,23].

As λQ binds to NusA-NTD [27] we used a series of NMR-based competition experiments to elucidate if this interaction also induced a repositioning of NusA-NTD, reminiscent of λN-dependent AT where λN forms a complex with NusA-NTD that binds to the FTH while the NusA-NTD:αCTD interaction is disrupted and NusA-NTD is repositioned [15,16]. We show that λQ displaces NusA-NTD from the FTH, both with $\beta flap^{\Delta}$ and complete RNAP, and no NusA-NTD:λQ:FTH complex is formed. Moreover, in stark contrast to λN-dependent AT, the NusA-NTD:αCTD interaction stays intact so that NusA-NTD remains bound to the RNAP even if it looses contact to the FTH. We hypothesize that the NusA-NTD:αCTD interaction may serve as pivot point to allow NusA to adopt a termination resistant conformation.

Although the NusA-NTD binding sites for αCTD and λQ overlap and are mutual exclusive [27], the presence of λQ does not disrupt the NusA-NTD:αCTD interaction under the chosen experimental conditions. However, at high concentration λQ can disturb the NusA-NTD:αCTD complex as well as the NusA-AR2:αCTD interaction [27], which might result in the release of NusA, eliminating the enhancing effect of NusA on λQ-dependent AT. This finding is in agreement with a report on Q82 AT where high concentrations of Q82 inhibit the stimulating effect of NusA upon terminator read-through [66].

During recruitment of λQ, holo RNAP pauses at a σ^{70}-dependent pause site and scrunches downstream DNA. Now λQ engages with this complex by establishing interactions with the QBE and the FTH, forming a stable complex that alters the elongation properties of RNAP [17-19,21]. Transcription resumes, but σ^{70} remains bound to the σ^{70}-dependent pause site, resulting in extended scrunching [21]. DNA scrunching together with the λQ-mediated destabilization of the σ^{70}:RNAP interaction have been suggested to be the driving forces for pause escape [21–23].

Competition experiments showed that λQ can indeed displace σ^{70} from the FTH (Fig. 6A) and that the σ^{70}:RNAP complex is destabilized significantly by λQ (Fig. 6B), although σ^{70} makes extensive contacts to RNAP via at least five distinct sets of interactions [7,8]. Additionally, λQ

contacts σ^{70}_{R4} and stabilizes the transcription complex in a non-standard conformation (Fig. S5B) [65]. Overall, our results support the hypothesis that destabilization of σ^{70}:RNAP interaction by λQ is a key element to overcome the σ^{70}-dependent pause. NusA-NTD, in contrast, is able to neither displace σ^{70} from the FTH (Supplementary Fig. S5C) nor destabilize the σ^{70}:RNAP complex (Supplementary Fig. S5E), suggesting that it does not actively support σ^{70} dissociation. This is in agreement with the finding that NusA engages with the transcription complex after dissociation of σ^{70} [67].

Our results also suggest that λQ causes a rearrangement of the position of NusA-NTD, forcing NusA to adapt a new conformation, which, in turn, may alter the effect NusA exerts on transcription. Thus, repositioning of NusA-NTD seems to be a general scheme to fine-tune transcription regulation by NusA, especially in the context of pausing and AT.

REFERENCES

1. Werner, F. & Grohmann, D. Evolution of multisubunit RNA polymerases in the three domains of life. *Nat Rev Microbiol* **9**, 85–98 (2011).
2. Murakami, K. S. Structural biology of bacterial RNA polymerase. *Biomolecules* **5**, 848–864 (2015).
3. Ishihama, A. Functional modulation of *Escherichia coli* RNA polymerase. *Annu. Rev. Microbiol.* **54**, 499–518 (2000).
4. Lonetto, M., Gribskov, M. & Gross, C. A. The sigma 70 family: sequence conservation and evolutionary relationships. *Journal of Bacteriology* **174**, 3843–3849 (1992).
5. Paget, M. S. B. & Helmann, J. D. The sigma70 family of sigma factors. *Genome Biol.* **4**, 203 (2003).
6. Murakami, K. S. X-ray Crystal Structure of *Escherichia coli* RNA Polymerase σ^{70} Holoenzyme. *J. Biol. Chem.* **288**, 9126–9134 (2013).
7. Kuznedelov, K. *et al.* A role for interaction of the RNA polymerase flap domain with the sigma subunit in promoter recognition. *Science* **295**, 855–857 (2002).
8. Geszvain, K., Gruber, T. M., Mooney, R. A., Gross, C. A. & Landick, R. A hydrophobic patch on the flap-tip helix of *E.coli* RNA polymerase mediates sigma(70) region 4 function. *J. Mol. Biol.* **343**, 569–587 (2004).
9. Hawley, D. K. & McClure, W. R. Compilation and analysis of *Escherichia coli* promoter DNA sequences. *Nucl Acids Res* **11**, 2237–2255 (1983).
10. Mooney, R. A., Darst, S. A. & Landick, R. Sigma and RNA polymerase: an on-again, off-again relationship? *Mol. Cell* **20**, 335–345 (2005).
11. Ray-Soni, A., Bellecourt, M. J. & Landick, R. Mechanisms of Bacterial Transcription Termination: All Good Things Must End. *Annu. Rev. Biochem.* **85**, 319–347 (2016).
12. Roberts, J. W. Termination factor for RNA synthesis. *Nature* **224**, 1168–1174 (1969).
13. Nudler, E. & Gottesman, M. E. Transcription termination and anti-termination in *E. coli*. *Genes to Cells* **7**, 755–768 (2002).
14. Roberts, J. W. *et al.* Antitermination by bacteriophage lambda Q protein. *Cold Spring Harb. Symp. Quant. Biol.* **63**, 319–325 (1998).
15. Said, N. *et al.* Structural basis for λN-dependent processive transcription antitermination. *Nat Microbiol* **2**, 17062 (2017).

16. Krupp, F. *et al.* Structural Basis for the Action of an All-Purpose Transcription Anti-termination Factor. *Molecular Cell* **74**, 143-157.e5 (2019).

17. Grayhack, E. J., Yang, X. J., Lau, L. F. & Roberts, J. W. Phage lambda gene Q antiterminator recognizes RNA polymerase near the promoter and accelerates it through a pause site. *Cell* **42**, 259–269 (1985).

18. Ring, B. Z., Yarnell, W. S. & Roberts, J. W. Function of *E. coli* RNA polymerase sigma factor sigma 70 in promoter-proximal pausing. *Cell* **86**, 485–493 (1996).

19. Marr, M. T., Datwyler, S. A., Meares, C. F. & Roberts, J. W. Restructuring of an RNA polymerase holoenzyme elongation complex by lambdoid phage Q proteins. *Proc. Natl. Acad. Sci. U.S.A.* **98**, 8972–8978 (2001).

20. Yarnell, W. S. & Roberts, J. W. The phage lambda gene Q transcription antiterminator binds DNA in the late gene promoter as it modifies RNA polymerase. *Cell* **69**, 1181–1189 (1992).

21. Strobel, E. J. & Roberts, J. W. Regulation of promoter-proximal transcription elongation: enhanced DNA scrunching drives λQ antiterminator-dependent escape from a σ70-dependent pause. *Nucleic Acids Res.* **42**, 5097–5108 (2014).

22. Shi, J. *et al.* Structural basis of Q-dependent transcription antitermination. *Nat Commun* **10**, 2925 (2019).

23. Yin, Z., Kaelber, J. T. & Ebright, R. H. Structural basis of Q-dependent antitermination. *Proc. Natl. Acad. Sci. U.S.A.* **116**, 18384–18390 (2019).

24. Perdue, S. A. & Roberts, J. W. A backtrack-inducing sequence is an essential component of *Escherichia coli* σ(70)-dependent promoter-proximal pausing. *Mol. Microbiol.* **78**, 636–650 (2010).

25. Deighan, P. & Hochschild, A. The bacteriophage lambdaQ anti-terminator protein regulates late gene expression as a stable component of the transcription elongation complex. *Mol. Microbiol.* **63**, 911–920 (2007).

26. Yang, X. J., Goliger, J. A. & Roberts, J. W. Specificity and mechanism of antitermination by Q proteins of bacteriophages lambda and 82. *J. Mol. Biol.* **210**, 453–460 (1989).

27. Dudenhoeffer, B. R., Borggraefe, J., Schweimer, K. & Knauer, S. H. NusA directly interacts with antitermination factor Q from phage λ. *Scientific Reports* **10**, 6607 (2020).

28. Pan, T., Artsimovitch, I., Fang, X. W., Landick, R. & Sosnick, T. R. Folding of a large ribozyme during transcription and the effect of the elongation factor NusA. *Proc. Natl. Acad. Sci. U.S.A.* **96**, 9545–9550 (1999).

29. Guo, X. *et al.* Structural Basis for NusA Stabilized Transcriptional Pausing. *Mol. Cell* **69**, 816-827.e4 (2018).

30. Ha, K. S., Toulokhonov, I., Vassylyev, D. G. & Landick, R. The NusA N-terminal domain is necessary and sufficient for enhancement of transcriptional pausing via interaction with the RNA exit channel of RNA polymerase. *J. Mol. Biol.* **401**, 708–725 (2010).

31. Linn, T. & Greenblatt, J. The NusA and NusG proteins of *Escherichia coli* increase the *in vitro* readthrough frequency of a transcriptional attenuator preceding the gene for the beta subunit of RNA polymerase. *J. Biol. Chem.* **267**, 1449–1454 (1992).

32. Burns, C. M., Richardson, L. V. & Richardson, J. P. Combinatorial effects of NusA and NusG on transcription elongation and Rho-dependent termination in *Escherichia coli*. *J. Mol. Biol.* **278**, 307–316 (1998).

33. Cardinale, C. J. *et al.* Termination factor Rho and its cofactors NusA and NusG silence foreign DNA in *E. coli*. *Science* **320**, 935–938 (2008).

34. Prasch, S. *et al.* Interaction of the intrinsically unstructured phage lambda N Protein with *Escherichia coli* NusA. *Biochemistry* **45**, 4542–4549 (2006).

35. Prasch, S. *et al.* RNA-binding specificity of *E. coli* NusA. *Nucleic Acids Res.* **37**, 4736–4742 (2009).

36. Schweimer, K. *et al.* NusA interaction with the α subunit of *E. coli* RNA polymerase is via the UP element site and releases autoinhibition. *Structure* **19**, 945–954 (2011).

37. Worbs, M., Bourenkov, G. P., Bartunik, H. D., Huber, R. & Wahl, M. C. An extended RNA binding surface through arrayed S1 and KH domains in transcription factor NusA. *Mol. Cell* **7**, 1177–1189 (2001).

38. Mah, T. F., Kuznedelov, K., Mushegian, A., Severinov, K. & Greenblatt, J. The alpha subunit of *E. coli* RNA polymerase activates RNA binding by NusA. *Genes Dev.* **14**, 2664–2675 (2000).

39. Strauß, M. *et al.* Transcription is regulated by NusA:NusG interaction. *Nucleic Acids Res.* **44**, 5971–5982 (2016).

40. Dudenhoeffer, B. R., Schneider, H., Schweimer, K. & Knauer, S. H. SuhB is an integral part of the ribosomal antitermination complex and interacts with NusA. *Nucleic Acids Res.* **47**, 6504–6518 (2019).

41. Huang, Y.-H., Said, N., Loll, B. & Wahl, M. C. Structural basis for the function of SuhB as a transcription factor in ribosomal RNA synthesis. *Nucleic Acids Res.* **47**, 6488–6503 (2019).

42. Drögemüller, J. *et al.* Determination of RNA polymerase binding surfaces of transcription factors by NMR spectroscopy. *Sci Rep* **5**, 16428 (2015).

43. Eisenmann, A., Schwarz, S., Prasch, S., Schweimer, K. & Rösch, P. The *E. coli* NusA carboxy-terminal domains are structurally similar and show specific RNAP- and λN interaction. *Protein Sci* **14**, 2018–2029 (2005).

44. Zuber, P. K. *et al.* The universally-conserved transcription factor RfaH is recruited to a hairpin structure of the non-template DNA strand. *Elife* **7**, (2018).

45. Zhi, H. & Jin, D. J. Purification of highly-active and soluble *Escherichia coli* sigma 70 polypeptide overproduced at low temperature. *Meth. Enzymol.* **370**, 174–180 (2003).

46. Meyer, O. & Schlegel, H. G. Biology of aerobic carbon monoxide-oxidizing bacteria. *Annu. Rev. Microbiol.* **37**, 277–310 (1983).

47. Sambrook, J. & Russel, D. W. *Molecular Cloning: A Laboratory Manual*. vol. 3 (Cold Spring Harbor Press, 2001).

48. Sprangers, R. & Kay, L. E. Quantitative dynamics and binding studies of the 20S proteasome by NMR. *Nature* **445**, 618–622 (2007).

49. Sattler, M., Schleucher, J. & Griesinger, C. Heteronuclear multidimensional NMR experiments for the structure determination of proteins in solution employing pulsed field gradients. *Prog. Nucl. Magn. Reson. Spectrosc.* **34**, 93–158 (1999).

50. Cavanagh, J., Fairbrother, W. J., Palmer, A. G., Rance, M. & Skelton, N. J. *Protein NMR Spectroscopy Principles and Practice*. (Elsevier Academic Press, 2007).

51. Zuber, P. K., Schweimer, K., Rösch, P., Artsimovitch, I. & Knauer, S. H. Reversible fold-switching controls the functional cycle of the antitermination factor RfaH. *Nat Commun* **10**, 702 (2019).

52. Toulokhonov, I. & Landick, R. The flap domain is required for pause RNA hairpin inhibition of catalysis by RNA polymerase and can modulate intrinsic termination. *Mol. Cell* **12**, 1125–1136 (2003).

53. Toulokhonov, I., Artsimovitch, I. & Landick, R. Allosteric control of RNA polymerase by a site that contacts nascent RNA hairpins. *Science* **292**, 730–733 (2001).

54. Ma, C. *et al.* RNA polymerase-induced remodelling of NusA produces a pause enhancement complex. *Nucleic Acids Res.* **43**, 2829–2840 (2015).

55. Deighan, P., Diez, C. M., Leibman, M., Hochschild, A. & Nickels, B. E. The bacteriophage lambda Q antiterminator protein contacts the beta-flap domain of RNA polymerase. *Proc. Natl. Acad. Sci. U.S.A.* **105**, 15305–15310 (2008).

56. Kang, J. Y. *et al.* Structural basis of transcription arrest by coliphage HK022 Nun in an *Escherichia coli* RNA polymerase elongation complex. *Elife* **6**, (2017).

57. Kang, J. Y. *et al.* Structural Basis for Transcript Elongation Control by NusG Family Universal Regulators. *Cell* **173**, 1650-1662.e14 (2018).

58. Abdelkareem, M. *et al.* Structural Basis of Transcription: RNA Polymerase Backtracking and Its Reactivation. *Molecular Cell* **75**, 298-309.e4 (2019).

59. Vorobiev, S. M. *et al.* Structure of the DNA-binding and RNA-polymerase-binding region of transcription antitermination factor λQ. *Structure* **22**, 488–495 (2014).

60. Mekler, V. *et al.* Structural organization of bacterial RNA polymerase holoenzyme and the RNA polymerase-promoter open complex. *Cell* **108**, 599–614 (2002).

61. Murakami, K. S. Structural Basis of Transcription Initiation: RNA Polymerase Holoenzyme at 4 A Resolution. *Science* **296**, 1280–1284 (2002).

62. Vassylyev, D. G. *et al.* Crystal structure of a bacterial RNA polymerase holoenzyme at 2.6 A resolution. *Nature* **417**, 712–719 (2002).

63. Murakami, K. S. & Darst, S. A. Bacterial RNA polymerases: the wholo story. *Curr. Opin. Struct. Biol.* **13**, 31–39 (2003).

64. Belogurov, G. A. & Artsimovitch, I. Regulation of Transcript Elongation. *Annu. Rev. Microbiol.* **69**, 49–69 (2015).

65. Nickels, B. E., Roberts, C. W., Sun, H., Roberts, J. W. & Hochschild, A. The sigma(70) subunit of RNA polymerase is contacted by the (lambda)Q antiterminator during early elongation. *Mol. Cell* **10**, 611–622 (2002).

66. Wells, C. D., Deighan, P., Brigham, M. & Hochschild, A. Nascent RNA length dictates opposing effects of NusA on antitermination. *Nucleic Acids Res.* **44**, 5378–5389 (2016).

67. Mooney, R. A. *et al.* Regulator trafficking on bacterial transcription units *in vivo*. *Mol. Cell* **33**, 97–108 (2009).

DATA AVAILABILITY

The backbone resonance assignment for βflap construct has been deposited in the Biological Magnetic Resonance Bank Databank, accession number XXXX. For αCTD, NusA-NTD and λQ resonance assignments were taken from previous studies as indicated in the manuscript.

AUTHOR CONTRIBUTIONS

SHK supervised the project. The experiments were designed by SHK, KS, and BRD. JB and K.S. made the assignment of $\beta flap^{\Delta}$ (the corresponding NMR experiments were carried out by KS). All interactions studies and competition experiments were performed by BRD and MW. Data was analyzed and evaluated by BRD and SHK. SHK and BRD wrote the manuscript with input from all authors.

Conflict of interest statement. None declared.

ACKNOWLEDGEMENT

We thank Ramona Heissmann, Ulrike Persau, and Andrea Hager for excellent technical assistance and the Northern Bavarian NMR Centre (NBNC) for access to the NMR spectrometers. Furthermore, we thank Irina Artsimovitch for the plasmid encoding $RNAP^{\Delta\alpha CTD}$. This work was supported by the German Research Foundation (Ro617/21-1 to Paul Rösch).

Supplementary Information

Antitermination factor λQ mediates NusA-NTD rearrangement on RNAP βflap

Benjamin R. Dudenhoeffer, Marlon Wörner, Jan Bodenschlägel, Kristian Schweimer, Stefan H. Knauer*

Biopolymers, University of Bayreuth, Universitätsstraße 30, 95447 Bayreuth, Germany

*Correspondence to: stefan.knauer@uni-bayreuth.de

Contents

Supplementary Figure S1

Supplementary Figure S2

Supplementary Figure S3

Supplementary Figure S4

Supplementary Figure S5

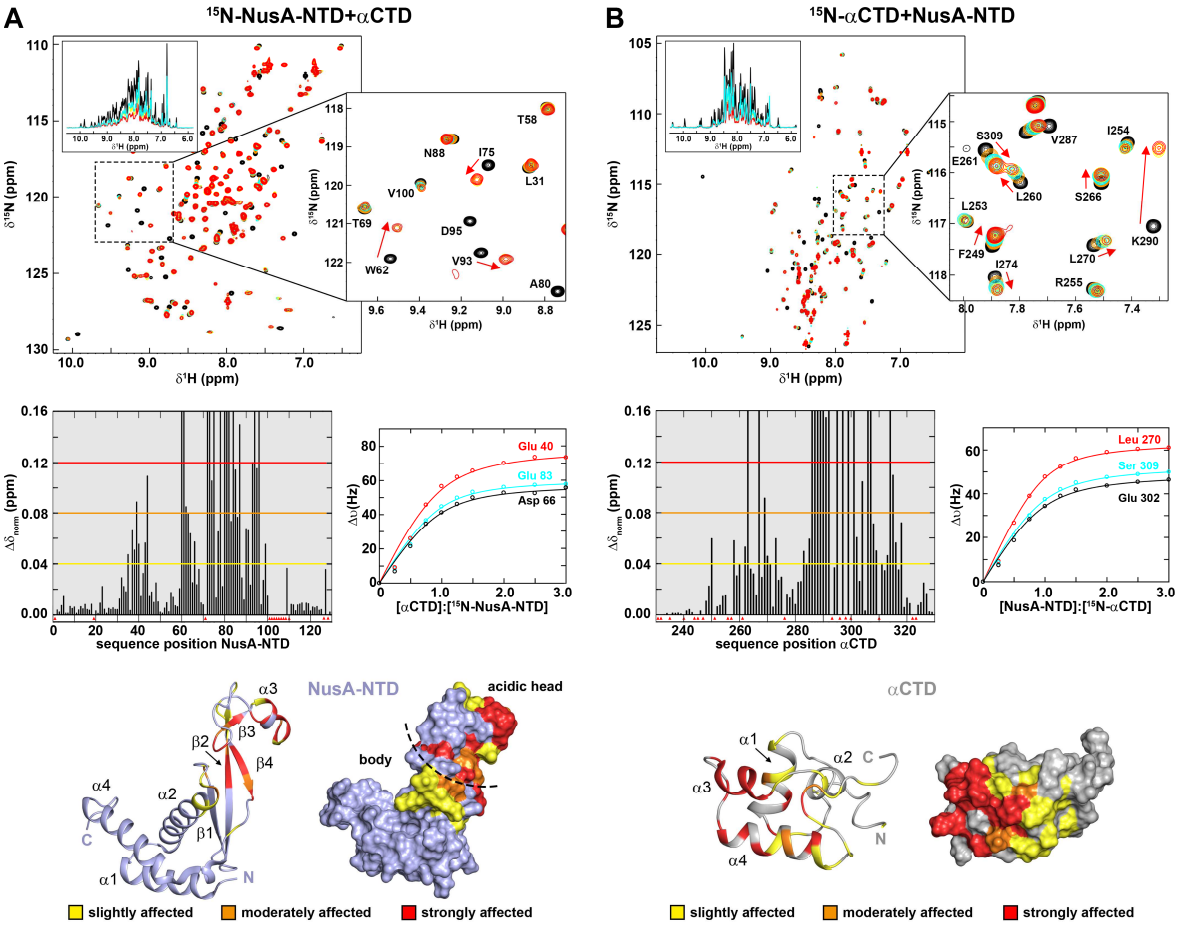

Supplementary Figure 1: Interaction of NusA-NTD with αCTD. (A) Titration of ^{15}N-NusA-NTD with αCTD. **(top)** 2D [^{1}H,^{15}N]-HSQC spectra. Molar ratios: 1:0, black; 1:0.5, orange; 1:1, cyan; 1:2, yellow; 1:3, red (concentration of ^{15}N-NusA-NTD: 200 µM; concentration of αCTD stock: 1 mM). The right panel shows a magnification of the boxed region. Selected signals are labelled. Arrows indicate changes of chemical shifts. The inset shows the 1D [^{1}H,^{15}N]-HSQC spectra of certain titration steps. **(middle, left)** Normalized chemical shift changes of ^{15}N-NusA-NTD versus sequence position. Thresholds for slightly (0.04 ppm ≤ $\Delta\delta_{norm}$ < 0.08 ppm), moderately (0.08 ppm ≤ $\Delta\delta_{norm}$ < 0.12 ppm), and strongly ($\Delta\delta_{norm}$ ≥ 0.12 ppm) affected residues are indicated by a yellow, orange, and red line. Unassigned residues are marked as red triangles. **(middle, right)** Titration curves of selected ^{15}N-NusA-NTD signals. The individual curves represent the best fit to a two-component, 1:1 binding equation, yielding an average K_D value of 27 ± 9 µM. **(bottom)** Mapping of affected residues on the structure of NusA-NTD (PDB ID: 2KWP; light blue) in ribbon (left) and surface (right) representation. The colour code is indicated. Termini and secondary structure elements are labelled, the body and acidic head region are indicated. **(B)** Titration of ^{15}N-αCTD with NusA-NTD **(top)** 2D [^{1}H,^{15}N]-HSQC spectra. Molar ratios: 1:0, black; 1:0.5, orange; 1:1, cyan; 1:2, yellow; 1:3, red (concentration of ^{15}N-αCTD: 200 µM; concentration of NusA-NTD stock: 1 mM). The right panel shows a magnification of the boxed region. Selected signals are labelled, chemical shift perturbations are indicated by arrows. The inset shows selected 1D [^{1}H,^{15}N]-HSQC spectra. **(middle, left)** Normalized chemical shift changes of ^{15}N-αCTD versus sequence position. Representation as in (A). **(middle, right)** Titration curves of selected residues of ^{15}N-αCTD. The binding curves were fitted to a two-component 1:1 binding equation, yielding a K_D value of 23 ± 6 µM. **(bottom)** Mapping of the affected residues from on the structure of ^{15}N-αCTD (PDB-ID: 1COO; grey). Representation and colour code as in (A).

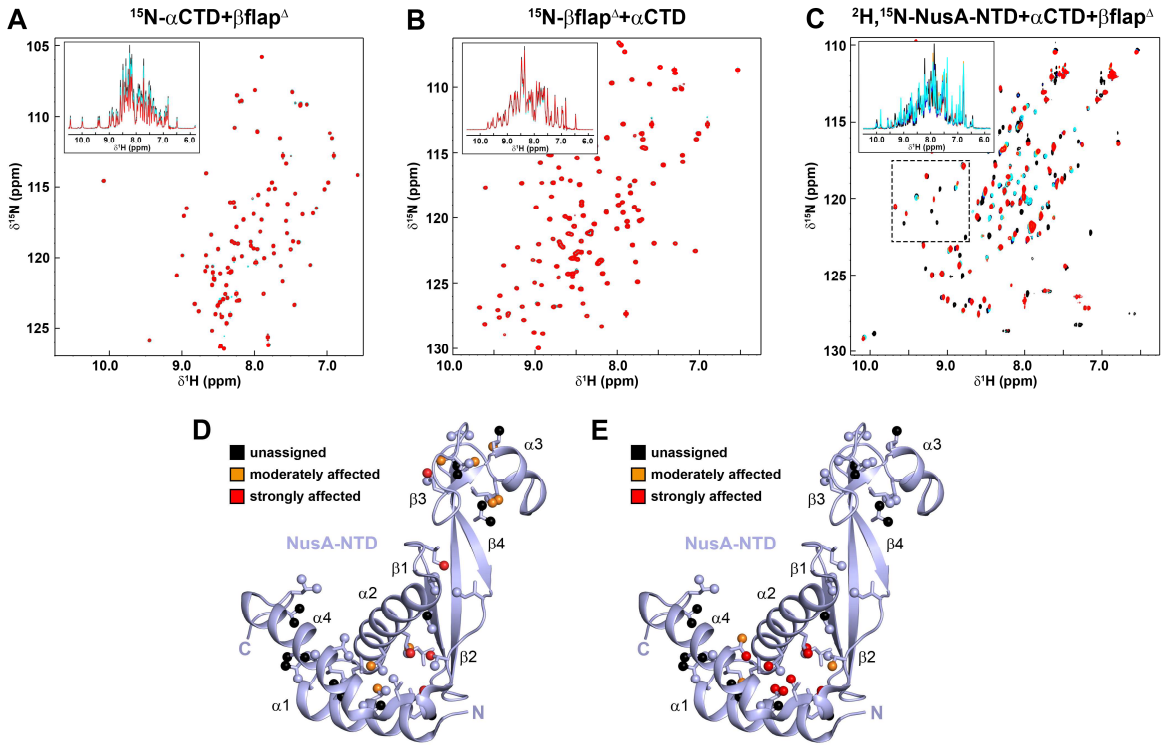

Supplementary Figure 2: NusA-NTD interacts with αCTD and βflap$^{\Delta}$ concurrently. (A,B) βflap$^{\Delta}$ does not interact with αCTD. **(A)** 2D [^{1}H,^{15}N]-HSQC spectra of the titration of 125 µM ^{15}N-αCTD with βflap$^{\Delta}$. Molar ratio of ^{15}N-αCTD:βflap$^{\Delta}$=1:0, black; = 1:1, cyan; = 1:2, red. The inset shows the 1D [^{1}H,^{15}N]-HSQC spectra of the titration. **(B)** 2D [^{1}H,^{15}N]-HSQC spectra of the titration of 125 µM ^{15}N-βflap$^{\Delta}$ with αCTD. Molar ratio of ^{15}N-βflap$^{\Delta}$:αCTD = 1:0, black; = 1:1, cyan; = 1:2, red. 1D [^{1}H,^{15}N]-HSQC spectra of the titration are shown as inset. **(C)** 2D [^{1}H,^{15}N]-HSQC spectra of the titration of 250 µM ^{2}H,^{15}N-NusA-NTD with αCTD and βflap$^{\Delta}$. Molar ratio of ^{2}H,^{15}N-NusA-NTD:αCTD:βflap$^{\Delta}$ = 1:0:0, black; = 1:1:0, blue; = 1:2:0, cyan; = 1:2:1, orange; = 1:2:2, red. The dashed box indicates the section shown in Fig. 3A. 1D [^{1}H,^{15}N]-HSQC spectra of the titration are shown as inset. **(D,E)** Interaction of ILV-NusA-NTD with RNAP **(D)** and RNAP$^{\Delta\alpha CTD}$ **(E)**. NusA-NTD residues affected by binding to RNAP or RNAP$^{\Delta\alpha CTD}$, respectively (see also Fig. 3B,C), are mapped on the structure of NusA-NTD (PDB ID: 2KWP; light blue; ribbon representation). Ile, Val and Leu residues are shown as sticks with carbon atoms terminal methyl groups depicted as spheres. The colour code is indicated. Termini and secondary structure elements are labelled.

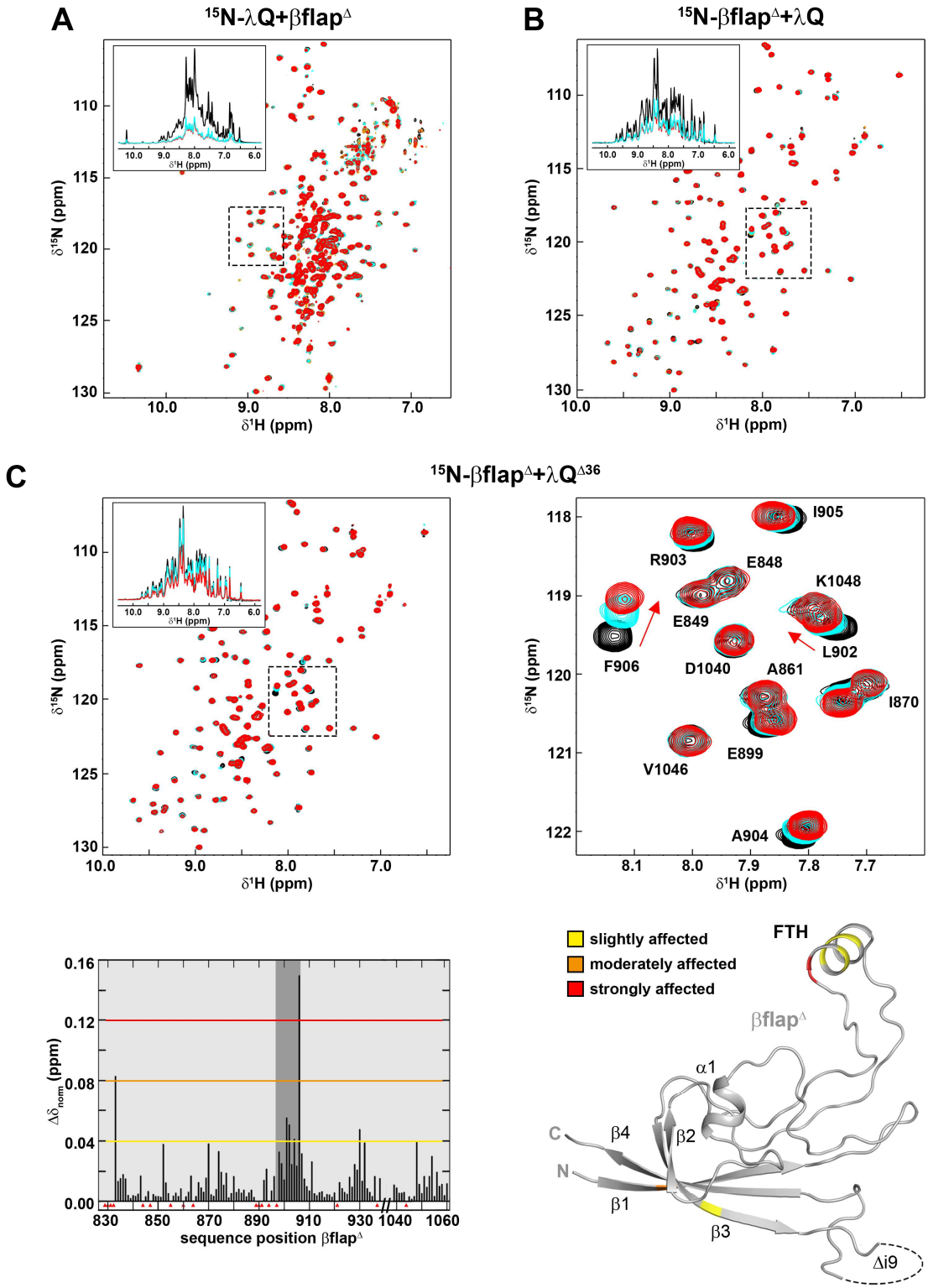

Supplementary Figure 3: Interaction of λQ with βflap$^{\Delta}$. **(A)** 2D [^{1}H,^{15}N]-BEST-TROSY spectra of the titration of 175 µM ^{15}N-λQ with βflap$^{\Delta}$. Molar ratio of ^{15}N- λQ:βflap$^{\Delta}$ = 1:0, black; = 1:0.5, orange; = 1:1, cyan; = 1:2, red. The dashed box indicates the section shown in Fig. 4A. 1D [^{1}H,^{15}N]-HSQC spectra of the titration are shown as inset. **(B)** 2D [^{1}H,^{15}N]-BEST-TROSY spectra of the titration of 175 µM ^{15}N-βflap$^{\Delta}$ with λQ. Molar ratio of ^{15}N-βflap$^{\Delta}$:λQ = 1:0, black; = 1:0.5, orange; = 1:1, cyan; = 1:2, red. The dashed box indicates the section shown in Fig. 4B. The inset shows 1D [^{1}H,^{15}N]-HSQC spectra of the titration. **(C)** Titration of ^{15}N-βflap$^{\Delta}$ with λQ$^{\Delta36}$. **(top)** 2D [^{1}H,^{15}N]-HSQC spectra of the titration of 125 µM ^{15}N-βflap$^{\Delta}$ with λQ$^{\Delta36}$.

Molar ratio of ^{15}N-βflap$^{\Delta}$:λQ$^{\Delta 36}$ = 1:0, black; = 1:1, cyan; = 1:2, red. 1D [^{1}H,^{15}N]-HSQC spectra are shown as inset. The boxed region marks the section shown in the right panel. Selected signals are labelled. Arrows indicate chemical shift changes. **(bottom, left)** Normalized chemical shift changes of ^{15}N-βflap$^{\Delta}$ in the presence of 2 equivalents λQ$^{\Delta 36}$ versus sequence position of βflap$^{\Delta}$. Thresholds for slightly (0.04 ppm ≤ $\Delta\delta_{norm}$ < 0.08 ppm), moderately (0.08 ppm ≤ $\Delta\delta_{norm}$ < 0.12 ppm), and strongly ($\Delta\delta_{norm}$ ≥ 0.12 ppm) affected residues are indicated by yellow, orange, and red lines. Unassigned residues are marked by red triangles. The FTH is highlighted in dark grey. **(bottom, right)** Mapping of affected residues on the structure of βflap$^{\Delta}$ (PDB ID: 4KMU; grey; ribbon representation). The colour code is indicated. Termini and secondary structure elements are labelled.

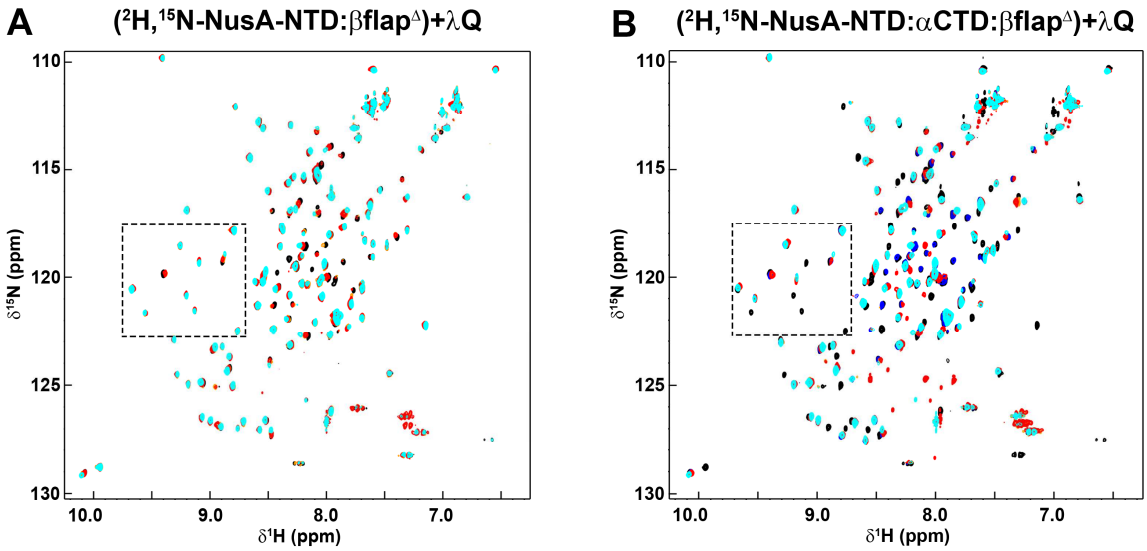

Supplementary Figure 4: λQ disrupts the NusA-NTD:βflap$^{\Delta}$ interaction. (A) λQ displaces NusA-NTD from βflap$^{\Delta}$. 2D [^{1}H,^{15}N]-HSQC spectra of a competition experiment of 250 µM ^{2}H,^{15}N-NusA-NTD with βflap$^{\Delta}$ and λQ. Molar ratio of ^{15}N-NusA-NTD:βflap$^{\Delta}$:λQ = 1:0:0, black; = 1:2:0, cyan; = 1:2:2, orange; = 1:2:2, red. The boxed region indicates the section shown in Fig. 4C. **(B)** λQ disrupts the NusA-NTD:βflap$^{\Delta}$ interaction in a NusA-NTD:βflap$^{\Delta}$:αCTD complex. 2D [^{1}H,^{15}N]-HSQC spectra of a competition experiment where λQ is added to a preformed ^{2}H,^{15}N-NusA-NTD:βflap$^{\Delta}$:αCTD ternary complex (initial concentration of ^{2}H,^{15}N-NusA-NTD: 250 µM). Molar ratios: ^{2}H,^{15}N-NusA-NTD:αCTD:βflap$^{\Delta}$:λQ = 1:0:0:0, black; = 1:2:0:0, cyan; = 1:2:2:0, blue; = 1:2:2:1 orange; 1:2:2:2, red. The boxed region indicates the section shown in Fig. 5A.

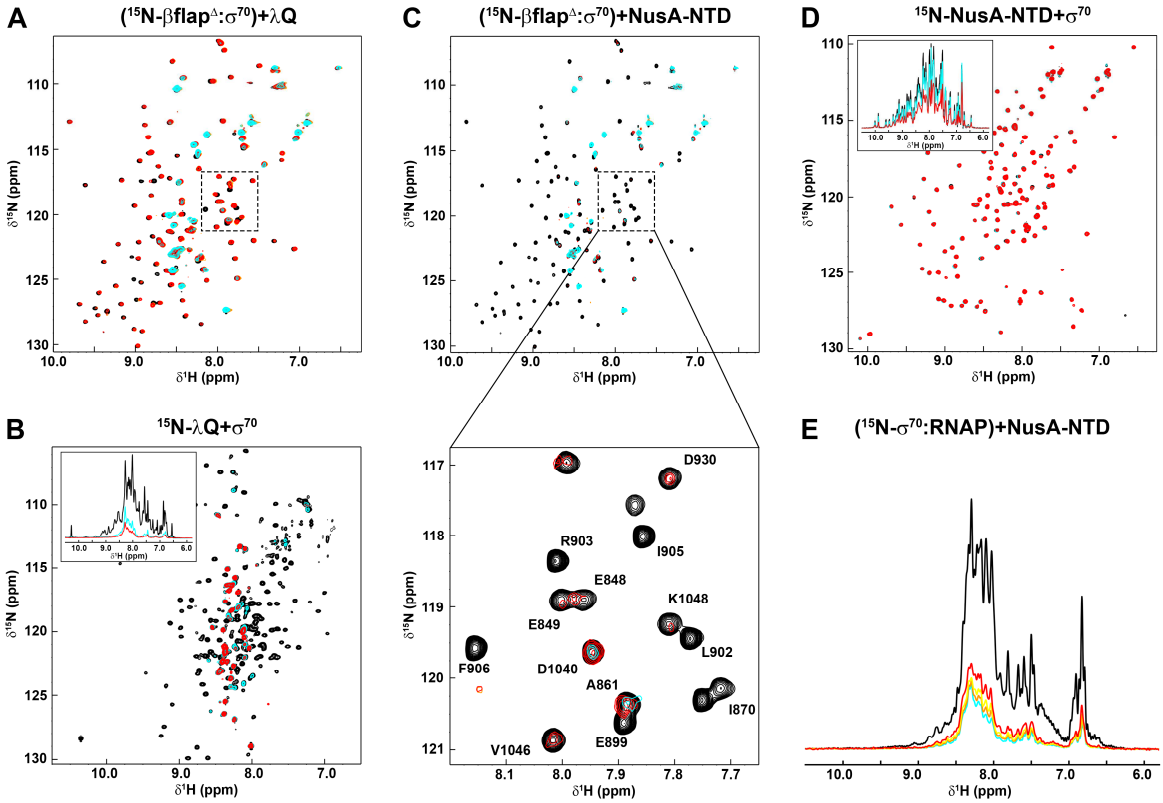

Supplementary Figure 5: λQ destabilizes σ^{70}:βflap interactions whereas NusA-NTD does not. (A) λQ displaces σ^{70}:βflap^{Δ}. 2D [^{1}H,^{15}N]-HSQC spectra of ^{15}N-βflap^{Δ} in the absence and presence of σ^{70} and upon subsequent titration with λQ (initial concentration of ^{15}N-βflap^{Δ}: 200 µM). Molar ratios of ^{15}N-βflap^{Δ}:σ^{70}:λQ = 1:0:0, black; = 1:1:0, cyan; = 1:1:1, orange; = 1:1:2 red. The boxed region indicates the section shown in Fig. 6A. **(B)** λQ directly interacts with σ^{70}. 2D [^{1}H,^{15}N]-BEST-TROSY spectra of the titration of 125 µM ^{15}N-λQ with σ^{70}. Molar ratio of ^{15}N-λQ:σ^{70} = 1:0, black; 1:1, cyan; 1:2, red. 1D [^{1}H,^{15}N]-HSQC spectra are shown in the inset. **(C)** NusA-NTD does not disrupt the ^{15}N-βflap:σ^{70} complex. 2D [^{1}H,^{15}N]-HSQC spectra of the titration of 125 µM ^{15}N-βflap with σ^{70} and NusA-NTD. σ^{70} Molar ratio of ^{15}N-βflap:σ^{70}:NusA-NTD = 1:0:0, black; = 1:1:0, cyan; = 1:1:1, orange; = 1:1:2, red. The boxed region indicates the section shown in the panel below. Selected signals are labelled. **(D)** NusA-NTD does not interact with σ^{70}. 2D [^{1}H,^{15}N]-HSQC spectra of the titration of 125 µM ^{15}N-NusA-NTD with σ^{70}. Molar ratio ^{15}N-NusA-NTD: σ^{70} = 1:0, black; = 1:1, cyan; = 1:2 red. The inset shows the corresponding 1D [^{1}H,^{15}N]-HSQC spectra. **(E)** NusA-NTD does not disrupt σ^{70}:RNAP interaction. 1D [^{1}H,^{15}N]-HSQC spectra of ^{15}N-σ^{70} in the absence (black, 40 µM ^{15}N-σ^{70}) and presence of RNAP (cyan, molar ratio 1:1, 40 µM ^{15}N-σ^{70}), and upon subsequent titration with NusA-NTD (molar ratio = 1:1:1, orange; = 1:1:2, yellow; = 1:1:5, red).

8 Publikationsliste

Benjamin R. Dudenhoeffer, Hans Schneider, Kristian Schweimer und Stefan H. Knauer (2019): **SuhB is an integral part of the ribosomal antitermination complex and interacts with NusA.** *Nucleic Acids Research* **47**, 6504–6518.

Benjamin R. Dudenhoeffer, Jan Borggraefe, Kristian Schweimer und Stefan H. Knauer (2020): **NusA directly interacts with antitermination factor Q from phage λ.** *Scientific Reports* **10,** 6607-6621.

Benjamin R. Dudenhoeffer, Marlon Wörner, Jan Bodenschlägel, Kristian Schweimer und Stefan H. Knauer: **Antitermination factor λQ mediates NusA-NTD rearrangement on RNAP βflap.** Manuskript.

9 Danksagung

Mein Dank gilt zunächst Prof. Dr. Paul Rösch, welcher mir ermöglichte meine Doktorarbeit am Lehrstuhl Biopolymere zu beginnen. Besonders danken möchte ich Dr. Stefan Knauer, welcher mir bereits vor der Übernahme meiner Betreuung immer mit Rat und Tat bei kleinen und großen Problemen zur Seite stand. Insbesondere für die Ideen, Diskussionen und Anregungen, welche allesamt diese Arbeit verbesserten, bin ich ihm sehr dankbar. Auch möchte ich mich bei Prof. Dr. Birgitta Wöhrl, welche stets ein offenes Ohr für meine Probleme hatte sowie bei Dr. Kristian Schweimer für seine Hilfe bei allen Fragen zur NMR-Spektroskopie bedanken.

Andy Hager möchte ich für die Laborорganisation und Ulrike Persau für ihre Unterstützung bei Klonierungen sowie in allen Fragen der Molekularbiologie bedanken. Insbesondere möchte ich auch meinen Dank Ramona Heißmann für die Vielzahl und in großen Mengen hergestellten Proteine aussprechen. Anja Groh danke ich für ihre Unterstützung bei Verwaltungsangelegenheiten sowie ihre aufmunternden Worte und Rainer Hofmann danke ich für die Hilfe bei allen PC-Problemen.

Bei Thessa Jacob und Philipp Zuber bedanke ich mich für die stets angenehme und konstruktive Arbeitsatmosphäre. Daneben gilt mein besonderer Dank auch Vanessa Boritzki für ihr Zuhören bei allen meinen Problemen, ihr hierbei gezeigtes Verständnis sowie ihr Durchhaltevermögen mit mir im Büro. Ganz besonders danken möchte ich auch all meinen Freunden, die Bayreuth zu meiner Heimat gemacht haben.

10 (Eidesstattliche) Versicherungen und Erklärungen

(§ 8 Satz 2 Nr. 3 PromO Fakultät)

Hiermit versichere ich eidesstattlich, dass ich die Arbeit selbstständig verfasst und keine anderen als die von mir angegebenen Quellen und Hilfsmittel benutzt habe (vgl. Art. 64 Abs. 1 Satz 6 BayHSchG).

(§ 8 Satz 2 Nr. 3 PromO Fakultät)

Hiermit erkläre ich, dass ich die Dissertation nicht bereits zur Erlangung eines akademischen Grades eingereicht habe und dass ich nicht bereits diese oder eine gleichartige Doktorprüfung endgültig nicht bestanden habe.

(§ 8 Satz 2 Nr. 4 PromO Fakultät)

Hiermit erkläre ich, dass ich Hilfe von gewerblichen Promotionsberatern bzw. –vermittlern oder ähnlichen Dienstleistern weder bisher in Anspruch genommen habe noch künftig in Anspruch nehmen werde.

(§ 8 Satz 2 Nr. 7 PromO Fakultät)

Hiermit erkläre ich mein Einverständnis, dass die elektronische Fassung der Dissertation unter Wahrung meiner Urheberrechte und des Datenschutzes einer gesonderten Überprüfung unterzogen werden kann.

(§ 8 Satz 2 Nr. 8 PromO Fakultät)

Hiermit erkläre ich mein Einverständnis, dass bei Verdacht wissenschaftlichen Fehlverhaltens Ermittlungen durch universitätsinterne Organe der wissenschaftlichen Selbstkontrolle stattfinden können.

…….

Ort, Datum, Unterschrift